Technical Report Documentation Page

1. Report No. FHWA/TX-13/0-6416-1	2. Government Accession No.	3. Recipient's Catalog No.	
4. Title and Subtitle Strength and Serviceability Design of Reinforced Concrete Inverted-T Beams		5. Report Date October 2012, Rev. March 2013, Published June 2013	
		6. Performing Organization Code	
7. Author(s) Nancy Larson, Eulalio Fernández Gómez, David Garber, Oguzhan Bayrak, and Wassim Ghannoum		8. Performing Organization Report No. 0-6416-1	
9. Performing Organization Name and Address Center for Transportation Research The University of Texas at Austin 1616 Guadalupe, Suite 4.202 Austin, TX 78701		10. Work Unit No. (TRAIS)	
		11. Contract or Grant No. 0-6416	
12. Sponsoring Agency Name and Address Texas Department of Transportation Research and Technology Implementation Office P.O. Box 5080 Austin, TX 78763-5080		13. Type of Report and Period Covered Technical Report 9/1/2009 – 8/31/2012	
		14. Sponsoring Agency Code	

15. Supplementary Notes
Project performed in cooperation with the Texas Department of Transportation and the Federal Highway Administration.

16. Abstract
Significant diagonal cracking in reinforced concrete inverted-T straddle bent caps has been reported throughout the State of Texas. Many of the distressed structures were recently constructed and have generally been in service for less than two decades. The unique nature of the problem prompted a closer look into the design and behavior of such structural components. An experimental study was conducted in which 33 reinforced concrete inverted-T beam specimens were tested. The effects of the following variables were evaluated: ledge depth and length, quantity of web reinforcement, number of point loads, member depth, and a/d ratio. A strut-and-tie design method proposed by TxDOT Project 0-5253, initially calibrated for compression-chord loaded deep beams, was investigated. It was concluded that the strut-and-tie method was a simpler and accurate design method and was recommended for use in inverted-T beam design. A recommendation was also made on the amount of minimum web reinforcement needed for strength and serviceability considerations. A simple service-load check was proposed for the purpose of limiting diagonal cracking under service loads. Lastly, a chart was created to aid in the distress evaluation of a diagonally-cracked inverted-T bent cap in the field.

17. Key Words Inverted-T Bent Caps, Strut-and-Tie Modeling, Crack Widths, Diagonal Cracking, Serviceability, Full-scale	18. Distribution Statement No restrictions. This document is available to the public through the National Technical Information Service, Springfield, Virginia 22161; www.ntis.gov.		
19. Security Classif. (of report) Unclassified	20. Security Classif. (of this page) Unclassified	21. No. of pages 234	22. Price

Form DOT F 1700.7 (8-72) Reproduction of completed page authorized

Strength and Serviceability Design of Reinforced Concrete Inverted-T Beams

Nancy Larson
Eulalio Fernández Gómez
David Garber
Oguzhan Bayrak
Wassim Ghannoum

Disclaimers

Author's Disclaimer: The contents of this report reflect the views of the authors, who are responsible for the facts and the accuracy of the data presented herein. The contents do not necessarily reflect the official view or policies of the Federal Highway Administration or the Texas Department of Transportation (TxDOT). This report does not constitute a standard, specification, or regulation.

Patent Disclaimer: There was no invention or discovery conceived or first actually reduced to practice in the course of or under this contract, including any art, method, process, machine manufacture, design or composition of matter, or any new useful improvement thereof, or any variety of plant, which is or may be patentable under the patent laws of the United States of America or any foreign country.

Engineering Disclaimer

NOT INTENDED FOR CONSTRUCTION, BIDDING, OR PERMIT PURPOSES.

Project Engineer: Oguzhan Bayrak
Professional Engineer License State and Number: Texas No. 106598
P. E. Designation: Research Supervisor

Acknowledgments

Table of Contents

x

List of Figures

xiii

List of Tables

CHAPTER 1
Introduction

1.1 OVERVIEW

Diagonal web cracking of recently built inverted-T straddle bent caps has been reported with increasing frequency in Texas, triggering concerns about current design procedures for such elements. To address these concerns, the Texas Department of Transportation (TxDOT) funded Project 0-6416 with the objectives of obtaining a better understanding of the behavior of inverted-T beams and developing strength and serviceability design criteria that will minimize such cracking in the future.

Inverted-T straddle bent caps are beam elements with girder loads applied to ledges at the bottom of the section (bottom- or tension-chord loading). The loads are transferred in the transverse direction from the ledges to the bottom of the web, then vertically to the compression chord, and finally in the longitudinal direction to the supports. This three-dimensional flow of forces, in addition to the deep beam loading conditions commonly encountered in bent caps, generate regions of stress discontinuities that have been traditionally designed using empirical equations. In the past two decades, US structural design codes have adopted strut-and-tie modeling as a more rational option for the design of deep beams and other structures with discontinuities like those present in the inverted-T bent caps.

Most inverted-T bent caps in Texas are designed using the traditional empirical procedures outlined in the TxDOT Bridge Design Manual LRFD (2011) that follows closely the AASHTO LRFD Bridge Design Specifications (2012). Given the observed cracking in inverted-T bent caps, it was the intent of this study to investigate the applicability of STM procedures developed for rectangular deep beams to improve the design of inverted-T bent caps. The TxDOT Project 0-5253 provisions (Strength and Serviceability Design of Reinforced Concrete Deep Beams) provided several improvements on the AASHTO (2012) STM procedures that, if found to be accurate and conservative, could be readily implemented to the design of inverted-T bent caps.

Due to scarcity of experimental investigations on inverted-T beams, a comprehensive experimental program was undertaken to examine the behavior of such structural elements and assess the accuracy and validity of implementing the STM design. Thirty three specimens were fabricated and tested as part of the current research program. Unlike those found in the literature, the test specimens in the current project were considered more representative of inverted-T beams designed in practice in terms of their size and reinforcement details.

1.2 PROJECT OBJECTIVE

This research report was funded by the Texas Department of Transportation (TxDOT). Since the inclusion of strut-and-tie modeling (STM) provisions in the AASHTO LRFD specifications in 1994, TxDOT engineers have been examining the impact that the provisions have on the design of bent caps. A recently completed research project, TxDOT Project 0-5253, examined the application of strut-and-tie models to the design of rectangular bent caps. From that project, recommendations were made to the AASHTO LRFD specifications to improve the strength and serviceability behavior of bent caps. A subsequent investigation, TxDOT Report 5-5253, provided additional recommendations and STM design examples for several structural bridge components.

The current project aims to evaluate the applicability of the recommended provisions, which were calibrated for compression-chord loaded beams, to inverted-T, or tension-chord loaded beams. An extensive experimental program was conducted to reveal what, if any, changes will be required for the proposed strut-and-tie modeling provisions for inverted-T bent caps. Field inspections of distressed inverted-T bent caps provided the basis for the test variables investigated in the experimental program.

1.3 PROJECT SCOPE

In order to accomplish the objectives mentioned above, the following tasks are addressed in TxDOT Project 0-6416:

1. Conduct a comprehensive literature review to expose the current state of knowledge on inverted-T beams.

2. Conduct a detailed assessment of the condition of distressed in-service bent caps

3. Conduct experimental investigations to uncover the main factors affecting the web diagonal cracking behavior of inverted-T beams:

    i. Determine the influence that the length of the ledge has on the strength and serviceability behavior of an inverted-T beam (Section 4.3).

    ii. Determine the influence that the depth of the ledge has on the strength and serviceability behavior of an inverted-T beam (Section 4.4).

    iii. Determine the influence that the web reinforcement ratio has on the strength and serviceability behavior of an inverted-T beam (Section 4.5).

    iv. Determine the influence that the number of point loads has on the strength and serviceability behavior of an inverted-T beam (Section 4.6).

<blockquote>
v.   Determine the influence that the depth of the web has on the strength and serviceability behavior of an inverted-T beam (Section 4.7).

vi.   Determine the effect of tension-chord loading on the strength and serviceability of deep beams (Section 4.8).
</blockquote>

4. Make a recommendation on the application of TxDOT Project 0-5253 STM provisions for the design of inverted-T bent caps (Section 5.2).

5. Make a recommendation on the feasibility of limiting diagonal cracking under service loads (Section 5.3).

6. Make a recommendation for relating the maximum diagonal crack width of an inverted-T beam to its residual capacity (Section 5.4).

Assembly of an inverted-T database produced 130 test results from the literature and the current project. However, most of the tests were either not applicable to the inclined cracking focus of this project or conducted on beams drastically smaller than the bent caps in service in Texas. Moreover, very limited serviceability information regarding diagonal crack widths was available in the literature. It was therefore deemed necessary to conduct a comprehensive experimental program of full-scale inverted-T beam specimens to achieve project goals.

Thirty three full-scale tests were conducted with several specimens measuring among the largest reinforced concrete deep beams ever tested to determine shear capacity. Based on the results of the experimental series treated in this project, design recommendations for strength of inverted-T beams were developed and are presented in this report. Serviceability criteria for minimizing diagonal cracking in inverted-T beams under service loads were developed based on the test results. A minimum reinforcement ratio required to restrain diagonal crack widths is also recommended. Finally a chart designed to correlate the crack width with inverted-T beam residual capacity was developed.

1.4   ORGANIZATION

A general background of the design and behavior of inverted-T bent caps is presented in Chapter 2. An overview of the distressed bent caps in service is also presented along with the assembly of the inverted-T database from the literature.

In Chapter 3, the experimental program is described in detail. An overview of the specimens, a description of the six experimental series, and the fabrication of the specimens is presented. The test setup and instrumentation are described and the overall test procedure is outlined.

Experimental results are presented in Chapter 4. Criteria for strength and serviceability evaluation are detailed. Comparisons of strength, diagonal cracking load, and the crack width progression are presented for the experimental variables covered in this project.

Analysis of the experimental results is provided in Chapter 5. A discussion of the failure modes is provided along with an assessment of the accuracy of the STM design method. The serviceability design considerations are evaluated in terms of the sizing the member to prevent or limit diagonal cracking and providing minimum reinforcement to restrain crack widths.

Descriptions of the in-service inverted-T bent caps inspected as part of this project are summarized in Chapter 6. An overview of the design recommendations are presented in Chapter 7. All of the findings and conclusions of the research program are summarized in Chapter 8.

CHAPTER 2
Background of Inverted-T Straddle Bent Caps

2.1 OVERVIEW

Included in this Chapter is an overview of the theoretical background of inverted-T beam design and behavior. A summary of the distressed in-service inverted-T bent caps are presented to frame the problem observed in Texas bridges. All cap inspections are described in detail in Chapter 6. Background information on inverted-T beams and strut-and-tie modeling is provided to familiarize the reader. The AASHTO LRFD Bridge Design Specifications and TxDOT Bridge Design Manual are discussed and the proposed TxDOT 0-5253 STM provisions are summarized for the design of inverted-T beams. Lastly, the inverted-T deep beam database is presented along with the filtering process implemented to remove specimens that were not considered to be representative of the field structures.

2.2 FIELD OBSERVATIONS

Several recently built Texas inverted-T bent caps have shown significant inclined cracking triggering concern about current design procedures for such structures. For this reason TxDOT funded Project 0-6416 to obtain a better understanding of the structural behavior of inverted-T bent caps and develop new design criteria to minimize/eliminate such cracking in the future.

One of the tasks of the current project was to conduct a thorough inspection of eight in-service bent caps that had evidence of significant diagonal cracking. In general, the measured crack widths were small ($\leq$ 0.016 in.) posing only aesthetic and durability concerns. Several of the bents were much more severely distressed with diagonal crack widths measuring up to 0.040 in. (Figure 2-1). In all cases, the observed cracking patterns on both faces of the distressed bent caps were symmetric about the longitudinal axis of the beams, indicating shear issues rather than torsional problems. While cracking is expected in reinforced concrete, the crack widths observed in some caps suggest structural deficiencies or overloading, prompting the field inspections.

Figure 2-1: Severely distressed inverted-T bent cap in El Paso.

A summary of the results obtained from inspections of the bent caps is provided in Table 2-1. The vertical reinforcement ratio, ρ_v, is evaluated as the cross-sectional area of the vertical reinforcement (stirrups) divided by the width of the section times the spacing of the stirrups. Similarly, the horizontal reinforcement ratio, ρ_h, is the ratio of the horizontal skin reinforcement to the web width times the skin spacing. The shear span-to-depth ratio, a/d, is evaluated as the distance from the center of the support to the closest load point divided by the effective depth of the section. The ledge length was determined by examining the amount the ledge was continued past the exterior bearing pad; with cut-offs terminated right at the bearing, short lengths extended a distance at least equal to the depth of the ledge, and long lengths extending to the support. More information on these variables is provided in Chapter 3. As shown in the table, the maximum diagonal crack widths of the inspected bent caps varied between 0.010 and 0.040 in. The field inspections are discussed in depth in Chapter 6.

Table 2-1: Crack width summary of in-service bent caps.

Bent	ρ_v	ρ_h	a/d	Ledge Length	Ledge Height / Cap Height	Max Diagonal Crack Width
Austin IH-35 / Tx-290 Bent 3M	0.43%	0.37%	1.4	Short	35%	0.02 in.
Austin IH-35 / Tx-290 Bent 6K	0.43%	0.37%	1.7	Short	35%	0.016 in.
Austin IH-35 / Tx-290 Bent 28K	0.43%	0.37%	1.4	Short	35%	0.03 in.
San Antonio IH-35 S Exit 165	Not available		1.85*	Long	33%*	0.015 in.
El Paso IH-10 / Geronimo Bent 4	0.57%	0.19%	1.7	Cut-Off	29%	0.04 in.
El Paso IH-10 / Geronimo Bent 5	0.57%	0.19%	3.4	Cut-Off	29%	0.02 in.
Waco IH-35 / LP340 Bent 17	0.46%	0.30%	2.5	Short	36%	0.01 in.
Waco IH-35 / LP340 Bent 19	0.46%	0.30%	2.5	Short	36%	0.015 in.

* Approximated based on field observations

2.3 BACKGROUND ON INVERTED-T BENT CAPS

In this section, a background on inverted-T beam behavior is given. The difference between tension-chord loaded beams and typical reinforced concrete deep beams is examined and the unique characteristics of inverted-T beams are discussed.

2.3.1 Tension-Chord vs. Compression-Chord Loaded Beams

Inverted-T bent caps are often used in bridge construction to reduce the elevation of bridges and/or to improve available clearance beneath the beams. The bridge girders are supported on ledges near the bottom of the beam, effectively loading the cap along its tension chord as shown in Figure 2-2. This arrangement generates a tension field in the web at the loading points as forces are "hung" from the tension chord to the top of the beam. In contrast, compression-chord loaded beams are not subjected to such concentrated tension fields in the web as the load is applied to the top of the beam.
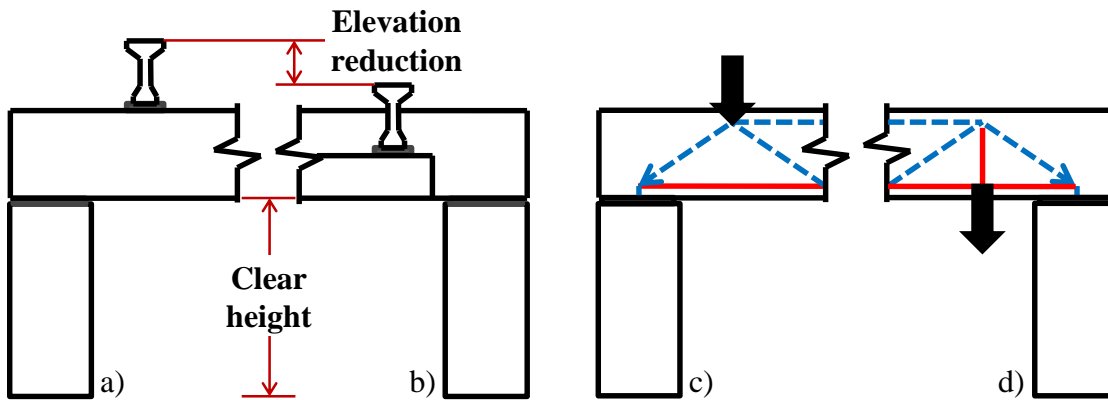
Figure 2-2: Left (a) rectangular bent cap, (b) inverted-T bent cap; right: flow path of forces in strut-and-tie models: (c) Compression-chord loaded beam, (d) tension-chord loaded beam (Fernandez 2012).

2.3.2 Components of an Inverted-T Beam

Inverted-T beams have two main components, as shown in Figure 2-3. Load is applied to the ledges of the beam, and is then transferred into the stem or web. The web then carries the shear and flexure forces to the supports.
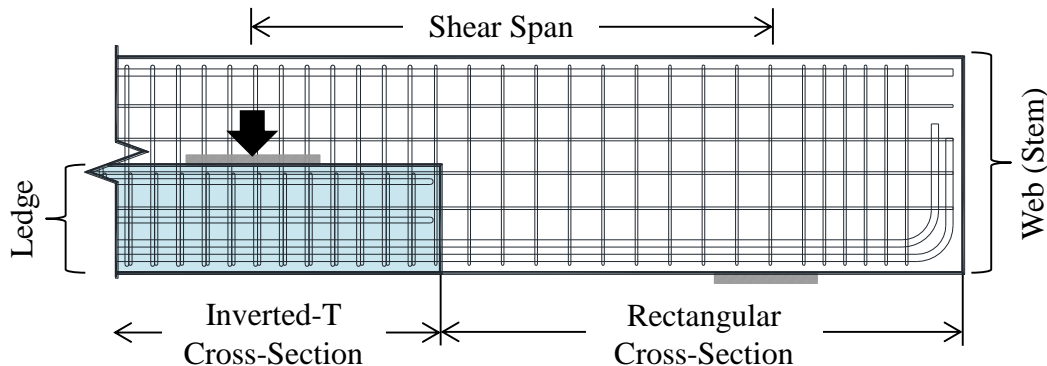
Figure 2-3: Longitudinal elevation of an inverted-T bent cap with discontinuous ledges.

Two additional types of reinforcement are required in an inverted-T beam compared to that of the typical reinforcement layout of a rectangular beam. Ledge reinforcement is necessary to resist flexural tension forces in the cantilevered ledge and allow the applied load to flow into the web of the beam. Additional vertical bars, or hanger reinforcement, are then used to "hang" the load transferred from the ledge at the bottom of the beam to the compression-chord at the top. The reinforcement layout for inverted-T beams is illustrated in Figure 2-4.
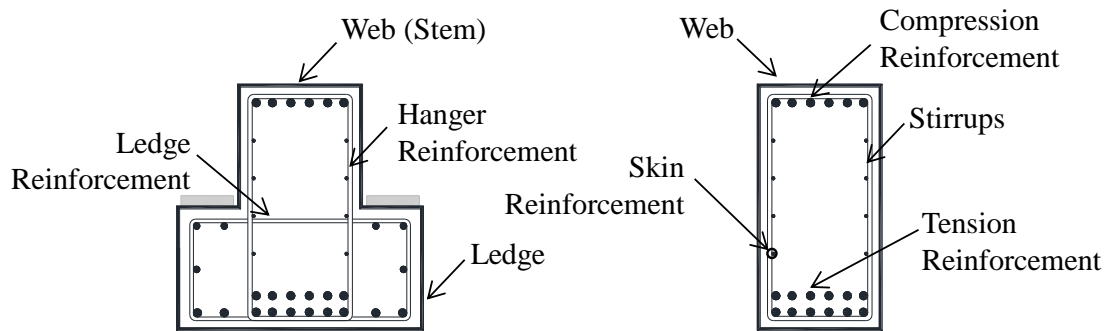
Figure 2-4: Typical details of inverted-T bent caps.

2.4 DISCONTINUITY REGIONS OF BEAMS

Typically, reinforced concrete beams are designed based on the assumption that plane sections remain plane; referred to as the Bernoulli hypothesis or beam theory. Within that theory, the strains in the beam are presumed to vary linearly at a section and the beam is said to be dominated by sectional behavior. As shown in Figure 2-5, these regions of linear stress (or strain) are referred to as B-regions (with the "B" standing for beam or Bernoulli).
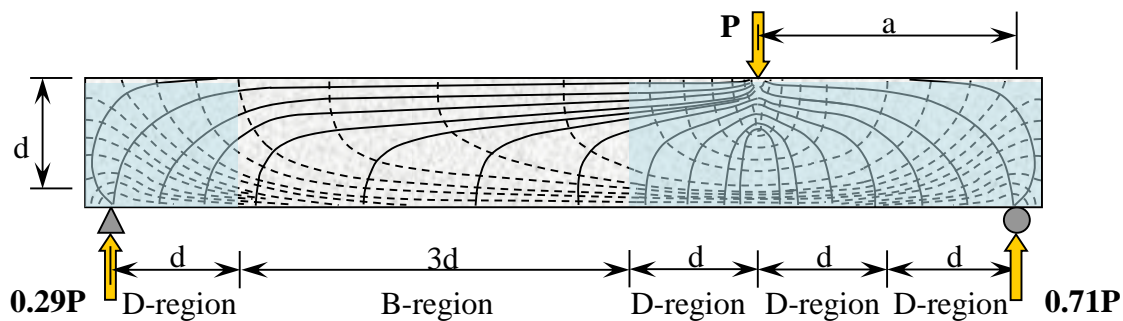
Figure 2-5: Stress trajectories within B- and D-regions (adapted from Birrcher, et al. 2009)

A D-region (with "D" standing for discontinuity or disturbed) can typically be found on either side of a B-region. These regions cannot be designed using the sectional procedures because the assumptions used to derive the beam theory are no longer valid. As illustrated in Figure 2-5, the strains are distributed nonlinearly throughout the D-regions. These disturbances are caused either by abrupt changes in geometry or loading. Frame corners, dapped ends, openings, and ledges are examples of geometric discontinuities. Point loads such as girder bearings or support reactions also result in nonlinear strains. According to St. Venant's Principle, an elastic stress analysis would indicate that a disturbance dissipates at about one member depth away from the

9

discontinuity. In other words, a D-region is assumed to extend one member depth, *d*, from the load or geometric discontinuity.

A deep beam is one in which the entire span is assumed to be dominated by nonlinear behavior. For this to be true, the shear span, *a*, must be less than about 2 to 2.5 times the member depth, *d*. The right shear span in Figure 2-5 is entirely composed of D-regions and is thus considered a deep beam. A beam with a greater a/d ratio, as shown in the left span, is assumed to behave according to beam theory and can be designed using the sectional procedures. Deep beams, however, require the use of non-sectional design procedure such as the strut-and-tie modeling procedure discussed below.

2.5 THEORETICAL BACKGROUND OF STRUT-AND-TIE MODELING

Strut-and-tie modeling (STM) offers a rational approach for obtaining lower-bound solutions for the strength design of deep beams. In the models, the complex state of stresses in a member is idealized as a system of uniaxial force elements acting as a truss within the concrete member as shown in Figure 2-6. This system will yield a conservative design if the resulting truss model is in equilibrium with the external forces and the concrete has enough deformation capacity to accommodate the assumed distribution of forces (Schlaich et al. 1987). The compressive forces must not exceed the factored concrete strengths and, likewise, the tensile forces must not exceed the factored tie capacities. It is also crucial that proper anchorage of the reinforcement is achieved.
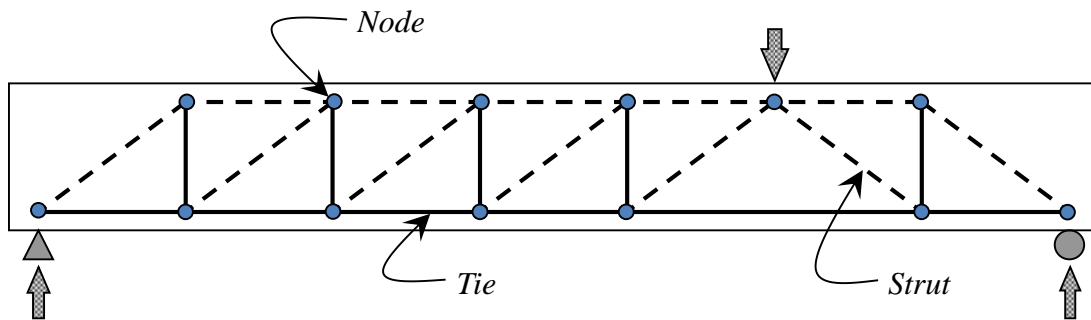
Figure 2-6: Strut-and-tie model: Simply supported beam supporting a concentrated load (adapted from Birrcher et al., 2009).

Strut-and-tie models consist of three components: struts, ties, and nodes assembled together to represent the flow of forces through a structure, as shown in the simply supported beam illustrated in Figure 2-6. After calculating the external reactions and defining the geometry of the STM, the individual member forces of the truss are determined through statics. The compression members are referred to as struts, the tension members as ties, and the regions in which they intersect are nodes.

The versatility of strut-and-tie modeling allows it to be used to design of any D-region and accommodate various load transfer mechanisms. Its adaptability is a significant advantage but can also pose major design challenges as no one "correct" STM exists for any particular structure. As long as the principles required to achieve a lower-bound solution are met, any model can be considered a safe design. A model should, to the best extent possible, follow the actual stress field as determined by an elastic stress analysis. If the model varies substantially from the structure's stress field, the structure will undergo substantial deformations leading to an increased chance of cracking. Many examples of strut-and-tie modeling can be found in the literature, including TxDOT Report 5-5253 (Williams et al., 2011) which aides engineers in developing strut-and-tie models for structural components of highway bridges. For further explanation of the theoretical background of STM, the reader is encouraged to reference the TxDOT Project 0-5253 report (Birrcher et al., 2009).

2.5.1   Struts

Struts are compression elements that vary in shape depending on their location within a structure. Idealized as dashed lines, struts can be bottle-shaped if allowed to spread along their length, or prismatic in regions of uniform stresses such as the compression zone of a beam's flexural region. Often bottle-shaped struts are idealized as prismatic struts as shown in Figure 2-7. It is important to provide transverse reinforcement in the vicinity of these diagonal bottle-shaped struts to carry the tensile forces, strengthen the strut, and control the bursting cracks that develop with the spreading.
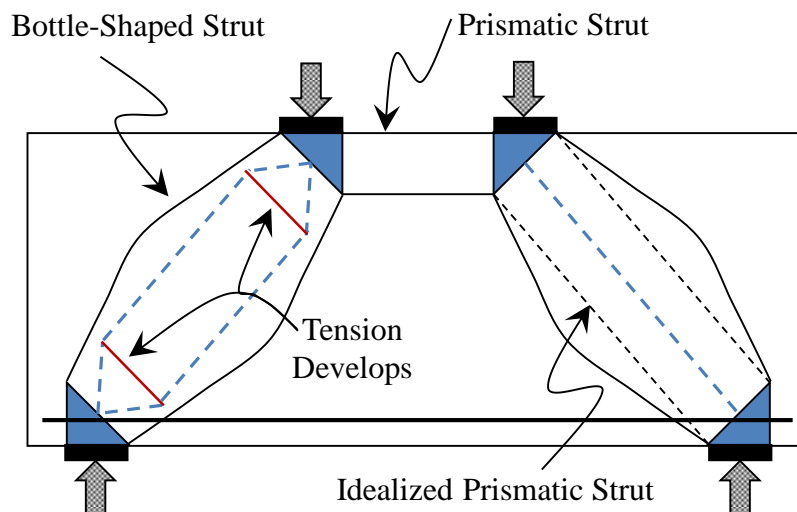
Figure 2-7: Prismatic and bottle-shaped struts (adapted from Birrcher et al., 2009)

2.5.2 Ties

STM tension elements, or ties, are generally made up of reinforcing steel and denoted by solid lines in Figure 2-7 and throughout this report. Enough reinforcement must be provided to carry the tensile demand of the tie and should be distributed so that its centroid coincides with the tie location. Details such as bar spacing and anchorage need to be considered for proper strut-and-tie modeling.

2.5.3 Nodal Zones

Due to the concentration of stresses from intersecting truss members, the nodes are the most highly stressed regions of a structural member. Three types of nodes can exist within an STM and are named based on the elements framing into them, as shown in Figure 2-8. Within the nodal designations, "C" refers to a compression element, such as a strut or an externally applied load, and "T" stands for tension, such as a tie.

- CCC: nodes where only struts intersect
- CCT: nodes where tie(s) intersect in only one direction
- CTT: nodes where ties intersect in two different direction

Struts are often resolved together to reduce the number of members intersecting at a node, such as the CCC node illustrated in Figure 2-8. The type of node governs its behavior and thus its strength. Additional information on strut-and-tie modeling for inverted-T design is provided in Section 2.6.2.
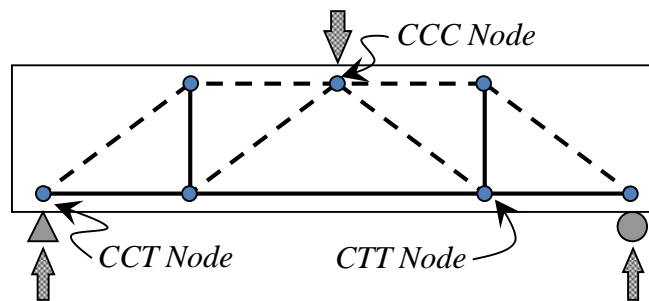
Figure 2-8: Node designations.

2.6 INVERTED-T DESIGN PROVISIONS

In this section, the current design provisions for inverted-T beams in AASHTO LRFD Bridge Design Specifications (2012) and the TxDOT Bridge Design Manual-LRFD (2011) are discussed. The design procedure used in the experimental portion of this project, the TxDOT Project 0-5253 STM provisions, is also presented.

2.6.1 AASHTO LRFD Bridge Design Specifications (2012)

AASHTO LRFD specifies two design methods for inverted-T beams: Strut-and-tie modeling of the beam or a series of separate design provisions for the web portion and the ledge portion.

The TxDOT Design Manual utilized a slightly modified version of the second method. For the web portion of inverted-T beams, sectional design provisions apply. To design the ledge portion, a set of checks outlined in the provisions of Articles 5.13.2.5.2 through 5.13.2.5.5 are used. These provisions focus on designing beam ledges to resist forces in various location of the ledge, including flexure, shear and horizontal forces at the ledge to web interface, tension force in the top of the ledge, punching shear through the ledge, and bearing forces.

If the shear span-to-depth ratio of a beam is less than about 2.0, the AASHTO Code specifies that strut-and-tie modeling should be considered. AASHTO (2012) Clause 5.6.3.1 specifies: *"The strut-and-tie model should be considered for the design of deep footings and pile caps or other situations in which the distance between the centers of applied load and the supporting reactions is less than about twice the member thickness."* This definition is not clear and can easily be taken to mean two things. Either the shear span is defined as the distance between the center of the column (support) and the center of the first load (girder) or the distance between the column and the center of all the applied loads (girders). Based on the second assumption, most if not all inverted-T bent caps would be considered slender and designed using sectional shear provisions as the center of the applied load (bridge girders) would be near the center of the bent itself. With large loads applied at distinct locations along the ledge, the first assumption, with the shear span defined as the distance from the support to the first load point is likely to be more appropriate when the actual behavior of the beam is considered.

In cases where the ledge of an inverted-T beam is within twice the web depth for the support regardless of where the loads are applied, the web can be considered as a D-region and STM may be appropriate. AASHTO LRFD is silent on the treatment of geometric discontinuities such as ledges in inverted-T beams.

Based on the geometric and loading discontinuities, strut-and-tie modeling is considered a more appropriate design procedure than sectional shear for inverted-T beams and will be investigated in the experimental program. A detailed overview of the STM provisions of AASHTO (2008) can be found in Birrcher (2009) and will not be covered here. Note that these provisions changed little in AASHTO (2012).

2.6.2   TxDOT Project 0-5253 STM Provisions

The proposed changes to the STM provisions in the AASHTO LRFD Bridge Design Specifications (Project 0-5253) and their application to the inverted-T beams in the experimental program are summarized herein. Further discussion on the recommendations derived from this project for STM of inverted-T caps is provided in Chapter 7.

2.6.2.1   *Recommended Changes to AASHTO LRFD STM Provisions*

TxDOT Project 0-5253 and subsequently Project 5-5253 improved upon the current strut-and-tie (STM) modeling provisions and recommended modifications to both the ACI 318 and AASHTO LRFD codes. These recommendations are presented in their entirety in Birrcher et al. (2009) and Williams et al.(2011). The most significant modifications that affect the design of inverted-T beams focused on the strength of the nodes, particularly the strut-to-node interfaces.

Three types of nodes exist in strut-and-tie modeling. For inverted-T beams, two of these nodes are present as shown in Figure 2-9. Hydrostatic nodes are proportioned to have equal stresses applied to each face. Such nodal constraints result in unrealistic nodal geometries and impractical reinforcement layouts. Only non-hydrostatic nodes are therefore recommended in the design of inverted-T beams, as they more closely correspond to the actual stress concentrations at the nodal regions. For additional details on hydrostatic and non-hydrostatic nodes refer to Birrcher et al, (2009).
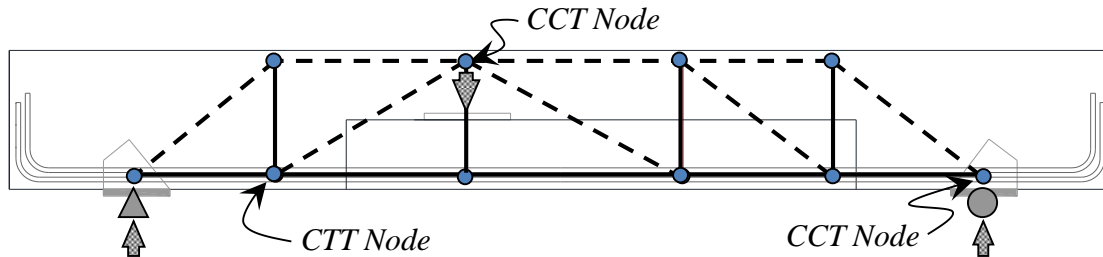
Figure 2-9: Node designations in an inverted-T beams

The CCT node at the support in Figure 2-9 is shown in detail in Figure 2-10. The length of the bearing face, l_b, corresponds to the dimension of the bearing plate. The length of the back face, w_t, is defined by the width of the tie corresponding to the longitudinal reinforcement. It is taken as twice the distance from the bottom of the beam to the centroid of the longitudinal steel.
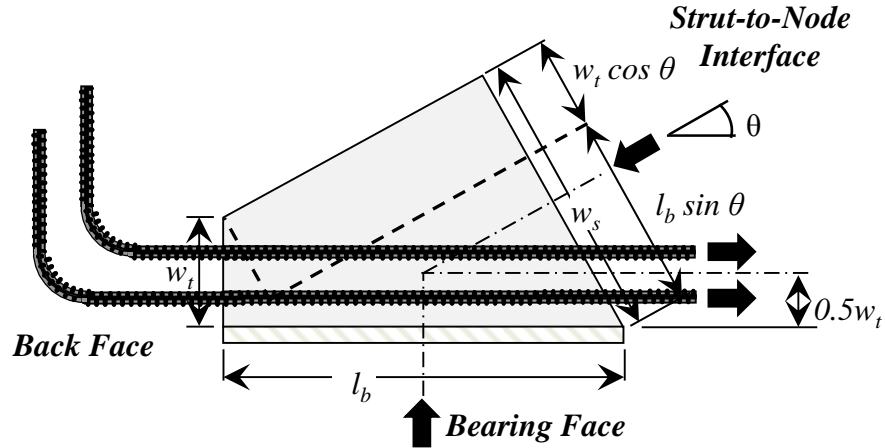
Figure 2-10: Geometry of a CCT node (adapted from Birrcher et al., 2009).

The strut-to-node interface is the face at which the diagonal strut frames into the node. This surface is perpendicular to the angle, θ, of the diagonal strut, and thus the length, w_s, depends on the angle. From the geometry of the node, the following equation for w_s can be derived with the previously defined node variables:

$$w_s = l_b sin\theta + w_t cos\theta \qquad \text{(2-1)}$$

For CCC nodes, such as the one under the load of the compression-chord loaded beam in Figure 2-8, adjacent struts are often resolved together to reduce the number of forces acting on the node. The node is then divided into two parts since the diagonal struts enter the node from the right and the left. In the design of inverted-T beams, however, no CCC nodes exist as the loads are applied to the ledge near the tension chord and "hung up" to the top chord of the beams. The resulting node at the compression chord is thus a CCT node, as shown in Figure 2-9. It is proportioned in a manner similar to that of a CCC at a load point in a typical rectangular beam.

The struts that intersect the vertical tie at the CCT hanger node are shown in Figure 2-11(a). To simplify the nodal geometry, the adjacent struts are resolved together, resulting in the diagonal struts presented in Figure 2-11(b). The compressive forces F_1 and F_2 have combined together to form the force F_R. A similar process is repeated but not shown for the struts on the right side.

15
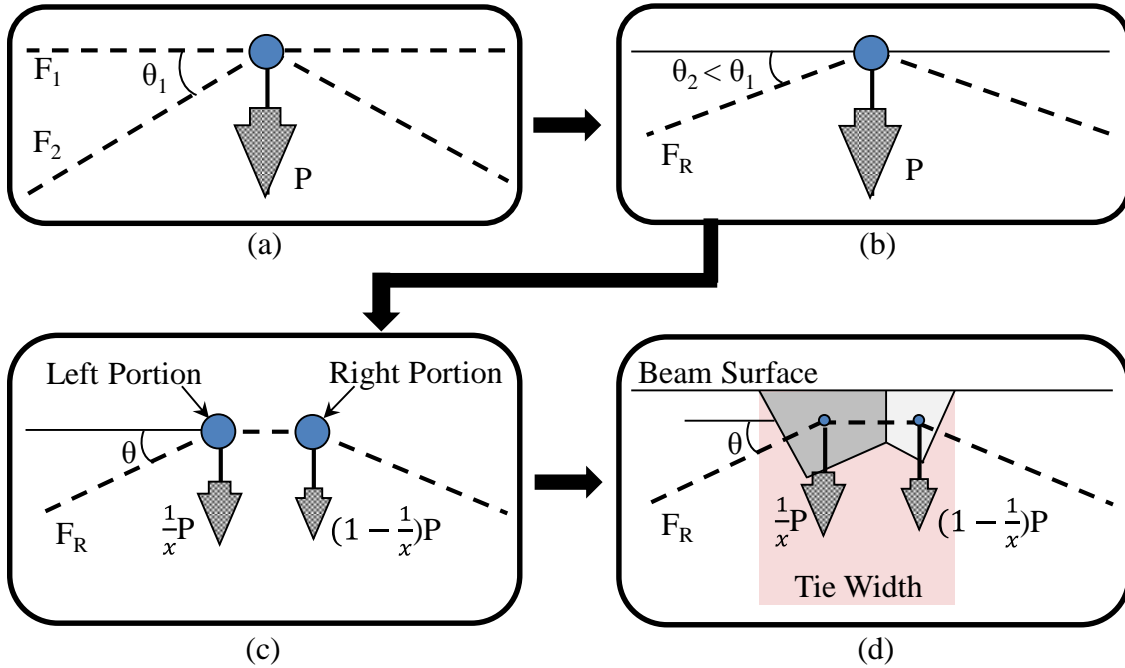
Figure 2-11: CCT hanger node- (a) Original geometry of the STM; (b) adjacent struts resolved together; (c) node divided into two parts; (d) final node geometry (adapted from Williams et al., 2011).

The node is divided into two parts when diagonal struts enter from both sides (Figure 2-11(c)). Each section is dimensioned proportionally to the fraction of the applied load P that the adjacent strut transfers to each support. From statics, if $1/_xP$ flows to the left support, the load acting on the left portion of the node will be $1/_x P$ and $(1-1/_x)P$ will act on the right portion.

The geometry of the CCT hanger node, shown in Figure 2-11(d) and Figure 2-12 can now be defined. The length of the node in the longitudinal direction, l_h, is determined by the width of the hanger tie. Since $1/_x$ of the applied load P acts on the left portion of the node, it occupies $1/_x$ of the total node length, l_h. The length of the face of the left portion of the node is therefore taken as $1/_x l_h$.
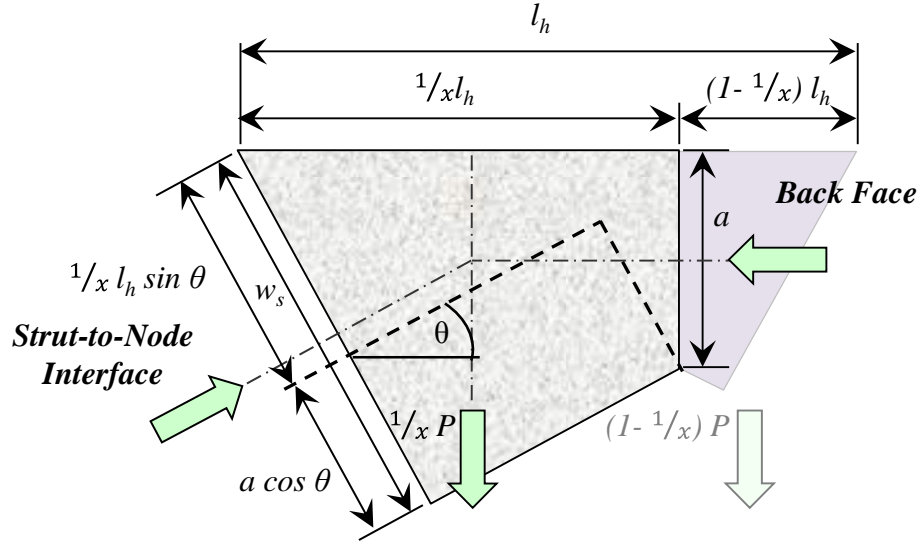
Figure 2-12: Geometry of a hanger CCT node (adapted from Birrcher et al., 2009)

The length, a, of the back face is taken as the depth of the compression stress block as defined in a typical flexural analysis. Using this assumption, the value of a for a rectangular web is determined using the following equation:

$$a = \frac{A_s f_y - A_s' f_y'}{0.85 b_w f_c'} \tag{2-2}$$

where:

A_s	=	area of longitudinal tension steel (in.^{2})
f_y	=	yield strength longitudinal tension steel (psi)
A_s'	=	area of longitudinal compression steel (in.^{2})
f_y'	=	yield strength longitudinal compression steel (psi)
b_w	=	web width (in.)
f_c'	=	specified compressive strength of concrete (psi)

Although a traditional flexural analysis is not valid in a D-region due to the nonlinear distribution of strains, defining a using the equation above is conservative according to Williams et al., (2011). The assumption is well-established in practice and will be used to design the inverted-T specimens in the current experimental program.

The length of the strut-to-node interface, w_s, is determined from the same equation as the support CCT node, Equation 2-1, except the variable w_t is replaced with a.

CTT nodes, such as the node denoted in the strut-and-tie model in Figure 2-9, are often interior nodes and can be classified as smeared nodes. Smeared nodes do not have a geometry that is restricted by a bearing plate or geometric boundaries and thus cannot be fully defined. The CTT node shown in Figure 2-13 is similar to the CCT node illustrated

in Figure 2-10, but instead of being defined by a bearing surface, the size of the exterior face, l_a, is dependent on the width of the vertical tie.
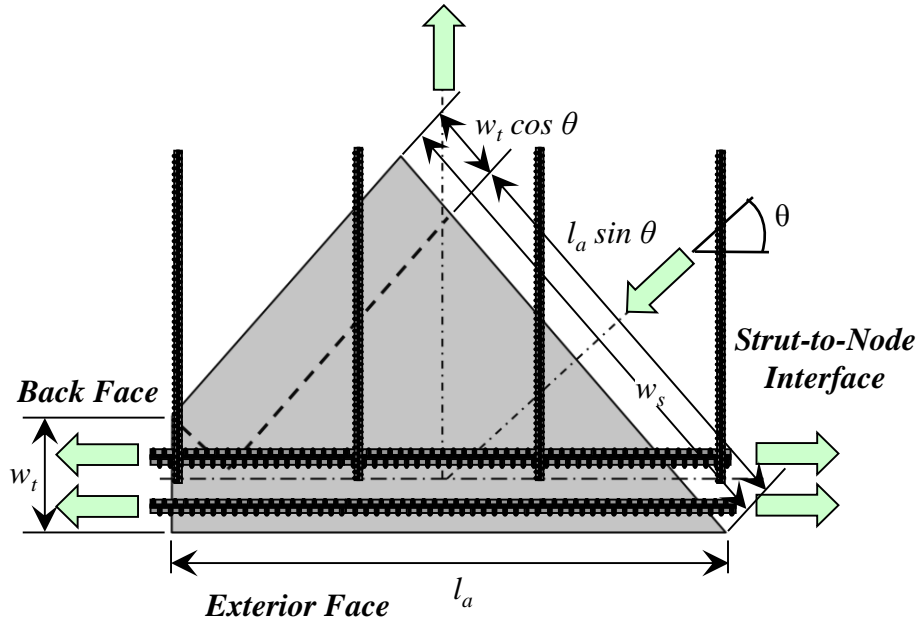
Figure 2-13: Geometry of CTT node(adapted from Birrcher et al., 2009)

In order to proportion the exterior face l_a, TxDOT Project 0-5253 utilizes a method recommended by Wight and Parra-Montesinos (2003). They propose that any stirrup that intersects an adjacent strut at an angle greater than 25 degree can be engaged as part of the vertical tie in the CCT node. The tie width or the exterior face, l_a, can then be conservatively estimated as the entire distance between the outermost stirrups included in the vertical tie. For the inverted-T specimens in the experimental program, the vertical tie was considered to be bounded by the 25 degree line on one side and the end of the hanger load spread, l_h, on the other as illustrated in Figure 2-14.
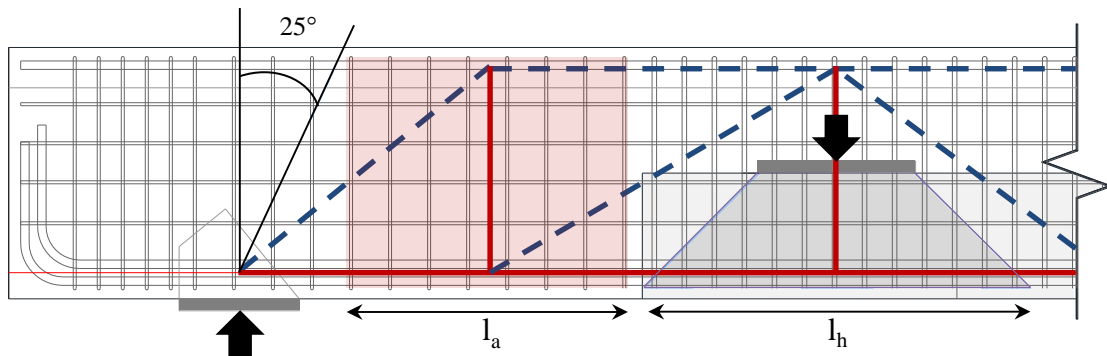
Figure 2-14: Determination of CTT vertical tie

The back face, w_t of the node is calculated the same way as the CCT node at the support and is equal to twice the distance to the centroid of the tension steel, measured from the tension surface of the beam. The width of the strut-to-node interface, w_s, is determined as in the previous node descriptions, with the angle of the strut framing into the strut-to-node interface is based on the truss geometries.

After the geometry of a node is defined, the design strength of each face is calculated and compared to the applied force. The design strength of the nodes was governed by the limiting compressive stresses at the faces of the node, f_{cu}, multiplied by the effective cross sectional area of the faces, A_{cn}. The cross-sectional area is obtained by multiplying the length of the face as described in Figure 2-10, Figure 2-12, and Figure 2-13 by the width of the node perpendicular to the plane of the page. If the node is defined by a bearing plate, the width of the node is taken as the width of the plate. In other cases, such as the CCT node above the ledge in an inverted-T beam, the width of the node is the same as the width of the member, b_w. The limiting compressive stress at the face of the node is calculated in design using the following equation:

$$f_{cu} = m \cdot v \cdot f_c' \qquad \text{(2-3)}$$

Where m is the triaxial confinement factor, v is the concrete efficiency factor, and f'_c is the specified compressive strength of the concrete. When evaluating test specimens, the measured concrete compressive strength was used in this study; as determined from cylinders tested in accordance with ASTM C39.

If the node is defined by a bearing area with a width smaller than that of the structural member, the concrete strength for all the faces in that node can be increased due to triaxial confinement. The triaxial confinement factor, m, is calculated using the following equation.

$$m = \sqrt{A_1 / A_2} \leq 2.0 \qquad \text{(2-4)}$$

Where A_1 is the loaded area and A_2 is measured on the plane defined by the location at which a line with a 2 to 1 slope extended from the loading area meets the edge of the member as shown in Figure 2-15. This modification factor is found in Article 5.7.5 of AASHTO LRFD (2011) and §10.14.1 of ACI 318-11.
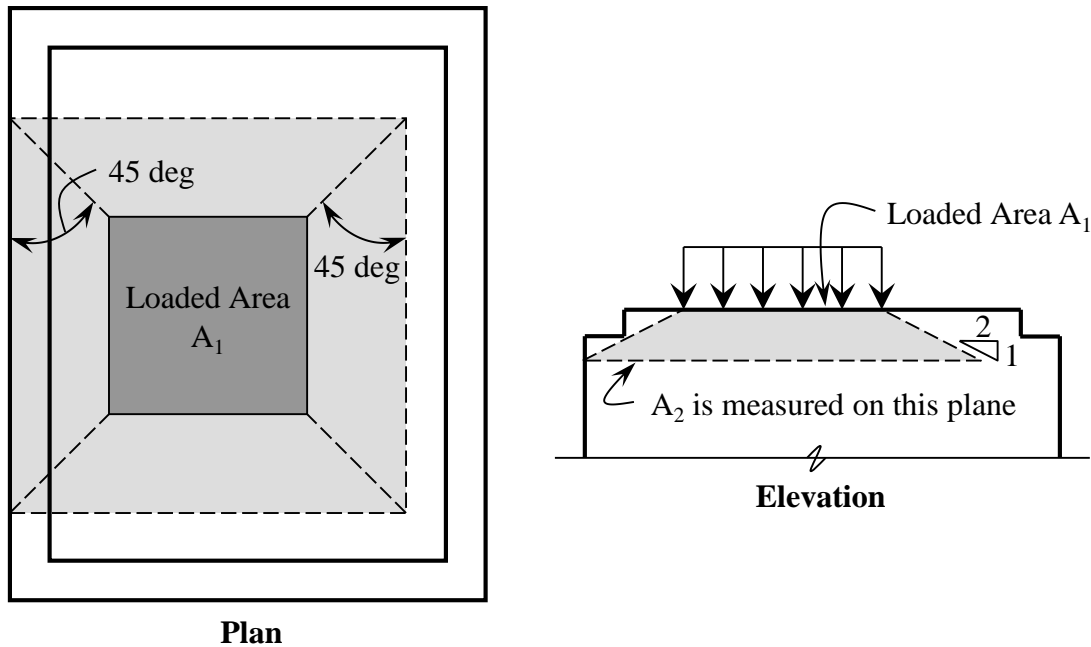
Figure 2-15: Determination of A$_2$ for stepped or sloped supports (from ACI 318-11)

The concrete efficiency factors, v, are used to reduce the compressive strength of the concrete in the node depending on the type of node (CCC, CCT, or CTT) and face (bearing face, back face, strut-to-node interface) under consideration. The factors developed in TxDOT Project 0-5253 are summarized in Table 2-2. These factors correspond directly to the strength of the node and thus were used to determine the nominal capacity of the specimens in the experimental program.

Table 2-2: TxDOT Project 5-5253-01 concrete efficiency factors, v

Face	Node Type		
	CCC	**CCT**	**CTT**
Bearing Face	0.85	0.70	$0.45 \leq 0.85 - \dfrac{f'_c}{20} \leq 0.65$
Back Face			
Strut-to-Node Interface*	$0.45 \leq 0.85 - \dfrac{f'_c}{20} \leq 0.65$	$0.45 \leq 0.85 - \dfrac{f'_c}{20} \leq 0.65$	

* If crack control reinforcement requirement of AASHTO Art. 5.6.3.5 is not satisfied, use v = 0.45 for the strut-to-node interface

It can be noted from Table 2-2 that the efficiency factor at a strut-to-node interface is given as the same for both CCC and CCT nodes. Current recommendations therefore do not reduce the nodal strength due to the presence of a tension field in an inverted-T beam. In compression-chord loaded members, the node below the applied load is a CCC node.

However, the same node in a tension-chord loaded inverted-T member is a CCT node. This report aims to explore potential differences between tension- and compression-chord loaded members that may affect efficiency factors of CCT nodes.

The design of struts is simplified by focusing on the strut-to-node interfaces, which implicitly accounts for the strut capacity and eliminates trivial checks.

Ties are simple in that their design capacity is the total cross-sectional area multiplied by the yield strength of the bars. As before, no strength reduction factors were used in this report in order to investigate the nominal strength of the specimens. The ties must be properly anchored to ensure that the structure can achieve the stress distribution assumed by the STM. STM procedures require that the yield strength of the tie be developed at the critical point where the centroid of the tie meets the end of the extended nodal zone; otherwise known as the edge of the diagonal strut as shown in Figure 2-16.
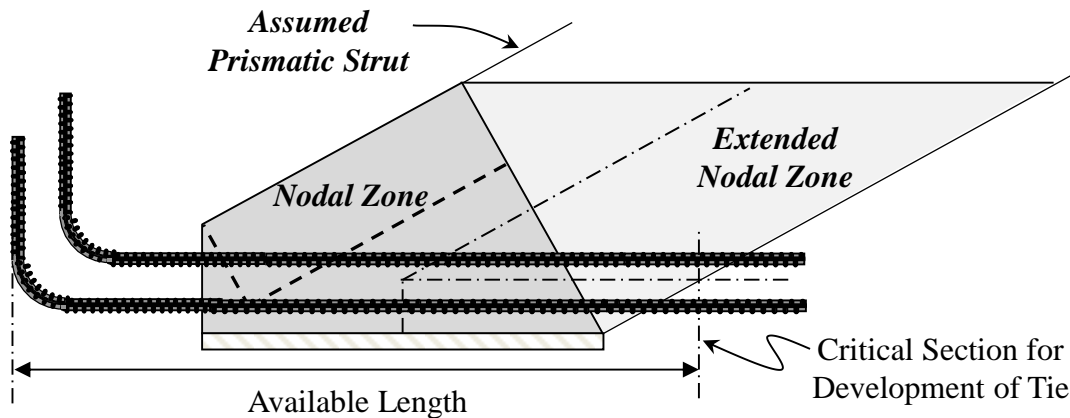
Figure 2-16: Available development length for ties (adapted from Birrcher et al., 2009)

2.6.2.2 Outline of Strut-and-tie Modeling of Inverted-T Bent Specimens

TxDOT Project 0-5253 demonstrated the effectiveness of the modifications proposed to the AASHTO LRFD STM design procedures for rectangular deep beams. TxDOT Project 5-5253 provided several additional modifications to the provisions. Due to the geometry of inverted-T beams, certain assumptions not treated in the available STM procedures had to be made in designing the inverted-T specimens. The design procedures used to design test specimens are summarized below. The validity of the proposed application of STM provisions of TxDOT Project 0-5253 and 5-5253 to inverted-T beams is investigated in Chapter 5.

Inverted-T bent caps transfer the loads in multiple dimensions: from the ledges to the web, from the tension- to the compression-chord, and from the loading points to the supports. In order to properly model this behavior it is necessary to consider a three-

dimensional strut-and-tie model as the one shown in Figure 2-17. The model can be divided into two 2-dimensional models to simplify the analysis, provided that the interaction between them is considered as follows: first, the external loads are applied to the longitudinal model and forces are calculated for the hanger ties, then, these calculated hanger forces are applied to the cross-sectional models.
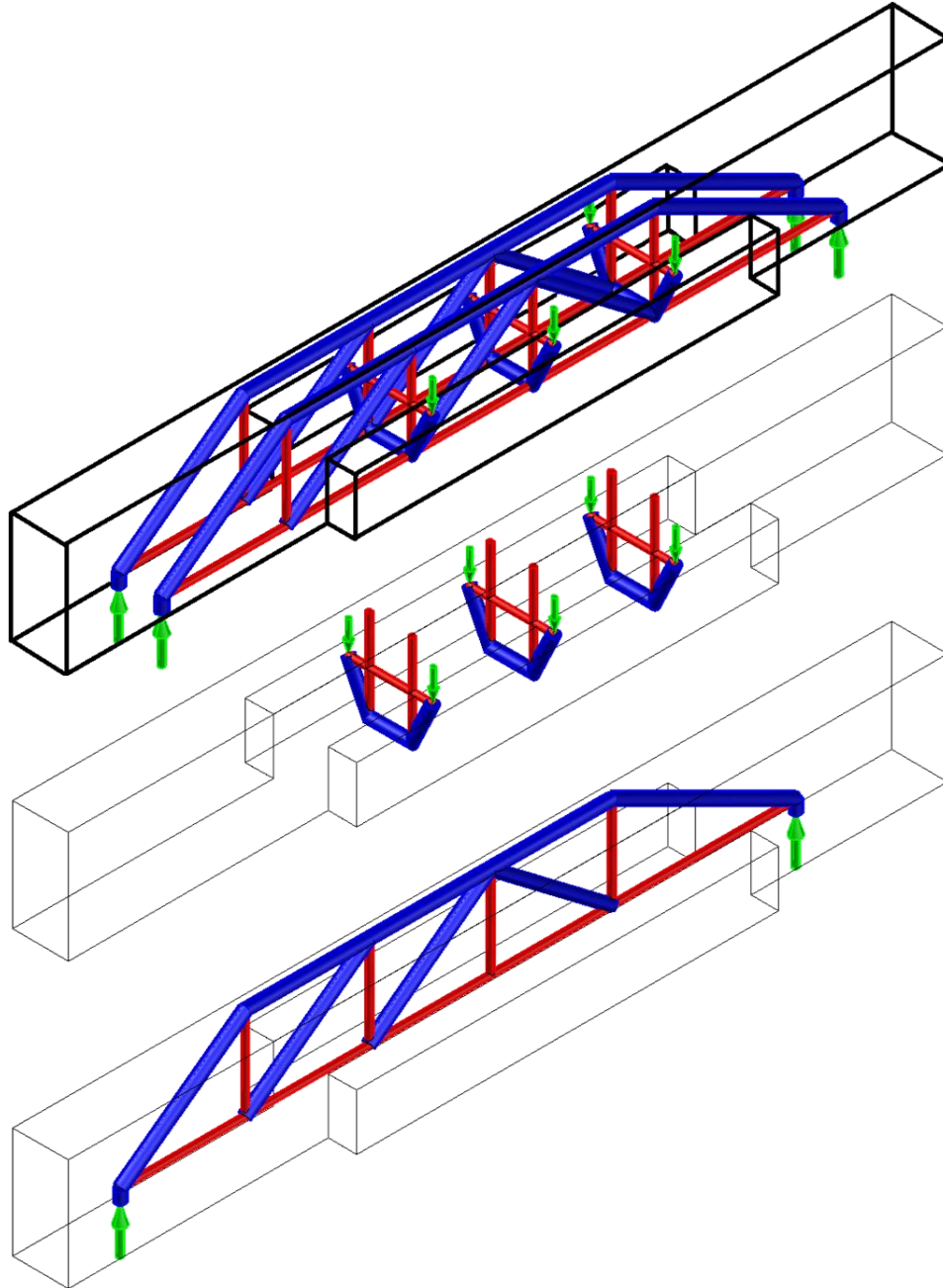
Figure 2-17: Strut-and-tie model of an inverted-T bent cap; top: tri-dimensional model, center: cross-sectional models, bottom: longitudinal model (from Fernandez 2102)

1 *Define loads and solve statics*

As the majority of an inverted-T beam is often adjacent to sections with point loads and geometric discontinuities, it is therefore appropriate to use the STM procedure to design the beam in its entirety. Once the cross-sectional area of inverted-T specimen is decided upon, the loads were defined and the reactions determined.

2 *Define geometry of the longitudinal strut-and-tie model*

In general, each tie must be aligned with the centroid of the reinforcing bars provided to carry the load. Vertical hanger reinforcement is placed at each load point with the location of the tie corresponding to the center of the bearing pad. A 45-degree spread under the loading plates is assumed to define width of hanger ties; as shown in Figure 2-18. For cut-off ledges, such as at the leftmost load point in Figure 2-18, load spread is limited by the length of the ledge.
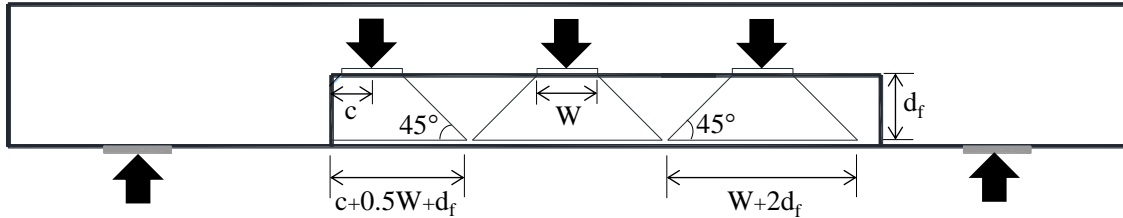
Figure 2-18: Hanger tie widths for beams with short and cut-off ledges

The horizontal strut along the top of the beam is assumed to be prismatic. The depth, a, of the compression stress block is defined from a typical flexural analysis as discussed in the proportioning of hanger CCT nodes in Section 2.6.2.1 (Figure 2-19).

The horizontal tie along the bottom of the beam is aligned with the centroid of the bottom flexural reinforcement. The width of that tie is assumed to be twice the distance from the extreme tension fiber to the centroid of the steel (Figure 2-19).
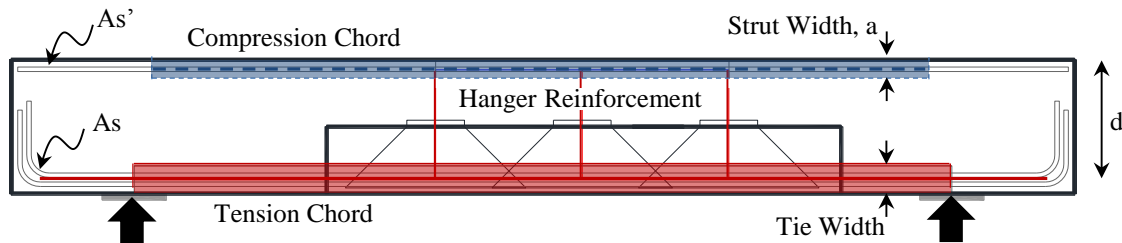
Figure 2-19: Widths of compression and tension chords

The location of the intermediate tie, Tie BC in Figure 2-20, for the two panel models in longer shear spans is determined using the technique proposed by Wight and Parra-Montesinos (2003). A line is projected at a 25 degree angle from the edge of the support

plate at Node A to the top of the beam to define the limit of the tie. Tie BC is then centered half way between the 45-degree projection from the loading plate at DE and the 25-degree projection from support plate at Node A (Figure 2-20).
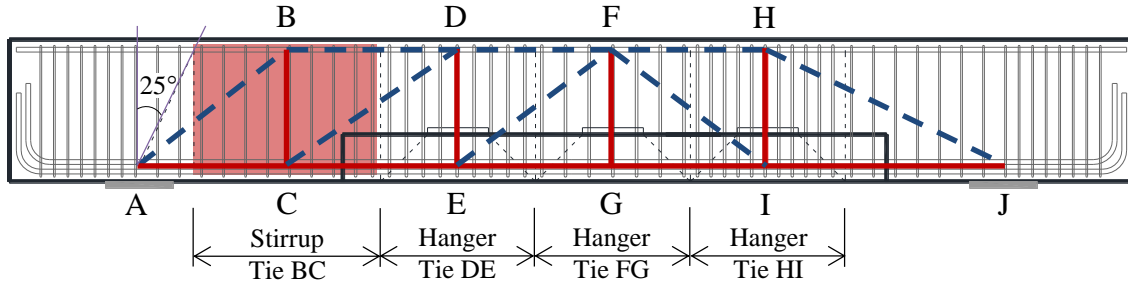
Figure 2-20: Development of strut and tie model

Diagonal bottle-shaped struts, idealized as dashed lines, are then connected to complete the flow of forces in the longitudinal strut-and-tie model. The angles between the strut and ties should be checked to ensure that they are greater than or equal to 25 degrees. Once the longitudinal model is completed, the forces in each element can be calculated using statics.

3 *Define geometry of the cross-sectional strut-and-tie model*

Along with the longitudinal model, a strut-and-tie model for the cross section at each load point is required to design the ledge of the inverted-T beam. The external loads are applied equally to both sides of the web as shown in Figure 2-21. For unequal spans, it is conservative to design for the longer span and the resulting greater load. The hanger ties discussed in the longitudinal STM are located at the center of the vertical reinforcement. The closed loop ledge reinforcement is positioned next to the hanger reinforcement, with the top of the loop corresponding to the horizontal ledge tie. The centroid of the horizontal compression strut is positioned at the depth of the flexural reinforcement from the longitudinal model. A diagonal strut transfers the applied load from the loading plate to the bottom of the hanger reinforcement, as shown in Figure 2-21.
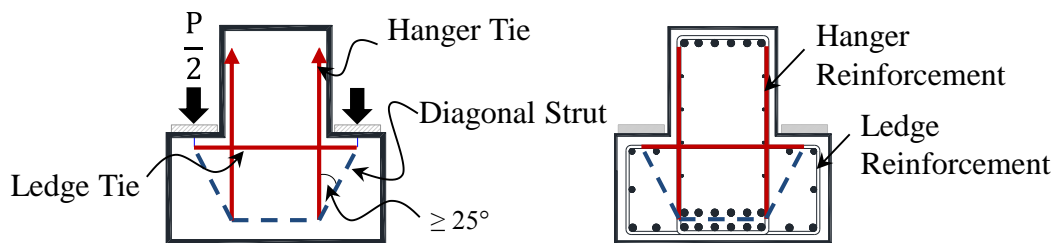
Figure 2-21: Forces in cross-sectional models

24

The angle between the diagonal strut and hanger tie must be checked to ensure it is greater than or equal to 25 degrees but less than 65 degrees. This limit is enforced to prevent an incompatability of strains. A smaller angle would result in the tension tie overlapping more of the diagonal strut, decreasing its effectiveness. If the angle is too small, a wider or shallower ledge is required.

4 *Perform nodal strength checks*

As the test specimens were designed using TxDOT Project 0-5253 STM provisions, the nodes were sized and detailed as specified in Section 2.6.2.1. For specimens tested at an a/d ratio of 1.85, the strut-to-node interface at either the support node or the node above the closest load point was found to govern the strength of the strut-and-tie model. Thus the capacity of the specimens tested at the shorter shear span-to-depth ratios were determined by the strength of the nodes.

5 *Determined required steel area for each tie*

Once the forces in the truss members were calculated and the nodes checked, the required steel area was determined to satisfy the tensile forces in the ties. The strength of each tie was taken as the total area of the reinforcement multiplied by the yield strength of the steel. After testing the coupon bars obtained with each order of rebar, the yield strength would be recalculated with the actual material properties. Proper anchorage of the ties was also ensured within the extended nodal regions.

The bars required for the hanger reinforcement were uniformly distributed within the load spread area shown in Figure 2-18. The ledge reinforcement was typically paired with the hanger bars. The effective load spread area was considered to be $W+5a_f$ or $2c$ as defined in AASHTO 5.13.2.5.3 and illustrated in Figure 2-22. If additional tie capacity was required, the size of the reinforcing bars was increased from No. 5 to No. 6 bars.
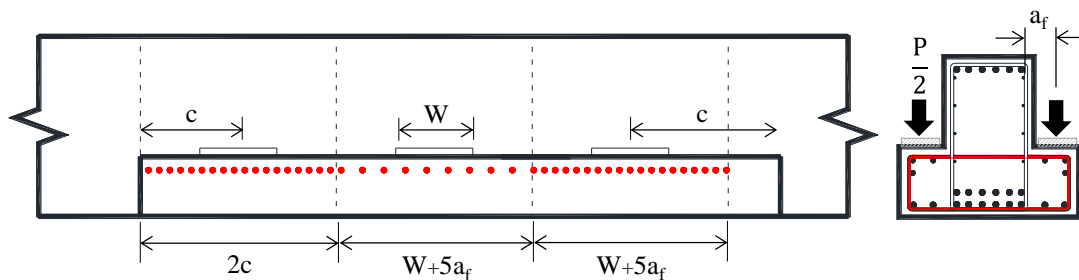
Figure 2-22: Load spread area for ledge reinforcement

The size and spacing of the stirrups in the intermediate tie was predetermined by the two reinforcement ratios investigated in the experimental program. A reinforcement ratio of 0.3% was achieved through spacing No. 4 bars at 6.5 in. on center and 0.6% was

achieved with No. 5 bars at 5 in. on center. Additional discussion on the reinforcement ratio is provided in Section 3.2.4.
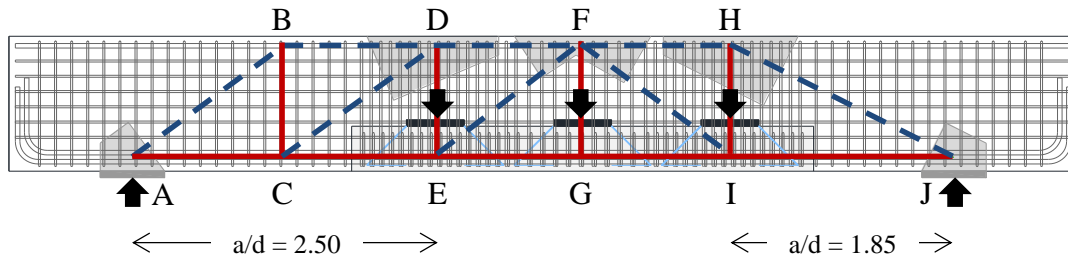
Figure 2-23: STM for inverted-T test specimen

A final strut-and-tie model for a beam loaded with three point loads is illustrated in Figure 2-23. Shear spans of 1.85d and 2.50d were examined in this specimen with shallow, short ledges. Resistance and load factors are required for STM design but were neglected for the purpose of this report as nominal strengths were computed and compared with experimental strengths. In general, no serviceability checks were made before testing the specimens. Rather, the cracking data obtained from loading the beams was used to validate current serviceability equations and/or make recommendations for application to inverted-T beams as discussed in Chapter 5.

For complete strut-and-tie design examples for inverted-T bent caps, refer to TxDOT Report 5-5253 (Williams et al., 2011). A sample specimen design is provided in Appendix A.

2.7 INVERTED-T DEEP BEAM DATABASE

In addition to the experimental and field investigation portions of the current research program, a database of deep inverted-T beam shear tests (a/d ≤ 2.50) was assembled. The purpose of this database is to provide a concise collection of specimens that, along with the results from the experimental program, can be used to verify the accuracy of proposed design provisions. The database and its filtration criteria are modeled after the deep beam database compiled as part of TxDOT Project 0-5253.

2.7.1 Literature Review

The first stage in constructing the database consisted of an exhaustive gathering of all the inverted-T specimens in the literature and collecting all the pertaining information regarding geometry, reinforcement, boundary conditions, strength, and serviceability. Many of the specimens reported in the literature were found to be unrepresentative of the bent caps in Texas due to size alone. The initial survey was expanded and the primary outcomes of the full literature review are highlighted herein.

Initially, the literature review considered experimental studies on reinforced concrete corbels. While similarities were encountered with respect to the ledge failure mechanisms, the corbel specimens did not provide insights into the shear strength and serviceability of inverted-T members. Corbel test data were therefore not included in the database.

A total of 97 tension-chord loaded specimens reported within 13 unique sources were ultimately compiled in the literature review. Many of the tests were not applicable to the current study due to missing plate size information, irregular support conditions, irregular reinforcement details, impractical cross-section size, and loading conditions that were not comparable to the in-service bent caps under investigation. The unique aspects and shortcomings of each reference are noted here. The scaled cross sections of the test specimens are illustrated in Figure 2-24.

- *Graf, O., Brenner, E., & Bay, H. (1943)*: One tension-chord-loaded specimen was tested in this study. The specimen had a tapered web at the support locations, with rectangular section in between measuring 118.1 x 3.9 in. (depth x width). Plate sizes were not reported. The specimen was loaded at five points to simulate a uniformly distributed load.

- *Ferguson, P. M. (1956)*: One tension-chord-loaded specimen was tested in this study. The specimen was indirectly supported on one end of the beam and loaded with two concentrated loads. The specimen had a web measuring 12 x 4 in. (depth x width). Plate sizes were not reported.

- *Schütt, H. (1956)*: Six tension-chord-loaded specimens were tested in this study. The specimens had a tapered web at the support locations and a rectangular section in between measuring 39.4 x 2.8 in. or 21.7 x 2.8 in. (depth x width). Plate sizes were not reported.

- *Taylor, R. (1960)*: Five tension-chord-loaded specimens were tested in this study. The specimens had no shear reinforcement. Specimens were indirectly supported on both ends of the beam and loaded at two points. Specimens measured 12 x 6 in. (depth x width). Plate sizes were not reported.

- *Leonhardt, F., & Walther, R. (1966)*: Four tension-chord-loaded specimens were reported in this study. Specimens measured 63 x 3.9 in. (depth x width). Specimens had six point loads simulating a uniformly distributed load.

- *Furlong, Ferguson, & Ma, (1971)*: Twenty-four inverted-T specimens were tested in this study. Specimens measured 62 x 24 in., 59 x 24in., and 21 x 8in. (depth x width). The larger specimens exceeded the test setup capacity and could not reach failure; except for one specimen that observed local failure of the ledge. The smaller specimens (21 x 8 in.) were subjected to failures in shear, flexure, punching shear, and shear friction. Some specimens were loaded on both chords simultaneously or in cantilever portions of the beam to generate negative bending.

Open stirrups were used in some of the specimens. Support plate sizes were not reported.

- *Furlong, R. W., & Mirza, S. A. (1974)*: Twenty seven inverted-T specimens were tested in this study. Specimens measured 21 x 8 in. (depth x width). Most of the specimens were post-tensioned and were loaded in positive and negative flexure with torsional couples. Support plate sizes were not reported.

- *Smith, K. N., & Fereig, S. M. (1974)*: Four tension-chord-loaded specimens were reported in this study. Specimens measured 24 x 3 in. and 12 x 3 in. (depth x width). Specimens were indirectly supported on both ends of the beam. Plate sizes were not reported. Some specimens had no shear reinforcement.

- *Fereig, S. M., & Smith, K. N. (1977)*: Two tension-chord-loaded specimens were tested in this study. Specimens measured 12 x 6 in. (depth x width). Specimens were indirectly supported on both ends of the beam. Plate sizes were not reported. One specimen did not have shear reinforcement.

- *Cussens, A. R., & Besser, I. I. (1985)*: Five tension-chord-loaded specimens were reported in this study. Specimens measured 39.4 x 2.8in. (depth x width). Specimens had six point loads simulating a uniformly distributed load. Cracking loads are available in the report.

- *Tan, K. H., Kong, F. K., & Weng, L. W. (1997)*: Six tension-chord-loaded specimens were reported in this study. Specimens measured 19.7 x 4.3in. (depth x width). Specimens had two point loads. Cracking loads are available in the report.

- *Zhu, R. R.-H., Dhonde, H., & Hsu, T. T. (2003)*: Four inverted-T specimens were tested in this study. Specimens measured 26 x 21 in. (depth x width). Specimens had negative and positive bending generated by four point loads, two on the main span, and one on each cantilever end of the beam. Diagonal reinforcement was used at the re-entrant corners in the cross-section to control the crack forming between the ledge and the web. Failure modes were not reported.

- *Galal, K., & Sekar, M. (2007)*: Four tension-chord-loaded specimens were constructed in this study. Specimens measured 24 x 7.1in. (depth x width). Specimens were loaded to failure, then repaired using CRFP and re-tested. Specimens had two point loads. Cracking loads are available in the report.

A scaled comparison of the cross-sections of the specimens from the literature, the inverted-T beams tested in the current project, and distressed in-service bent caps within the State of Texas is presented in Figure 2-24. A notable difference in size between the in-service bent caps (hatched blue) and the specimens found in the literature (shaded black) can be observed.
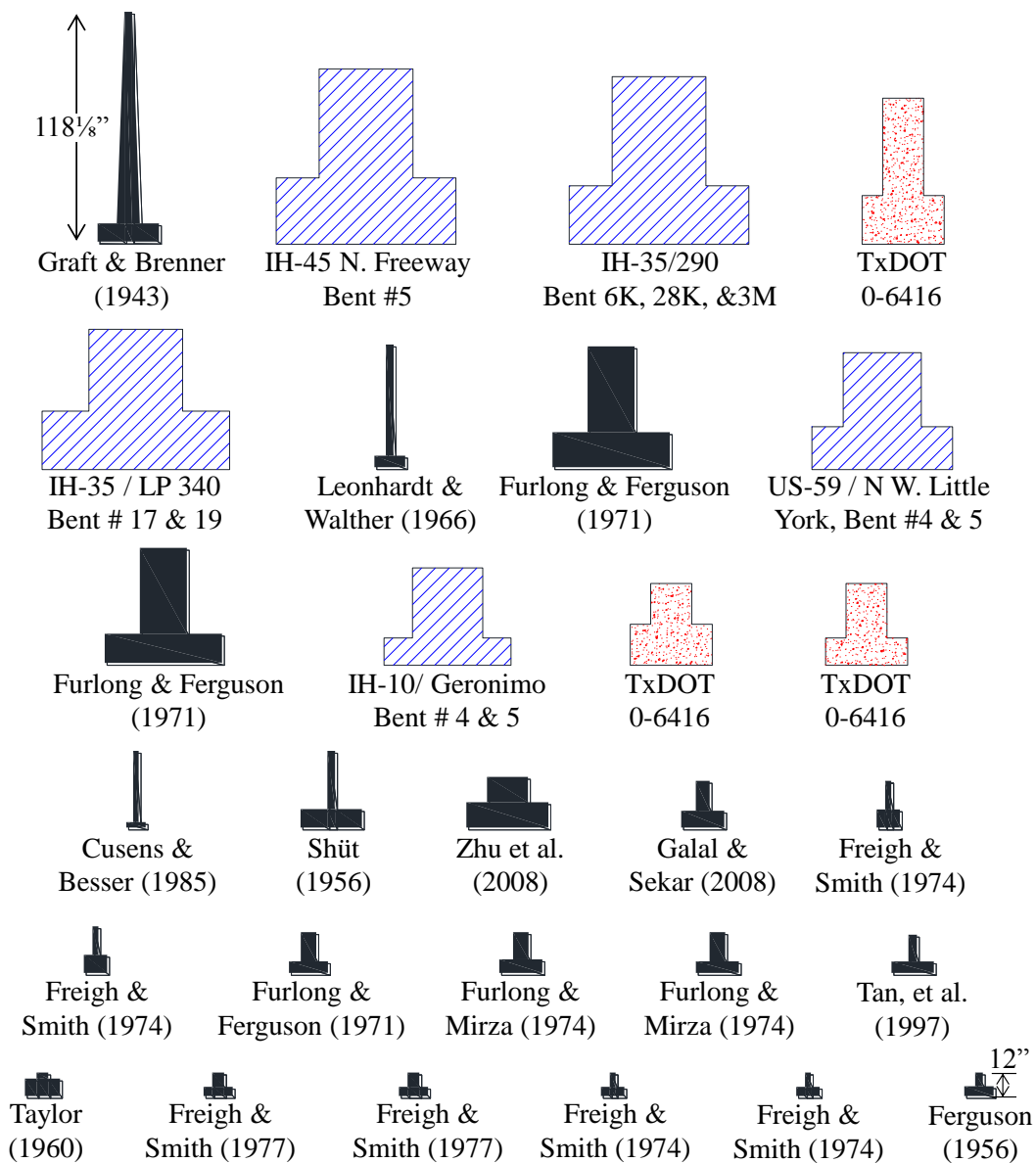
Figure 2-24: Scaled cross-sections of literature review specimens and in-service bent caps.

The sources identified in Figure 2-24 form a comprehensive image of the currently available literature on inverted-T members. Due to the lack of relevant, complete test date, the literature review reinforced the need for an extensive experimental program to evaluate the strength and serviceability effects of tension chord loading. The collection database was compiled based on the research papers described above and supplemented with results from the current experimental program. A total of 130 specimens from 14 different sources compose the collection database; including thirty three tests conducted within Project 0-6416.

2.7.2 Filtered Database

As complete test results were required in the inverted-T database, many of the specimens collected from the literature could not be used. This stage of the database construction consisted in removing forty one specimens for the following reasons.

In ten of the tests, the specimens were not loaded to failure. Ultimate capacity information is essential to evaluate the performance of the specimens and calibrate the new design provisions for inverted-T beams and is thus required for the database. Filtering based on the actual mode of failure was not performed as it is the intent of the project to perform a comprehensive assessment of all design provisions for inverted-T beams (not just those applicable to web shear). As such some beams in the filtered database were subjected to ledge or flexural failures.

The reports of ten additional specimens were lacking plate size information essential for the construction of strut-and-tie models to evaluate the performance of the specimens.

Two specimens had no shear reinforcement; an unrealistic condition, as in-service beams generally have a minimum amount of transverse reinforcement.

Nineteen specimens were found to have complicated support conditions, geometry, or reinforcement details- conditions were unrealistic when compared to in-service beams.

In summary, the filtered database was reduced to results from 89 specimens that have adequate details necessary to perform reliable strut-and-tie analyses.

2.7.3 Evaluation Database

The majority of the specimens found in the literature were unrepresentative of the bent caps in service in Texas, and thus another set of filters were required. Most of the inverted-T specimens presented in Figure 2-24 have shear areas of less than 200 in.^{2}. Texas bent caps typically have shear areas of 1,200 in.^{2} or greater. Also, a significant number of specimens in the literature review have an aspect ratio greater than 4; some have a depth over 12 times greater than their width. Such a high aspect ratio is unrealistic for inverted-T bent caps. Conventional beams have an aspect ratio of approximately one to three.

In order to construct a useful inverted-T database for the purposes of this project, further refinement was required to remove specimens that were unrepresentative of the distressed field members. In this stage 56 tests were filtered due to the following reasons.

Eleven specimens with a web depth-to-web width aspect ratio greater than four were removed due to the fact that specimens under this condition resemble walls. Their

behavior is different from that of bent caps with typical aspect ratios on the order of one to three.

Nine specimens with web widths smaller than 4.5 in. were filtered out of the database. The minimum limit was selected as the required width to accommodate two number five longitudinal bars with 1 in. of clear space between them, with a No. 3 stirrup and a clear cover of ¾ in.

Nine additional specimens were tested with a combined tension- and compression-chord loading. This condition is unrepresentative of the field specimens that are not subjected to significant loads on both chords and thus the specimens were removed.

Twenty seven specimens were subjected to torsional loads. These specimens were filtered out as the distressed field members showed no signs of torsional problems, only web shear deficiencies (in all cases the observed cracking pattern is consistent with web shear distress).

In summary, a total of one hundred thirty specimens from fourteen different sources were included in the collection database (Figure 2-25). The database filtering record is provided in Table 2-3. Thirty three specimens remained in the evaluation database, all of them conducted within the TxDOT Project 0-6416. This fact highlighted the importance of the current experimental program and reinforced the need for a large number of test specimens to fully evaluate the strength and serviceability behavior of inverted-T bent caps.
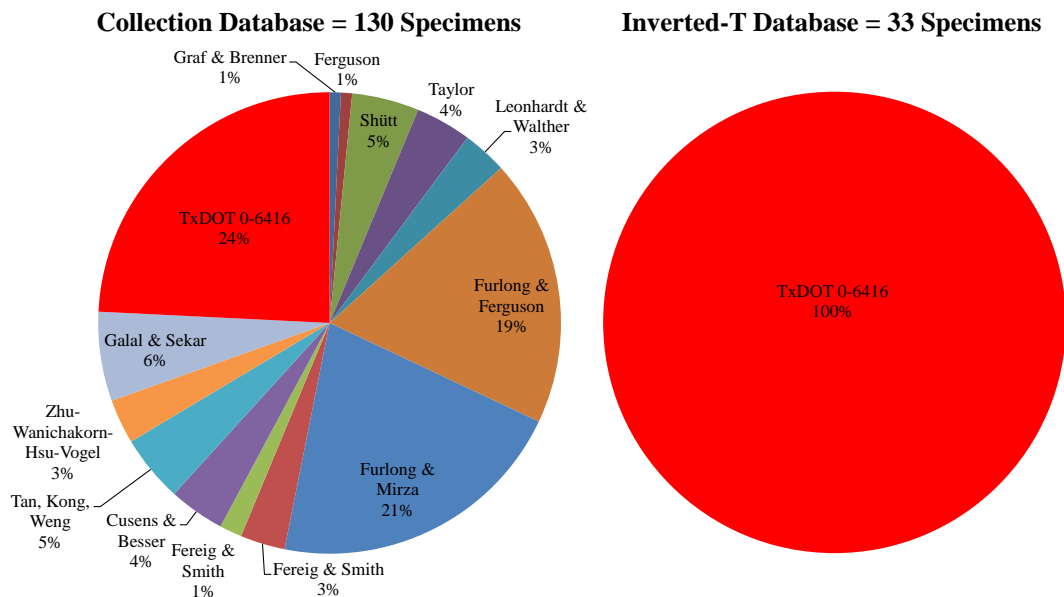
Figure 2-25: Sources of the inverted-T database.

Table 2-3: Inverted-T database assembly.

Collection Database			130 tests
Stage 1 Filtering	specimen did not fail	-	*10 tests*
	incomplete plate size information	-	*10 tests*
	no shear reinforcement	-	*2 tests*
	complicated supports/geometry/reinforcement	-	*19 tests*
Filtered Database			**89 tests**
Stage 2 Filtering	h / bw > 4	-	*11 tests*
	bw < 4.5in.	-	*9 tests*
	tension- and compression-chord loaded	-	*9 tests*
	torsional loads	-	*27 tests*
Inverted-T Database			**33 tests**

2.8 SUMMARY

Four topics were reviewed in this chapter. First, an overview of distressed inverted-T bent caps in service in Texas were presented including diagonal crack width information. Next, background information on strut-and-tie modeling design and behavior of inverted-T beams was presented. Then, design provisions for inverted-T beams from the AASHTO LRFD code, TxDOT bridge design manual, and TxDOT project 5253 were summarized. Finally, assembly of the inverted-T deep beam database was presented.

CHAPTER 3
Experimental Program

3.1 OVERVIEW

In this chapter, details of the design, fabrication, and load testing of the specimens in the experimental program are provided. Thirty three tests were conducted on beams with various web reinforcement details, ledge geometries, section sizes, number of point loads, and a/d ratios.

3.2 TESTING PROGRAM

To accomplish the objectives of the current project, it was necessary to develop an extensive testing program. Data in the literature was generally insufficient to address the tasks of the project due to the scarcity of research related to tension-chord loaded specimens. One of the major objectives of this project was to examine the serviceability performance of inverted-T deep beams and very little relevant information, including diagonal crack width data, was available in the literature. Furthermore, the cross-sectional dimensions of inverted-T beams tested in the past, especially those that led to the development of shear provisions in the TxDOT bridge design manual, are drastically smaller than those of in-service members. In order to properly address both the strength and serviceability objectives of this study it was deemed necessary to fabricate full-scale specimens within the experimental program.

The experimental program comprised several large-scale tests that encompassed the variables found in the in-service bridge bents exhibiting problems in the field. The objective of the tests was to investigate the influence of the following variables on the strength and serviceability of inverted-T bent caps:

1. The length of the ledge beyond the bearing of the exterior stringer
2. The depth of the ledge with respect to the total member depth
3. The amount of web reinforcement (transverse and longitudinal)
4. The number of point loads (stringers) on the ledge
5. The overall depth of the member
6. Chord loading (tension or compression)

3.2.1 Overview of Test Specimens

An overview of the thirty three specimens is presented in this section. Load testing was conducted as described in Section 3.6. The test specimens were designed such that they fail by web shear. Final designs for all test specimens was achieved through use of the strut-and-tie modeling provisions of TxDOT Project 5253 as implemented for inverted-T

members in Section 2.6.3. Six possible failure modes can be expected for inverted-T beams (Furlong, et al. (1974)):

1. Flexure.
2. Torsion.
3. Web Shear (This failure mode is the focus of the current project).
4. Yielding of hanger reinforcement.
5. Punching shear in ledge.
6. Shear friction in ledge.

Strut-and-tie models inherently consider all failure modes identified above. The specimens were tested at a shear span-to-depth (a/d) ratio of 1.85 or 2.50. Specimens with an a/d ratio of 1.85 capture the deep beam behavior of transferring shear from the load point to the support through a direct compression strut. Specimens with an a/d ratio of 2.50 transfer shear forces through a double strut (or double panel) system and are considered to be at the limit of sectional shear behavior (Birrcher et al., 2009). The two a/d ratios were also selected to be directly comparable with the compression-chord loaded specimens of TxDOT Project 0-5253.

In order to ensure web shear failures, the models were adjusted such that specimen capacities were controlled by the elements carrying the web shear; i.e. strut-to-node interfaces for beams with an a/d ratio of 1.85 and the intermediate web tie for beams with an a/d ratio of 2.50; as shown in Figure 3-1.
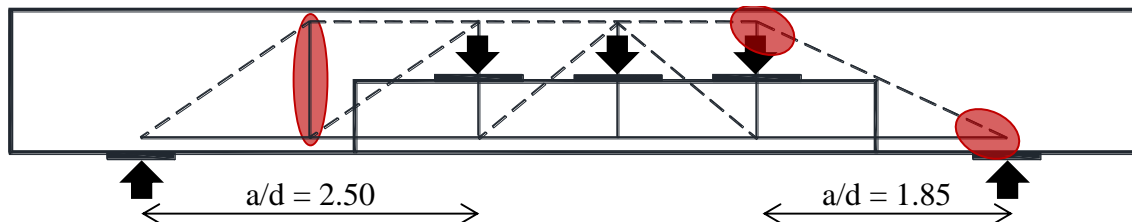
Figure 3-1: Simplified strut-and-tie model showing elements limiting shear capacity

The shear span-to-depth ratio is defined within the context of this report as the ratio of the distance from the center of the support to the center of the nearest loading point, *a*, with respect to the effective depth of the specimen *d*, measured from the centroid of the longitudinal tension steel to the extreme compressive fiber of the web (Figure 3-2). Such a definition of shear span is thought to be more appropriate for inverted-T beams than that provided by AASHTO LRFD (Art. 5.6.3.1) since inverted-T beams are essentially comprised of D-regions adjacent to large point loads (girders) and geometric discontinuities (ledges).
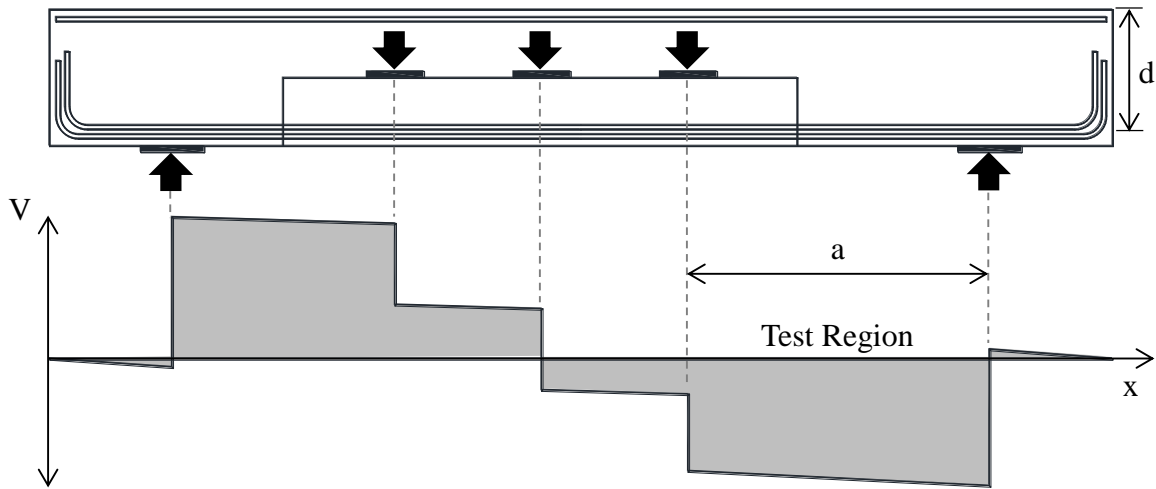
Figure 3-2: Free body and shear diagram for a specimen subjected to three point loads

In order to distinguish the specimens from one another and provide a quick insight into their defining characteristics, the nomenclature presented in Figure 3-3 was developed. Each numeral is a variable within the testing program.

Web reinforcement ratio (0.3%, 0.6%)

Shear span-to-depth ratio

DS1-42-1.85-03

Web Height (in)

No. of Point Loads

Ledge Length (C = Cut-off, S = Short, L = Long)

Ledge Depth (D = Deep, S = Shallow)
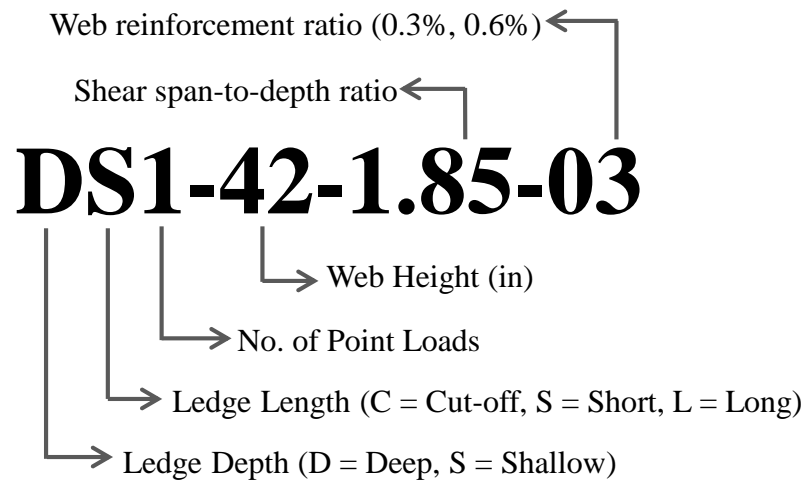
Figure 3-3: Specimen nomenclature.

The testing program was divided into five series based on the parameters under investigation. A summary of the variables used in each series is provided in Table 3-1. A brief description of each testing series and the details of the variables under investigation are provided in Sections 3.2.2 to 3.2.6.

Table 3-1: Variables in Testing Program.

Series I Ledge Length	Series II Ledge Depth	Series III Web Reinforcement		Series IV Number of Point Loads	Series V Web Depth
Cut-off	Shallow (h/3)	$\rho_v = 0.3\%$	$\rho_h = 0.3\%$	1	42 in.
Short	Deep (h/2)	$\rho_v = 0.6\%$	$\rho_h = 0.6\%$	3	75 in.
Long		$\rho_v = 0.6\%$	$\rho_h = 0.3\%$		

The width of the beams was proportioned in order to maximize the cross-sectional area of the specimen, while keeping it narrow enough to ease installation and removal from the test setup. A constant web width of 21 in. was used for each beam in the experimental program. The width of the ledge was also the same, 10.5 in. on each side, for each of the beams. All other dimensions varied between the beams. Typical specimen geometries and reinforcing details are shown in Figure 3-4 and Figure 3-5.

Longitudinal Elevation

42-in. Deep Ledge
Cross-Section
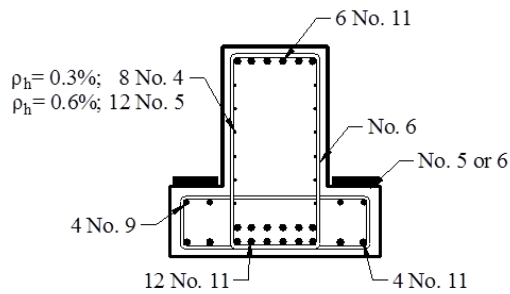
42-in. Shallow Ledge
Cross-Section
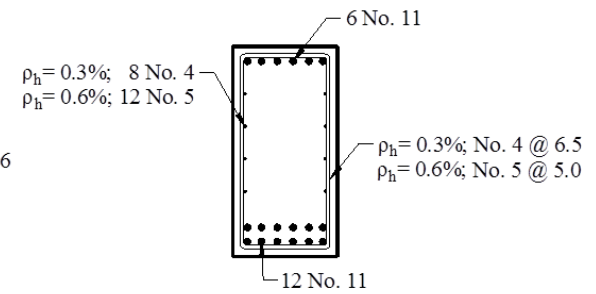
42-in. Rectangular
Cross-Section

75-in. Shallow Ledge
Cross-Section

Note: Clear Cover = 1.5" (ledge), 2" (web)

Figure 3-4: Typical specimen geometries

37

Figure 3-5: Typical reinforcement details.

38

3.2.2 Series I: Ledge Length

The purpose of the Series I specimens was to evaluate the influence of the ledge length on the strength and serviceability of inverted-T beams. The results from twenty tests were organized into eight groups of two or three directly comparable specimens, in which every parameter was kept constant except the length of the ledge.

The varying ledge lengths of inverted-T bent caps have been simplified to three types as shown in Figure 3-6. A "cut-off" ledge is one in which the ledge was interrupted just past the edge of the bearing pad of the outermost stringer. If the ledge runs continuously from support to support it was considered a "long" ledge. In a bent cap with a "short" ledge, the ledge is allowed to continue a distance equal to the depth of the ledge past the outermost stringer. Additional details of the Series I specimens are provided in Section 3.2.8 in Table 3-2. Inspected bent caps in the field contained a variety of ledge length ranging from cut-off to long.
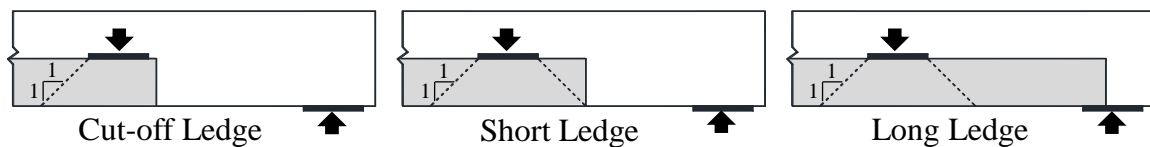
Figure 3-6: Ledge lengths

As discussed in Section 2.3, inverted-T bent caps are tension chord loaded structures in which the loads from bridge stringers have to be "hung" up to the compression chord before being transferred to the support. This induces a tension field in the web, the size of which is determined by the ledge length as shown in Figure 3-7. In the case of short and long ledges, the tension field can spread to engage as many "hanger" bars as possible. The width of this field is estimated to be equal to the width of the bearing pad plus twice the ledge height. In the case of cut-off ledges, the force can only spread on one side of the bearing plate thus concentrating the load in a smaller area and increasing the tensile stresses in the beam.
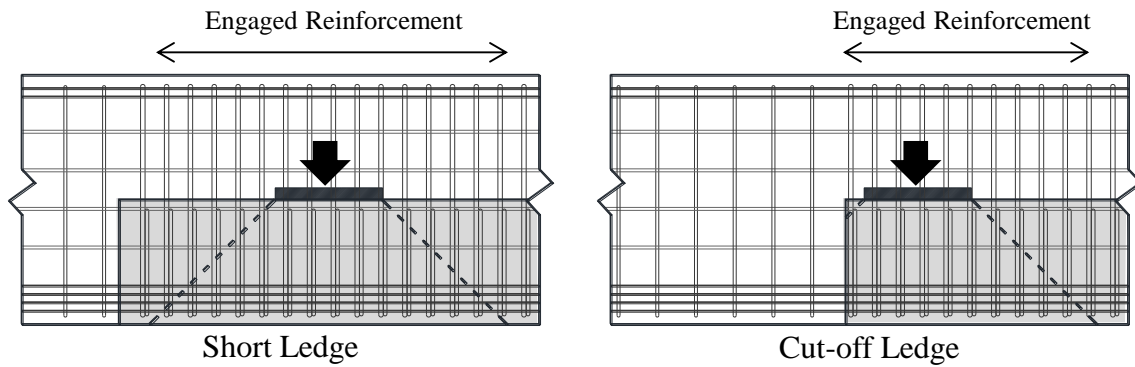
Figure 3-7: Load spread in specimens with short and cut-off ledges

Furthermore, by extending a ledge the entire length of a beam, the capacity of the support node may increase. The additional cross-sectional area provided by the ledge can provide confinement in the nodal region and increase the bearing width at the support as compared to beams with short and cut-off ledges as illustrated in Figure 3-8.
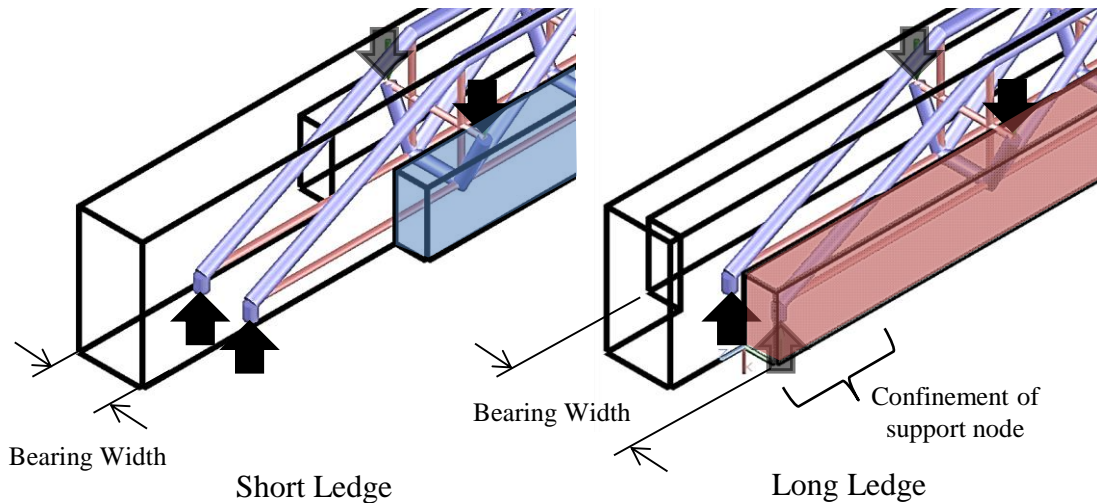
Figure 3-8: Ledge length effect on support region.

3.2.3 Series II: Ledge Depth

The specimens in Series II were evaluated to investigate the effect of the depth of the ledge on the strength and serviceability performance of inverted-T deep beams. Twenty tests were organized into ten pairs of directly comparable specimens, in which every parameter was kept constant except the ledge depth. This allowed for a thorough examination of the results, which are provided in Section 4.4.

In order to better capture the effect of ledge geometry, the specimens in this series were designed with two ledge depths. Shallow ledge specimens had depth equal to one-third and deep ledge specimens were one-half the total height of the beam (Figure 3-9). Ledges

shallower than one third of member depth could not be used due to concerns of local ledge failures. Additional details of the Series II specimens are provided in Section 3.2.8 in Table 3-2.
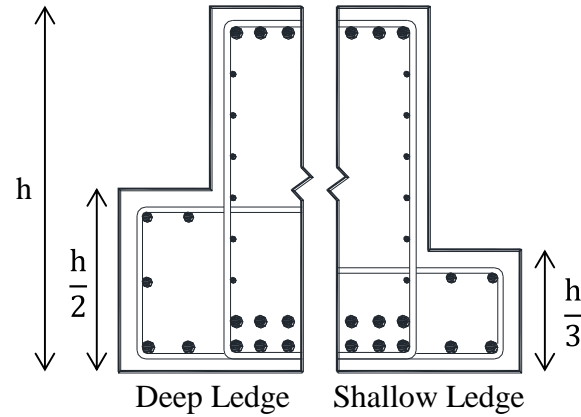
Figure 3-9: Ledge depths

The specimen ledge depths were chosen to give and adequate range of the configurations used in practice. The distressed in-service bent caps had ledge depths, h_{le}, between 0.28 and 0.42 times the total height of the beam, h. A comparison between the ledge depth to beam depth ratio of the in-service beams and those included in the Series III investigation is shown in Figure 3-10.
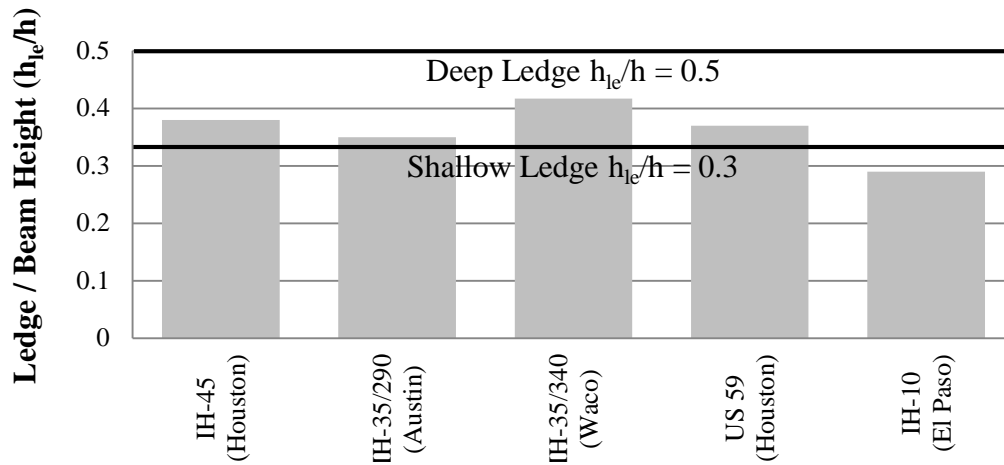
Figure 3-10: Ledge depth to beam height ratios of cracked in-service bent caps

As mentioned in Section 3.2.2, loading on the ledge of an inverted-T induces a tension field in the web, as the forces have to be "hung" up to the compression chord. As seen with the ledge length, the ledge depth also has a direct effect on the width over which this tension field spreads. Deeper ledges allow the forces to spread over a wider area,

consequently decreasing the tensile stress in the web whereas a shallow ledge would theoretically lead to a more concentrated stress (Figure 3-11).
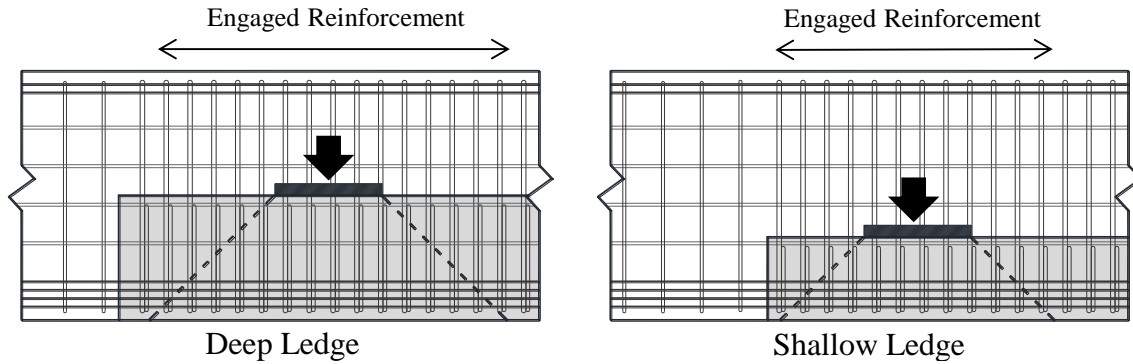
Figure 3-11: Load spread in specimens with deep and shallow ledges

3.2.4 Series III: Web Reinforcement Ratio

The effects of web reinforcement on the strength and serviceability of inverted-T deep beams was evaluated in Series III. Two amounts of web reinforcement were investigated with areas of steel equal to 0.3% and 0.6% of the effective web area as illustrated in Figure 3-12. Fourteen tests were organized into six groups of two or three directly comparable specimens, in which every parameter was kept constant except the web reinforcement ratio.
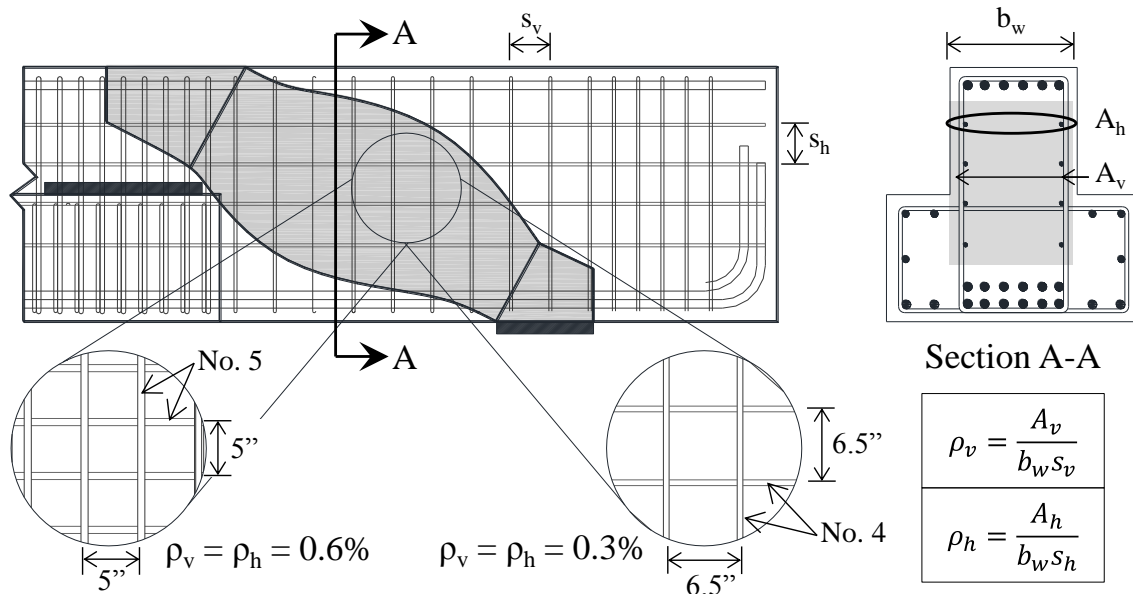
Figure 3-12: Web reinforcement ratios

An orthogonal grid of reinforcement is required at each face such that the ratio of total reinforcement to the gross concrete area is equal to the desired reinforcement ratio. In

most tests, the amount of vertical and horizontal web reinforcement was kept equal. Two specimens had 0.3% in the horizontal direction (skin reinforcement) and 0.6% in the vertical direction (shear stirrups). The reinforcement ratio of 0.003 (0.3%) is achieved through spacing No. 4 bars at 6.5 in. on center at each face of the beam. Likewise a 0.006 (0.6%) ratio corresponds to No. 5 bars at 5 in. on center. Additional details of the Series III specimens are provided in Section 3.2.8 in Table 3-2.

The lower limit of 0.3% corresponds to the minimum required skin reinforcement according to the TxDOT Bridge Design Manual – LRFD (2011), the AASHTO LRFD Bridge Design Specification 2012, and the findings of TxDOT Project 0-5253. The upper limit of 0.006 (0.6%) was selected to encompass the maximum reinforcement ratio (0.57%) found in the in-service distressed bents. The size and spacing of the bars were chosen to provide crack control. According to Project 0-5253, adequate crack control was ensured for web bar spacing less than 12 in. or $d/4$.

3.2.5   Series IV: Number of Point Loads

The purpose of Series IV was to examine the effect of single and multiple loading points on the strength and serviceability of inverted-T beams. Twelve tests were conducted in six pairs of directly comparable specimens, in which every parameter was kept constant except the number of point loads. The specimens in this series were loaded with either one or three point loads, as shown in Figure 3-13. Specimens with a single load point were used for direct comparison with compression-chord loaded specimens from TxDOT Project 0-5253, all of which were tested with a single load point.

One Point Load
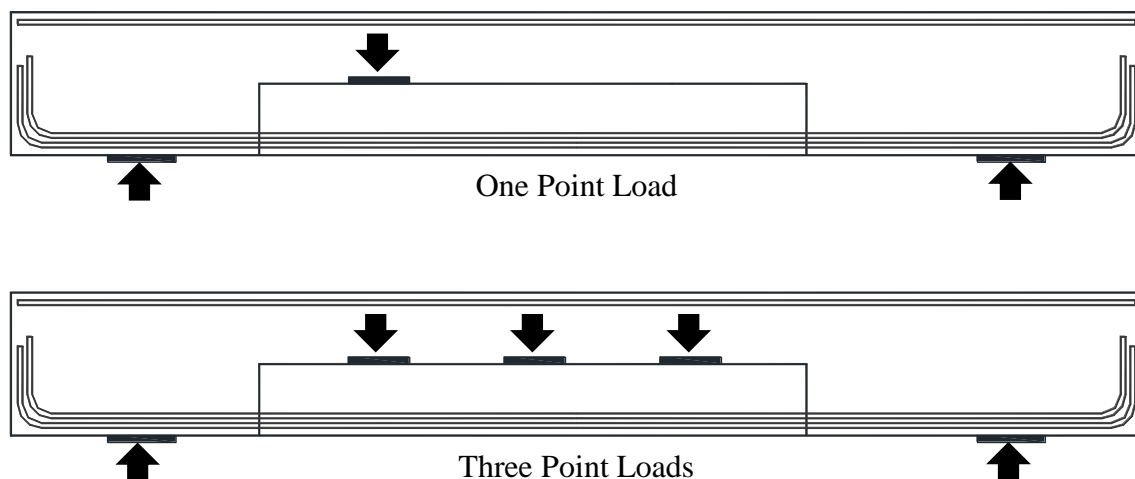
Three Point Loads

Figure 3-13: Inverted-T number of point loads

Specimens with three point loads allowed for shallower ledges by distributing the total force to multiple locations and helping prevent local failure of the ledge. They were also

used to help quantify the effect of multiple girders on bridge bent caps. The number of girders on each side of the bent caps inspected as part of this program ranged from two U-beams to six box beams.

Three point loads were also chosen because the resulting load spacing was representative of that of in-service girders. Laboratory testing constraints also factored in the decision. Additional details of the Series IV specimens are provided in Section 3.2.8 in Table 3-2 and the test results are discussed in Section 4.6.

3.2.6   Series V: Web Depth

Series V was developed to compare the effect of web depth on the strength and serviceability of the inverted-T beams. A review of the literature revealed a significant difference in the size of the in-service bent caps when compared to the specimens used to calibrate the shear provisions in the current design code (TxDOT Bridge Design Manual – 2011). Full-scale specimens with web depths of 42 and 75 in were constructed and tested for the experimental program. This series contains two groups of two directly comparable specimens, in which every parameter was kept constant except the web depth.

As with the 42 in. specimens, the web width for the larger beams was limited to 21 in.. By keeping the same web width, the effect of the depth of the beam could be directly investigated. Each 75-in. beam was constructed with a short, shallow ledge. Providing enough ledge and hanger reinforcement was not feasible in a cut-off ledge and crane weight restrictions prevented the construction of a long ledge.
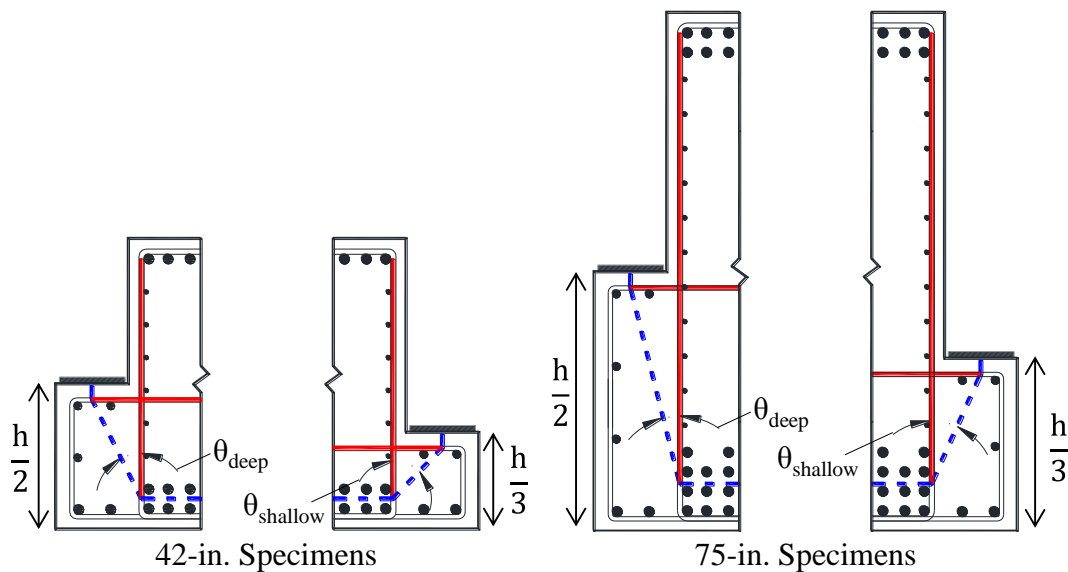
Figure 3-14: Inclination angle of ledge strut in cross-sectional STM

The design of deep ledges in the 75-in. specimens were restricted due to geometric and strut-and-tie intersection limitations. The ledge depth defines the inclination of the ledge strut in the cross-sectional STM as shown in Figure 3-14. The angle of the strut impacts the strength of the ledge and may lead to the incompatibility of strains in the associated nodes when the strut intersects a tie at an angle less than 25 degrees as discussed in Section 2.6.2.2. This incompatibility was seen when 75-in. deep specimen was designed with a deep ledge and thus only shallow ledges were constructed and tested. Additional details of the Series V specimens are provided in Section 3.2.8 in Table 3-2 and the test results are discussed in Section 4.7.

3.2.7 Series VI: Loaded Chord

A final series was added to evaluate the effects of tension chord loading on the strength and serviceability of reinforced concrete deep beams. As discussed in Section 2.4, ledge loading introduces additional tensile forces into inverted-T beams that are not present in rectangular bent caps. It is likely that varying the location at which the load is applied on the cross-section (Figure 3-15) could result in significant changes in the behavior of the beam.

Compression Chord Loading   Tension Chord Loading
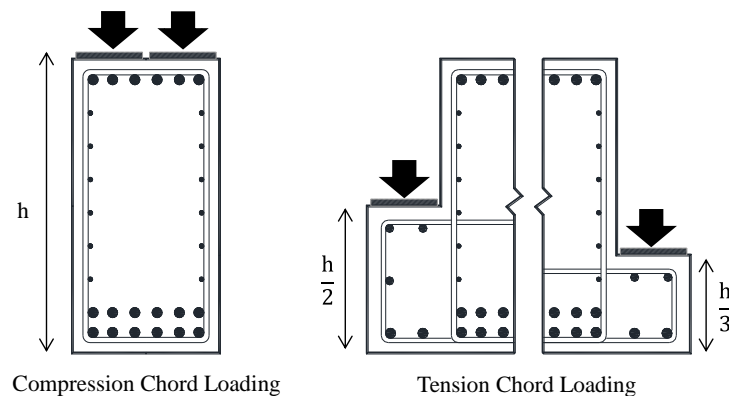
Figure 3-15: Cross-section loading

Twenty two tests were examined in four groups of directly comparable specimens, in which every parameter was kept constant except the loaded chord. Results from fourteen inverted-T and one compression-chord loaded specimens tested in this project are compared to six compression-chord loaded specimens from TxDOT Project 0-5253 in Section 4.8. A compression-chord loaded beam, C1-42-1.85-06, was designed and constructed as part of the current inverted-T experimental program to provide a direct comparison for reinforcement ratio of 0.6% in each orthogonal direction. Additional details of the loaded chord specimens are provided in Section 3.2.8 in Table 3-2 and the test results are discussed in Section 4.7.

3.2.8 Summary of Test Specimen Details

Thirty three inverted-T beam tests were conducted in the current experimental program. The inverted-T deep beams tested in this research project represent some of the largest deep beam shear test available in the literature. As shown in Figure 3-16, the specimens from the current study populate the upper bound of the inverted-T deep beam data in the literature as measured by the shear area of the beam (b_wd). As previously noted, the objectives of the current study necessitated the testing of specimens of comparable size to field members. A comparison between the investigated in-service bent caps, the beams in the current study, and beams from previous research projects is provided in Figure 3-16.
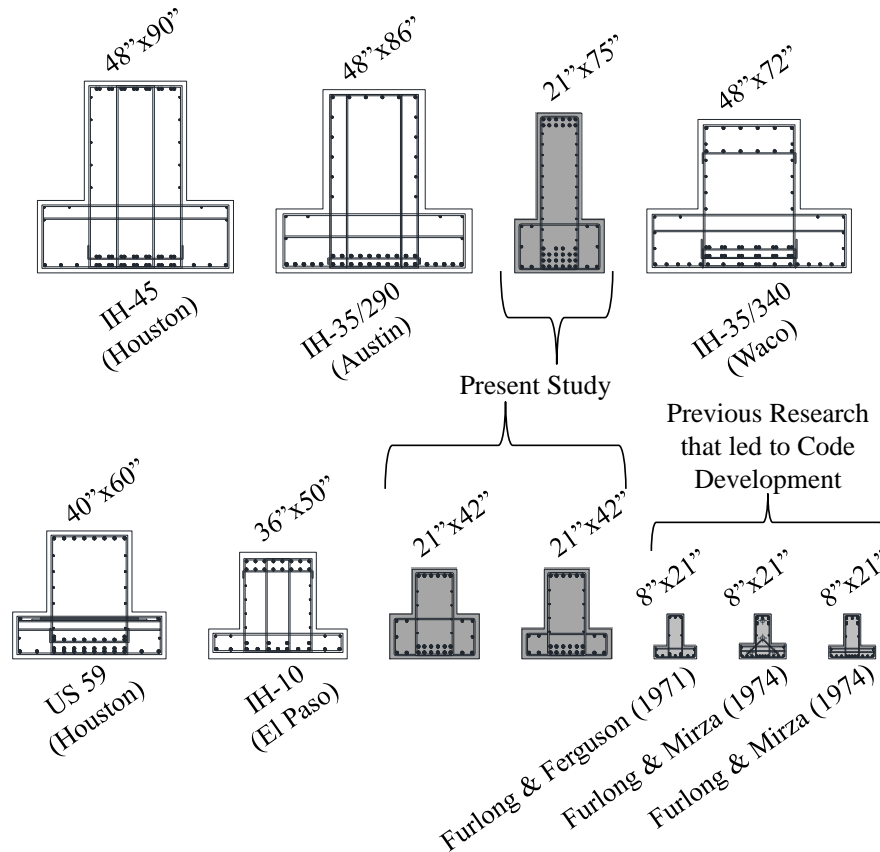
Figure 3-16: Scaled comparison of actual bent caps and IT beams included in current and past research programs.

A summary of the details for the thirty three inverted-T tests in the experimental program is presented in Table 3-2. Two specimens were specially designed with ledge lengths equal to the length of the bearing plate and are designated with *b* at the end of the specimen notation. Because of the large number of variables, each specimen was used in at least one series. The experimental results for the test specimens are provided and discussed in Chapter 4.

Table 3-2: Summary of beam details

Specimen	Ledge Depth	Ledge Length	Load Points	d (in)	a / d ratio	Support Plate	Load Plate	ρ_v	ρ_h
DS1-42-1.85-03	h/2	Short	1	37.6	1.96	16" x 20"	26" x 9"	0.3%	0.3%
DS1-42-2.50-03	h/2	Short	1	37.6	2.65	16" x 20"	26" x 9"	0.3%	0.3%
DS1-42-1.85-06	h/2	Short	1	37.6	1.85	16" x 20"	26" x 9"	0.6%	0.6%
DS1-42-2.50-06	h/2	Short	1	37.6	2.50	16" x 20"	26" x 9"	0.6%	0.6%
DL1-42-1.85-06	h/2	Long	1	37.6	1.85	16" x 20"	26" x 9"	0.6%	0.6%
DL1-42-2.50-06	h/2	Long	1	37.6	2.50	16" x 20"	26" x 9"	0.6%	0.6%
SS3-42-1.85-03	h/3	Short	3	37.6	1.85	16" x 20"	18" x 9"	0.3%	0.3%
SS3-42-2.50-03	h/3	Short	3	37.6	2.50	16" x 20"	18" x 9"	0.3%	0.3%
SS3-42-2.50-06	h/3	Short	3	37.6	2.50	16" x 20"	18" x 9"	0.6%	0.6%
SC3-42-2.50-03	h/3	Cut-off	3	37.6	2.50	16" x 20"	18" x 9"	0.3%	0.3%
SC3-42-1.85-03	h/3	Cut-off	3	37.6	1.85	16" x 20"	18" x 9"	0.3%	0.3%
DS3-42-2.50-03	h/2	Short	3	37.6	2.50	16" x 20"	18" x 9"	0.3%	0.3%
DL1-42-1.85-03	h/2	Long	1	37.6	1.85	16" x 20"	26" x 9"	0.3%	0.3%
DL1-42-2.50-03	h/2	Long	1	37.6	2.50	16" x 20"	26" x 9"	0.3%	0.3%
SL3-42-1.85-03	h/3	Long	3	37.6	1.85	16" x 20"	18" x 9"	0.3%	0.3%
SL3-42-1.85-06	h/3	Long	3	37.6	1.85	16" x 20"	18" x 9"	0.6%	0.6%
C1-42-1.85-06	-	-	1	37.6	1.85	16" x 20"	30" x 20"	0.6%	0.6%
DC1-42-1.85-06	h/2	Cut-off	1	37.6	1.85	30" x 21"	30" x 10"	0.6%	0.6%
SS1-75-1.85-03	h/3	Short	1	68.2	1.87	16" x 20"	30" x 10"	0.3%	0.3%
DC3-42-1.85-03	h/2	Cut-off	3	37.6	1.85	16" x 20"	18" x 9"	0.3%	0.3%
DS3-42-1.85-03	h/2	Short	3	37.6	1.85	16" x 20"	18" x 9"	0.3%	0.3%
SS1-42-2.50-03	h/3	Short	1	37.6	2.50	16" x 20"	26" x 9"	0.3%	0.3%
SS1-42-1.85-03	h/3	Short	1	37.6	1.85	16" x 20"	26" x 9"	0.3%	0.3%
DC1-42-2.50-03	h/2	Cut-off	1	37.6	2.50	16" x 20"	18" x 9"	0.3%	0.3%
DL3-42-1.85-03	h/2	Long	3	37.6	1.85	16" x 20"	18" x 9"	0.3%	0.3%
SL1-42-2.50-03	h/3	Long	1	37.6	2.50	16" x 20"	26" x 9"	0.3%	0.3%
SC1-42-2.50-03	h/3	Cut-off	1	37.6	2.50	16" x 20"	26" x 9"	0.3%	0.3%
DS1-42-1.85-06/03	h/2	Short	1	37.6	1.85	16" x 20"	26" x 9"	0.6%	0.3%
DS1-42-2.50-06/03	h/2	Short	1	37.6	2.50	16" x 20"	26" x 9"	0.6%	0.3%
SC1-42-1.85-03	h/3	Cut-off	1	37.6	1.85	30" x 20"	26" x 9"	0.3%	0.3%
DC1-42-1.85-03	h/2	Cut-off	1	37.6	1.85	30" x 20"	26" x 9"	0.3%	0.3%
SC1-42-1.85-03*	h/3	Cut-off	1	37.6	1.85	30" x 20"	30" x 10"	0.3%	0.3%
DC1-42-1.85-03*	h/2	Cut-off	1	37.6	1.85	30" x 20"	30" x 10"	0.3%	0.3%
SS1-75-2.50-03	h/3	Short	1	68.2	2.50	16" x 20"	30" x 10"	0.3%	0.3%

Plate dimensions: [in direction of span] x [transverse to direction of span]

* Ledge length set equal to bearing pad length

3.3 FABRICATION OF SPECIMENS

The specimens in the current project were constructed using conventional materials and methods. Steel formwork was used to expedite the fabrication process and to ensure dimensional accuracy. In general, the assembly of the reinforcement cage, installation of strain gauges, placement of concrete, and removal of formwork took about three weeks to complete per specimen. Beams were tested approximately 28 days after concrete placement. The following sections describe in detail the construction process and materials used.

Concrete Mixture Design

Typically, TxDOT engineers specify the compressive strength of concrete used in inverted-T bent caps to be between 3600 and 5000-psi. Proportions of the typical 5000-psi concrete mix are presented in Table 3-3. Actual compressive strengths measure the same day of testing varied from 3000 to 6400-psi as shown in Table 3-4. During the placement of concrete for each beam, standard 4 in. x 8 in. cylinders were prepared in accordance with ASTM C31 and tested in accordance with ASTM C39.

Table 3-3: Typical concrete mixture properties

Material	Quantity
Type I Portland Cement	388 lb/cy
Flys Ash	94 lb/cy
CA: 3/4" Limestone	1650 lb/cy
FA: Sand	1528 lb/cy
Water	24 gallons/cy
HRWR Admixture	24 oz/cy
Set Retardant Admixture	5 oz/cy
Water/Cement Ratio	0.52
Slump	6 ± 2 inches

*HRWR: High Range Water Reducing (i.e. *Superplasticizer*)

Reinforcement Properties

Domestic Grade 60 deformed bars satisfying the requirements of ASTM A 615 were used for all steel reinforcement (rebar). Cross sectional dimensions of the bars complied with the nominal sizes given in ASTM A615.

Each order delivered to the Ferguson Laboratory was accompanied by a set of four coupons for each bar size. The tensile strength of the coupons was measured in accordance with ASTM A370 and is provided in the material properties in Table 3-4.

Table 3-4: Specimen material strengths

Specimen	# 11 Bars f_y (ksi)	# 6 Bars f_y (ksi)	# 5 Bars f_y (ksi)	# 4 Bars f_y (ksi)	f'_c (psi)
DS1-42-1.85-03	69.24	63.38	64.69	63.14	5258
DS1-42-2.50-03	69.24	63.38	64.69	63.14	5389
DS1-42-1.85-06	64.13	63.38	60.68	N/A	5024
DS1-42-2.50-06	64.13	63.38	60.68	N/A	5088
DL1-42-1.85-06	67.90	63.38	64.69	N/A	4830
DL1-42-2.50-06	67.90	63.38	64.69	N/A	4986
SS3-42-1.85-03	68.60	64.68	62.75	67.25	5891
SS3-42-2.50-03	68.60	64.68	62.75	67.25	5891
SS3-42-2.50-06	69.50	61.83	60.90	N/A	6255
SC3-42-2.50-03	66.20	63.50	60.25	64.27	5873
SC3-42-1.85-03	66.20	63.50	60.25	64.27	5873
DS3-42-2.50-03	63.60	62.63	60.22	64.58	5687
DL1-42-1.85-03	71.01	61.90	64.29	64.43	4929
DL1-42-2.50-03	71.01	61.90	64.29	64.43	4929
SL3-42-1.85-03	75.18	60.62	63.58	65.57	5037
SL3-42-1.85-06	70.38	63.26	64.80	62.62	5250
C1-42-1.85-06	73.30	63.98	60.81	N/A	3727
DC1-42-1.85-06	73.30	63.98	60.81	N/A	3727
SS1-75-1.85-03	66.10	61.97	64.69	65.08	3127
DC3-42-1.85-03	63.63	66.00	63.09	63.16	4568
DS3-42-1.85-03	63.63	66.00	63.09	63.16	4568
SS1-42-2.50-03	65.44	69.57	77.76	66.58	5703
SS1-42-1.85-03	65.44	69.57	77.76	66.58	5721
DC1-42-2.50-03	70.06	64.13	69.77	62.44	4035
DL3-42-1.85-03	70.06	64.13	69.77	62.44	4202
SL1-42-2.50-03	68.70	71.41	N/A	64.47	4281
SC1-42-2.50-03	68.70	71.41	N/A	64.47	4281
DS1-42-1.85-06/03	65.80	70.92	64.94	65.18	4173
DS1-42-2.50-06/03	65.80	70.92	64.94	65.18	4173
SC1-42-1.85-03	66.36	64.04	N/A	67.28	4330
DC1-42-1.85-03	66.36	64.04	N/A	67.28	4303
SC1-42-1.85-03b	70.47	63.12	N/A	68.56	3013
DC1-42-1.85-03b	70.47	63.12	N/A	68.56	2996
SS1-75-2.50-03	65.22	63.85	63.62	63.76	5158

3.3.1 Construction of Specimens

The steel reinforcement was supplied by a local steel manufacturer and delivered in the specified lengths and with the appropriate bends. The reinforcement cages were assembled in the laboratory and, upon completion and instrumentation, were moved into the formwork in the casting area. The specimens were cast in the same orientation that they were tested. As they were loaded from beneath, the primary flexural reinforcement was located at the top of the section as shown in Figure 3-17.

The concrete used to fabricate the specimens was provided from a local ready-mix supplier. Upon the arrival of the concrete truck, a slump test was performed according to ASTM C143. If necessary, additional water was added to increase the slump to approximately 6 ± 2 in. The additional amount of water added did not exceed the amount of water that was held back at the batch plant as indicated on the ticket. 4-in. diameter cylinders were prepared in accordance with ASTM C31. They were covered and cured under the same ambient conditions as the beam.

Figure 3-17: Fabrication of specimens

Two trucks were ordered for each 75-in. deep beam and one truck was required for each 42-in. deep beam. For the larger pours, each truck was filled with the same mixture design from the same batch plant. The second truck was scheduled to arrive 30 minutes after the first truck to minimize idling and prevent the formation of a cold joint. The compressive strength from one truck generally differed from the other by less than 20 percent.

Concrete was placed via a one-cubic yard bucket lifted by an overhead crane. Proper consolidation was achieved through the use of external pneumatic vibrators that moved along the length of the formwork and internal rod vibrators, or stingers, that were placed in the concrete from the top as shown in Figure 3-17. After initial setting, the top surface of the beam was finished and the beam was covered with a plastic sheet and cured under the ambient laboratory conditions.

Seven days after casting, the specimens were uncovered and stripped of their forms. The cylinders were likewise uncovered and removed from their molds. The specimens were then moved into the test setup with an overhead crane and allowed to reach an age of at least 28 days before testing.

3.4 TEST SETUP

The specimens were tested at the Phil M. Ferguson Structural Engineering Laboratory at the University of Texas at Austin. The test setup was originally constructed for TxDOT Project 0-5253 and was designed for an upside-down simply-supported beam test. Minor modifications were required for use in the current project. The load was applied via a 5 million pound capacity, double-acting hydraulic ram for single point load tests, and three 2 million pound capacity rams for multiple point load specimens. U-shaped frames were introduced to spread loads around the web and apply load evenly to the ledges on both faces of the test specimens. The strong floor consisted of a 96,000-lb steel platen. At each support, six 3-in. diameter threaded rods reacted against a 7,000-lb transfer girder to resist the applied load. In the current configuration shown in Figure 3-18, the test set setup can resist a shear force of approximately 1.5 million pounds or an applied load at midspan of approximately 3 million pounds. For additional details of the test setup design and construction, refer to Huizinga (2007).
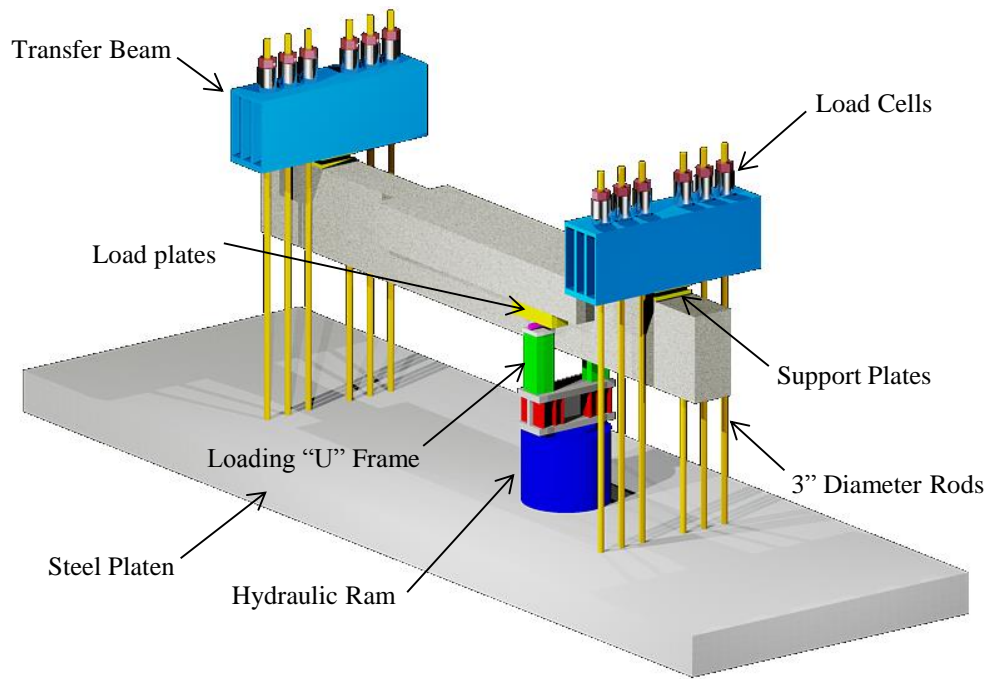
Figure 3-18: Test setup

At each support, pin connections were achieved by the use of a 2-in. diameter steel bar between two 2-in. steel plates. The steel bar was welded to the bottom plate which was placed on top of a thin layer of hydrostone that provided a planar bearing surface on top of the beam. Horizontal movement was permitted by the flexibility of the six threaded rods. Similarly, at the applied load, rotation was permitted by a 3-in. diameter roller which was allowed to roll freely between a 5-in. or 7-in. thick plate and the top of the U-frame. A smaller ½-in. thick steel plate was placed on top of the larger plate to achieve the desired size of the load plate. A ¼-in. neoprene bearing pad was placed between the concrete ledge and load plate to ensure a uniform load distribution.

3.5 INSTRUMENTATION

The instruments used during testing to obtain and record data included steel electrical strain gauges, linear potentiometers, load cells, and crack comparator cards. Further details regarding each of these are provided in the following sections.

3.5.1 Strain Measurements

Strain gauges were affixed to the steel reinforcement to measure the change in strain in areas of particular interest including flexural reinforcement, hanger and ledge bars, skin reinforcement, and shear stirrups. The gauge type was model *FLA-3-11-5LT*

manufactured by Tokyo Sokki Kenkyujo Co. The width and length of the gauges were 1.5 and 3 mm, respectively, with a resistance of 120-ohms (± 0.5).

Typical locations of strain gauges are illustrated in Figure 3-19. Strain gauges were attached to the stirrups and horizontal skin reinforcement along the assumed centerline of the inclined strut in all of the test specimens. Beams with a shear span-to-depth ratio of 1.85 were instrumented along the axis of the direct strut that spans from the support to the first loading point. Beams with the longer shear span-to-depth ratio of 2.50 were instrumented along the axis of the first strut in the multiple panel model as well as the line between the load and the support. The purpose of installing a gauge along the proposed strut centerline was to measure steel strains at or close to the primary diagonal splitting crack. Strain gauges were also affixed to the primary flexural reinforcement in several locations including the load point to monitor the maximum strain in the reinforcement as the beam was loaded to failure.

Two Panel Model (a/d = 2.5)   **Direct Strut (a/d = 1.85)**

Gauges on Stirrups   Gauges on Stirrups

Gauges on Longitudinal Bars   Gauges on Ledge and Hanger Bars
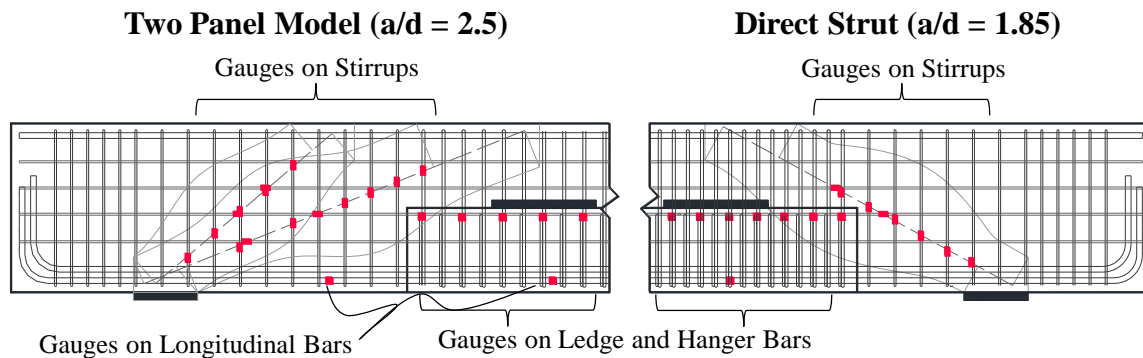
Figure 3-19: Typical location of strain gauges in longitudinal section

Strain gauges were used to monitor the hanger and ledge reinforcement in the regions of the load plates as shown in Figure 3-20. They served to verify the assumed 45 degree load-spread and the associated number of hanger bars that transferred the applied loads to the compression chord.

Assumed Load Spread

IT Cross Section
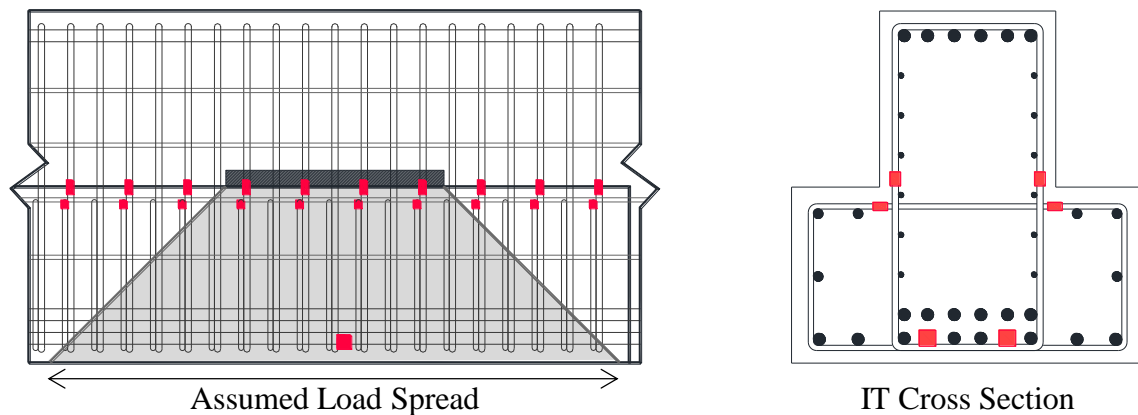
Figure 3-20: Strain gauges on the hanger and ledge reinforcement

The installation procedure of the gauges is shown in Figure 3-21. The deformations on the bars were removed with a grinder and polished to provide a smooth planar surface for the application of the gauges. Care was taken to not significantly reduce the cross-sectional area of the bar. The surface was cleaned and the strain gauges were glued to the reinforcement. A butyl rubber tape was applied to protect and water proof the gauges, which were then wrapped in foil tape to further isolate them from the concrete.
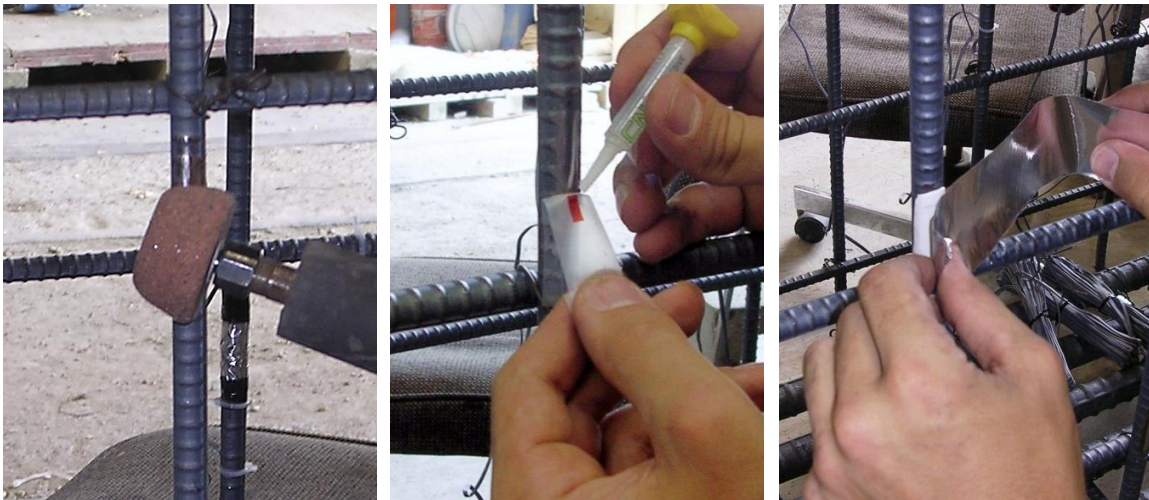
Figure 3-21: Steel strain gauge installation

3.5.2 Load and Displacement Measurements

The force applied to the beam during testing was measured by 500-kip capacity load cells placed between the transfer beam and the reaction nut at each of the twelve rods, six at each support as shown in Figure 3-22. Because the load cells were located at either end, the shear in the test region could be accurately measured throughout the loading history.

Care was taken to balance the reaction at each side of the supports to prevent torsion in the test specimen and overloading of a single rod.
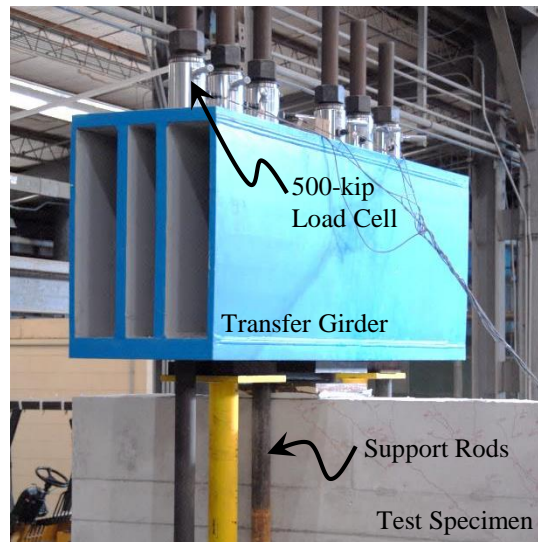
Figure 3-22: Load cell arrangement at supports

Beam deflection and rigid body motion were measured using an arrangement of five 6-in. linear potentiometers with one located at each support, one at mid-span, and two at the load point closest to the support as shown in Figure 3-23. The purpose of the linear potentiometers was to measure the deflections of the beam throughout the test. The specimens underwent rigid body motion as they were lifted off their supports at the start of the test and as the reaction rods elongated. The displacement measured at the support was used to subtract this motion from the beam midspan deflections. The two linear potentiometers at the load point allowed for observation of rotation of the beam along the longitudinal axis.
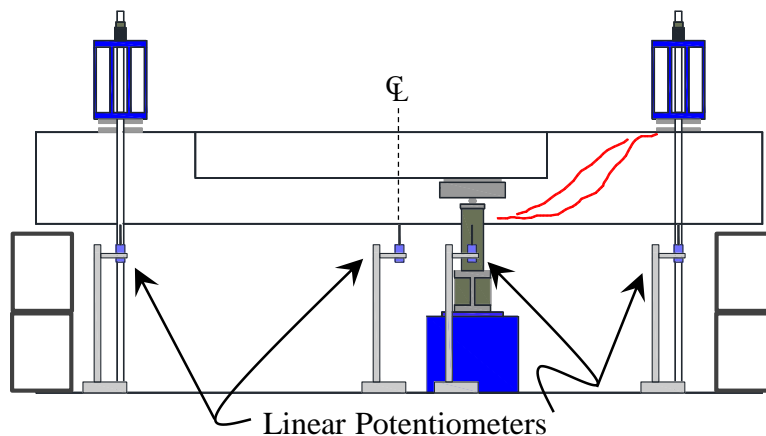
Linear Potentiometers
Figure 3-23: Deflection measurement locations

3.5.3 Crack Width Measurements

Diagonal crack widths were measured and recorded for each test specimen as part of the serviceability considerations of the experimental program. At each load increment, the maximum width of any diagonal crack was collected for each face of the shear span under investigation. Several cracks were also arbitrarily selected to be monitored at the same location throughout the entire test. Independent measurements were obtained by two students with the use of a crack comparator card as shown in Figure 3-24. The crack widths were averaged to produce the diagonal crack width data. No distinction was made between web-shear or flexure-shear cracks. As long as the crack formed at a significant angle from the beam longitudinal axis it was considered a diagonal crack. In general, the location of the maximum width of the diagonal cracks was near or slightly above the mid-height of the member.
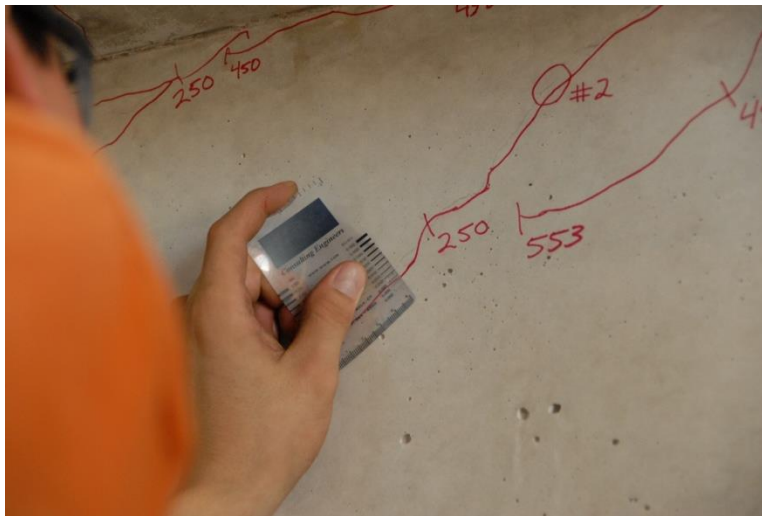
Figure 3-24: Measuring crack widths with a comparator card

3.6 TEST PROCEDURE

Test specimens were monotonically loaded in 50-kip increments up the appearance of the first diagonal crack, then in 100-kip increments up to failure. After each load increment, cracks were marked and the widths of the widest diagonal shear cracks were measured. Photographs were taken after each load increment and the failure was recorded with a video camera.

Two tests were conducted on each beam. Specimens with a single point load were loaded a distance from one support corresponding to the desired a/d ratio. After a shear failure was achieved, the load was removed and post-tensioning clamps were installed to strengthen the first test region. The hydraulic ram and U-frame were then moved to the opposite end of the beam and the test procedure was repeated. Both test regions cracked

during the first test on each beam, therefore the cracking load was not able to be recorded for the second test region for beams with single point loads.
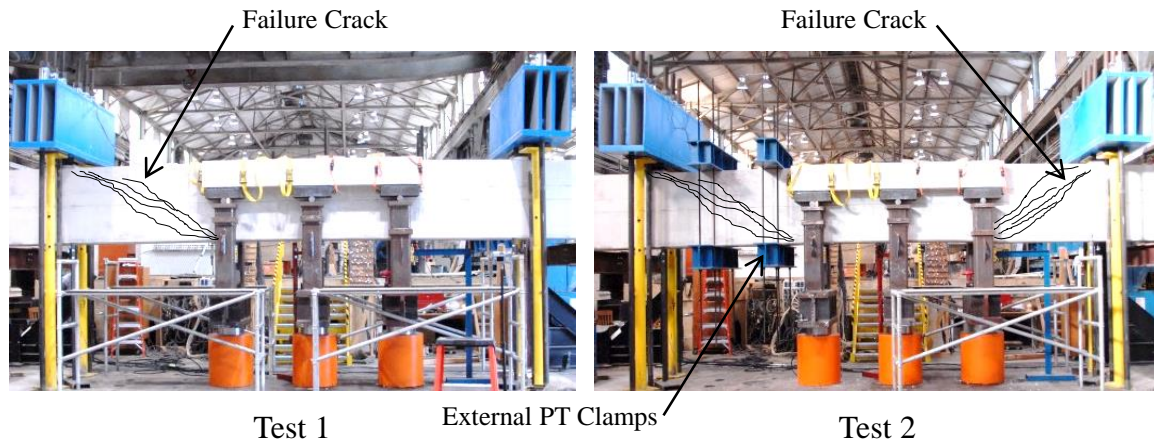
Figure 3-25: Three point loads, first and second test

Specimens with three loading points were designed such that both ends were tested simultaneously as shown in Figure 3-25. For those specimens, the cracking load was obtained for the two test regions, both of which were monitored until a shear failure was achieved at one end of the beam. At that point the load was removed, post-tensioned clamps were installed in the failed test region, and the load was reapplied at the same location until the opposite end of the beam failed in shear. Two tests were also conducted simultaneously for the 75-in. specimens. In this case, the size of the specimen was chosen such that the resulting a/d ratios on each side of the beam matched the appropriate a/d ratios of the experimental program.

Although the beams in the experimental program were tested in an inverted, simply-supported manner, the photographs and drawings of the test regions in the rest of the report will be shown upside down. This is to maintain consistency with the conventional manner of the in-service inverted-T beams (i.e. with tension steel at the bottom of the beam).

3.7   SUMMARY

The details of the experimental program were provided in this chapter. The experimental variables studied in this project were: (1) ledge length, (2) ledge depth, (3) web reinforcement, (4) number of point loads, and (5) web depth. The test specimens were designed to evaluate the effect of these variables on the strength and serviceability of inverted-T beams, thus requiring specimens of comparable size to field members. Thirty three tests were conducted on beams with widths of 21 in. and depths of 42 in. and 75 in. at shear span-to-depth ratios of 1.85 and 2.50.

In addition, the details of the fabrication and testing procedure were provided in this chapter. Two tests were performed on each beam with the help of external post-tensioned clamps for strengthening the off-span. Instrumentation that measured steel strains, applied loads, and beam deflations were monitored throughout the test. Crack width measurements were also taken between each load increment. The results for the experimental program are provided in Chapter 4. The analysis of the experimental results and the additional design objectives of the current project are presented in Chapter 5.

CHAPTER 4
Experimental Results

4.1 OVERVIEW

In this chapter, the experimental results of the testing program are presented in detail. Thirty three tests were conducted on full-scale specimens with the following six parameters investigated:

- length of the ledge (Section 4.3)
- depth of the ledge (Section 4.4)
- amount of web reinforcement (Section 4.5)
- number of point loads (Section 4.6)
- member depth (Section 4.7)
- tension- versus compression-chord loading (Section 4.8)

Prior to discussing the effects of the various parameters, a summary of the experimental results for all of the test specimens is provided. In addition, pertinent information regarding the evaluation of the strength and serviceability data is given to facilitate the interpretation of results.

4.2 SUMMARY OF EXPERIMENTAL RESULTS

The strength and serviceability results of all tests conducted in the experimental program are summarized in Table 4-1. Other important details were provided previously in Table 3.2. The variables presented in Table 4-1 are defined as follows:

b_w =   beam web width, in.

d =   distance from extreme compression fiber to centroid of tensile reinforcement, in.

f'_c =   compressive strength of concrete at the time of testing measured in accordance with ASTM C39, psi.

f_{yl} =   yield strength of longitudinal reinforcement measured in accordance with ASTM A370, ksi.

f_{yv} =   yield strength of transverse reinforcement measured in accordance with ASTM A370, ksi.

f_{yh} =   yield strength of skin reinforcement measured in accordance with ASTM A370, ksi.

$\mathbf{f_{yha}}$ =   yield strength of hanger reinforcement measured in accordance with ASTM A370, ksi.

a/d ratio = shear span-to-depth ratio

$\mathbf{V_{crack}}$ =   shear carried in the test region at the formation of the first diagonal crack, kip.

Specific details regarding the determination of the diagonal cracking load are presented in Section 4.2.2.

$\mathbf{V_{test}}$ =   maximum shear carried in the critical section of the test region, including self-weight of the specimen and test setup.

Specific details regarding the determination of the applied shear are presented in Section 4.2.1.

It should be noted that the majority of the specimens sustained web shear failures, but in a few cases flexural failure, diagonal strut failure in the cross section, punching shear, or ledge-to-web shear friction failures were observed. The value reported for V_{test} is the maximum shear carried at the critical section at the onset of strength loss, regardless of the failure mode. A note was added in Table 4-1 to the specimens that experienced a failure mode different than web shear.

Table 4-1: Summary of experimental results

Specimen	b_w (in.)	d (in.)	$f'c$ (psi)	f_{yl} (ksi)	f_{yv} (ksi)	f_{yh} (ksi)	f_{yha} (ksi)	a/d ratio	V_{crack} (kip)	$\dfrac{V_{crack}}{\sqrt{f'_c}b_wd}$	$\dfrac{V_{crack}}{V_{test}}$	V_{test} (kip)	$\dfrac{V_{test}}{f'_cb_wd}$	$\dfrac{V_{test}}{\sqrt{f'_c}b_wd}$
DS1-42-1.85-03	21	37.64	5258	69	63	63	64	1.96	172	2.99	0.24	712	0.17	12.42
DS1-42-2.50-03	21	37.64	5389	69	63	63	64	2.65	N/A	N/A	N/A	406	0.10	6.99
DS1-42-1.85-06	21	37.64	5024	64	61	61	64	1.85	188	3.35	0.30	621	0.16	11.09
DS1-42-2.50-06	21	37.64	5088	64	61	61	64	2.50	N/A	N/A	N/A	503	0.13	8.93
DL1-42-1.85-06	21	37.64	4830	68	61	61	64	1.85	168	3.06	0.23	741	0.19	13.48
DL1-42-2.50-06	21	37.64	4986	68	61	61	64	2.50	N/A	N/A	N/A	622	0.16	11.15
SS3-42-1.85-03	21	37.64	5891	69	67	67	65	1.85	126	2.08	0.24	523	0.11	8.62
SS3-42-2.50-03	21	37.64	5891	69	67	67	65	2.50	140	2.31	0.31	447	0.10	7.38
SS3-42-2.50-06 (f)	21	37.64	6255	70	61	61	62	2.50	115	1.84	0.22	516	0.10	8.25
SC3-42-2.50-03	21	37.64	5873	66	64	64	64	2.50	113	1.87	0.34	329	0.07	5.44
SC3-42-1.85-03	21	37.64	5873	66	64	64	64	1.85	90	1.48	0.19	483	0.10	7.98
DS3-42-2.50-03	21	37.64	5687	64	65	65	63	2.50	143	2.40	0.33	430	0.10	7.21
DL1-42-1.85-03	21	37.64	4929	71	64	64	62	1.85	242	4.36	0.39	626	0.16	11.28
DL1-42-2.50-03	21	37.64	4929	71	64	64	62	2.50	N/A	N/A	N/A	510	0.13	9.19
SL3-42-1.85-03	21	37.64	5037	75	66	66	64	1.85	172	3.06	0.30	571	0.14	10.17
SL3-42-1.85-06	21	37.64	5250	70	65	65	63	1.85	154	2.69	0.21	744	0.18	13.00
DC1-42-1.85-06	21	37.64	3727	69	61	61	64	1.85	107	2.23	0.21	519	0.18	10.76
C1-42-1.85-06	21	37.64	3727	69	61	61	64	1.85	N/A	N/A	N/A	637	0.22	13.21

(f) Flexural failure

61

Table 4-1(Cont.'d): Summary of experimental results

Specimen	b_w (in.)	d (in.)	$f'c$ (psi)	f_{yl} (ksi)	f_{yv} (ksi)	f_{yh} (ksi)	f_{yha} (ksi)	a/d ratio	V_{crack} (kip)	$\dfrac{V_{crack}}{\sqrt{f'_c}b_w d}$	$\dfrac{V_{crack}}{V_{test}}$	V_{test} (kip)	$\dfrac{V_{test}}{f'_c b_w d}$	$\dfrac{V_{test}}{\sqrt{f'_c}b_w d}$
SS1-75-1.85-03	21	68.20	3127	66	65	65	62	1.87	346	4.51	0.46	745	0.17	9.31
DC3-42-1.85-03	21	37.64	4568	64	63	63	66	1.85	152	2.84	0.38	395	0.11	7.39
DS3-42-1.85-03	21	37.64	4568	64	63	63	66	1.85	164	3.07	0.36	454	0.13	8.49
SS1-42-2.50-03	21	37.64	5703	65	67	67	70	2.50	157	2.63	0.39	398	0.09	6.67
SS1-42-1.85-03	21	37.64	5721	65	67	67	70	1.85	N/A	N/A	N/A	583	0.13	9.75
DC1-42-2.50-03	21	37.64	4035	70	62	62	64	2.50	70	1.40	0.19	365	0.11	7.28
DL3-42-1.85-03 (f)	21	37.64	4202	70	62	62	64	1.85	276	5.39	0.44	629	0.19	12.27
SL1-42-2.50-03	21	37.64	4281	69	64	64	71	2.50	167	3.24	0.34	498	0.15	9.62
SC1-42-2.50-03 (r)	21	37.64	4281	69	64	64	71	2.50	N/A	N/A	N/A	319	0.09	6.18
DS1-42-2.50-06/03	21	37.64	4173	66	65	65	71	2.50	115	2.25	0.21	539	0.16	10.59
DS1-42-1.85-06/03	21	37.64	4173	66	65	65	71	1.85	N/A	N/A	N/A	739	0.22	14.49
SC1-42-1.85-03 (le)	21	37.64	4330	66	67	67	64	1.85	N/A	N/A	N/A	463	0.13	8.67
DC1-42-1.85-03	21	37.64	4303	66	67	67	64	1.85	127	2.45	0.25	517	0.15	9.97
SC1-42-1.85-03b	21	37.64	2996	70	69	69	63	1.85	N/A	N/A	N/A	456	0.19	10.54
DC1-42-1.85-03b	21	37.64	3013	70	69	69	63	1.85	N/A	N/A	N/A	424	0.18	9.77
SS1-75-2.50-03 (p)	21	68.20	5158	65	64	64	64	2.50	225	2.19	0.35	649	0.09	6.31

(f) Flexural failure

(r) Shear friction failure of the web-to-ledge interface

(le) Ledge tie failure

(p) Punching shear failure

4.2.1 Evaluation of Strength Data

The shear strength of the test specimens, V_{test}, was defined as the maximum shear carried at the critical section. The critical section was considered to be the point halfway between the support and the nearest load in the test region of interest. V_{test} was determined by summing the reactions measured by the load cells at the support, R_A or R_B, the corresponding portion of the self-weight of the specimen, ω_{SW}, and the weight of a transfer girders, P_{TR}, as shown in Figure 4-1. The self-weight was assumed to be uniform along the entire length of the beam
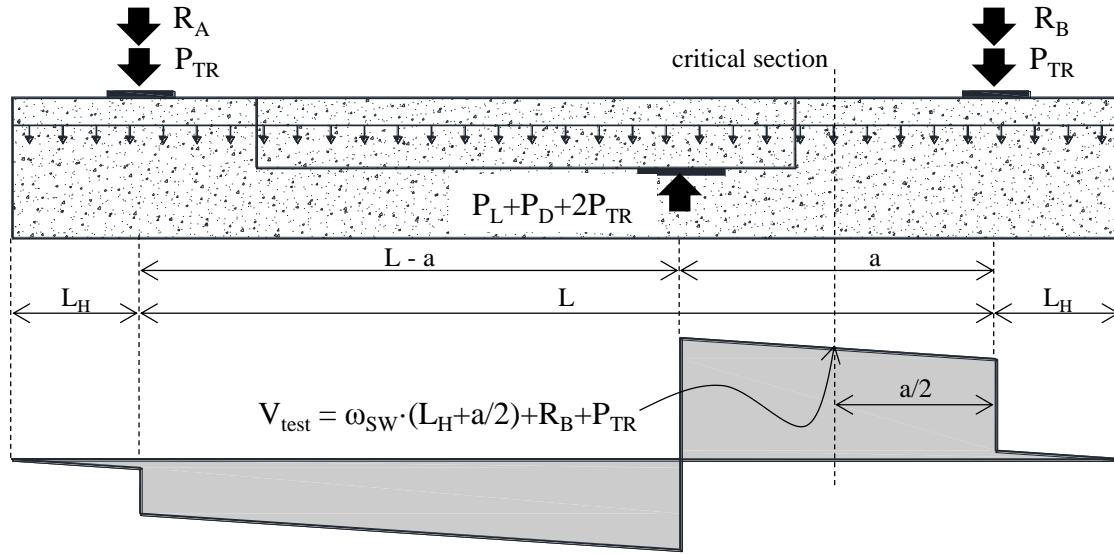
Where:
$$P_L = R_A + R_B \qquad\qquad L = 255.25 \text{ in.}$$
$$P_{TR} = 7.8 \text{ kip} \qquad\qquad L_H = 38.375 \text{ in.}$$
$$P_D = \omega_{SW}(2_{LH} + L) \qquad \omega_{SW} = \text{Specimen self-weight, kip/ft}$$

Figure 4-1: Load and shear force diagram for typical beam test.

The shear capacity of the test specimens presented in this chapter is normalized by the cross-sectional area and the strength of the concrete. Depending on the a/d ratio the failure mechanism can depend on the tension and/or compressions strengths of the concrete. At higher a/d ratios (> 2.0), sectional shear (diagonal tension) generally controls the strength of a member. The shear capacity in these beams is therefore related to the tensile strength of concrete or its proxy $\sqrt{f'_c}$. The capacity of deep beams (a/d < 2.0) is related to the compression strength and to some extent the tensile strength of concrete as failure occurs in such beams due to crushing and splitting of the concrete struts and nodes. The ultimate capacity of the test specimens were therefore normalized by both $f'_c b_w d$ and $\sqrt{f'_c} b_w d$ so that more direct comparisons between the various beams

capacities can be made In Table 4-1, the diagonal cracking loads of the test specimens, which depend on the tensile strength of the concrete, are normalized by $\sqrt{f'_c}b_w d$.

4.2.2 Evaluation of Serviceability Data

In order to evaluate the serviceability performance of the specimens, two parameters were considered: the first diagonal cracking load, and the progression of maximum crack width with increasing shear.

The load corresponding to the first shear crack was recorded during testing by visual inspection of the test region. Upon examination of the test data, the first cracking load, V_{crack}, was determined at the load when a sudden increase in strain was measured by the gauges affixed to the stirrups. This load was confirmed with the observations made during testing. As noted in Section 3.6, the diagonal cracking loads were only obtained for the first test on each specimen, unless both spans were tested simultaneously. An illustration of the data used to determine V_{crack} is presented in Figure 4-2.
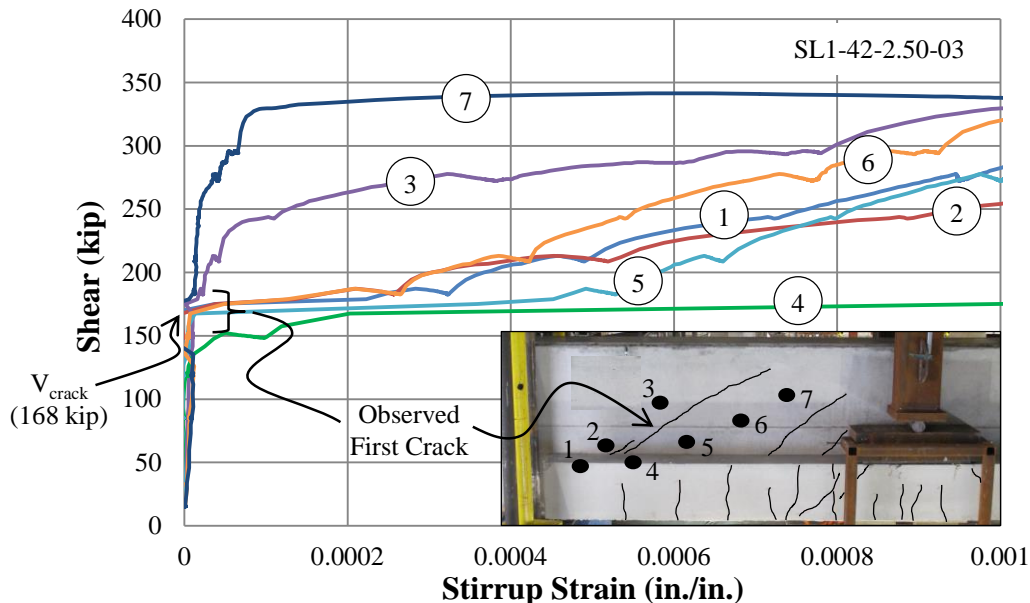
Figure 4-2: Visual and experimental determination of first cracking load.

At each load increment, the beam was inspected and cracks were marked. The maximum diagonal crack width was measured with a crack comparator card and recorded along with the corresponding applied load. An example of crack width progression is given in Figure 4-4.

In order to characterize the cracking performance of test specimens at service load levels, a benchmark crack width of 0.016 in. was selected. Maximum crack widths recorded below that threshold were deemed acceptable for long-term serviceability considerations.

The selected value is consistent with the tolerable service crack widths listed in ACI 224R-01 and fib-1999 for dry exposure, as well as with TxDOT Project 0-5253. ACI 224R-01 reports that crack width limits are expected to be exceeded by a significant portion of the cracks thus the values are only meant as general guidelines to be used in conjunction with sound engineering judgment. Thus even though bent caps may be exposed to wet and dry cycles, the dry exposure crack limit was deemed acceptable for the evaluation of test specimens for which the actual maximum crack widths were recorded at every loading increment.

Along with the limit on maximum crack width, a service load level corresponding to 33% of the maximum applied load was selected as an approximate service load level for test specimens. This value is consistent with the value used in TxDOT Project 0-5253. Assumptions leading to the 33% value are detailed in Figure 4-3. Maximum diagonal crack width progressions of four typical tests are presented in Figure 4-4 in conjunction with the load and crack width serviceability criteria. In that figure, specimens with crack progression outside of the bottom right quadrant drawn by the selected limits are deemed to have acceptable detailing to limit crack widths at service loads. Crack width evaluations at service loads for all specimens tested are presented in Section 4.5.3.

$$\varphi \text{ Nominal Capacity} \quad \approx \quad \eta \text{ Service Load}$$

$$\frac{\varphi}{\eta} \quad \approx \quad \frac{\text{Service Load}}{\text{Nominal Capacity}}$$

Assumptions:

$\left.\begin{array}{l} \text{1). Load Case: } 1.25DL + 1.75LL \\ \text{2). } DL = 75\% \text{ of Service Load} \\ \quad\; LL = 25\% \text{ of Service Load} \end{array}\right\} \eta = 1.4$

3). Nominal = 2/3 Experimental

$$\frac{2}{3} \; \frac{0.70}{1.4} = 0.33 \quad \approx \quad \frac{\text{Service Loads}}{\text{Experimental Capacity}}$$

φ = strength reduction factor, 0.70
η = load factor
DL = dead load
LL = live load

Figure 4-3: Service load level estimation (Birrcher, Tuchscherer, et al., Strength and Serviceability Design of Reinforced Concrete Deep Beams 2008)
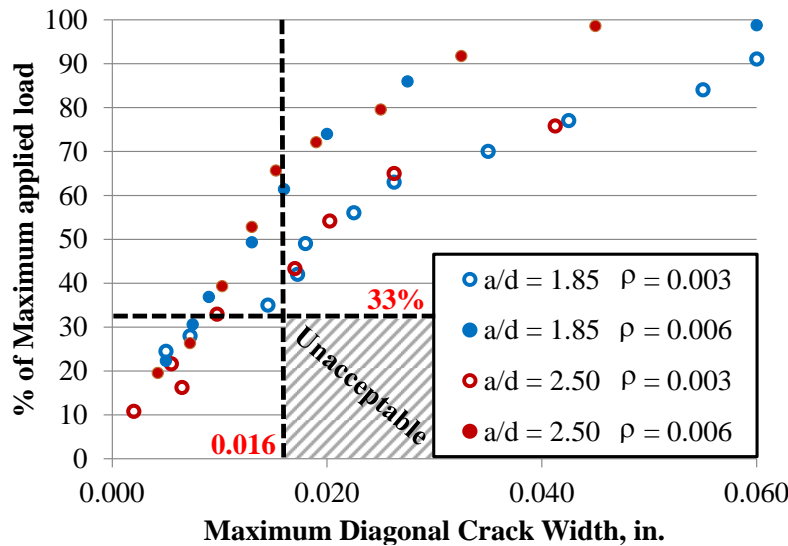
Figure 4-4: Typical crack width progression plot

4.3 SERIES I: LEDGE LENGTH

Different ledge lengths were investigated in the current study to evaluate the effect on the strength and serviceability of inverted-T straddle bent caps. The results of Series I will be used to develop design recommendations in regards to the length of ledges in bridge bent caps.

Three different ledge lengths were investigated. Beams with ledges that were interrupted right after the outermost stringer were "cut-off ledge" specimens. Bent caps in which the ledge ran from end to end of the beam were considered to be "long ledge" specimens. "Short ledge" specimens were the in-between case where the ledge was extended enough to allow a 45-degree force spread from the last bearing pad to the bottom of the beam, but did not continue all the way to the support. Section 3.2.2 provides additional background information on the ledge length series.

4.3.1 Experimental Results

Twenty tests produced eight groups of two or three directly comparable specimens in which every parameter including ledge depth, web reinforcement, number of point loads, and web depth was kept constant except the ledge length. A summary of the experimental results from this series is provided in Table 4-2. All variables are defined in Section 4.2. Strength results are normalized as discussed in Section 4.2.1.

All specimens in this series failed in web shear except DL3-42-1.85-03 and SC1-42-2.50-03. The test of Specimen DL3-42-1.85-03 was halted upon the onset of yielding of the flexural tensile reinforcement and crushing of the concrete in the flexural compression region. Specimen SC1-42-2.50-03 suffered a shear friction failure and the test was halted

upon the bending of the ledge longitudinal bars and the separation of the ledge from the web of the beam. The maximum shear values reported in Table 4-2 is the amount of shear carried at the critical section of the beam at the onset failure, regardless of the failure mode.

Table 4-2: Series I: Ledge Length- Experimental results.

Comparison	Specimen	f'_c (psi)	V_{test} (kip)	$\dfrac{V_{test}}{f'_c b_w d}$	$\dfrac{V_{test}}{\sqrt{f'_c} b_w d}$	V_{crack} (kip)	$\dfrac{V_{crack}}{\sqrt{f'_c} b_w d}$
D_1-42-1.85-03	DS1-42-1.85-03	5258	712	0.17	12.42	172	2.99
	DL1-42-1.85-03	4929	626	0.16	11.28	242	4.36
D_3-42-1.85-03	DC3-42-1.85-03	4568	395	0.11	7.39	152	2.84
	DS3-42-1.85-03	4568	454	0.13	8.49	164	3.07
	DL3-42-1.85-03 (f)	4202	629	0.19	12.27	276	5.39
S_3-42-1.85-03	SC3-42-1.85-03	5873	483	0.10	7.98	90	1.48
	SS3-42-1.85-03	5891	523	0.11	8.62	126	2.08
	SL3-42-1.85-03	5037	571	0.14	10.17	172	3.06
D_1-42-1.85-06	DS1-42-1.85-06	5024	621	0.16	11.09	188	3.35
	DL1-42-1.85-06	4830	741	0.19	13.48	168	3.06
D_1-42-2.50-03	DC1-42-2.50-03	4035	365	0.11	7.28	70	1.40
	DS1-42-2.50-03	5389	406	0.10	6.99	N/A	N/A
	DL1-42-2.50-03	4929	510	0.13	9.19	N/A	N/A
S_1-42-2.50-03	SC1-42-2.50-03 (r)	4281	319	0.09	6.18	N/A	N/A
	SS1-42-2.50-03	5703	398	0.09	6.67	157	2.63
	SL1-42-2.50-03	4281	498	0.15	9.62	167	3.24
S_3-42-2.50-03	SC3-42-2.50-03	5873	329	0.07	5.44	113	1.87
	SS3-42-2.50-03	5891	447	0.10	7.38	140	2.31
D_1-42-2.50-06	DS1-42-2.50-06	5088	503	0.13	8.93	N/A	N/A
	DL1-42-2.50-06	4986	622	0.16	11.15	N/A	N/A

(f) Flexural failure

(r) Shear friction failure of the web-to-ledge interface

4.3.2 Strength Results

The strength results of the twenty ledge depth specimens are directly compared in Figure 4-5 and Figure 4-6. Each of the eight plots represents a group in which every parameter was kept constant except the ledge length. V_{test} is normalized by $f'_c b_w d$ in Figure 4-5 and by $\sqrt{f'_c} b_w d$ in Figure 4-6. The first figure is often considered more appropriate for shorter shear spans (a/d < 2) and the second for longer (a/d > 2) but both are included for evaluation purposes.

D_1-42-1.85-03

D_3-42-1.85-03

S_3-42-1.85-03

D_1-42-1.85-06

D_1-42-2.50-03

S_1-42-2.50-03

S_3-42-2.50-03

D_1-42-2.50-06

(f) Flexural failure

(r) Shear friction failure of the web-to-ledge interface
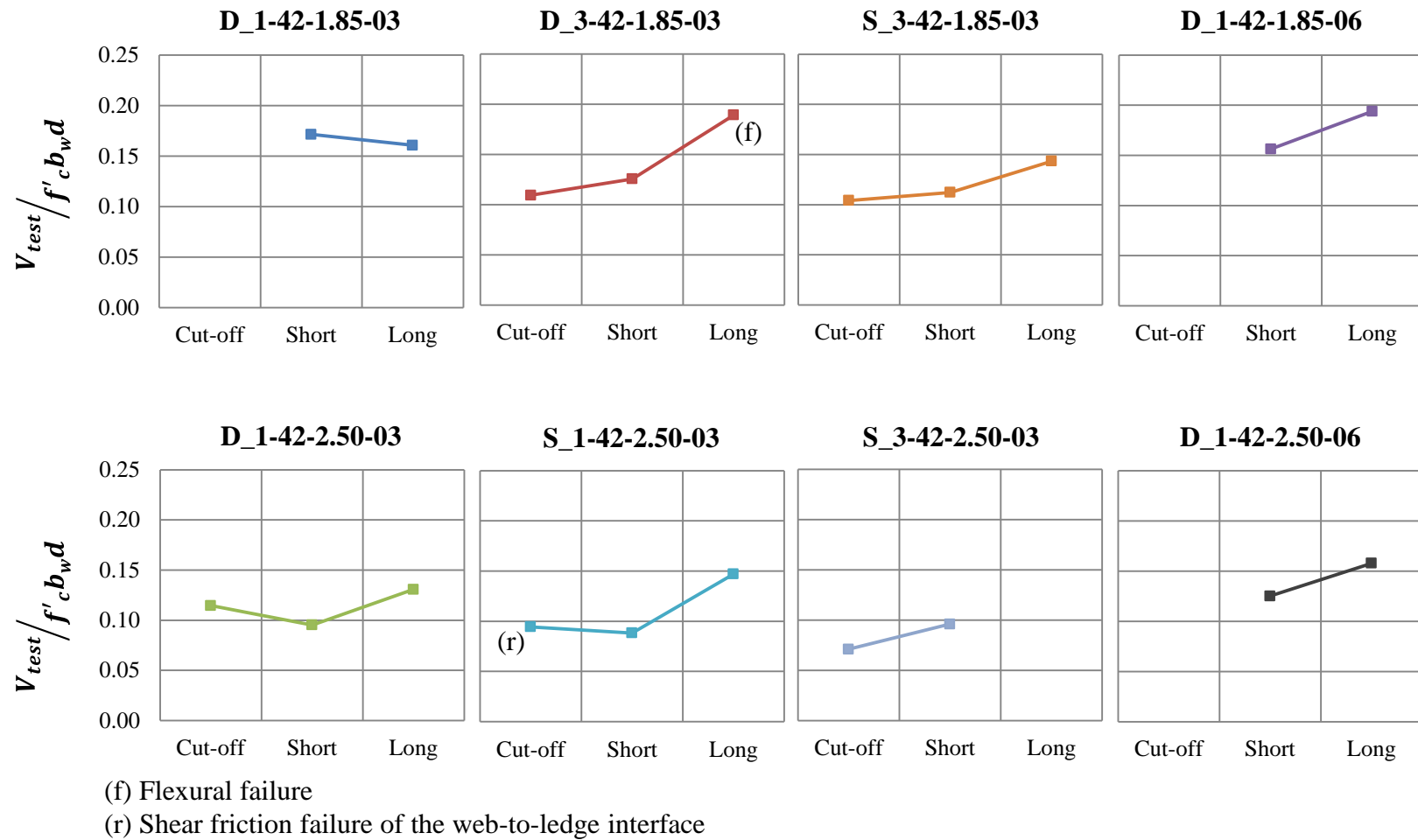
Figure 4-5: Series I: Ledge Length- Direct comparisons of V_test normalized by f'_c b_w d
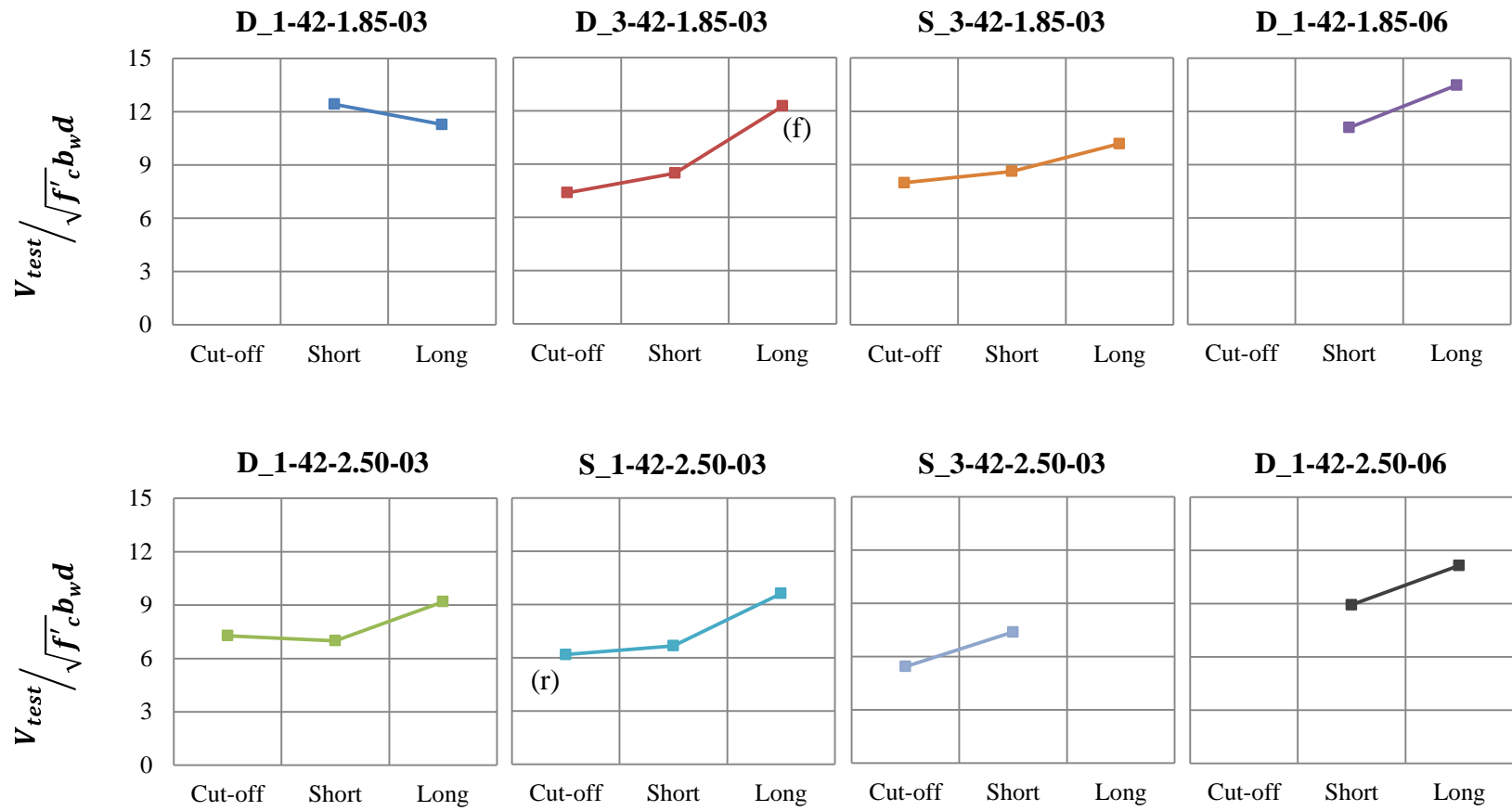
(f) Flexural failure

(r) Shear friction failure of the web-to-ledge interface

Figure 4-6: Series I: Ledge Length- Direct comparisons of V$_{test}$ normalized by $\sqrt{f'_c}$b$_w$d

The nomenclature for the comparison groups is similar to that of the specimens themselves. For example, D_1-42-1.85-03 is comprised of two specimens with deep ledges (D), tested with one point load (1), a total depth of 42 in. (42), a shear span-to-depth ratio of 1.85 (1.85) and 0.3% reinforcement in each direction (03). The blank (_) denotes the length of the ledge, the only variable that differs between the specimens. A similar nomenclature is used in each series with the blank (_) representing the variable currently under investigation.

The same trend was observed in both figures. The normalized shear strength appears to increase with the length of the ledge regardless of the a/d ratio, web reinforcement ratio, and ledge depth. This would suggest that increasing the length of the ledge of an inverted-T straddle bent cap would lead to an increase in shear capacity. It should also be noted that the two specimens that did not fail in web shear fell within the range of V_{test} values in their respective ledge length and a/d ratios- i.e. their capacity did not define a maximum or minimum normalized V_{test}.

4.3.3   Serviceability Results

In addition to the strength results, serviceability data was collected for each of the tests compared within Series I, including the first cracking load and crack widths at each load increment. As the first cracking load is associated with the concrete tensile strength, the values presented in Table 4-2 are normalized with respect to the square root of the compressive strength of the concrete.

Because the first cracking load could not be measured for the second test on most beams, only fourteen of the twenty tests are available in six groups of two or three directly comparable specimens A delay in cracking with respect to the normalized shear load is observed with increasing ledge lengths (Figure 4-7). The trend was observed for both a/d ratios and ledge depths.
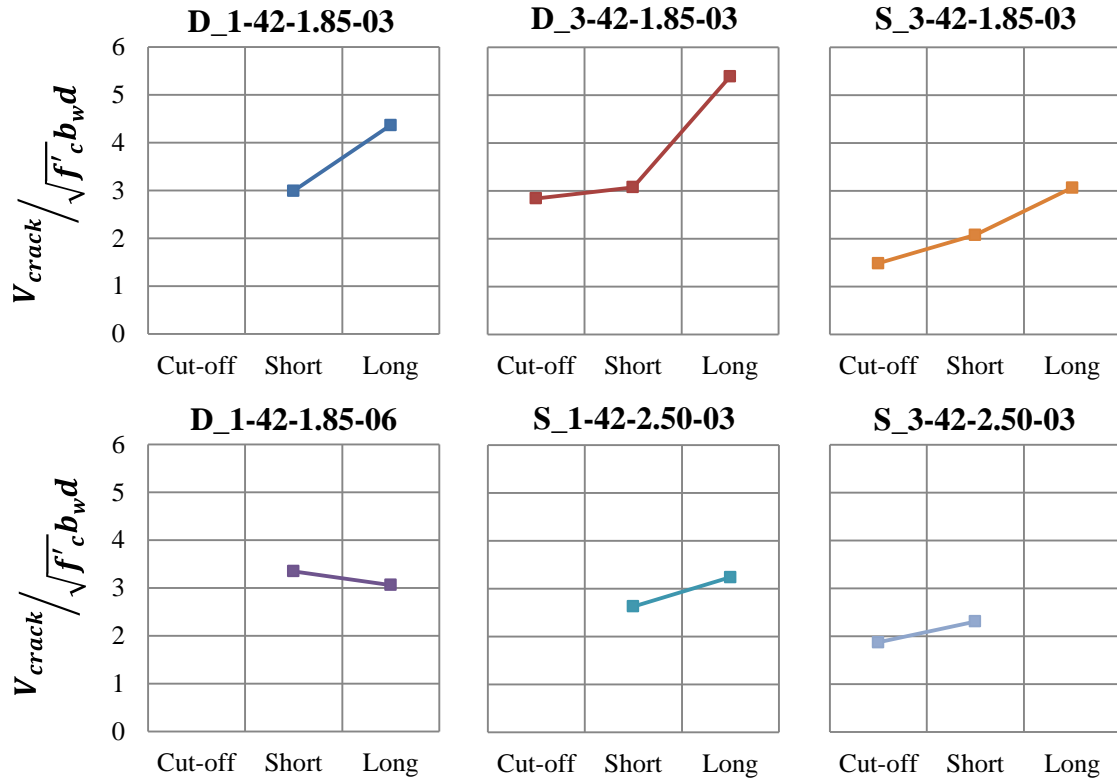
Figure 4-7: Series I: Ledge Length- Direct comparisons of V_{crack} normalized by $\sqrt{f'_c}b_w d$

The location and angle of first diagonal crack is shown for one group of directly comparable specimens in Figure 4-8. As with the normalized diagonal cracking load, the percent of ultimate capacity at which the beam first cracked increased with the ledge length. This is expected as the longer ledge slightly increases the size of the beam, thus delaying the first diagonal crack. The location and angle of the initial diagonal crack was similar for the cut-off and short ledge specimen, but appeared more shallow and further from the load point for the specimen with the deep ledge.

SC3-42-1.85-03: 17% ultimate load   SS3-42-1.85-03: 24% ultimate load

SL3-42-1.85-03: first crack at 30% ultimate load
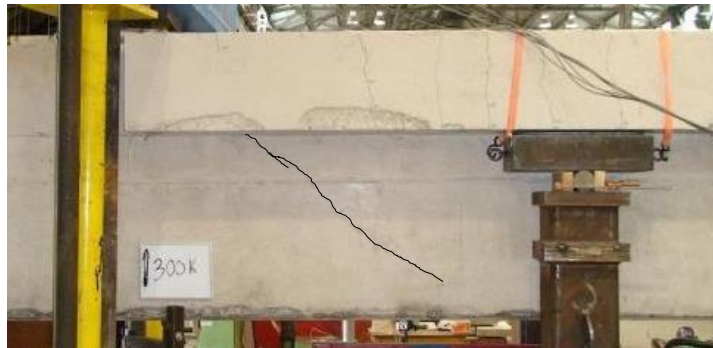
Figure 4-8: First diagonal crack comparison for ledge length specimens

Crack width progressions are shown in Figure 4-9 with twenty specimens presented in eight groups of two or three directly comparable specimens. Contrary to the observations of the first cracking load, no clear trend can be distinguished in the crack width progression plots. In some cases, specimens with longer ledges showed a more accelerated crack widening, whereas in other cases the widening of cracks in specimens with cut-off ledges were more accelerated. Therefore it was concluded that the length has no appreciable effect on the width of the diagonal cracks.
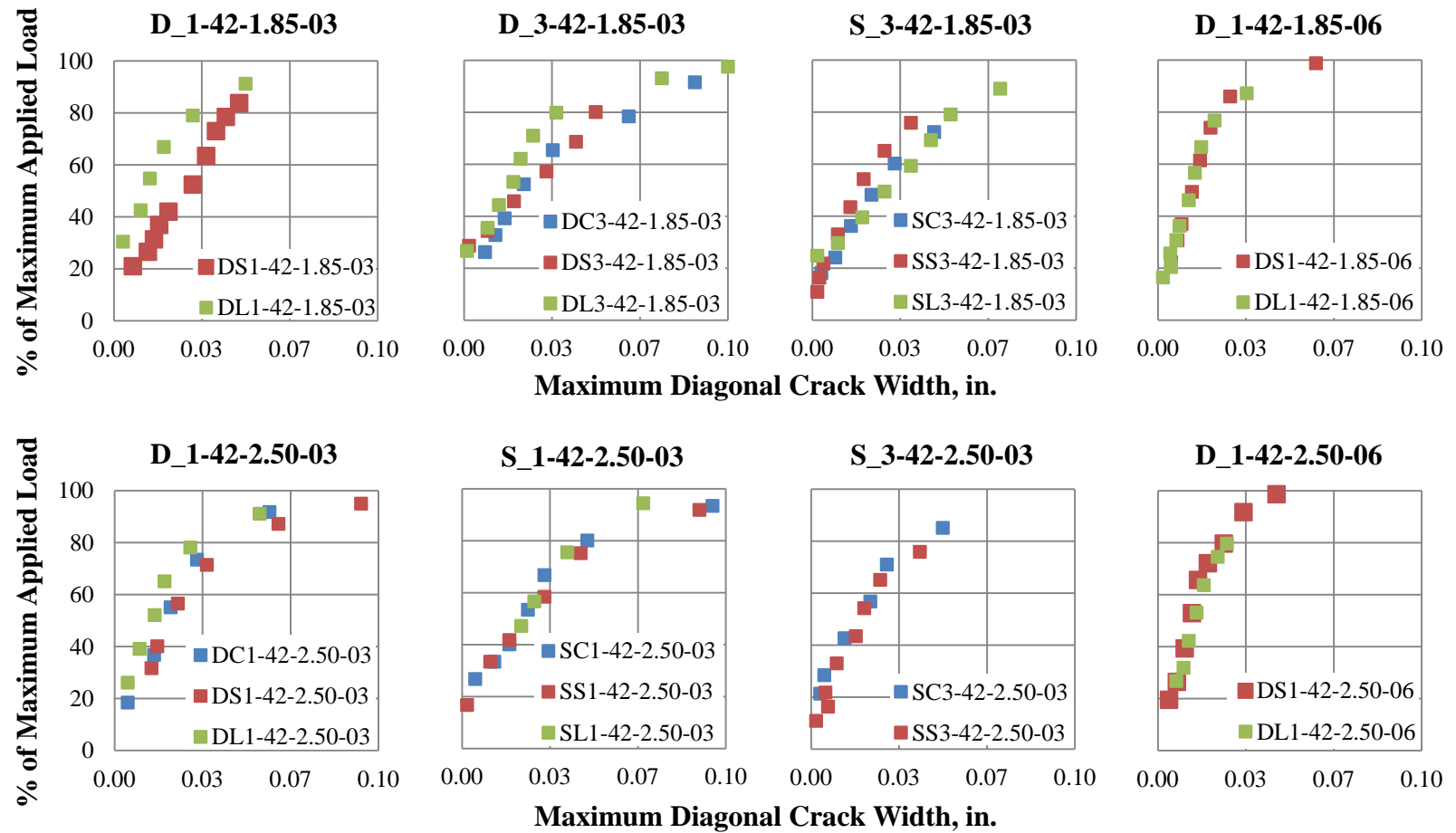
Figure 4-9: Series I: Ledge Length- Direct comparisons of crack width progression

In addition to widths, the crack patterns were also recorded by means of photographs taken at each loading increment. This enabled the formation of new cracks and the extension of existing cracks to be monitored. The location of the cracks at various percentages of ultimate applied load are shown in Figure 4-10 for a direct comparison, with deep ledges, tested at an a/d ratio of 1.85, and 0.3% reinforcement in each direction and three load points. The sketches have been oriented to represent beams in the field and it should be noted that no cracking could be observed directly above each load point as that was the location of the loading frame.

It is more difficult to observe cracking along the direct strut in the beams with long ledges due to the fact that the cracks did not propagate onto the ledge. The ledge length appears to have some effect on the angle of the crack between the load and support. The cut-off ledge results in a much steeper crack when compared to what can be observed for the beam with the long ledge, especially at lower levels of load. As the load increases the crack angle appears to decrease, tending more towards a straight line between the inner corner of the bearing plate and the center of the node above the load point. A similar trend can be observed in the beam with the short ledge, but the cracking pattern appears steeper at higher loads due to the fact that the cracks extend to the top of the beam above the load point. Overall the angle of the cracks observed on the beam with the deep, long ledge were shallower than those of the short and cut-off ledge. It should also be noted that the angle did not appear to change with higher levels of ultimate load.

A three point load direct comparison with shallow ledges is presented in Figure 4-11. The cracking pattern is very similar to the deep ledge specimens and indications of reinforcement stress, either yield or half of yield, is shown in this figure to demonstrate the effectiveness of the strain gauges. The gauges were installed along the assumed direct strut for these specimens tested at an a/d ratio of 1.85 as discussed in Section 3.5.1. The measured strain increases in the gauges as additional load is applied and the cracks form and widen. As with the effect of ledge length on the crack location, the reinforcement is shown to yield earlier in the specimen with the longer ledge when the general crack angle more closely resembles the angle of the assumed direct strut. At higher levels of load the cracking pattern and reinforcement stresses are almost indistinguishable.

DC3-42-1.85-03   DS3-42-1.85-03   DL3-42-1.85-03

30%

50%

60%

80%

90%

100%

Percent of Ultimate Load
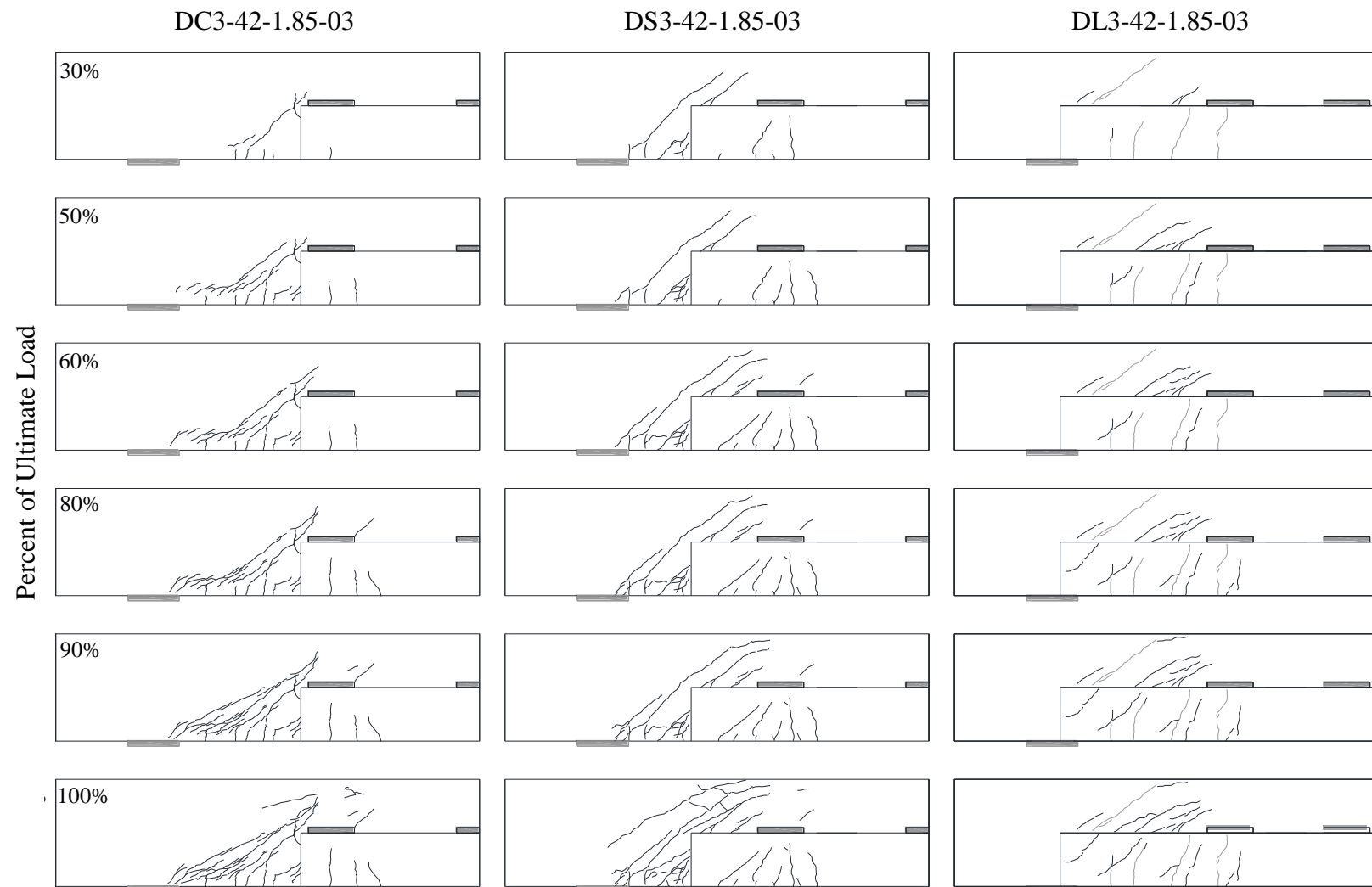
Figure 4-10: Crack patterns for D_3-42-1.85-03 (ledge length varies)

75

Column headers (left to right): SC3-42-1.85-03, SS3-42-1.85-03, SL3-42-1.85-03

Rows (top to bottom): 30%, 50%, 60%, 80%, 90%, 100%

Y-axis: Percent of Ultimate Load

Reinforcement Key: ● $f_s = f_y$ ■ $f_s = \frac{1}{2} f_y$
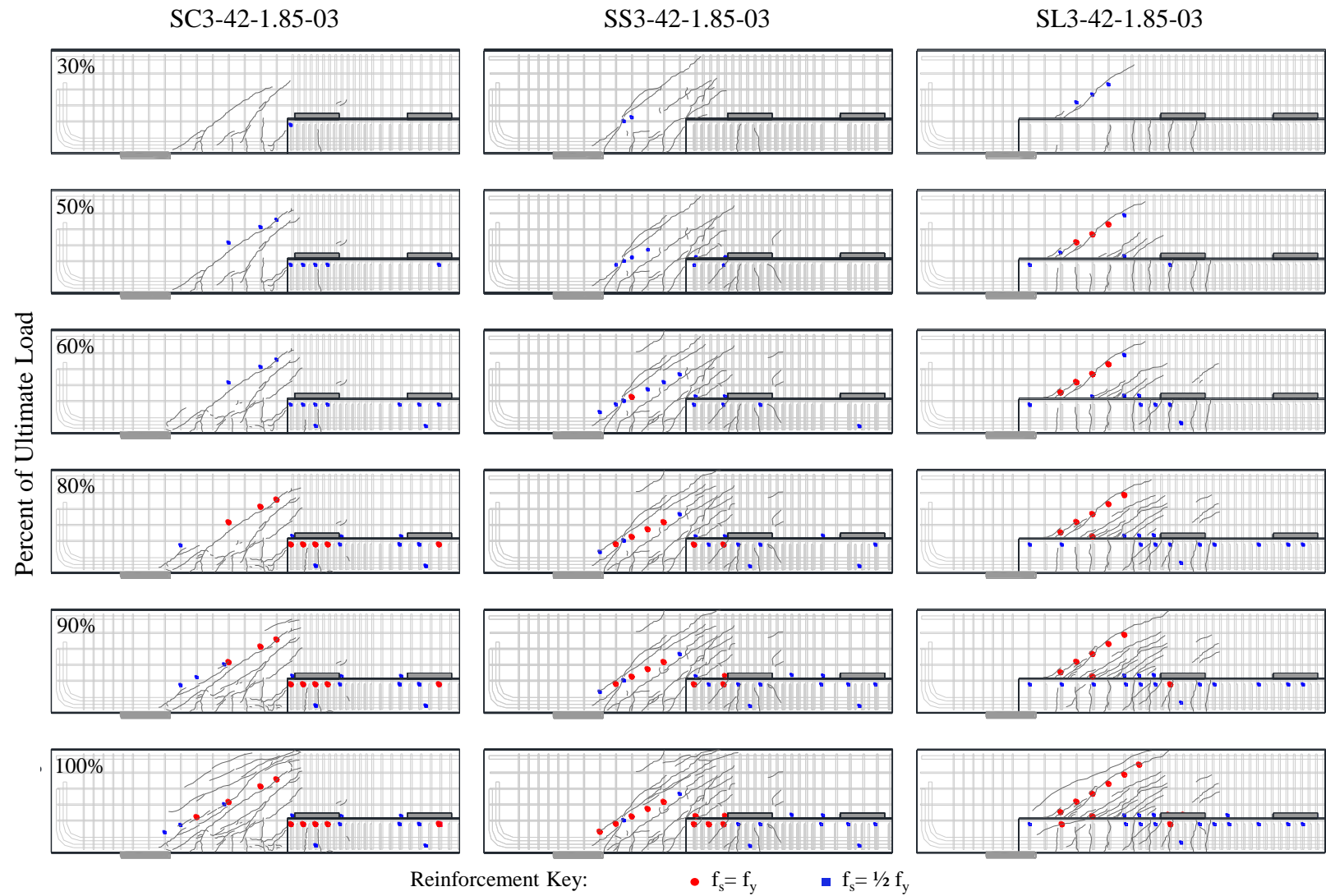
Figure 4-11: Crack patterns and strain gauges for S_3-42-1.85-03 (ledge length varies)

4.3.4   Summary- Series I: Ledge Length

Direct comparisons were presented in this section to evaluate the influence of the length of the ledge on the strength of inverted-T straddle bent caps, the appearance of the first diagonal crack, and the crack width progression.

The results from twenty two tests have shown that increasing the ledge length increases the strength of the inverted-T beam and delays the appearance of the first diagonal crack. Specimens with cut-off ledges were found to have the lowest normalized shear strength while long ledges generally resulted in greater strength as well as diagonal cracking loads. No significant difference was observed in the correlation between the maximum crack width and percent of maximum applied load for the three ledge lengths.

4.4   SERIES II: LEDGE DEPTH

This series was designed to evaluate the effects of the depth of the ledge on the strength and serviceability of inverted-T straddle bent caps. The results of Series II will be used to develop design recommendations in regards to the depth of ledges in similar bent caps.

In order to represent the various ledge geometry found in the inspected in-service bent caps, two different ledge depths were investigated. A ledge depth of half the total section height was considered a "deep ledge" and represented the upper bound of the range of ledge depth seen in the field. Similarly, a ledge depth of a third the total section height was a "shallow ledge" and represented the upper bound of the range of ledge depth seen in the field. Section 3.2.3 provides additional background information on the ledge depth series.

4.4.1   Experimental Results

Twenty of the tests produced ten pairs of directly comparable specimens in which every parameter was kept constant except the ledge depth. A summary of the experimental results from the ledge depth series is provided in Table 4-3. All variables are defined in Section 4.2.

Table 4-3: Series II: Ledge Depth- Experimental results.

Comparison	Specimen	f'_c (psi)	V_{test} (kip)	$\dfrac{V_{test}}{f'_c b_w d}$	$\dfrac{V_{test}}{\sqrt{f'_c} b_w d}$	V_{crack} (kip)	$\dfrac{V_{crack}}{\sqrt{f'_c} b_w d}$
_C1-42-1.85-03	SC1-42-1.85-03 (le)	4303	463	0.15	9.97	127	2.45
	DC1-42-1.85-03	4330	517	0.14	8.90	NA	NA
_C1-42-1.85-03b	SC1-42-1.85-03b	2996	456	0.19	10.54	NA	NA
	DC1-42-1.85-03b	3013	424	0.18	9.77	NA	NA
_S1-42-1.85-03	SS1-42-1.85-03	5721	583	0.13	9.75	NA	NA
	DS1-42-1.85-03	5258	712	0.17	12.42	172	2.99
_C3-42-1.85-03	SC3-42-1.85-03	5873	483	0.10	7.98	90	1.48
	DC3-42-1.85-03	4568	395	0.11	7.39	152	2.84
_S3-42-1.85-03	SS3-42-1.85-03	5891	523	0.11	8.62	126	2.08
	DS3-42-1.85-03	4568	454	0.13	8.49	164	3.07
_L3-42-1.85-03	SL3-42-1.85-03	5037	571	0.14	10.17	172	3.06
	DL3-42-1.85-03 (f)	4202	629	0.19	12.27	276	5.39
_C1-42-2.50-03	SC1-42-2.50-03 (r)	4281	319	0.09	6.18	0	0.00
	DC1-42-2.50-03	4035	365	0.11	7.28	70	1.40
_S1-42-2.50-03	SS1-42-2.50-03	5703	398	0.09	6.67	157	2.63
	DS1-42-2.50-03	5389	406	0.10	6.99	0	0.00
_L1-42-2.50-03	SL1-42-2.50-03	4281	498	0.15	9.62	167	3.24
	DL1-42-2.50-03	4929	510	0.13	9.19	0	0.00
_S3-42-2.50-03	SS3-42-2.50-03	5891	447	0.10	7.38	140	2.31
	DS3-42-2.50-03	5687	430	0.10	7.21	143	2.40

(le) Horizontal ledge tie failure in cross section model

(f) Flexural failure

(r) Shear friction failure of the web-to-ledge interface

All specimens failed in web shear except for three: DL3-42-1.85-03 failed in flexure, and SC1-42-1.85-03 and SC1-42-2.50-03 experienced local ledge failures. The maximum shear value, V_{test}, reported in Table 4-2, is the amount of shear carried at the critical section of the beam at the onset failure, regardless of the failure mode.

4.4.2   Strength Results

Strength results are compared in Figure 4-12 and Figure 4-13. Each plot is a direct comparison of two specimens in which the ledge depth is the only varying parameter. As discussed in Section 4.2.1, V_{test} is normalized by $f'_c b_w d$ in Figure 4-12 and by $\sqrt{f'_c} b_w d$ in Figure 4-13.
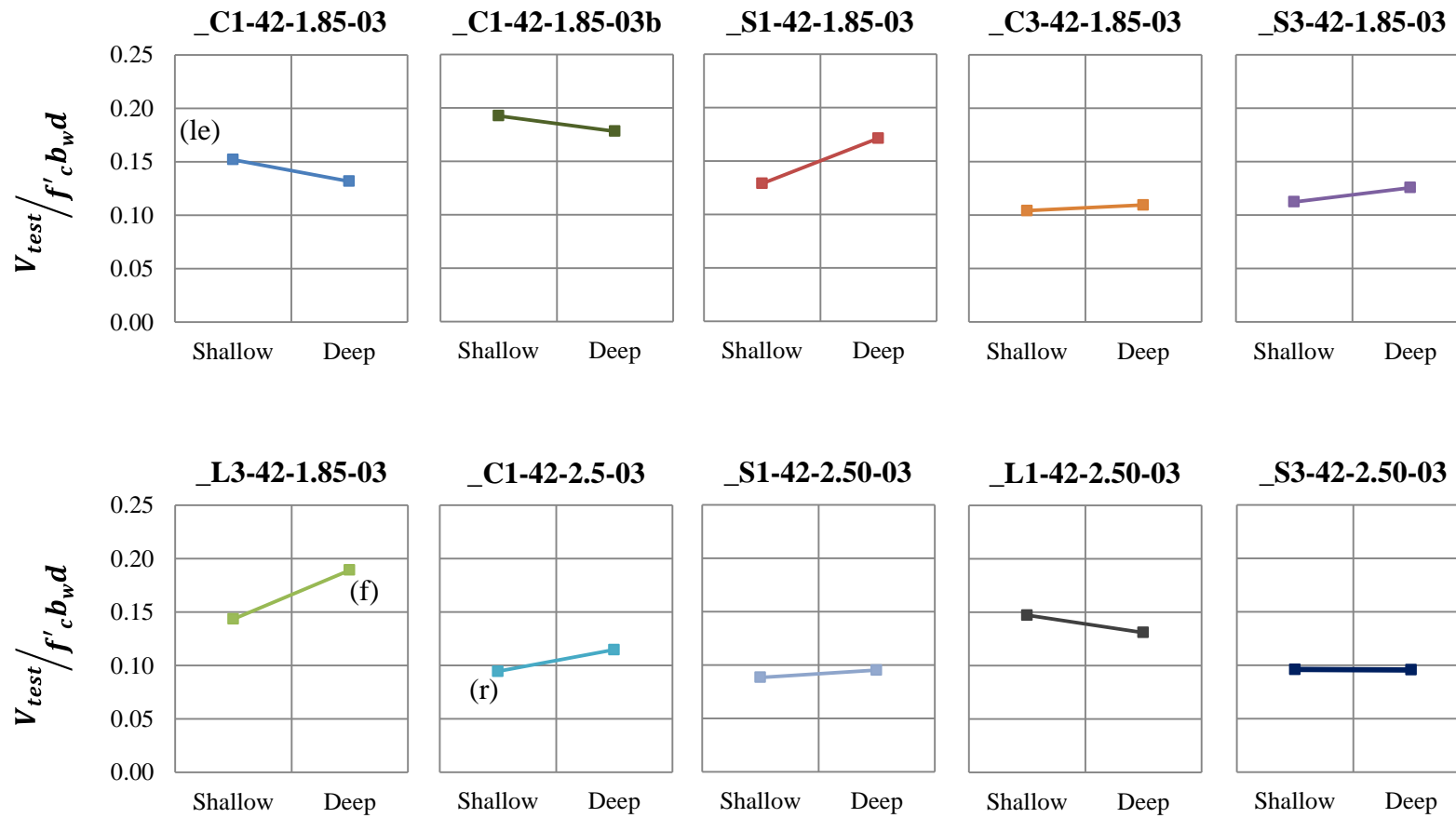
(le) Horizontal ledge tie failure in cross section model
(f) Flexural failure
(r) Shear friction failure of the web-to-ledge interface

Figure 4-12: Series II: Ledge Depth- Direct comparisons of V_{test} normalized by f'$_c$b$_w$d.
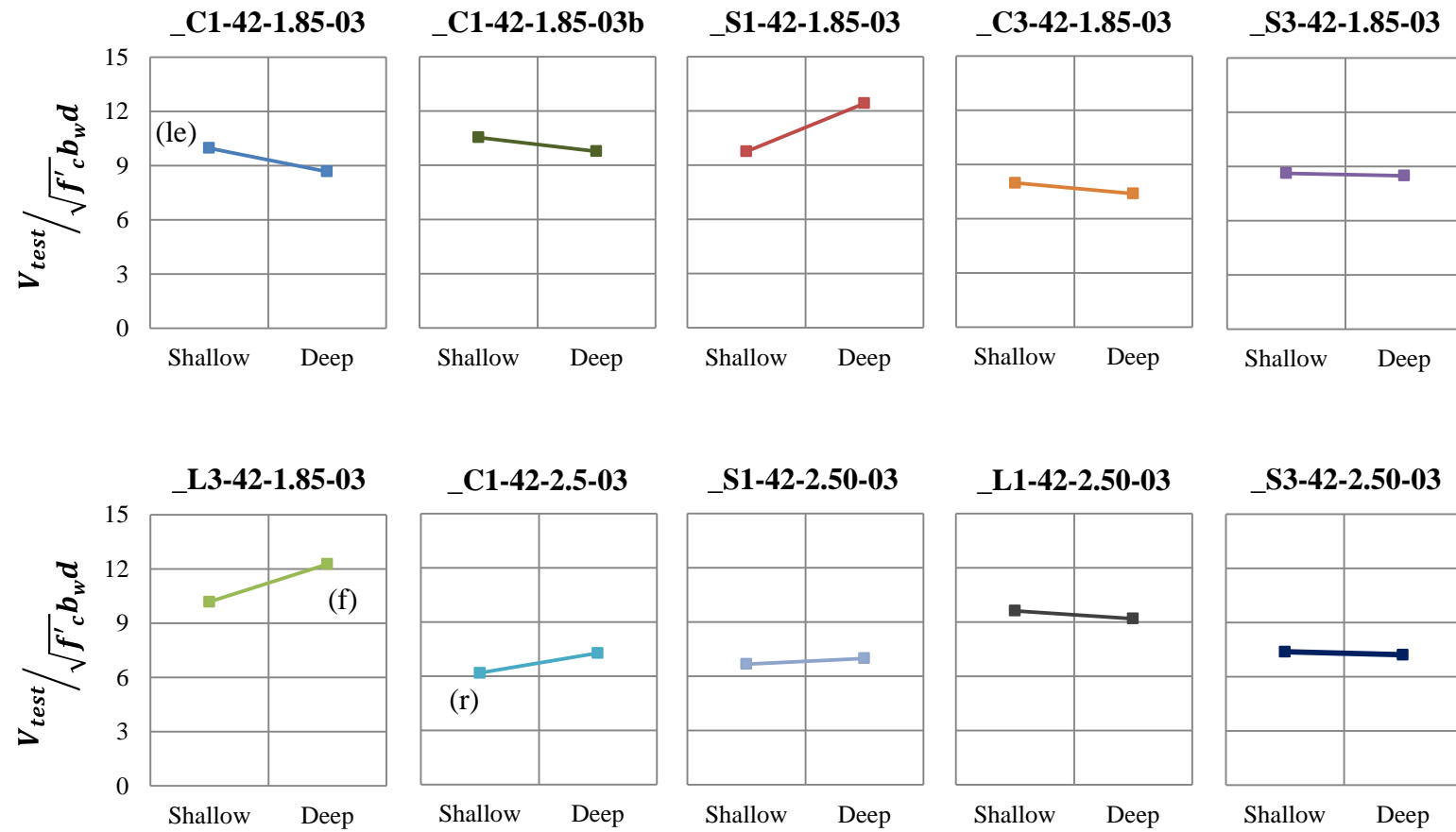
(le) Horizontal ledge tie failure in cross section model

(f) Flexural failure

(r) Shear friction failure of the web-to-ledge interface

Figure 4-13: Series II: Ledge Depth- Direct comparisons of V$_{test}$ normalized by $\sqrt{f'_c}b_wd$.

Two sets of 42-in. specimens with cut-off ledges, one point load, an a/d of 1.85 and 0.3% reinforcement were tested in the current experimental program. The second set, denoted by _C1-42-1.85-03b, resembled corbels in that the beams were designed with ledges with lengths equal to the length of the load plate. These specimens were used to directly examine the node above the load point when the load was confined to the width of the plate and not allowed to spread along the ledge in either direction.

The results shown in Figure 4-12 and Figure 4-13 indicate that the ledge depth does not influence shear strength. Only in two comparisons, _S1-42-1.85-03 and _L3-42-1.85-03 did the specimens with deep ledges exhibited significantly higher strengths than specimens with shallow ledges. Considering that about half of the comparisons revealed a slight decrease in the shear strength of deeper ledges and the inherent variability in shear tests, one can conclude that ledge depth has no significant effect in the shear strength.

4.4.3   Serviceability Results

The first cracking loads, V_{crack}, for the ledge depth series are presented in Figure 4-14. V_{crack} was normalized by $\sqrt{f'_c} b_w d$ due to the fact that the first cracking load is associated with the tensile strength of the concrete.
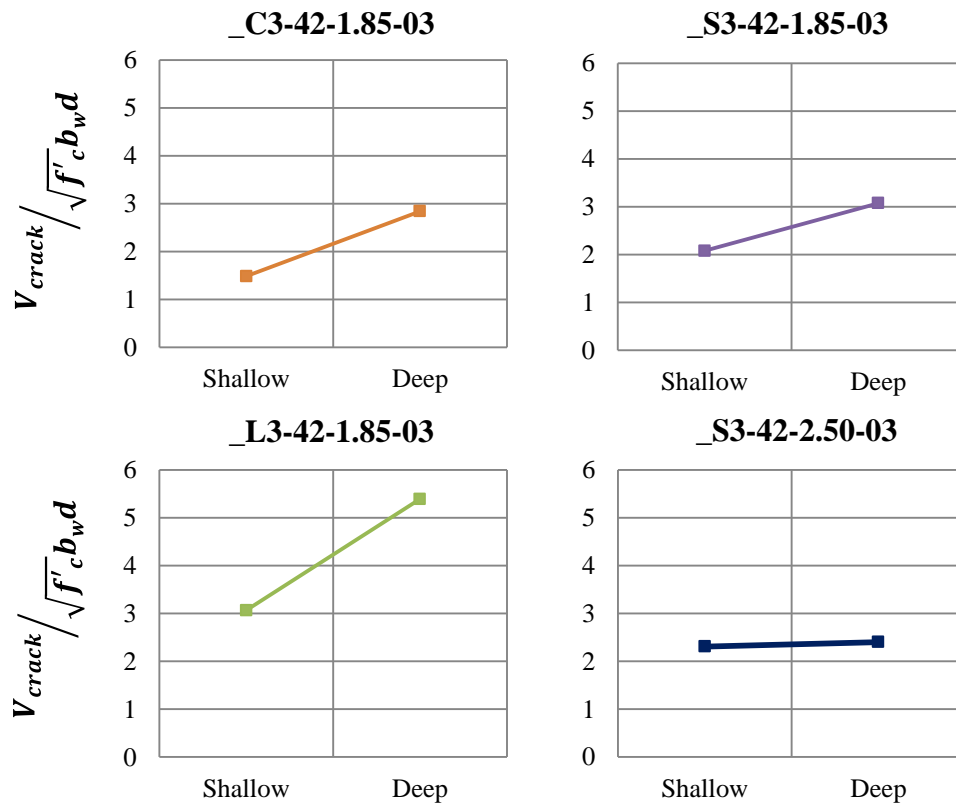
Figure 4-14: Series II: Ledge Depth- Direct comparisons of V_{crack} normalized by $\sqrt{f'_c} b_w d$.

Because the first test on a specimen resulted in cracks on the opposite span, the first cracking load was not recorded for many of the tests in this series. Only eight tests were available for direct comparisons in four groups of two specimens. A trend can be observed in Figure 4-14 in which the specimens with shallow ledges crack at a lower load than comparable specimens with deep ledges. In other words, increasing the depth of the ledge delays the appearance of diagonal cracks.

This was confirmed when examining the percentage of ultimate capacity at the appearance of the first diagonal crack for the direct comparison shown in Figure 4-15. An increase in diagonal cracking load was observed but the overall location and angle of the diagonal crack appears very similar. The crack in the deep ledge specimen does start slightly higher on the web of the beam.

SC3-42-1.85-03: 17% ultimate load   DC3-42-1.85-03: 38% ultimate load
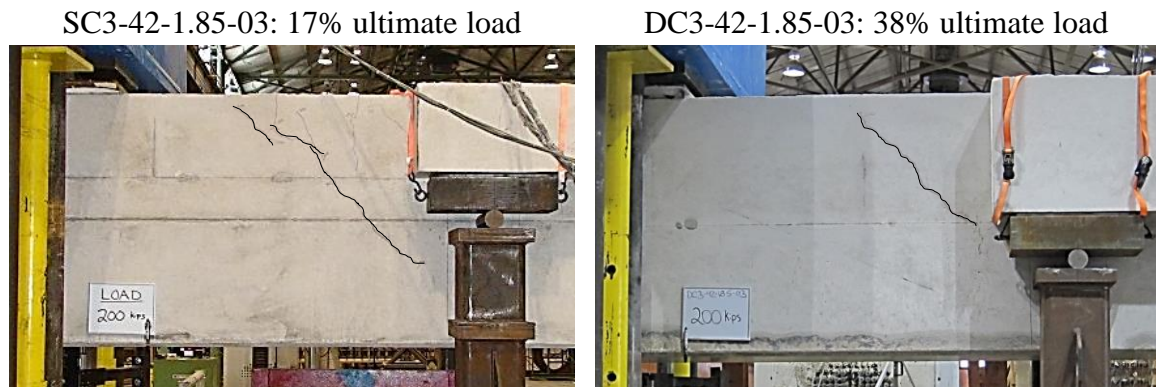
Figure 4-15: First diagonal crack comparison for ledge depth specimens

The progression of crack widths with respect to the applied load for the ledge depth series is illustrated in Figure 4-16. Twenty specimens are presented in ten groups of two directly comparable specimens in which the ledge depth was the only parameter varied.

Regarding the crack width progressions, no clear trend can be distinguished in Figure 4-16. In a few cases, the specimens with deeper ledges appeared to show a more accelerated crack widening but for the most part the maximum crack widths of the two specimen types were indistinguishable. Ultimately, it can be concluded that the depth of the ledge does not have a significant effect on the width of diagonal cracks when compared to the percentage of applied load.

Figure 4-16: Series II: Ledge Depth- Direct comparisons of crack width progression.
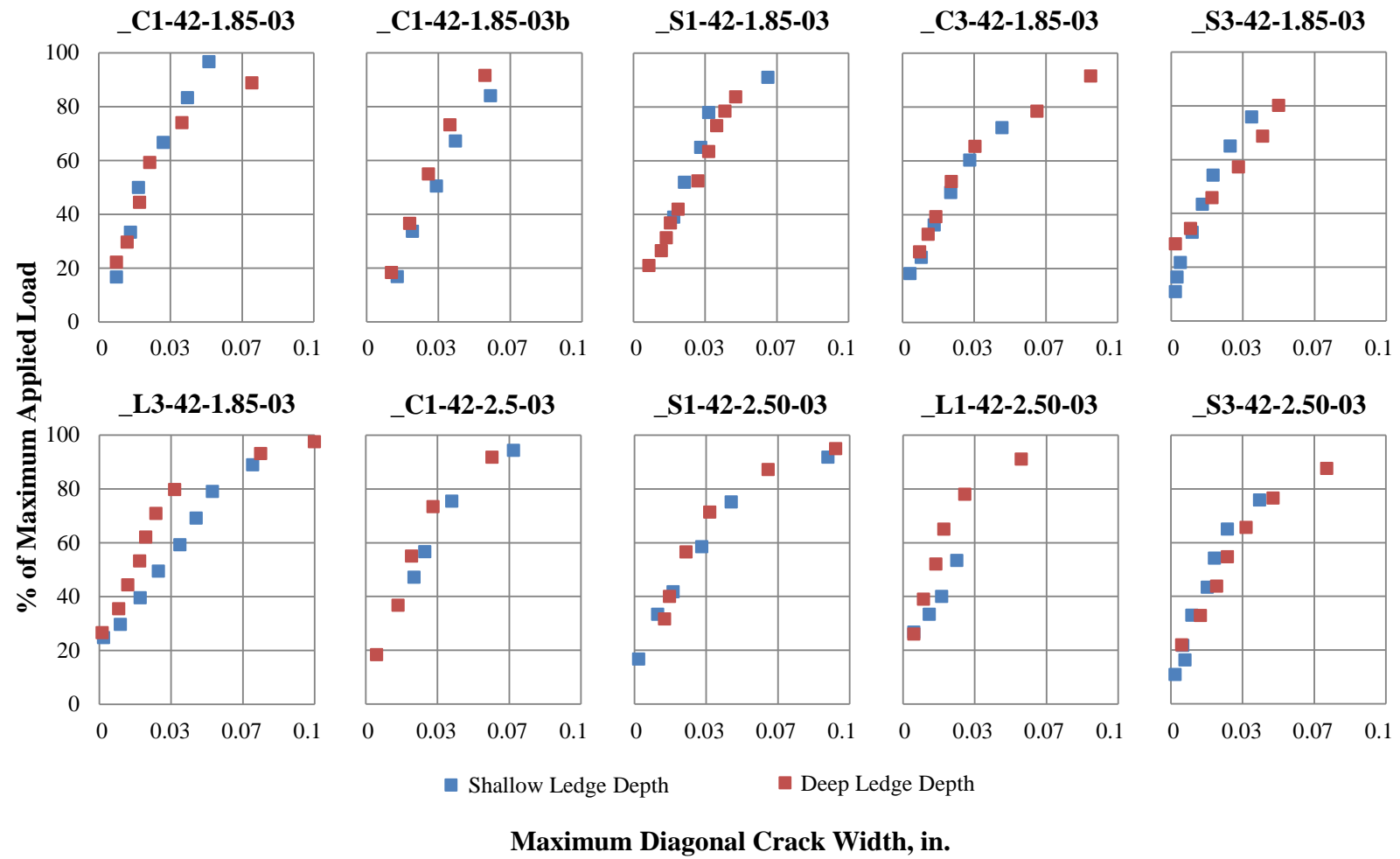
Examining the crack patterns and reinforcement strains shown in Figure 4-17, there appears to be little difference between the shallow and deep ledge specimen. The only chnage being the development of cracks above the approximate strut along the web strain gauges for the shallow ledge specimen. The ledge depth did not have an influence on the crack pattern or yielding of the reinforcement for the other direct comparison specimens.
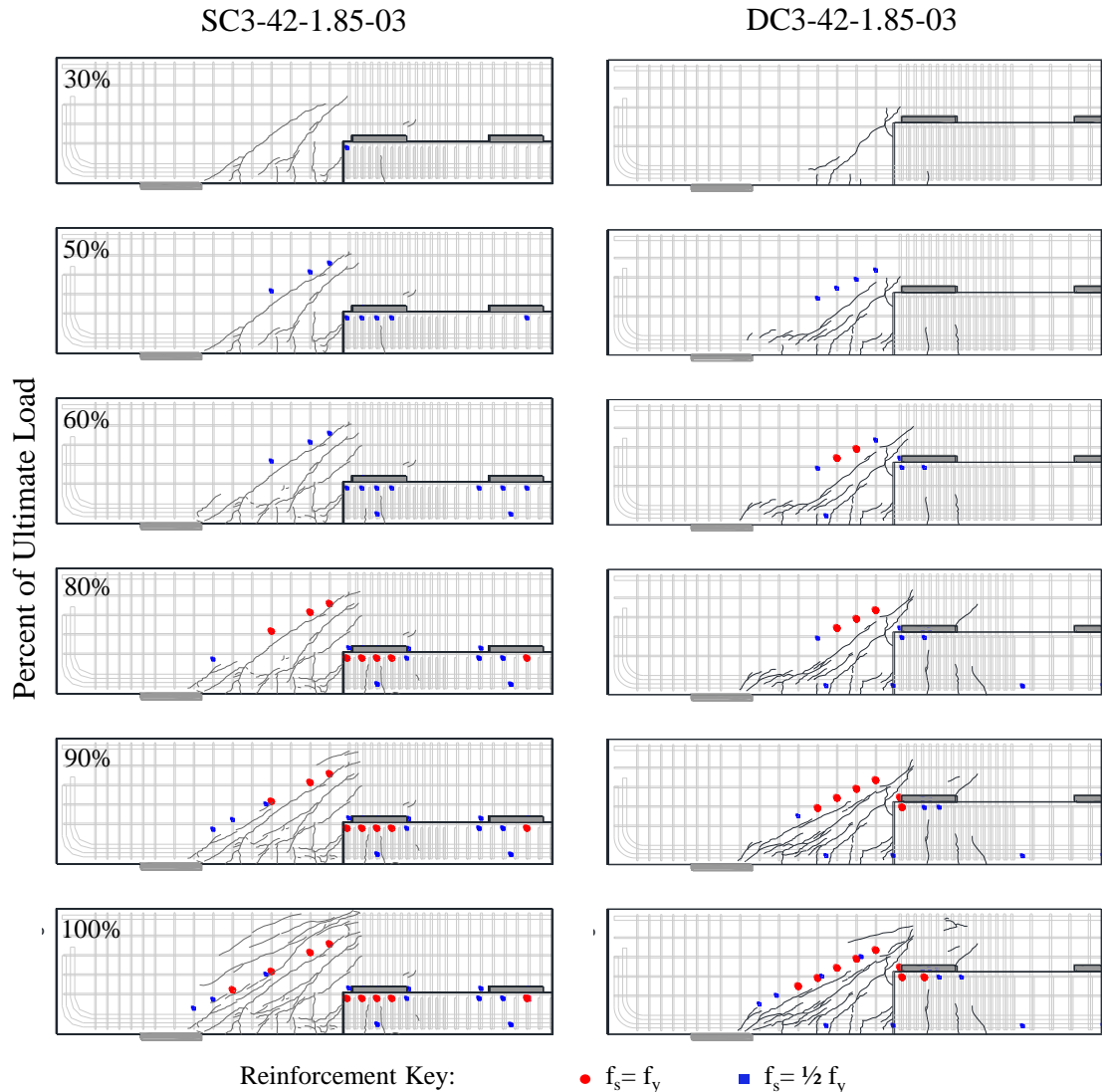
Figure 4-17: Crack patterns and strain gauges for _C3-42-1.85-03 (ledge depth varies)

4.4.4   Summary: Series II: Ledge Depth

Direct comparisons were presented in this section to evaluate the influence of the depth of the ledge on the shear strength of inverted-T straddle bent caps, the appearance of first diagonal crack, and the crack width progression.

The results from twenty tests have shown that increasing the ledge depth does not have a significant effect on the strength of the inverted-T beams. There was also no significant effect on the correlation between the maximum crack width and the percent of maximum applied load. It was, however, observed that increasing the depth of the ledge can delay the appearance of the first diagonal crack.

4.5   SERIES III: WEB REINFORCEMENT

This series was designed to evaluate the effects web reinforcement on the strength and serviceability behavior of the reinforced concrete inverted-T straddle bent caps. The results of Series III will be used to evaluate recommendations of minimum horizontal and vertical reinforcement.

Two different web reinforcement ratios were investigated. The minimum horizontal and vertical reinforcement requirement for deep beams designed using strut-and-tie models according to AASHTO LRFD 2012 is an orthogonal grid of reinforcement at each face such that the ratio of total reinforcement to the gross concrete area is equal to 0.003 (0.3%). The spacing of the reinforcement is limited to 12 in. The purpose of this requirement is to control the width of cracks and allow for the redistribution of internal stresses. For additional discussion on the minimum reinforcement requirements, refer to Birrcher (2008). By constructing and testing specimens with this reinforcement ratio, the performance of the minimum reinforcement ratio in inverted-T beams can be analyzed.

The reinforcement ratio of 0.006 (0.6%) was chosen to provide an upper bound on the maximum reinforcement ratio (0.57%) found in the in-service distressed bent caps. Two specimens were also constructed with a reinforcement ratio of 0.6% in the vertical direction and 0.3% in the horizontal. The purpose of these tests was to examine the effects of mixed reinforcement in inverted-T straddle bent caps; as is common in current design practices when sectional shear design is used. Section 3.2.4 includes additional background information on this series.

4.5.1   Experimental Results

Fourteen tests produced six groups of two or three directly comparable specimens in which every parameter was kept constant except the reinforcement ratio. A summary of the experimental results for Series III is provided in Table 4-4. All variables are defined in Section 4.2. Strength results are normalized as discussed in Section 4.2.1

Table 4-4: Series III: Web Reinforcement- Experimental results.

Comparison	Specimen	f'_c (psi)	V_{test} (kip)	$\dfrac{V_{test}}{f'_c b_w d}$	$\dfrac{V_{test}}{\sqrt{f'_c} b_w d}$	V_{crack} (kip)	$\dfrac{V_{crack}}{\sqrt{f'_c} b_w d}$
DS1-42-1.85-_	DS1-42-1.85-03	5258	712	0.17	12.42	172	3.00
	DS1-42-1.85-06/03	4173	739	0.22	14.49	NA	NA
	DS1-42-1.85-06	5024	621	0.16	11.09	188	3.35
DL1-42-1.85-_	DL1-42-1.85-03	4929	626	0.16	11.28	242	4.36
	DL1-42-1.85-06	4830	741	0.19	13.48	168	3.06
SL3-42-1.85-_	SL3-42-1.85-03	5037	571	0.14	10.17	172	3.06
	SL3-42-1.85-06	5250	744	0.18	13.00	154	2.69
DS1-42-2.50-_	DS1-42-2.50-03	5389	406	0.10	6.99	NA	NA
	DS1-42-2.50-06/03	4173	539	0.16	10.59	115	2.25
	DS1-42-2.50-06	5088	503	0.13	8.93	NA	NA
DL1-42-2.50-_	DL1-42-2.50-03	4929	510	0.13	9.19	NA	NA
	DL1-42-2.50-06	4986	622	0.16	11.15	NA	NA
SS3-42-2.50-_	SS3-42-2.50-03	5891	447	0.10	7.38	140	2.31
	SS3-42-2.50-06 (f)	6255	516	0.10	8.25	115	1.84

(f) Flexural failure

4.5.2   Strength Results

Direct comparisons of the strength results are provided in Figure 4-18 and Figure 4-19. Each plot is a direct comparison of two or three specimens. V_{test} is normalized by $f'_c b_w d$ in Figure 4-18 and by $\sqrt{f'_c} b_w d$ in Figure 4-19.
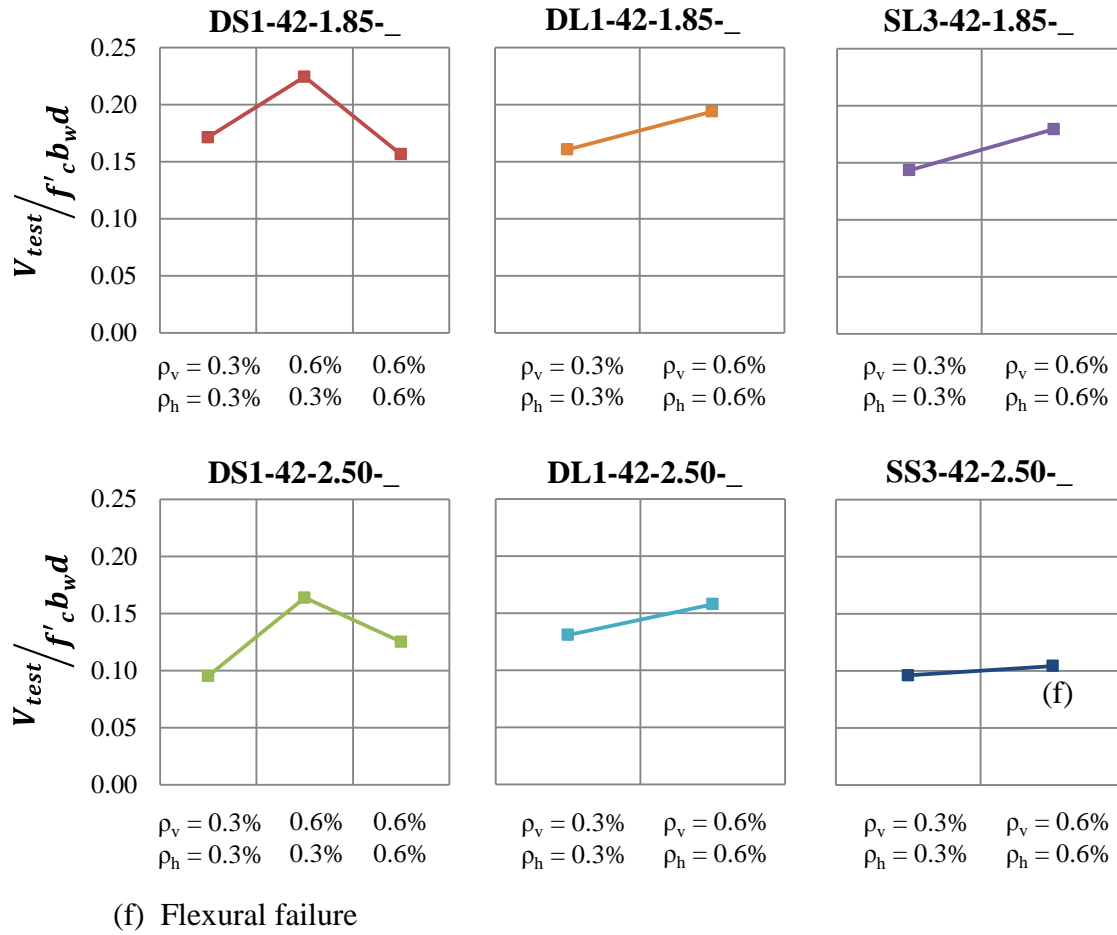
Figure 4-18: Series III: Web Reinforcement- Direct comparisons of V_{test} normalized by $f'_c b_w d$.

As seen in both Figure 4-18 and Figure 4-19, an increase in reinforcement ratio appears to lead to an increase in shear strength, even for beams with a/d ratios of 1.85. In specimens with a/d of 1.85, shear capacity is governed by the compression strut and nodes spanning from load to support. The purpose of the web reinforcement in single-panel beams (a/d=1.85) is to resist the transverse tensile forces that develop in a bottle-shaped strut. Increasing the amount of web reinforcement above a minimum amount required to resist transverse stresses was not found to increase strut capacity in the beams tested with reinforcement ratios of 0.2% and 0.3% in Project 0-5253. Although no difference was observed in the rectangular beams, increasing the reinforcement ratio from 0.3% to 0.6% appears to increase the strength of the direct strut in inverted-T beams. In specimens with a/d of 2.5 however, the tension tie in the shear span limits the shear capacity. It would therefore be expected that a larger increase in shear strength with a larger amount of web reinforcement would be recorded for the beams with a/d ratios of

2.50. However, this was not the case, which indicates that the concrete may play as large a role in the shear strength of longer beams as in shorter beams.
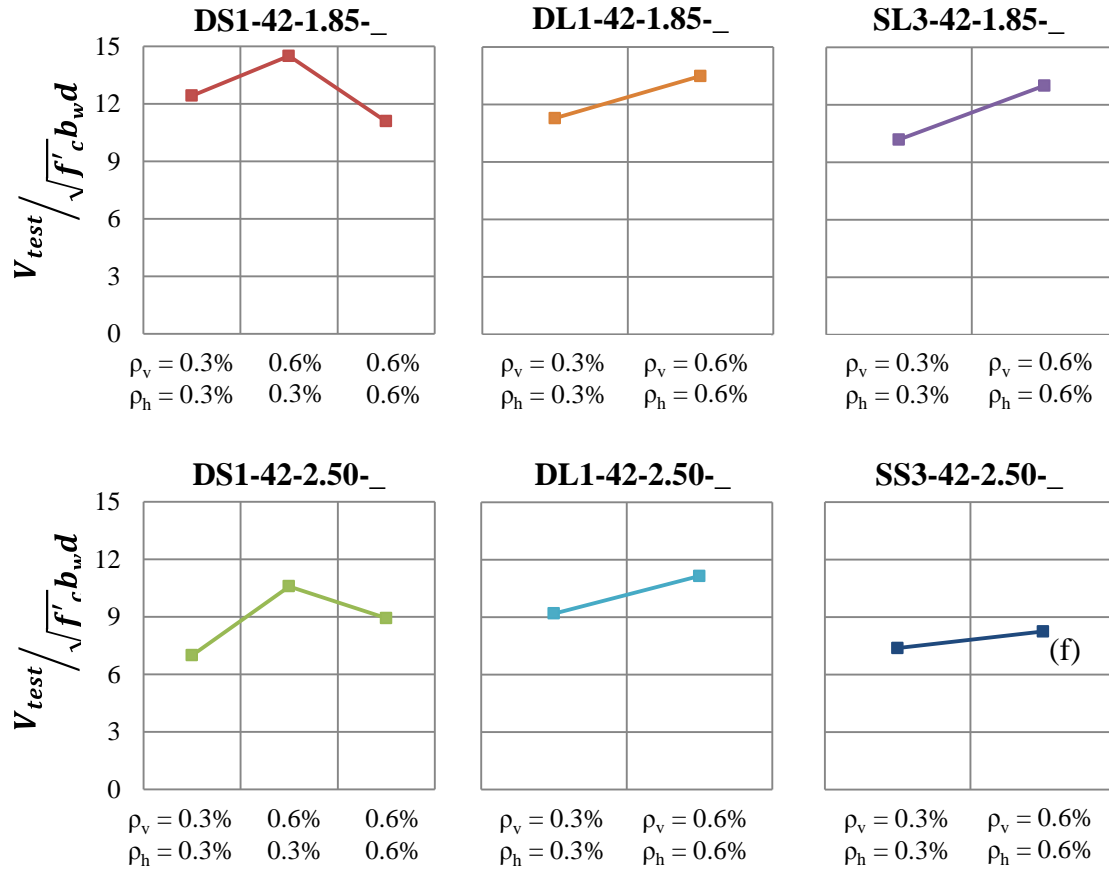
(f) Flexural failure

Figure 4-19: Series III: Web Reinforcement- Comparisons of V_{test} normalized by $\sqrt{f'_c}b_wd$.

All but two beams tested in the experimental program had equal reinforcement ratios in the horizontal and vertical direction. A significant increase in shear capacity can be seen in Figure 4-18 and Figure 4-19 between specimens with $\rho_v = 0.6\%$ to $\rho_h = 0.3\%$ and those with both ratios at 0.3%. In fact the specimens with $\rho_v = 0.6\%$ to $\rho_h = 0.3\%$ showed slightly higher shear strength than those with both ratios at 0.6%. This indicates that the vertical reinforcement ratio likely has a greater effect on the shear strength of inverted-T beams. In previous research of reinforced concrete deep beams, horizontal reinforcement above and beyond 0.3% was found to have little effect on the shear strength (Birrcher (2009)).

4.5.3 Serviceability Results

The cracking loads and the width of diagonal cracks were used to assess the effect of web reinforcement on the serviceability performance of the specimens in this series. As with the strength results, directly comparable specimens were used to evaluate the serviceability behavior on inverted-T deep beams. This allowed all other variables to be kept constant to isolate any effects that could be attributed directly to the amount of web reinforcement.

The diagonal cracking loads for the web reinforcement series are presented in Figure 4-20. Eight tests were available for comparisons in four groups. As seen in Figure 4-20, the results revealed a slight decrease in the normalized cracking load with an increase in the quantity of reinforcement for most of the beams. Such a result was not expected as significant strains are not typically experienced by the reinforcement prior to cracking . However, as the observed trend is slight, it may be concluded that the web reinforcement has no appreciable effect on the diagonal cracking load.
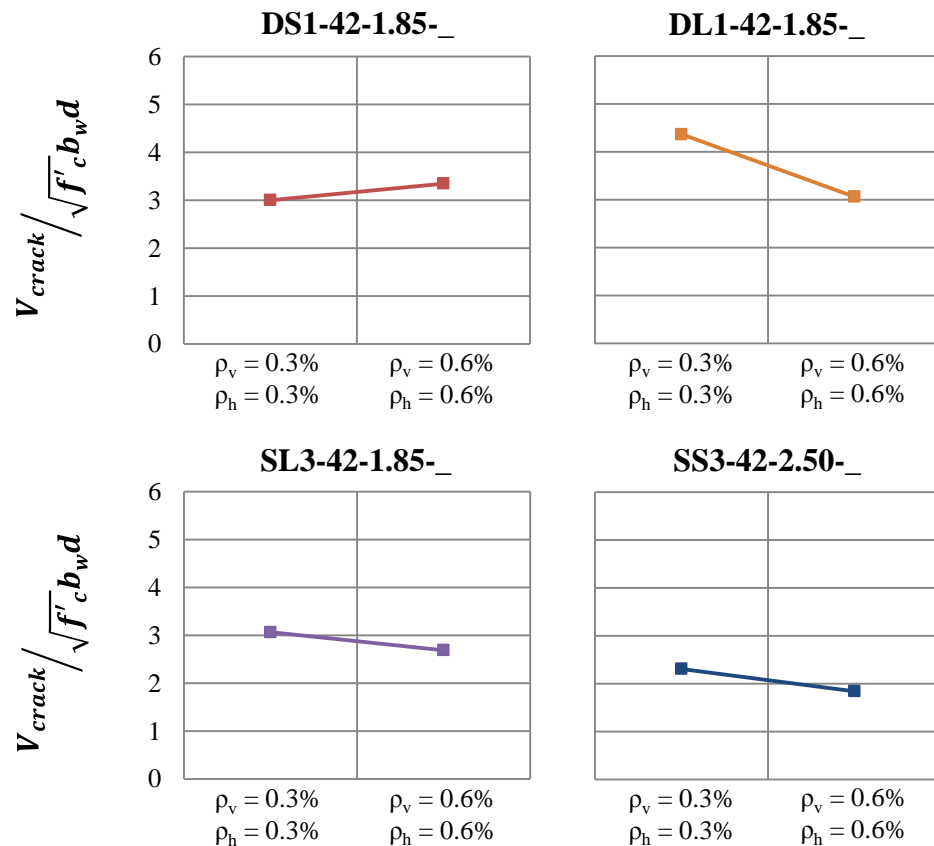
Figure 4-20: Series III: Web Reinforcement- Direct comparisons of normalized V$_{crack}$.

An example of the location and angle of the first diagonal crack for two directly comparable specimens is provided in Figure 4-21. The beam with 0.3% web

reinforcement in both directions cracked at a slightly lower ultimate load and had a slightly steeper diagonal crack.
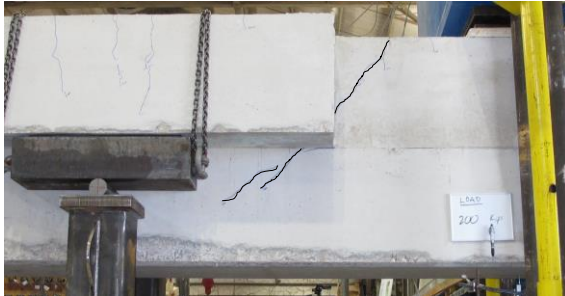
DS1-42-1.85-03: 24% ultimate load   DS1-42-1.85-06: 30% ultimate load

Figure 4-21: First diagonal crack comparison for reinforcement ratio specimens

The maximum diagonal crack widths were examined using all fourteen directly comparable beams as shown in Figure 4-22. It is interesting to note that in half of the comparisons, the web reinforcement ratio did not appear to greatly affect the maximum crack widths in terms of the percentage of the maximum applied load. In the other half of the groups, there was a significant difference. The specimens with a web reinforcement ratio of 0.3% were subjected to a given crack width at a smaller percentage of maximum applied than those with 0.6%. This indicated that inverted-T bent caps with larger amounts of web reinforcement are closer to their ultimate load at a given crack width. Conversely, at a given percent of ultimate load, higher reinforcement ratios result in narrower cracks. The two specimens with mixed reinforcement ratios showed crack widths between those of the two other reinforcement layouts. However, the mixed reinforcement specimen cracks were closer to those of the beams reinforced with 0.3% in both directions.
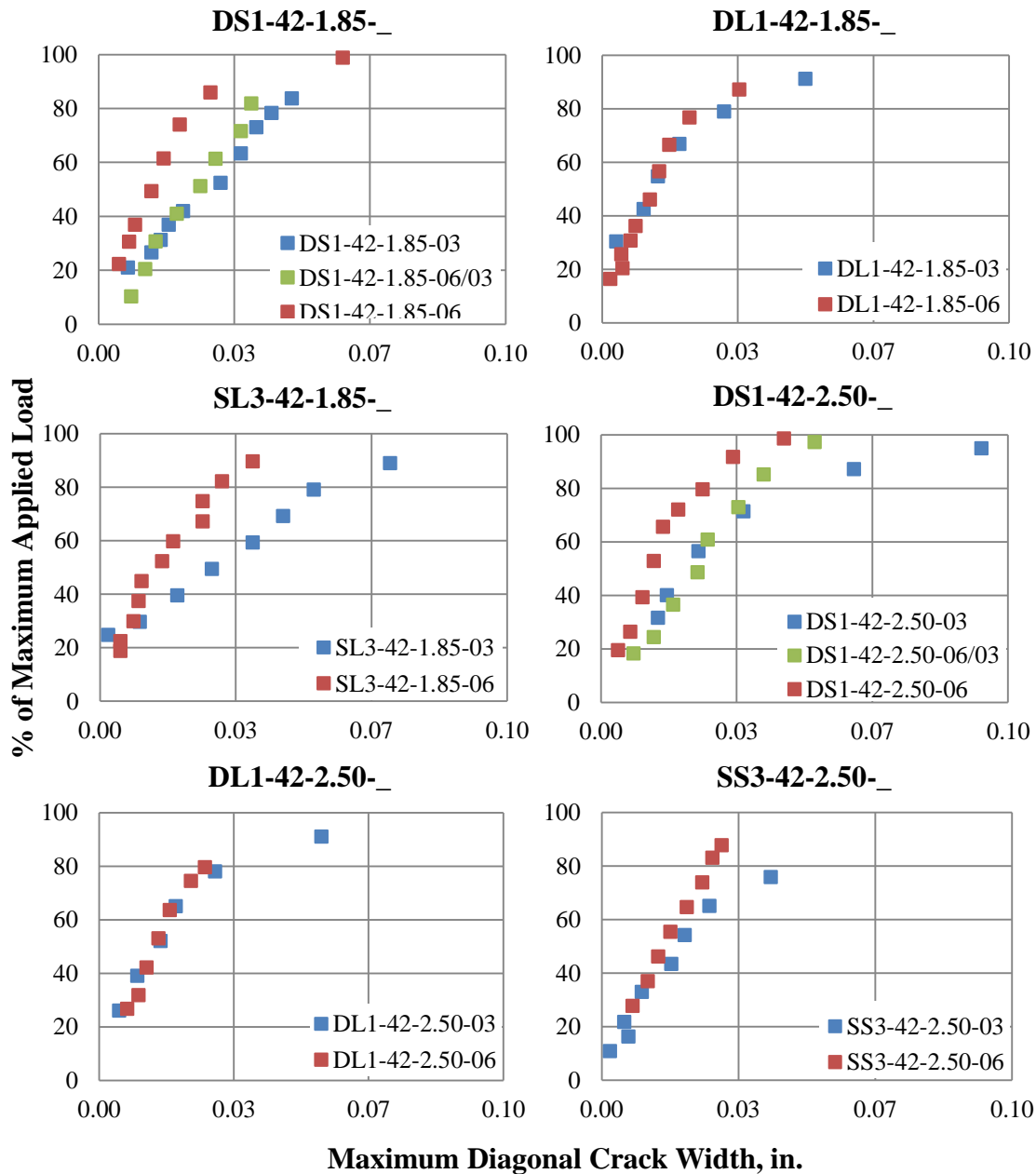
Figure 4-22: Series III: Web Reinforcement- Direct comparisons of crack width progression.

Similar trends can be observed when all test specimen maximum crack widths are investigated. The maximum diagonal crack widths for nineteen specimens from the experimental program that were tested at an a/d ratio of 1.85 are plotted versus the percentage of maximum applied load in Figure 4-23.

Although there is greater scatter in the data for beams with a reinforcement ratio of 0.3% in both orthogonal directions, the general trend clearly shows that quantity of web reinforcement has a direct impact on the width of diagonal cracks. As can be seen in the figure, a larger reinforcement ratio results narrower cracks for a given load ratio. Therefore a beam with 0.6% in each direction is closer to its ultimate capacity at a given crack width than a beam with a reinforcement ratio of 0.3%. The beam with 0.6% in the vertical direction and 0.3% in the horizontal direction had crack widths at lower loads comparable to those of beams reinforced with 0.3% in both directions. As the percentage of maximum applied load increased past 50% however, cracks width of the mixed reinforcement ratio specimens were in-between those of the two uniformly reinforced specimens.
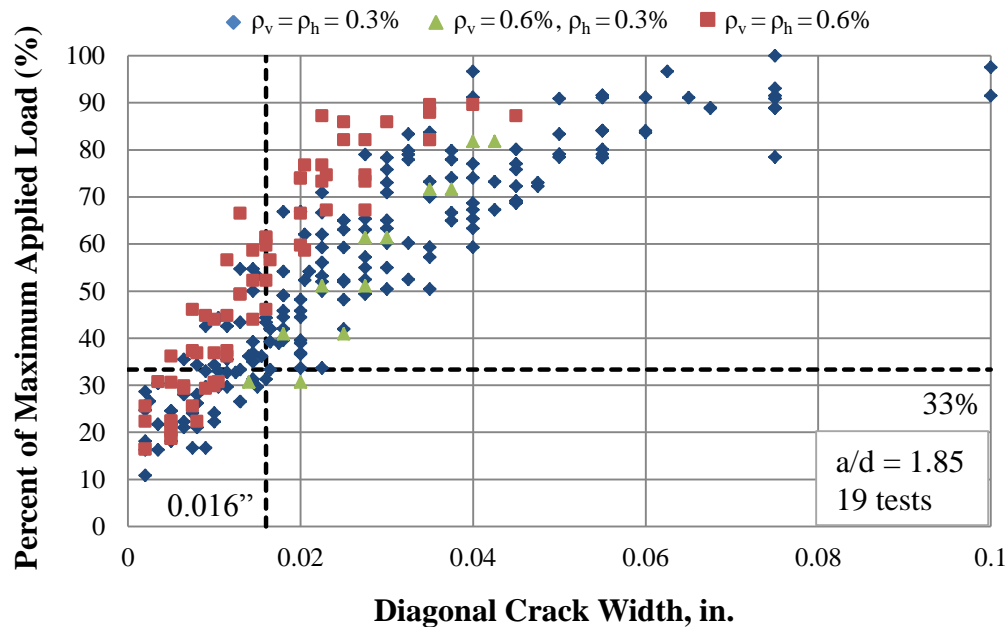
Figure 4-23: Diagonal crack widths for specimens tested at a/d of 1.85

The crack width data in Figure 4-23 can be compared to the crack width limit of 0.016 in. and the estimated service load of 33% ultimate capacity as discussed in Section 4.2.2. At the estimated service load, the maximum diagonal crack widths for the specimens with 0.3% web reinforcement in each direction were at or below the tolerable crack width limit. Near first cracking and at the expected service load, the specimens with 0.6% reinforcement ratio saw a limited reduction in the maximum diagonal crack widths compared with those of the more lightly reinforced specimens. The effects of higher reinforcement ratios only became more significant at load levels higher than service. One can therefore conclude that providing at least 0.3% reinforcement in each orthogonal

direction can adequately restrain the widths of diagonal cracks at service loads. Additional reinforcement beyond the recommended minimum would only have limited effect on crack widths at service level loads. It should be noted that the crack width of 0.016 in. and the estimated service load should not be treated as hard limits, but rather as a general benchmark to gauge the effectiveness of the reinforcement.

Crack width data from fourteen tests with a/d=2.5 are presented in Figure 4-24. Results for the longer shear spans are consistent with observations made for beams tested at an a/d of 1.85; but results showed less scatter.
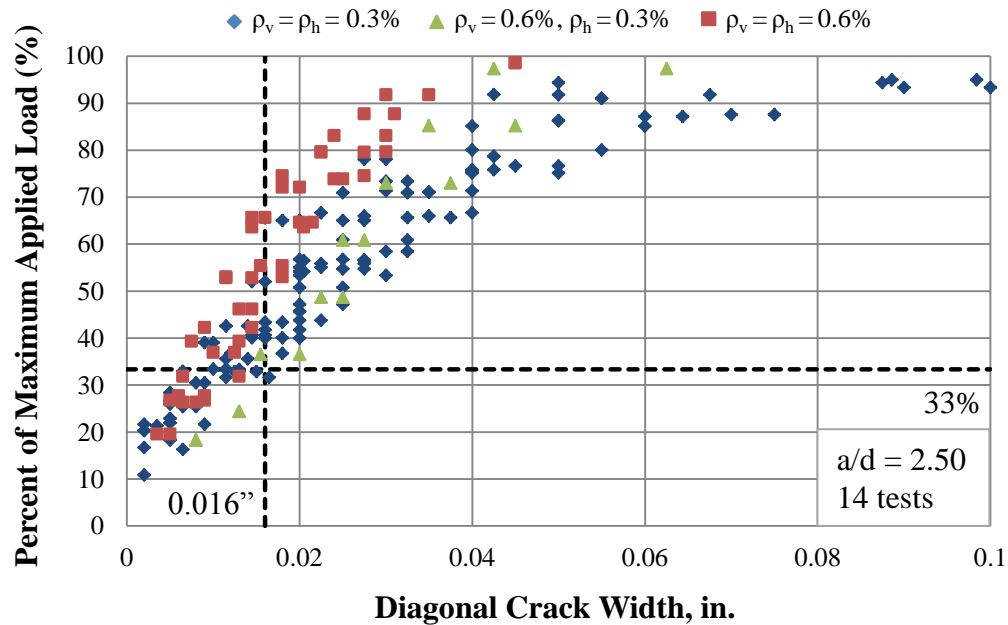
Figure 4-24: Diagonal crack widths for specimens tested at a/d of 2.50

As shown in Figure 4-25, increased amounts of web reinforcement was also shown to affect the crack distribution. It is understood that as the reinforcement ratio increased, the width of shear cracks is reduced (Figure 4-22) and the distribution becomes more spread out. This is confirmed for inverted-T beams as well by the increased amount of cracking in specimen SC3-42-1.85-06 shown in Figure 4-25. Not only did the additional stirrups and skin reinforcement increase the shear capacity of the specimens, it also delayed first yield of the web reinforcement slightly.
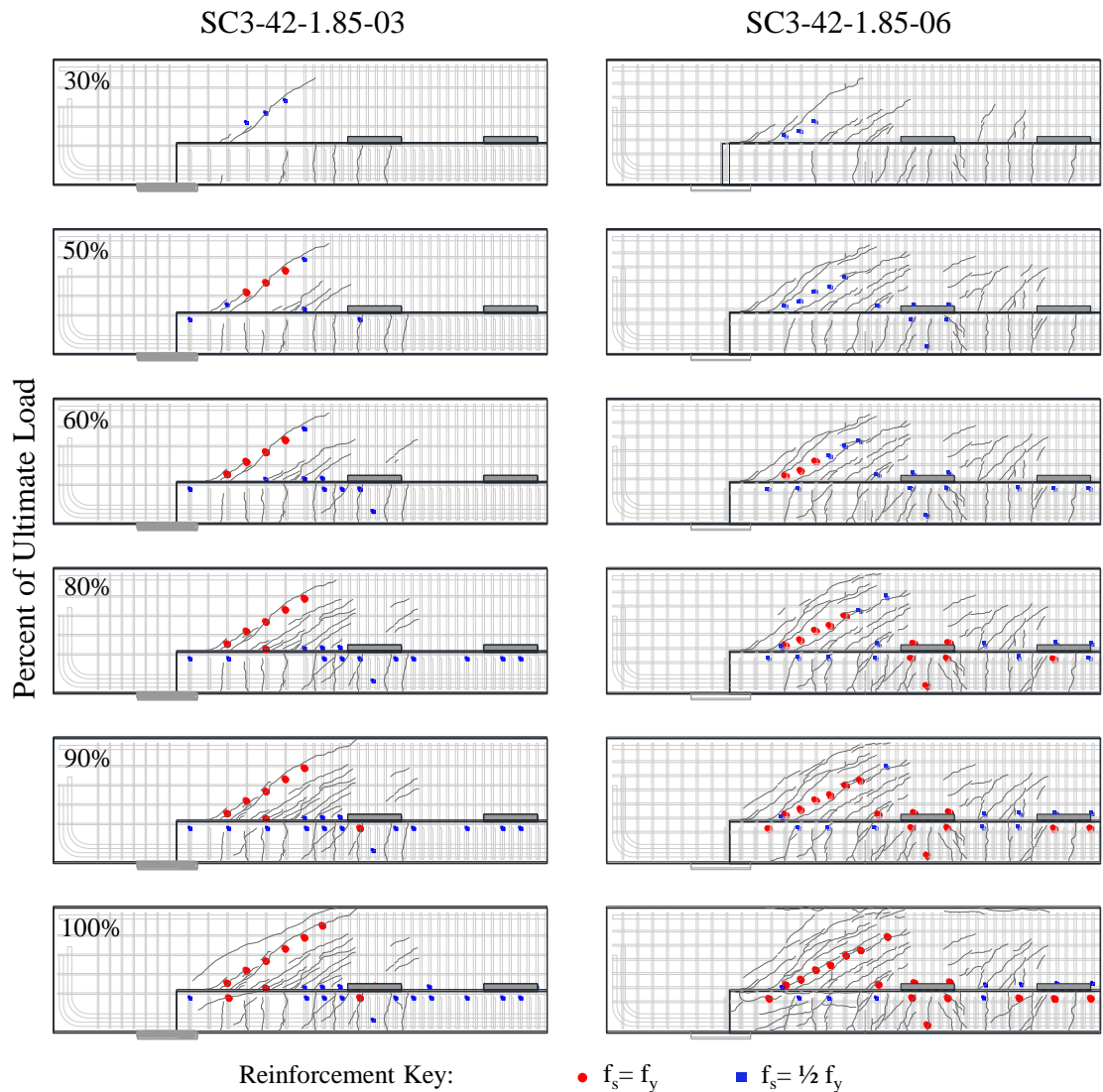
Figure 4-25: Crack patterns and strain gauges for SC3-42-1.85-_ (reinforcement varies)

4.5.4   Summary

The influence of the amount of web reinforcement on the strength, appearance of first diagonal crack, and the progression of the maximum crack width was investigated. Increasing the web reinforcement ratio was found to increase shear strength of inverted-T beams, both at a/d ratios of 1.85 and 2.50. The reinforcement ratio had little effect on the diagonal cracking load. Larger amounts of web reinforcement were found to better restrain the widths of diagonal cracks. Consequently, inverted-T beams with higher levels of web reinforcement are more likely to be closer to their ultimate capacity at a given crack width than those with a lower reinforcement ratio.

The minimum reinforcement ratio of 0.3% in each orthogonal direction recommended by TxDOT Project 0-5253 for adequate crack width restraint in deep beams was also found to adequately restrain cracks at service loads in inverted-T beams.

4.6 SERIES IV: NUMBER OF POINT LOADS

In this section, the effect of multiple point loads on the strength and serviceability behavior of inverted-T beams is investigated. In order to quantify the effect of multiple girders framing into bridge bent caps, twelve specimens were tested with either one load point or three load points along the length of the beam.

4.6.1 Experimental Results

Twelve tests were grouped into six pairs of directly comparisons in which the number of point loads, either one or three, was the only parameter that was varied. A summary of the experimental results from the number of point loads series is provided in Table 4-5. The strength results are normalized as discussed in Section 4.2.1.

Table 4-5: Series IV: Number of Point Loads- Experimental results.

Comparison	Specimen	f'_c (psi)	V_{test} (kip)	$\dfrac{V_{test}}{f'_c b_w d}$	$\dfrac{V_{test}}{\sqrt{f'_c} b_w d}$	V_{crack} (kip)	$\dfrac{V_{crack}}{\sqrt{f'_c} b_w d}$
SS_-42-1.85-03	SS1-42-1.85-03	5721	583	0.13	9.75	NA	NA
	SS3-42-1.85-03	5891	523	0.11	8.62	126	2.08
DS_-42-1.85-03	DS1-42-1.85-03	5258	712	0.17	12.42	172	2.99
	DS3-42-1.85-03	4568	454	0.13	8.49	164	3.07
DL_-42-1.85-03	DL1-42-1.85-03	4929	626	0.16	11.28	242	4.36
	DL3-42-1.85-03 (f)	4202	629	0.19	12.27	276	5.39
SC_-42-2.50-03	SC1-42-2.50-03 (r)	4281	319	0.09	6.18	NA	NA
	SC3-42-2.50-03	5873	329	0.07	5.44	113	1.87
SS_-42-2.50-03	SS1-42-2.50-03	5703	398	0.09	6.67	157	2.63
	SS3-42-2.50-03	5891	447	0.10	7.38	140	2.31
DS_-42-2.50-03	DS1-42-2.50-03	5389	406	0.10	6.99	NA	NA
	DS3-42-2.50-03	5687	430	0.10	7.21	143	2.40

(f) Flexural failure
(r) Shear friction failure

It is important to note that all specimens in this series failed in web shear except DL3-42-1.85-03 and SC1-42-2.50-03, which failed in flexure and shear friction respectively. The value reported for V_{test} is the maximum shear carried at the critical section at the onset of failure, regardless of the failure mode.

4.6.2 Strength Results

Direct comparisons of the strength results are provided in Figure 4-26 and Figure 4-27. V_{test} is normalized by $f'_c b_w d$ in Figure 4-26 and by $\sqrt{f'_c} b_w d$ in Figure 4-27. In each subplot the results are compared for specimens in which every parameter was kept constant except the number of point loads.

(f) Flexural failure
(r) Shear friction failure of the web-to-ledge interface
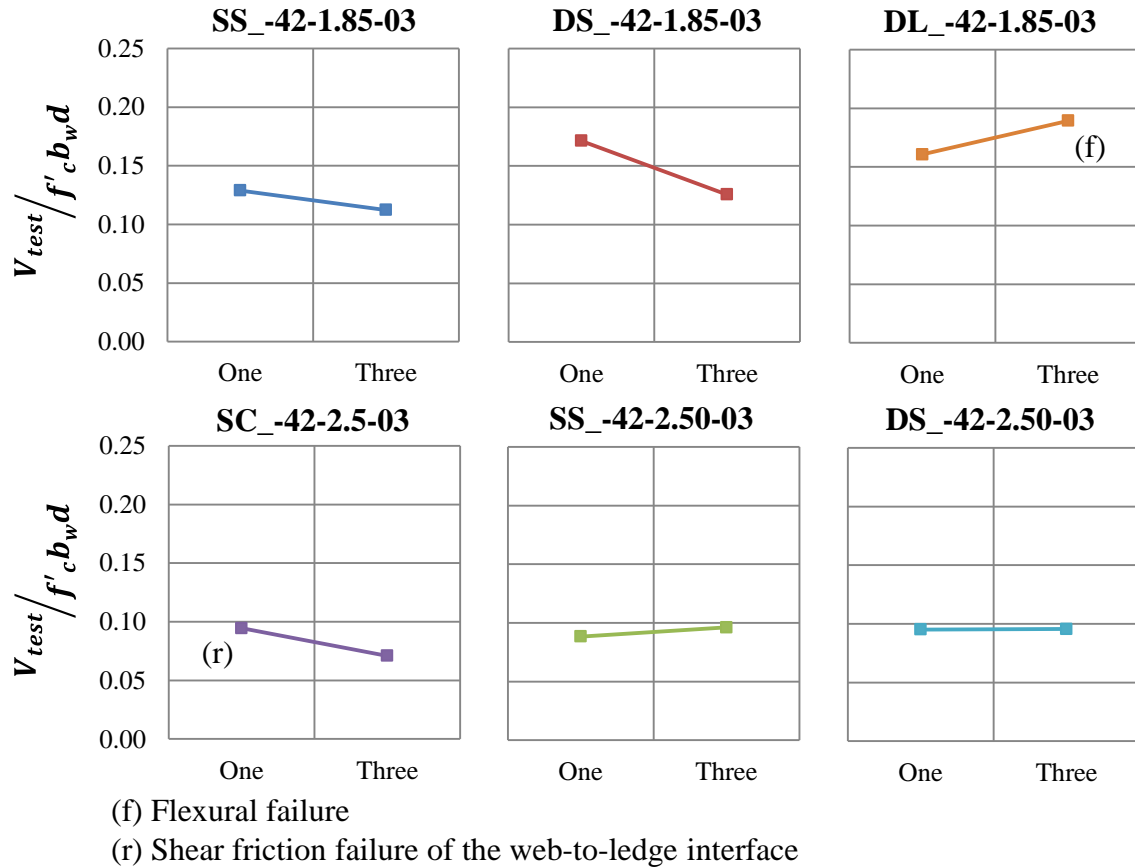
Figure 4-26: Series IV: Number of Point Loads- Direct comparisons of V_test normalized by f'_cb_wd.

Only two comparisons, DS_-42-1.85-03 and DL_-42-1.85-03, in Figure 4-26 and Figure 4-27 show a significant difference between the strength of the two directly comparable specimens. These specimens, however, reveal contradictory trends. The remaining plots suggest similar strengths for specimens with one and three point loads. Observations from the results indicated that the number of point loads does not have an appreciable effect on the strength of the inverted-T specimens within the range of parameters studied. This is a significant observation as experimental specimens are often tested with one point load due to laboratory restrictions, whereas in-service bent caps support multiple bridge girders. Since the number of loads did not affect the shear strength of the

specimens, test results from single point load specimens can be confidently used to develop design recommendations for beams subjected to multiple concentrated loads.

(f) Flexural failure
(r) Shear friction failure of the web-to-ledge interface
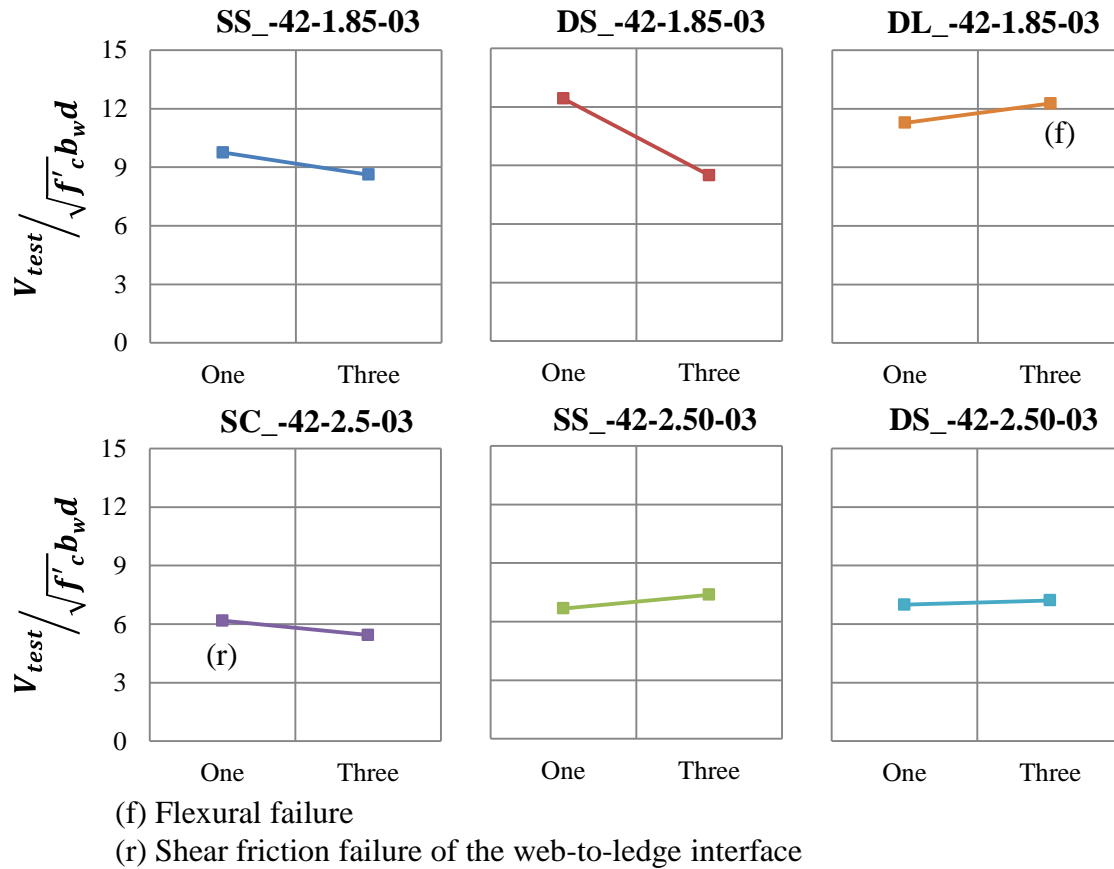
Figure 4-27: Series IV: Number of Point Loads- Direct comparisons of V_{test} normalized by $\sqrt{f'_c}b_wd$.

Not only was the normalized shear strength unaffected by the addition of load points, the failure mode was also unchanged. For beams tested at an a/d ratio of 2.50, yielding of the stirrups, consistent with a two panel tie failure, was observed to be the dominate failure mechanism. For the specimens tested at an a/d ratio of 1.85, crushing of the direct strut and the corresponding strut-to-node interfaces occurred for one and three point load tests. Therefore it can be concluded that shifting the center of the applied load further from the support for specimens with three loading points did not change the behavior of the inverted-T specimens.

4.6.3 Serviceability Results

First cracking loads, normalized by $\sqrt{f'_c}b_w d$, for the series are presented in Figure 4-28. The first cracking load of six tests were available for three pairs of comparable specimens in which every parameter was kept constant except the number of loading points.
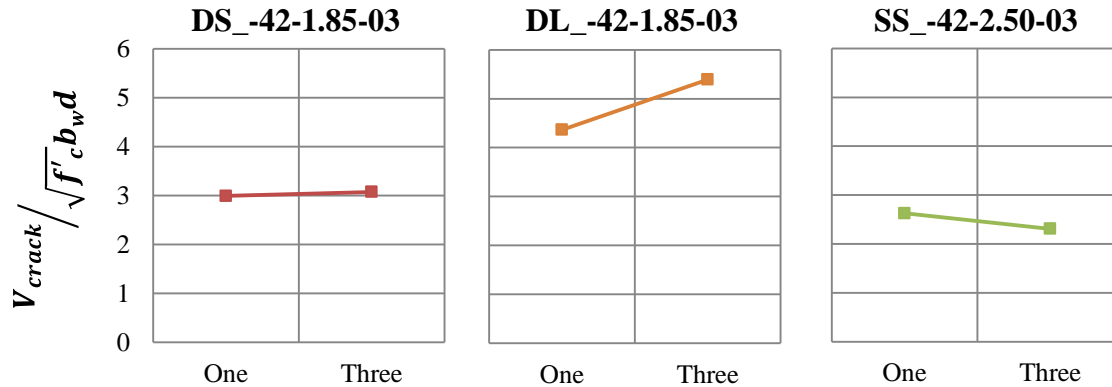
Figure 4-28: Series IV: Number of Point Loads- Direct comparisons of V$_{crack}$.

No clear trend is indicated by the results in Figure 4-28. One comparison shows a similar normalized cracking load, while another shows an increase, and the third indicated a slight decrease when the inverted-T beam was subjected to multiple point loads. Similar crack angles, with the beam tested at one point being slightly steeper are shown in Figure 4-29. It does, however show an increase in the percentage of ultimate load at which the first diagonal crack occurred. Based on these limited results it appears that no trend exists between the number of point loads and the load at which an inverted-T beam is likely to crack due to shear forces.

DS1-42-1.85-03: 24% ultimate load   DS3-42-1.85-03: 36% ultimate load
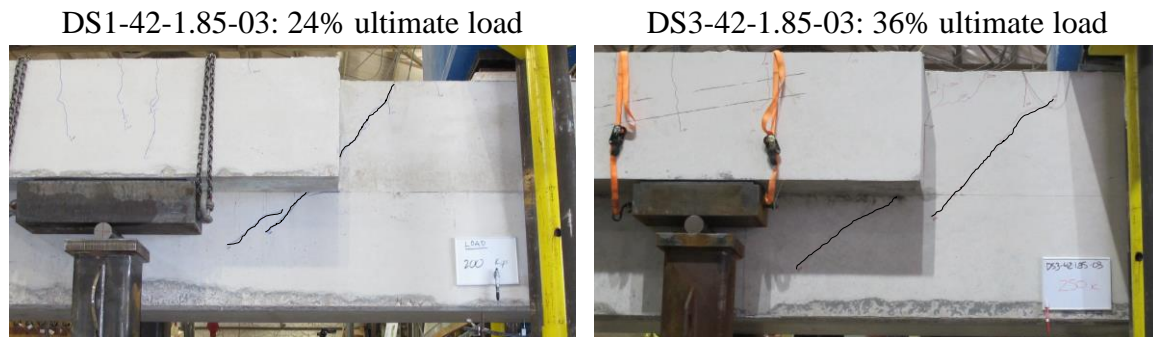
Figure 4-29: First diagonal crack comparison for number of point load specimens

The serviceability performance of the test specimens was also evaluated by plotting the progression of the maximum width of the diagonal cracks (Figure 4-30). No trend relating crack width progression and number of point loads can be observed in Figure 4-30. Therefore it can be concluded that multiple point loads do not have a significant

effect on the progression of crack widths with respected to the percentage of ultimate capacity. This confirms the applicability of experimental serviceability results from single point loaded specimens to in-service members subjected to multiple loads.
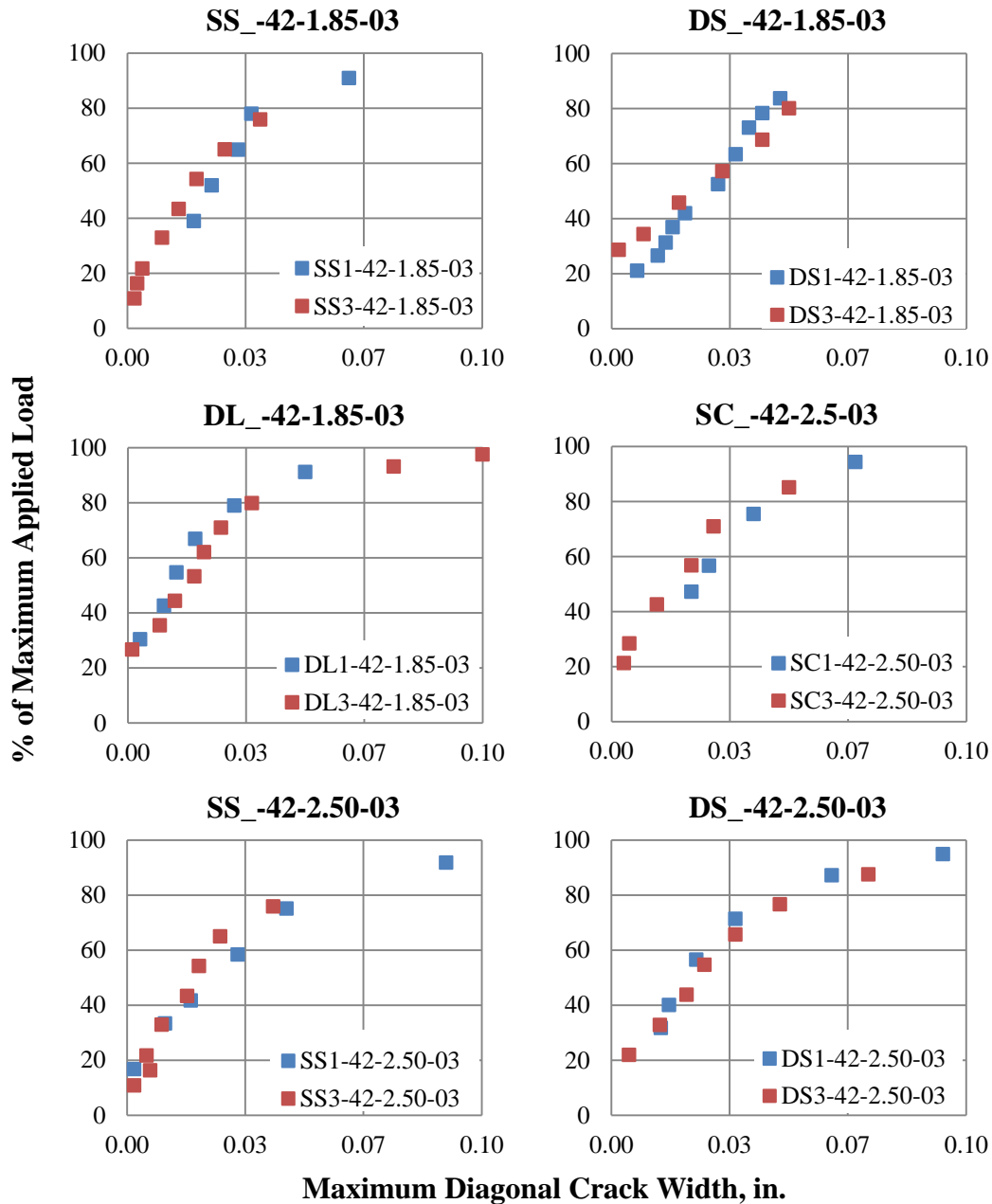
Figure 4-30: Series IV: Number of Point Loads- Direct comparisons of crack width progression.

As with the crack width progression, the location and development of cracks at various load stages did not indicated an effect due to the number of point loads as shown in

Figure 4-31. In general the cracks have the same angle of inclination and distribution between the two specimens compared in the figure. The arching action, or formation of the bottle-shaped strut, can be seen in the crack patterns of both figures, with a clearer picture in SS1-42-1.85-03. It should be noted that this was the second test on this beam so the one point loaded specimen did have a few preexisting cracks (marked in lighter gray).
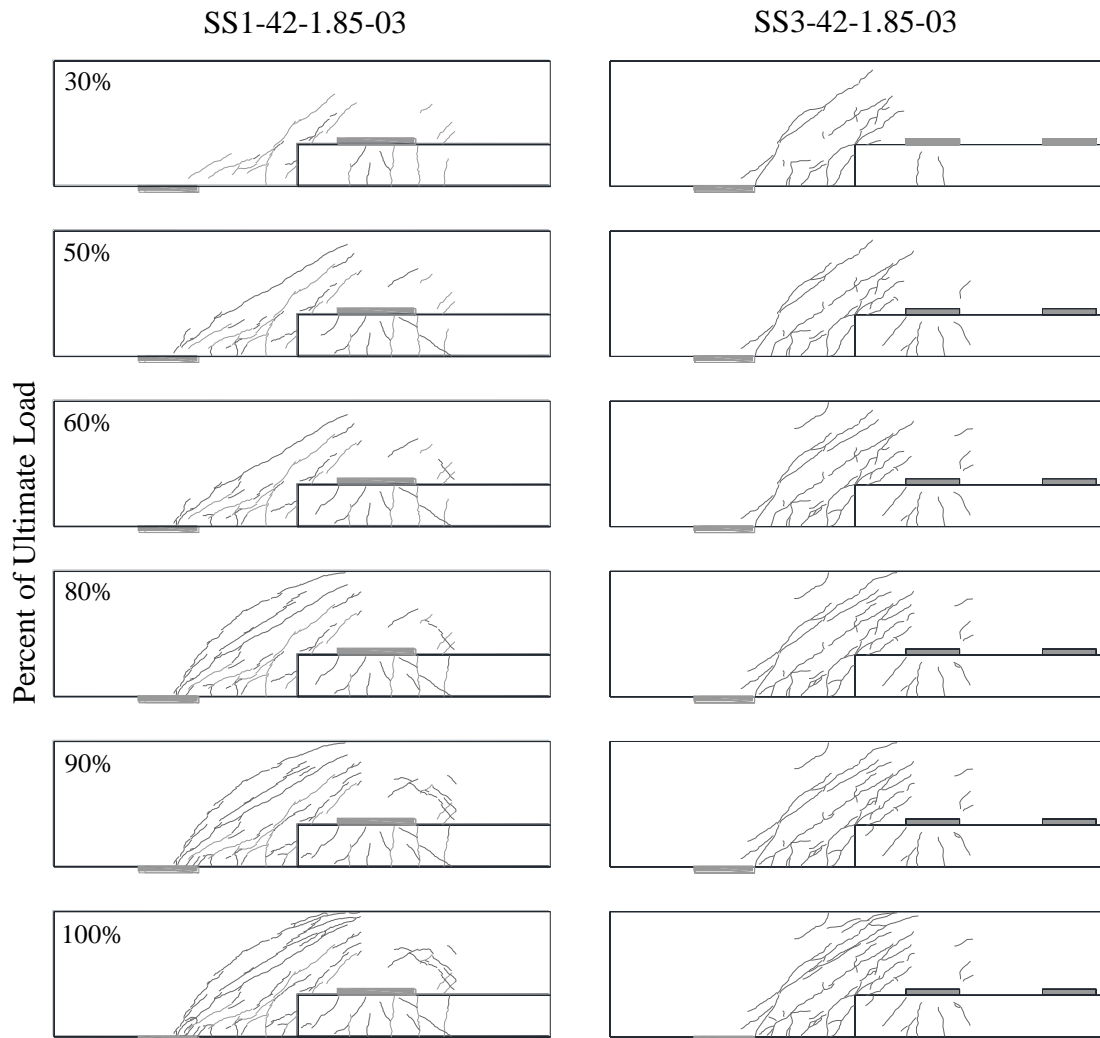
Figure 4-31: Crack patterns for SS_-42-1.85-03 (number of point loads varies)

4.6.4   Summary

The direct comparisons presented in this section have shown that the number of point loads has a negligible effect on the strength and the appearance of the first diagonal crack. No effect was observed on the crack width progression or crack distribution of inverted-T beams with the application of increasing loads.

4.7 SERIES V: WEB DEPTH

The effects of web depth on the strength and serviceability behavior of inverted-T beams, are presented in this section. The purpose of this series is to extend the conclusions drawn for the 42 in. deep specimens to larger inverted-T bent caps. Most of the specimens in the experimental program were constructed with a total depth of 42 in. Two beams had total depth of 75 in. and are discussed in in light of results from tests on the 42 in. deep specimens.

4.7.1 Strength Results

Although no comparable large-scale inverted-T tests were available in the literature, an investigation on the effect of web depth on compression-chord loaded beams was performed by TxDOT Project 0-5253. Based on previous research studies, the length of the bearing plates appeared to affect the strength results of deep beams as the effective depth increased. Rather than link the size of the bearing plates to the depth of the member, the plate dimensions were selected to create similar size nodal regions for each section depth.

The four tests, two of each depth, discussed in this section are summarized in Table 4-1. The strength results are normalized as discussed in Section 4.2.1.

Table 4-6: Series VI: Web Depth- Experimental results.

Comparison	Specimen	f'_c (psi)	V_{test} (kip)	$\dfrac{V_{test}}{f'_c b_w d}$	$\dfrac{V_{test}}{\sqrt{f'_c} b_w d}$	V_{crack} (kip)	$\dfrac{V_{crack}}{\sqrt{f'_c} b_w d}$
SS1-_-1.85-03	SS1-42-1.85-03	5721	583	0.13	9.75	NA	NA
	SS1-75-1.85-03	2867	745	0.18	9.72	346	4.51
SS1-_-2.50-03	SS1-42-2.50-03	5703	398	0.09	6.67	157	2.63
	SS1-75-2.50-03 (p)	5158	649*	0.09	6.31	225	2.19

(p) Punching shear failure

*Although this beam failed due to punching shear, it was determined to be within 10% of its ultimate capacity and the maximum measured shear is reported herein.

Direct comparisons of the strength results of two pairs of specimens are provided in Figure 4-32 and Figure 4-33. As discussed in Section 4.2.1, V_{test} is normalized by $f'_c b_w d$ in Figure 4-26 and by $\sqrt{f'_c} b_w d$ in Figure 4-27. It is interesting to note that for the specimens tested at an a/d of 1.85, there was an increase in shear strength when normalized by $f'_c b_w d$ in the first figure, but the shear strength is essentially equal when they are normalized by $\sqrt{f'_c} b_w d$. For the specimens tested at an a/d ratio of 2.50, there was essentially no difference between the normalized strength for the 42 in. and 75 in. deep

beams. Given the limited data set, a definitive conclusion cannot be made regarding beam size effects. However, it appears that there are no significant size effects within the size range tested. This indicates that strength results from 42 in. deep beams are applicable to larger beams.

SS1-_-1.85-03   **SS1-_-2.50-03**

(p) Punching shear failure
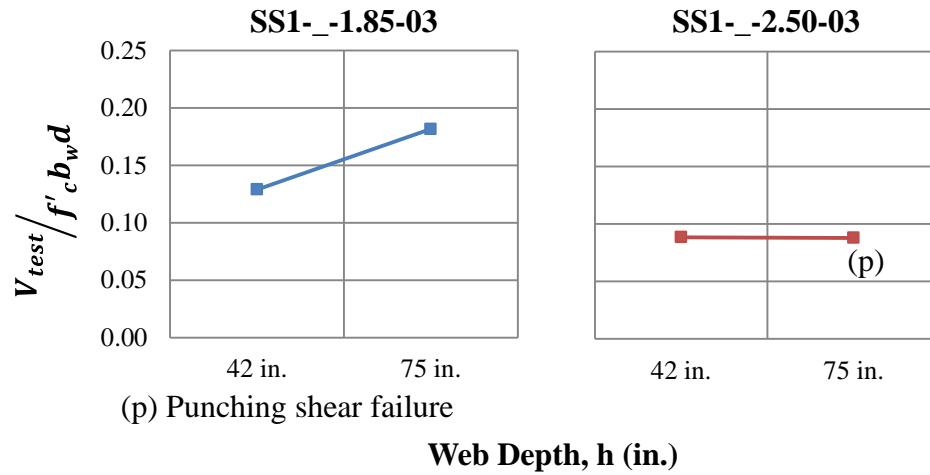
Web Depth, h (in.)

Figure 4-32: Series VI: Web Depth- Direct comparisons of V_{test} normalized by $f'_c b_w d$.

SS1-_-1.85-03   **SS1-_-2.50-03**

(p) Punching shear failure
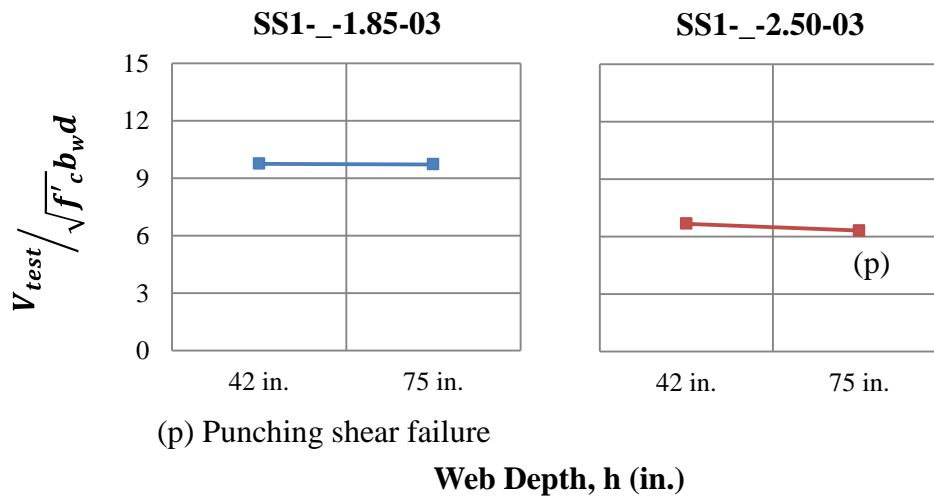
Web Depth, h (in.)

Figure 4-33: Series VI: Web Depth- Direct comparisons of V_{test} normalized by $\sqrt{f'_c} b_w d$.

4.7.2 Serviceability Results

The diagonal cracking loads for the web depth series is presented in Figure 4-34. The first cracking load, $V_{crack,}$ was not available for specimen SS1-42-1.85-03 so only one comparison can be made for the first diagonal cracking with respect to different web depths. As shown in Figure 4-34, there is a slight decrease in the normalized first cracking load with an increase in web depth.

SS1-_-2.50-03
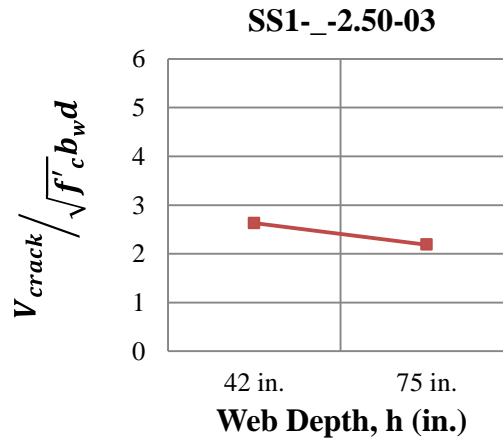
Figure 4-34: Series VI: Web Depth- Direct comparisons of V_{crack} normalized by $\sqrt{f'_c}b_w d$.

Comparing the angle and location of the first diagonal crack shows a very similar result in Figure 4-35. The percentage of ultimate load at the appearance of the first crack were also almost identical. Based on the limited data and conclusions from the compression-chord study, web depth does not appear to be a factor in the diagonal cracking load of an inverted-T beam.
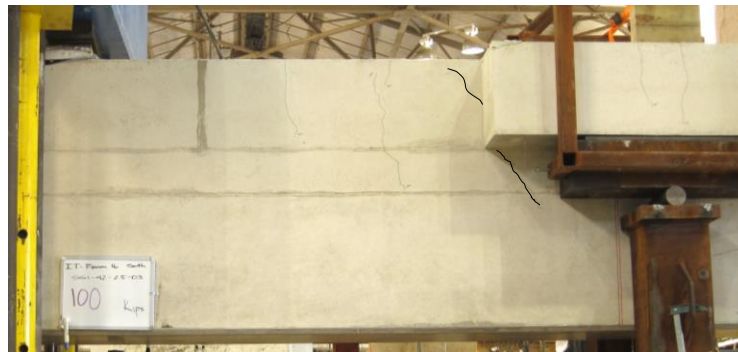
SS1-42-2.50-03: first crack at 39% ultimate load
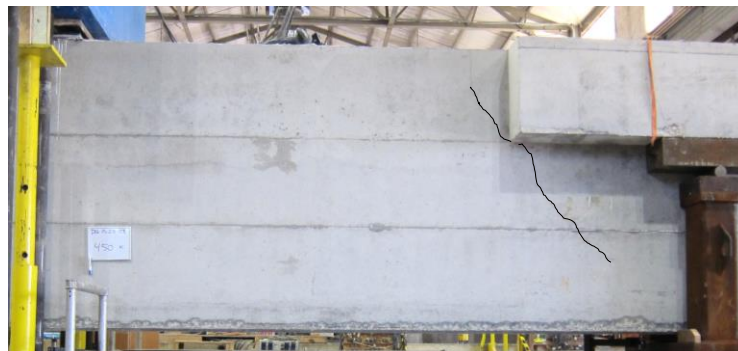
SS1-75-2.50-03: first crack at 35% ultimate load

Figure 4-35: First diagonal crack comparison for web depth specimens

The maximum diagonal crack widths are presented for the directly comparable specimens in Figure 4-36. It is interesting to note that regardless of the a/d ratio, there is no noticeable difference between the crack width progression of the 42-in. and 75-in. beam. This is an important observation as the relationship between the maximum diagonal crack width and the reserve strength does not depend on the depth of the inverted-T beam. Thus a correlation between the diagonal crack width and the ultimate capacity of a member can be made regardless of the height of the bent cap.
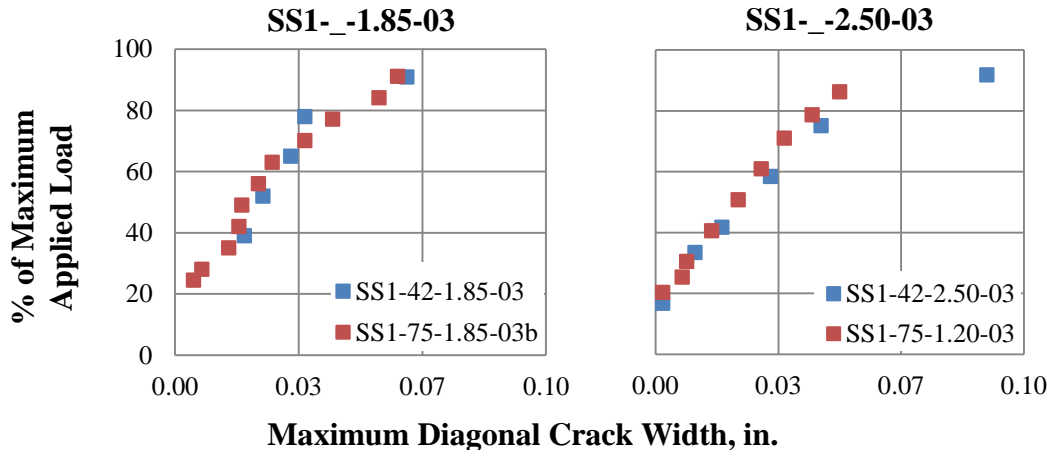
Figure 4-36: Series VI: Web Depth- Direct comparisons of crack width progression.

The plot of the maximum crack widths of the four specimens discussed in this section versus the corresponding percent of maximum applied load are presented in Figure 4-37. All four specimens had reinforcement ratios of 0.3% in each orthogonal direction. No trend could be discerned in crack width progression for the two web depths. The results readily suggest that the width of diagonal cracks are not dependent on web depth at a given percentage of maximum applied load as the data is pretty much indistinguishable for the four beams.
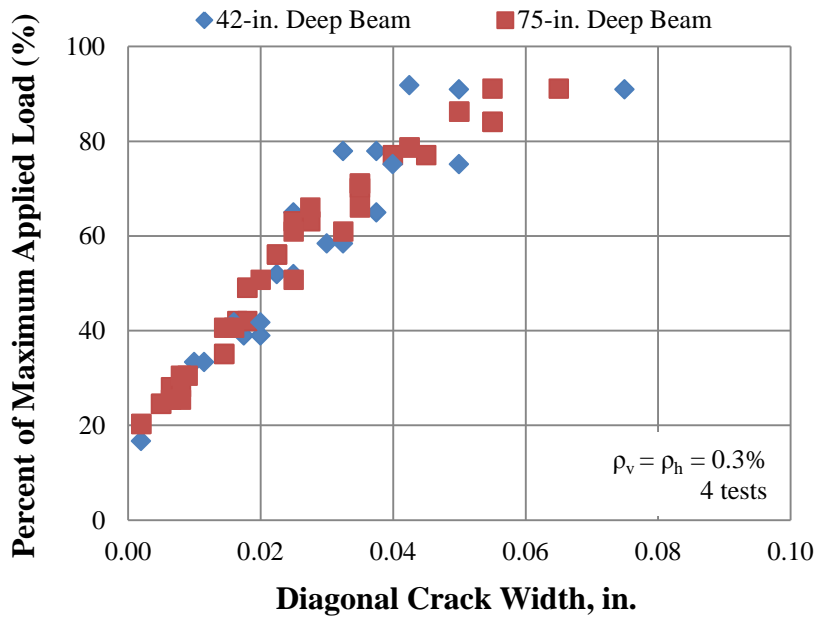
Figure 4-37: Diagonal crack widths for specimens with 0.3% reinforcement both directions

The distribution of cracks at various load stages is shown in Figure 4-38. Although a larger number of cracks form on the 75-in. deep specimen, the spacing between cracks and the overall pattern is very similar between the two beams. The cracks begin forming in a direct strut between the corner of the support plate and the area above the load plate. As the load is increased and the strut begins to spread, additional cracks form in an arching shape similar to the assumed bottle-shape of the strut.

SS1-42-1.85-03   SS1-75-1.85-03

30%

50%

60%

Percent of Ultimate Load

80%

90%

100%
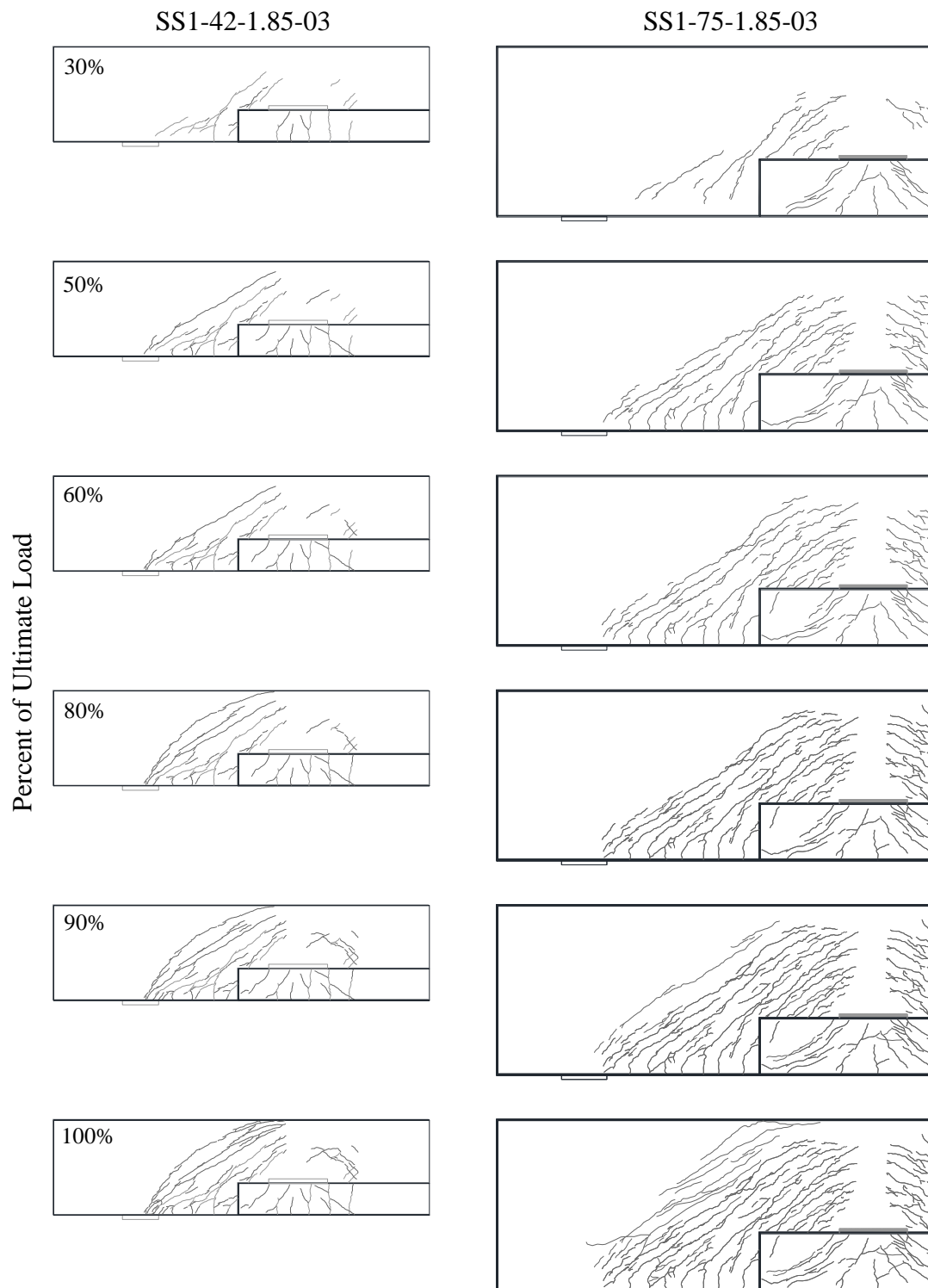
Figure 4-38: Crack patterns for SS1-_-1.85-03 (web depth varies)

106

4.7.3 Summary

From the limited direct comparisons between 75-in. and 42-in. deep beam tests performed in the experimental program, no notable effect of web depth was discovered on the strength and serviceability behavior of the inverted-T beams. Increasing the web depth appeared to increase the shear strength of the beam tested at an a/d ratio of 1.85, but only when normalized by $f'_c b_w d$. No difference was noted when it was normalized by $\sqrt{f'_c} b_w d$ or for the beam tested at an a/d ratio of 2.50 regardless of the normalization technique; which suggests that size effect was not an issue for these large-scale beams.

A slight but otherwise insignificant decrease in the first cracking load was observed for the 75-in. beam. There was also no effect on the correlation between the maximum crack width and the percent of maximum applied load. The larger beam did experience more cracking than the 42-in. beam but the overall spacing and pattern were the same.

4.8 SERIES VI: LOADED CHORD

The loaded chord series was created to examine the important strength and serviceability differences in behavior between tension- and compression-chord loaded beams. As previously discussed, loading on the ledge of an inverted-T beam induces additional tensile forces into the web that could result in changes of the behavior of the beam.

In the TxDOT Project 0-5253, different variables were examined in order to develop the strut-and-tie modeling provisions. This resulted in beams with various depths, web widths, reinforcement ratios, number of stirrup legs, bearing and loading plate sizes, and a/d ratios. Because some of these objectives differ greatly from the current project, which focuses more on ledge geometry, reinforcement ratio, and number of point loads, many of the tests from Project 0-5253 cannot be used in this comparison. Only rectangular beams with 21 in. web width, 42 in. or 75 in. web depth, 0.3% web reinforcement, and a/d ratios of 1.85 and 2.50 are included in this series.

Due to a lack of rectangular beams with 0.6% web reinforcement in both directions, a 42 in. specimen, C1-42-1.85-06, was constructed and loaded on its compression chord at an a/d ratio of 1.85. Section 3.2.7 provides additional background information on the loaded chord series.

4.8.1 Strength Results

The experimental strength of the twenty one beams examined in this test series is summarized in Table 4-7. Fourteen inverted-T beams were compared to seven compression-chord loaded specimens in four similar groups in Figure 4-39 and Figure 4-40. All variables presented in the table are defined in Section 4.2. The strength results were normalized as discussed in Section 4.2.1

Table 4-7: Series VI: Loaded Chord- Experimental results.

Comparison	Specimen	f'_c (psi)	V_{test} (kip)	$\dfrac{V_{test}}{f'_c b_w d}$	$\dfrac{V_{test}}{\sqrt{f'_c} b_w d}$	V_{crack} (kip)	$\dfrac{V_{crack}}{\sqrt{f'_c} b_w d}$
_1-42-1.85-03	DC1-42-1.85-03	4303	517	0.15	9.97	127	2.45
	DS1-42-1.85-03	5258	712	0.17	12.42	172	2.99
	DL1-42-1.85-03	4929	626	0.16	11.28	242	4.36
	SC1-42-1.85-03 (le)	4330	463	0.14	8.90	N/A	N/A
	SS1-42-1.85-03	5721	583	0.13	9.75	N/A	N/A
	III-1.85-03[1]	4990	412	0.10	7.20	137	2.39
	III-1.85-03b[1]	3300	471	0.18	10.12	114	2.45
	I-03-2[1]	5240	569	0.13	9.73	144	2.45
	I-03-4[1]	5330	657	0.15	11.14	N/A	N/A
_1-75-1.85-03	SS1-75-1.85-03b	2867	745	0.18	9.72	346	4.51
	IV-2175-1.85-03[1]	4930	842	0.12	8.29	218	2.15
_1-42-1.85-06	DC1-42-1.85-06	3727	519	0.18	10.76	107	2.23
	DS1-42-1.85-06	5024	621	0.16	11.09	188	3.35
	DL1-42-1.85-06	4830	741	0.19	13.48	168	3.06
	C1-42-1.85-06[2]	3727	637	0.22	13.21	N/A	N/A
_1-42-2.50-03	DC1-42-2.50-03	4035	365	0.11	7.28	70	1.40
	DL1-42-2.50-03	4929	510	0.13	9.19	N/A	N/A
	SC1-42-2.50-03 (r)	4281	319	0.09	6.18	N/A	N/A
	SS1-42-2.50-03	5703	398	0.09	6.67	157	2.63
	SL1-42-2.50-03	4281	498	0.15	9.62	167	3.24
	III-2.5-03[1]	5030	516	0.13	8.98	N/A	N/A

(le) Ledge tie failure

(r) Shear friction failure

[1] Compression-chord loaded rectangular beam from TxDOT Project 0-5253

[2] Compression-chord loaded rectangular beam from TxDOT Project 0-6416

Web shear failure was not achieved in two beams in this series due to inadequate ledge capacity. SC1-42-1.85-03 (le) failed due to ledge tie yielding and SC1-42-2.50-03 (r) failed due to shear friction failure. Both of these beams exceeded the predicted shear capacity and showed signs of being very close to web shear failure at their ultimate load.

Figure 4-39: Series VI: Loaded Chord- Direct comparisons of V_{test} normalized by f'_cb_wd.
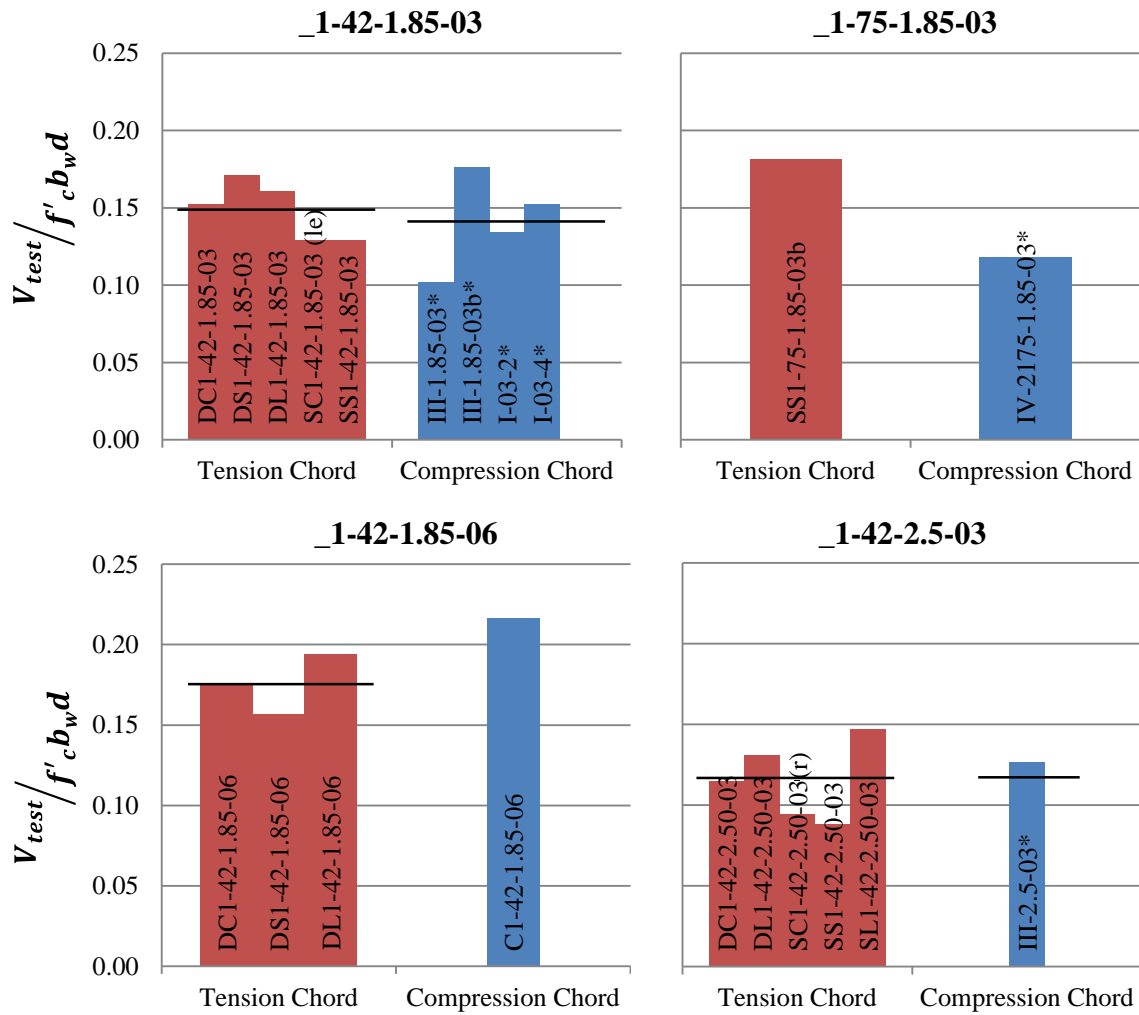
Figure 4-39: Series VI: Loaded Chord- Direct comparisons of V_{test} normalized by $f'_c b_w d$.

No trend is seen amongst the shear strength comparisons normalized by $f'_c b_w d$ in Figure 4-39. A similar lack in trend is shown in Figure 4-40 where the shear strength results were normalized by $\sqrt{f'_c} b_w d$.
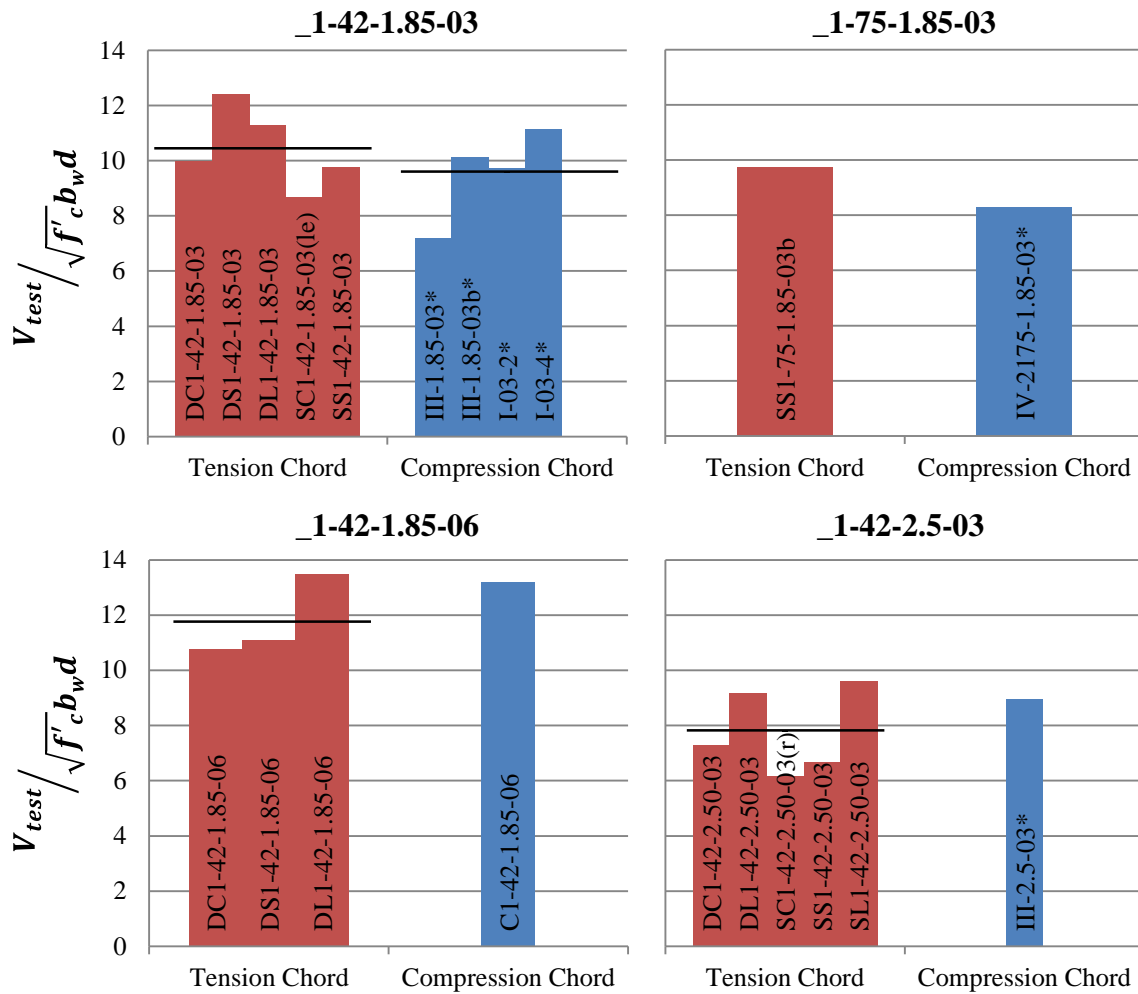
Figure 4-40: Series VI: Loaded Chord- Direct comparisons of V$_{test}$ normalized by $\sqrt{f'_c}$b$_w$d.

4.8.2   Serviceability Results

The diagonal cracking loads and the maximum width of the cracks were used to assess the effect of web reinforcement on the serviceability performance of ledge-loaded inverted-T beams versus rectangular beams loaded on their compression chord.

The available diagonal crack loads for the beams tested in this series were normalized by $\sqrt{f'_c}b_w d$ and plotted in Figure 4-41 by loaded chord. No first cracking loads were available for the compression-chord loaded beams in the _1-42-1.85-06 or _1-42-2.5-03 comparisons, so the corresponding inverted-T beams are omitted from the figure.
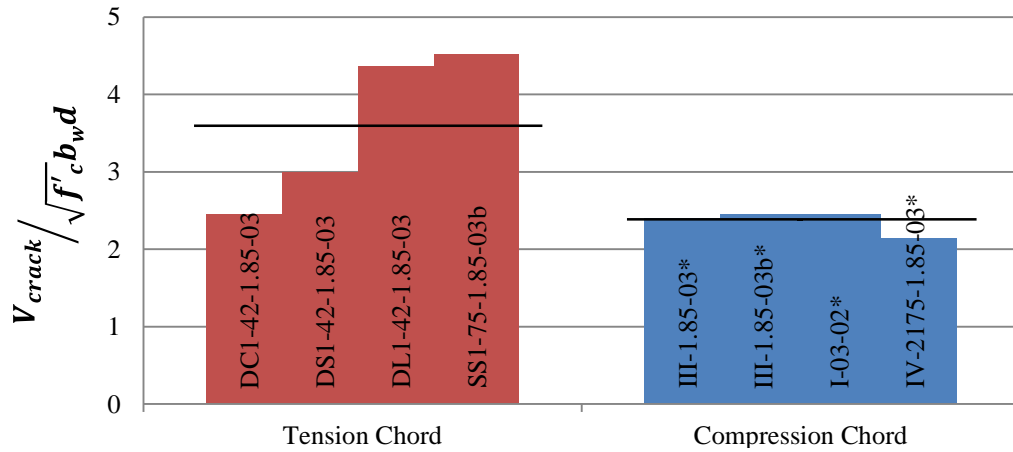
Figure 4-41: Series VI: Loaded Chord – Comparison of V$_{crack}$ normalized by $\sqrt{f'_c}$b$_w$d.

As shown in Figure 4-41, the location of the applied load on the cross section of a member has an effect on the amount of load at which the member cracks. For 42 in. deep beams with short and cutoff ledges, the cracking load is similar to that of compression-chord loaded specimens. Beams with long ledges on the other hand seem to have a larger first cracking load compared to rectangular beams. The 75 in. deep inverted-T beam shown in Figure 4-41 has a larger cracking load than rectangular beam even though it has a short ledge. Overall through, inverted-T beams appear to crack at a higher normalized load than traditional compression-chord loaded beams. Hence rectangular-beam cracking loads can be used as conservative reasonable and conservative estimates of inverted-T beam cracking loads, regardless of ledge geometry.

The maximum diagonal crack widths are plotted versus the corresponding maximum applied load in Figure 4-42. There are several general trends that can be observed in the plots. First, tension-chord loaded beams have more scatter with respect to the maximum diagonal crack width as indicated by the R^2 values from the power trend lines. Secondly, the tension-chord loaded beams tend to have smaller crack widths at a given percentage of ultimate load. This suggests that an inverted-T beam is closer to its ultimate capacity than a compression-chord loaded beam with the same width diagonal crack. This difference is not as clear for the first comparison, _1-42-1.85-03, but the trend is still present.
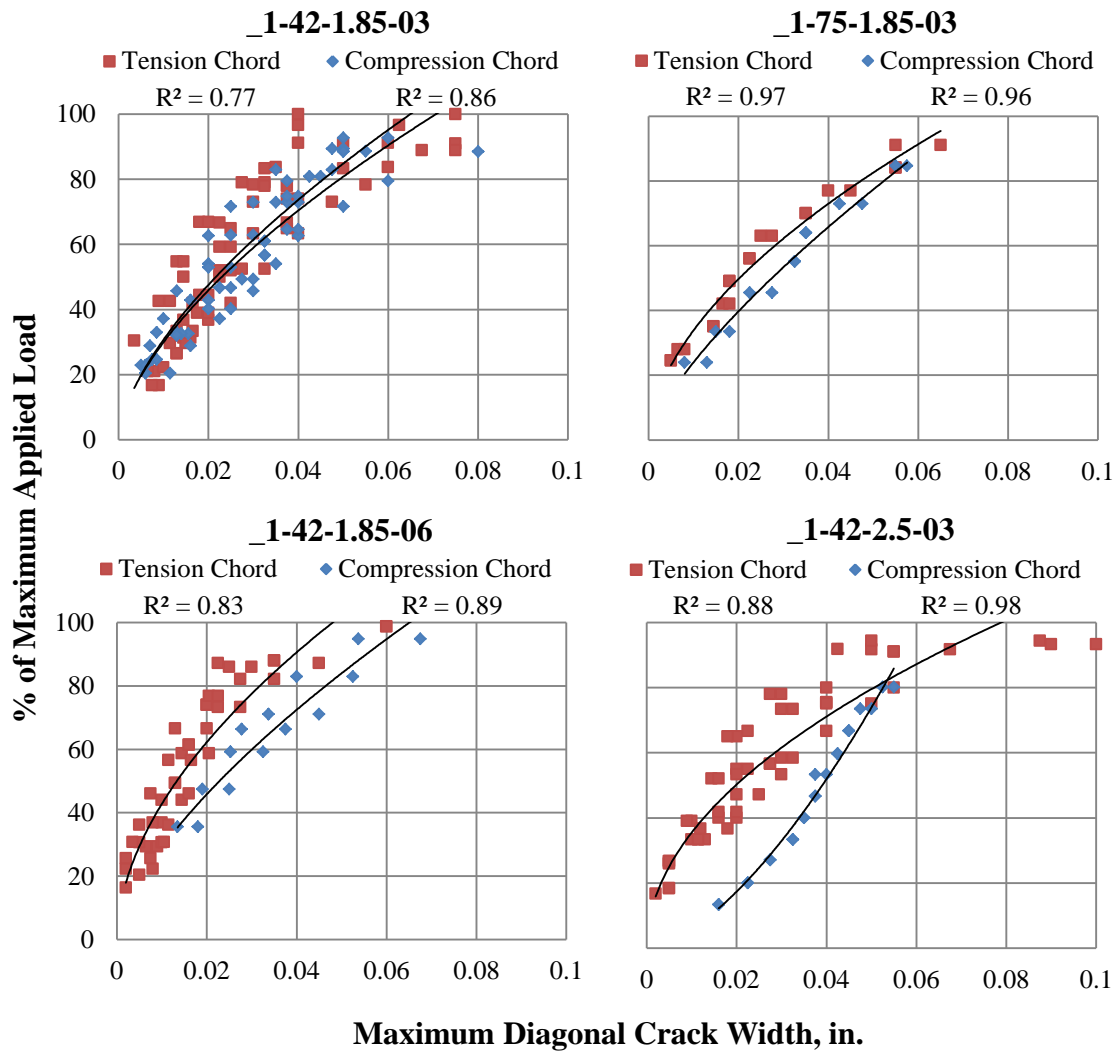
Figure 4-42: Series V: Loaded Chord- Direct comparisons of crack width progression.

The crack widths of the beams discussed in this series are plotted collectively in Figure 4-43. No distinction was made for a/d ratio, reinforcement ratio, or web height. Although there is a significant amount of scatter, there is also a noticeable difference between compression and tension cord loaded beams. This difference varies up to 10% and will be considered in the correlation of maximum diagonal crack width to capacity discussion in Section 5.4.
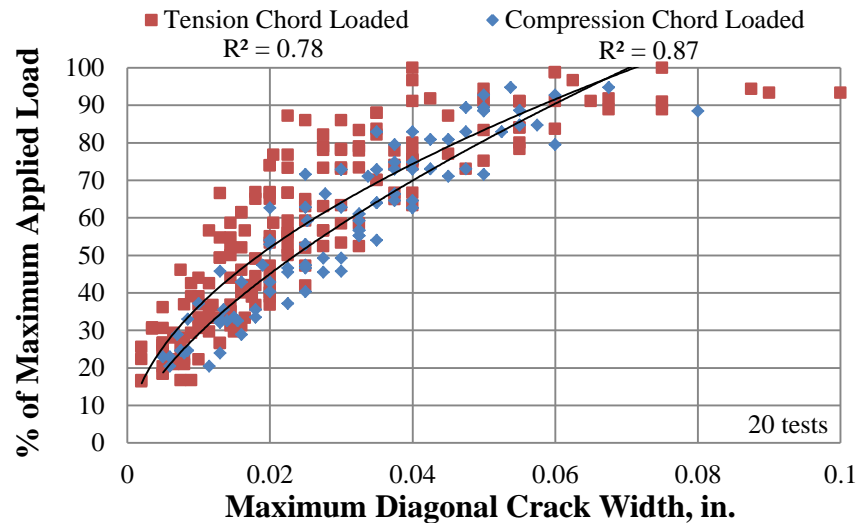
Figure 4-43: Series V: Loaded Chord- General comparisons of crack width progression.

4.8.3 Summary

General observations and direct comparisons have been presented in this section to illustrate the influence of the loaded chord on the strength, appearance of first diagonal crack, and the progression of the maximum crack width with respect to applied load.

It has been shown the applying load closer to the tension chord of a reinforced concrete member does not have a significant effect on its web shear strength. However, when the serviceability behavior is considered there is a noticeable difference. Inverted-T beams with long ledges tend to crack at a higher normalized load than comparable compression-chord loaded members. Inverted-T beams with short or cut-off ledges tend to crack at a similar normalized load than comparable compression-chord loaded members. The progression of diagonal crack widths was also affected by chord loading. The tension-chord loaded beams tended to have greater scatter with respect to the maximum diagonal crack widths but the general trend indicated that inverted-T beams have narrower crack widths at a given percentage of ultimate capacity than comparable compression-chord loaded members. This observation will be investigated further in Section 5.4- correlation of maximum diagonal crack width to member capacity.

4.9 SUMMARY OF EXPERIMENTAL RESULTS

Experimental results of specimens tested within TxDOT Project 0-6416 were included in this chapter. General conclusions regarding the evaluation of strength and serviceability criteria were made based on the normalization of strength results, the shear force at first inclined cracking, and the progression of the maximum diagonal crack widths as

compared to the percent of ultimate applied load. Effects of ledge length, ledge depth, web reinforcement ratio, number of point loads, and web depth were presented in detail.

Increasing the ledge length was observed to increase the shear strength of IT beams and delay the appearance of the first diagonal cracking. Ledge length was found to have no significant effect on crack width progression.

Ledge depth has no significant effect on the strength or crack width progression of inverted-T beams. However, it was observed that increasing the ledge depth delayed the appearance of the first diagonal cracking slightly.

An increased amount of web reinforcement was shown to increase the shear strength of the test specimens and slightly decrease the diagonal cracking load. Similar levels of shear strength increases with increasing reinforcement ratio were observed for specimens with both a/d ratios (i.e., 1.85 and 2.50). A significant effect on the maximum crack width progression was observed, with a greater degree of crack width restraint for specimens with higher web reinforcement ratios. The recommended minimum reinforcement ratio of 0.3% was also shown to adequately control crack widths at service level loads.

Loading inverted-T beams at multiple points resulted in a negligible effect on the shear strength of the member, the diagonal cracking load, and the crack width progression with applied load.

Increasing the web depth from 42 in. to 75 in. resulted in no notable effect on the strength of the inverted-T beams. Similarly the serviceability behavior was unchanged between the beams with different web depths.

When comparing compression- and tension-chord loaded beam, no notable trend was observed on the strength of the beams. A slight increase in first cracking load was observed for the inverted-T beams (dependent on ledge geometry) and the crack width progression suggests narrower cracks in inverted-T beams at the same percent of ultimate load.

CHAPTER 5
Analysis of Results

5.1 OVERVIEW

In this chapter, analyses of the data from the experimental program are presented to address the following tasks:

- Evaluating the applicability of existing strut-and-tie modeling provisions for design of inverted-T beams
- Providing recommendations for limiting diagonal cracking under service loads
- Correlating the maximum inclined crack width to member ultimate shear strength

5.2 STRENGTH ANALYSIS

A summary of the experimental versus calculated shear strengths (V_{test}/V_{calc}) for all tests conducted within this project is provided in Table 5-1. The calculations of V_{calc} for the specimens were discussed in Chapter 4.

V_{test} = maximum shear carried in the critical section of the test region, including self-weight of the specimen and test setup.

V_{calc} = shear capacity calculated using the measured material properties presented in Section 3.4 and TxDOT Project 0-5253 STM provisions as implemented for inverted-T beams in Section 2.5.1.

As can be seen in Table 5-1, all values of V_{test}/V_{calc} are higher than 1.0, which indicates that the STM provisions proposed by Project 0-5253 as implemented for inverted-T beams in Section 2.5.1 are conservative for all specimens tested. Values of V_{test}/V_{calc} lower than 1.2 are shaded in the table to highlight tests where the STM provisions had a relatively low safety margin. One should note however that strength reduction factors were not used in calculating V_{calc} and hence conservatism would be greater in design.

The calculated and observed failure modes are also summarized for all specimens in Table 5-1. From the test observations it was often difficult to distinguish between node and strut crushing, therefore both failure modes were referred to as "concrete crushing". All specimens were designed using the STM provisions to fail in web shear, either through yielding of the intermediate tie or through crushing of the strut-to-node interface. The calculated mode of failure was observed in all tests with the exception of the five shaded in Table 5-1. For those five tests, although the expected failure mode did not occur, each of these specimens failed well above the web shear capacity predicted by the strut-and-tie model. Thus the strength estimates were still conservative.

Table 5-1: V_{test}/V_{calc} results for 5253 STM provisions.

Specimen	Vtest kip	Observed Failure Mode	Vcalc kip	$\dfrac{V_{test}}{V_{calc}}$	STM Controlling Element
DS1-42-1.85-03	712	Concrete Crushing	463	1.54	Node at support
DS1-42-2.50-03	406	Sectional Shear	202	2.01	Intermediate tie
DS1-42-1.85-06	621	Concrete Crushing	479	1.30	Node at support
DS1-42-2.50-06	503	Sectional Shear	339	1.48	Intermediate tie
DL1-42-1.85-06	741	Concrete Crushing	464	1.60	Node at support
DL1-42-2.50-06	622	Sectional Shear	353	1.76	Intermediate tie
SS3-42-1.85-03	523	Concrete Crushing	456	1.15	Node at support
SS3-42-2.50-03	447	Sectional Shear	215	2.08	Intermediate tie
SS3-42-2.50-06	516	Flexure Failure	415	1.24	Intermediate tie
SC3-42-2.50-03	329	Sectional Shear	257	1.28	Intermediate tie
SC3-42-1.85-03	483	Concrete Crushing	427	1.13	Node at support
DS3-42-2.50-03	430	Sectional Shear	236	1.82	Intermediate tie
DL1-42-1.85-03	626	Concrete Crushing	468	1.34	Node at support
DL1-42-2.50-03	510	Sectional Shear	235	2.17	Intermediate tie
SL3-42-1.85-03	571	Concrete Crushing	409	1.39	Node at support
SL3-42-1.85-06	744	Concrete Crushing	424	1.76	Node at support
C1-42-1.85-06	637	Concrete Crushing	428	1.49	Node at load
DC1-42-1.85-06	519	Concrete Crushing	428	1.21	Node at load
SS1-75-1.85-03	745	Concrete Crushing	389	1.92	Node at support
DC3-42-1.85-03	395	Concrete Crushing	370	1.07	Node at support
DS3-42-1.85-03	454	Concrete Crushing	370	1.23	Node at support
SS1-42-2.50-03	398	Sectional Shear	205	1.94	Intermediate tie
SS1-42-1.85-03	583	Concrete Crushing	501	1.16	Node at support
DC1-42-2.50-03	365	Sectional Shear	259	1.41	Intermediate tie
DL3-42-1.85-03	629	Flexure Failure	359	1.75	Node at support
SL1-42-2.50-03	498	Sectional Shear	261	1.91	Intermediate tie
SC1-42-2.50-03	319	Shear Friction	259	1.23	Intermediate tie
DS1-42-1.85-06/03	739	Concrete Crushing	416	1.78	Node at support
DS1-42-2.50-06/03	539	Sectional Shear	362	1.49	Intermediate tie
SC1-42-1.85-03	463	Ledge Tie	443	1.05	Node at load
DC1-42-1.85-03	517	Concrete Crushing	474	1.09	Node at load
SC1-42-1.85-03b	456	Concrete Crushing	362	1.26	Node at load
DC1-42-1.85-03b	424	Concrete Crushing	362	1.17	Node at load
SS1-75-2.50-03	649	Punching Shear	357	1.82	Intermediate tie

5.2.1 Failure Modes

Web shear failure was observed in all specimens except for five in which flexure, shear friction, ledge tie failures, or punching shear occurred (SS3-42-2.50-06, DL3-42-1.85-03, SC1-42-2.50-03, SC1-42-1.85-03, and SS1-75-2.50-03) as shown in Figure 5-1.
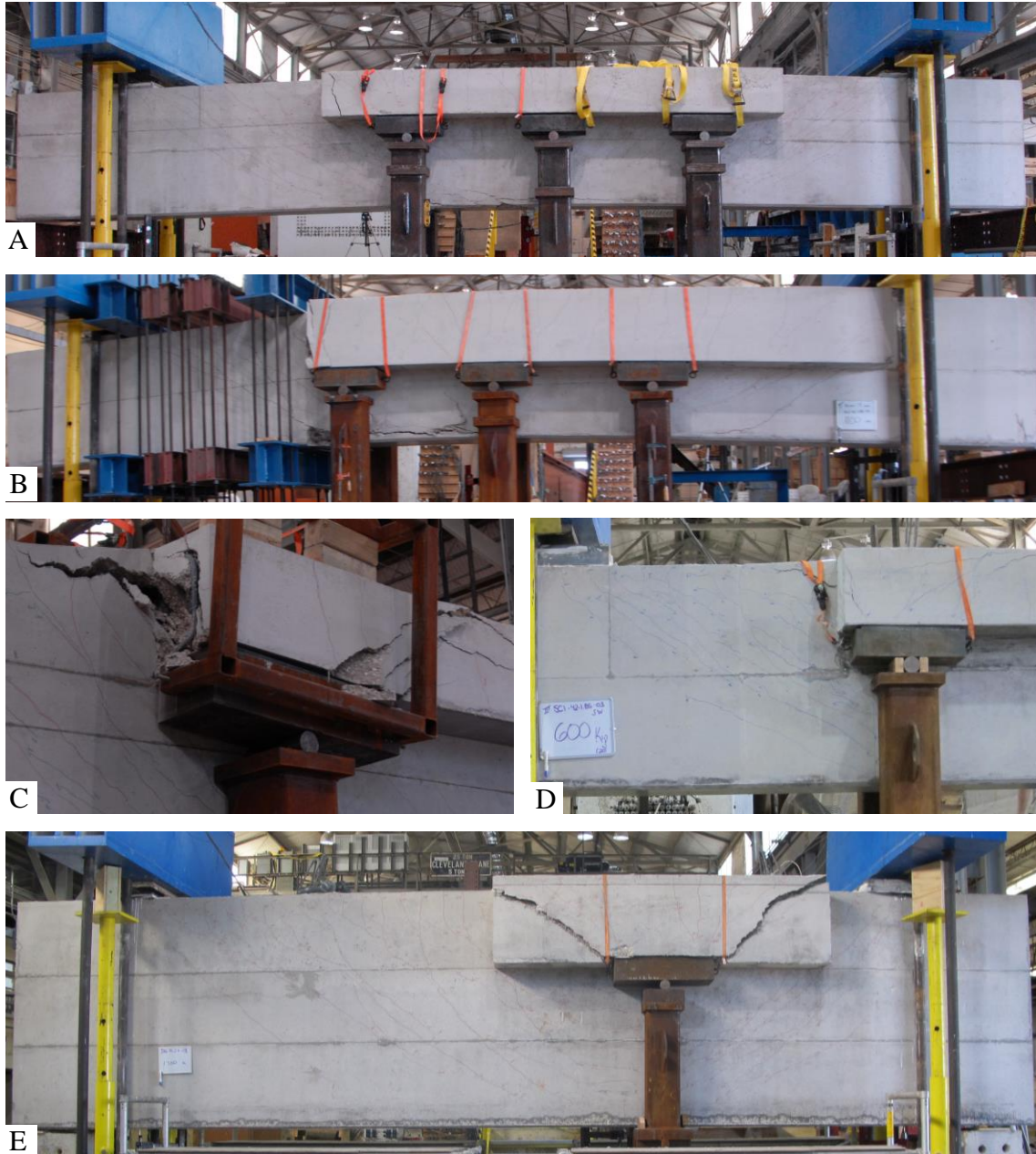
Figure 5-1: Failure modes- (A) SS3-42-2.50-06 flexure, (B) DL3-42-1.85-03 flexure, (C) SC1-42-2.50-03 shear friction, (D) SC1-42-1.85-03 ledge tie yielding, and (E) SS1-75-2.50-03 punching shear.

For specimen SS3-42-2.50-06, a flexural mode of failure was observed (Figure 5-1A). During specimen design, web shear failure was predicted using a strut-and-tie model and specified material properties. However, when measured material strengths were considered the flexural capacity was estimated to be only 6% higher than the web shear strength; which partly explains the flexural failure mode. Nevertheless the specimen was able to exceed the capacity calculated using the TxDOT Project 0-5253 STM provisions.

Specimen DL3-42-1.85-03 also failed in flexure (Figure 5-1B). The strut-and-tie model was controlled by web shear with a predicted overstrength of 38% over the flexural strength. As with the previous test, the ultimate strength of the specimen was well above the estimated strengths with V_{test}/V_{calc} ratio of 1.75.

Shear friction failure of the ledge was observed in SC1-42-2.50-03 (Figure 5-1C). The STM design was controlled by web shear, with overstrengths of 83% and 135% over ledge tie and strut strengths respectively. No indication of local failure was anticipated in the design phase. It is interesting to note that this specimen had a shallow, cut-off ledge and a single loading point; which indicates that these parameters may have influenced the weaker than anticipated ledge strength. The V_{test}/V_{calc} ratio was still conservative at 1.23.

Specimen SC1-42-1.85-03 sustained a local failure in the ledge (Figure 5-1D). As with the previous specimen with ledge failure, this beam also had a shallow, cut-off ledge and a single loading point. The STM design was governed by web shear; however, when the actual material strengths were considered the ledge strut and ledge tie were calculated to be only 10% stronger than the strut-to-node interface in the web. Hanger reinforcements had an overstrength of 20%. Since the concrete strength was higher than anticipated in the original design, web shear-strength was greater than anticipated and the calculated safety against local ledge failure was compromised.

Specimen SS1-75-2.50-03 failed due to punching shear in the ledge (Figure 5-1E). This beam had a short, shallow ledge that was not able to carry the higher than anticipated load. At yielding of the hanger bars, crack widths were recorded and it was determined that the beam was within approximately 10% of its failure load. Retesting through application of load to the web of the beam confirmed this observation and it was determined that the test provided valid information on the shear strength and behavior of a 75-in. deep beam.

For the remaining twenty nine specimens, all of the observed web shear failures similar to those shown in Figure 5-2 and were correctly predicted using the STM provisions of TxDOT Project 0-5253. Overall the STM provisions resulted in accurate predictions of the actual failure modes. In the 12% of the cases where web shear was not the limiting factor, the actual failure mode involved the next weakest element in the STM.

Concrete Crushing Failure   Stirrup Yielding Failure
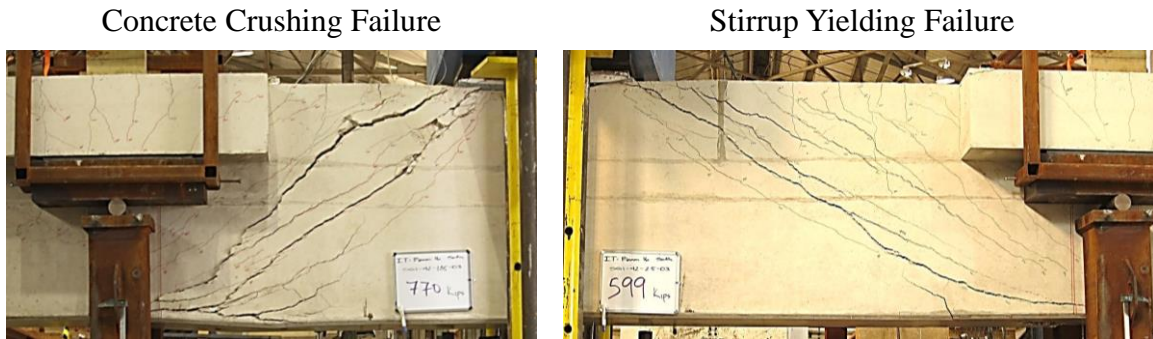
Figure 5-2: Shear failure: concrete crushing for a/d = 1.85 and stirrup yielding for a/d =2.50

5.2.2 Ledge Design

Although the ledge length and depth were variables considered in this report, the factors affecting the strength of the ledge itself were not directly investigated. Each specimen was designed such that its shear strength would govern its capacity. In order for that to occur, the ledge and cross sectional model was required to have greater strength. This is another advantage to strut-and-tie modeling; the desired failure mode can be chosen by identifying the weakest link and strengthening other components. For example, in specimens tested at an a/d ratio of 2.50 it was necessary for the shear stirrups to yield before the ledge or hanger reinforcement (shown in Figure 5-3), and the reinforcement was proportioned accordingly. If crushing of the diagonal strut in the cross section was governing the model, the concrete strength can be increased.
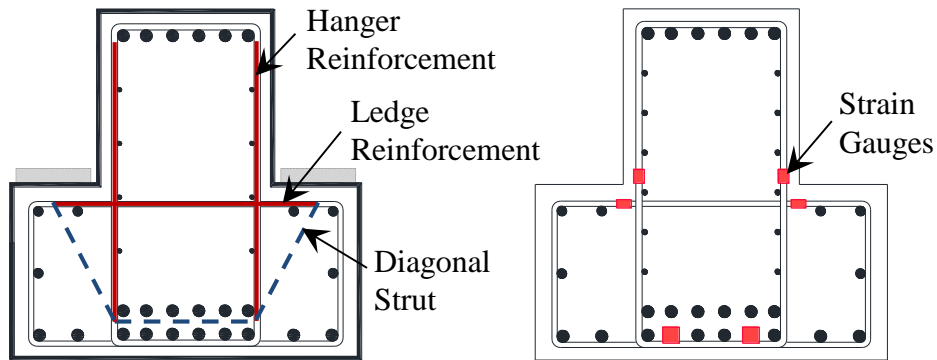
Figure 5-3: Inverted-T Cross Section STM and Strain Gauges

As discussed in Section 2.6.2.2, certain assumptions were required to apply the STM provisions that were developed for rectangular beams to the design of inverted-T beams. In order to determine the number of required hanger bars, the applied load was assumed to spread at a 45-degree. Therefore, hanger ties were given a width equal to the length of the bearing plate (W) plus twice the depth of the ledge (d_f) for short and long ledges. In cut-off ledges, the hanger tie was restricted and could only spread in one direction, as

119

shown in Figure 5-4. The same assumptions are found in AASHTO Eq. 5.13.2.5.5-3 for calculating the strength of hanger reinforcement.
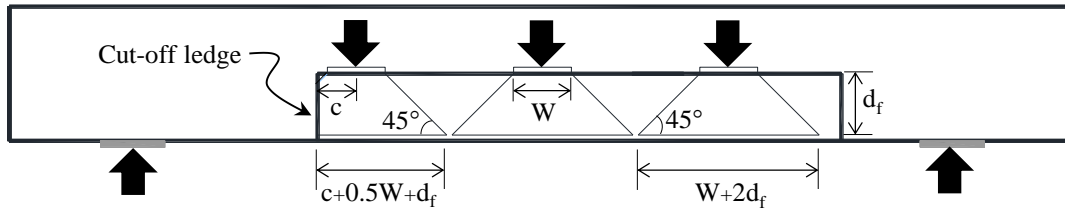
Figure 5-4: Load Spread for Cross Section Design

The hanger tie width assumptions were validated by measuring strains using electrical strain gauges described in Section 3.5.1, the locations of which are shown in the cross section Figure 5-3. Yield was determined for each bar size and specimen as described in Section 3.3. Typical measured strains normalized by yielding strains for the hanger reinforcement are shown in Figure 5-5.

One Point Load, Short Shallow Ledge (SS1-42-1.85-03)

Three Point Loads, Cut-off and Short, Deep Ledges (DC1- & DS1-42-1.85-03)

Reinforcement Key: ● $\varepsilon_s \geq \varepsilon_y$ ■ $\varepsilon_s \geq \frac{1}{2}\varepsilon_y$ ■ $\varepsilon_s \geq \frac{1}{4}\varepsilon_y$ □ $\varepsilon_s \leq \frac{1}{4}\varepsilon_y$
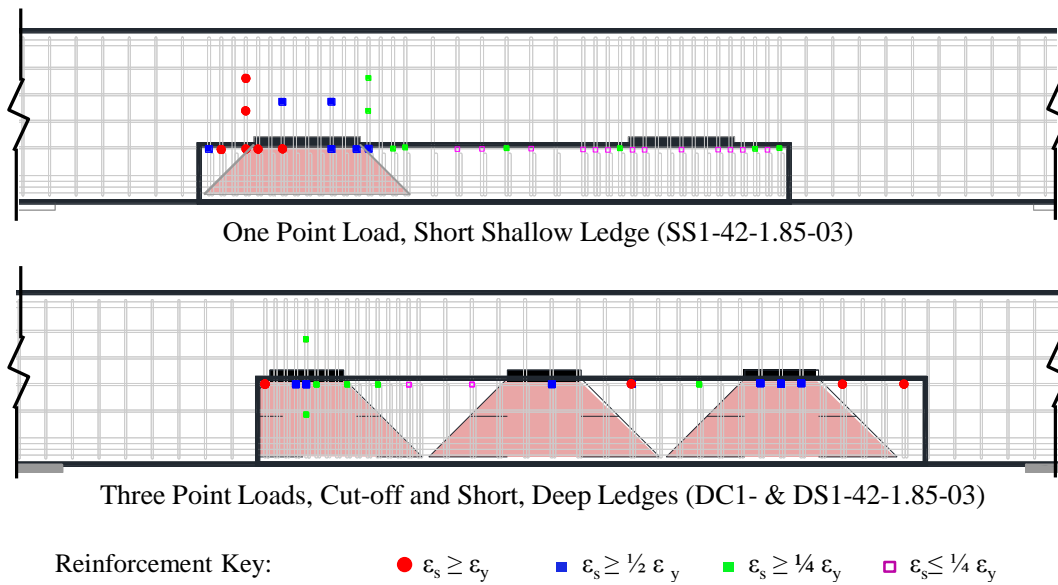
Figure 5-5: Typical Hanger Stains

In the above figure, higher strains can be seen to concentrate within the assumed load spread length, with a tendency for the load to spread towards the closest support. Similar distributions observed in most specimens. Strain gauge measurements thus indicate that the 45-degree load spread assumption is reasonable and conservative.

Also, as discussed in Section 5.2.1, only three of the thirty three inverted-T specimens had ledge-related failure modes. The actual failure mode was typically the second weakest element in the STM and occurred only after the calculated shear capacity was surpassed. It is important to note that these failures also occurred in specimens loaded at

one point, which is not typical in field applications with multiple bridge girders. It is therefore recommended to calculate the hanger tie widths as shown in Figure 5-4.

5.2.3 Ultimate Strength

The statistical results for the strength ratios of the thirty three tests in the experimental program are summarized in Table 5-2. As shown in the table, all ratio values fall above 1.0, indicating that the design method yielded conservative estimations of strength. The mean strength ratio for all tests is 1.50, which indicates fairly accurate strength calculations.

Table 5-2: Overall accuracy of TxDOT Project 0-5253 STM provisions

33 tests	V_{test}/V_{calc}
Min	1.05
Max	2.17
Mean	1.50
Unconservative[*]	0%
Standard deviation	0.33
Coefficient of Variation**	0.22

* Unconservative = % of tests for which $V_{test}/V_{calc} < 1.0$

** Coefficient of Variation = Standard Deviation / Mean

In order to evaluate more closely the TxDOT Project 0-5253 STM design provisions for inverted-T beams, direct comparisons of the experimental shear strength, V_{test}, and the nominal capacity, V_{calc}, calculated per the strut-and-tie models are made in the following sections for the individual series.

5.2.3.1 Effects of Ledge Length

Specimens were constructed with three different ledge lengths: cut-off, short and long ledges. The V_{test}/V_{calc} values from the ledge length series specimens are summarized in Table 5-3. The ratio of test to calculated strengths are organized into eight groups of two or three directly comparable specimens as illustrated in Figure 5-6. Presenting the data in this manner allows for observations to be made on specimens in which all variables are kept constant except the length of the ledge.

Table 5-3: Series I: Ledge Length

Comparison	Specimen	f'_c (psi)	V_{test} (kip)	V_{calc} (kip)	$\dfrac{V_{test}}{V_{calc}}$
D_1-42-1.85-03	DS1-42-1.85-03	5258	712	463	1.54
	DL1-42-1.85-03	4929	626	468	1.34
D_3-42-1.85-03	DC3-42-1.85-03	4568	395	370	1.07
	DS3-42-1.85-03	4568	454	370	1.23
	DL3-42-1.85-03 (f)	4202	629	359	1.75
S_3-42-1.85-03	SC3-42-1.85-03	5873	483	427	1.13
	SS3-42-1.85-03	5891	523	456	1.15
	SL3-42-1.85-03	5037	571	409	1.39
D_1-42-1.85-06	DS1-42-1.85-06	5024	621	479	1.30
	DL1-42-1.85-06	4830	741	464	1.60
D_1-42-2.50-03	DC1-42-2.50-03	4035	365	259	1.41
	DS1-42-2.50-03	5389	406	202	2.01
	DL1-42-2.50-03	4929	510	235	2.17
S_1-42-2.50-03	SC1-42-2.50-03 (r)	4281	319	259	1.23
	SS1-42-2.50-03	5703	398	205	1.94
	SL1-42-2.50-03	4281	498	261	1.91
S_3-42-2.50-03	SC3-42-2.50-03	5873	329	257	1.28
	SS3-42-2.50-03	5891	447	215	2.08
D_1-42-2.50-06	DS1-42-2.50-06	5088	503	339	1.48
	DL1-42-2.50-06	4986	622	353	1.76

(f) Flexural failure

(r) Shear friction failure of the web-to-ledge interface

The difference in ledge length is accounted for in the strut-and-tie models by the size of the node above the load point. When the ledge length is shortened, the hanger load is concentrated and the resulting node size is decreased as illustrated in Figure 3-7. As long as this node controls the strength of the model, the strut-and-tie method would capture the effect of the ledge length on the web-shear strength of the inverted-T beam. For the specimens tested at an a/d ratio of 1.85, the node at the support typically controlled the predicted capacity of the beam. For the specimens tested at an a/d ratio of 2.50, the vertical tension tie was designed to govern the beam's shear strength. Therefore varying the ledge length was not expected to have an effect on the calculated capacity of the specimens according to the strut-and-tie models.

(f) Flexural failure
(r) Shear friction failure of the web-to-ledge interface
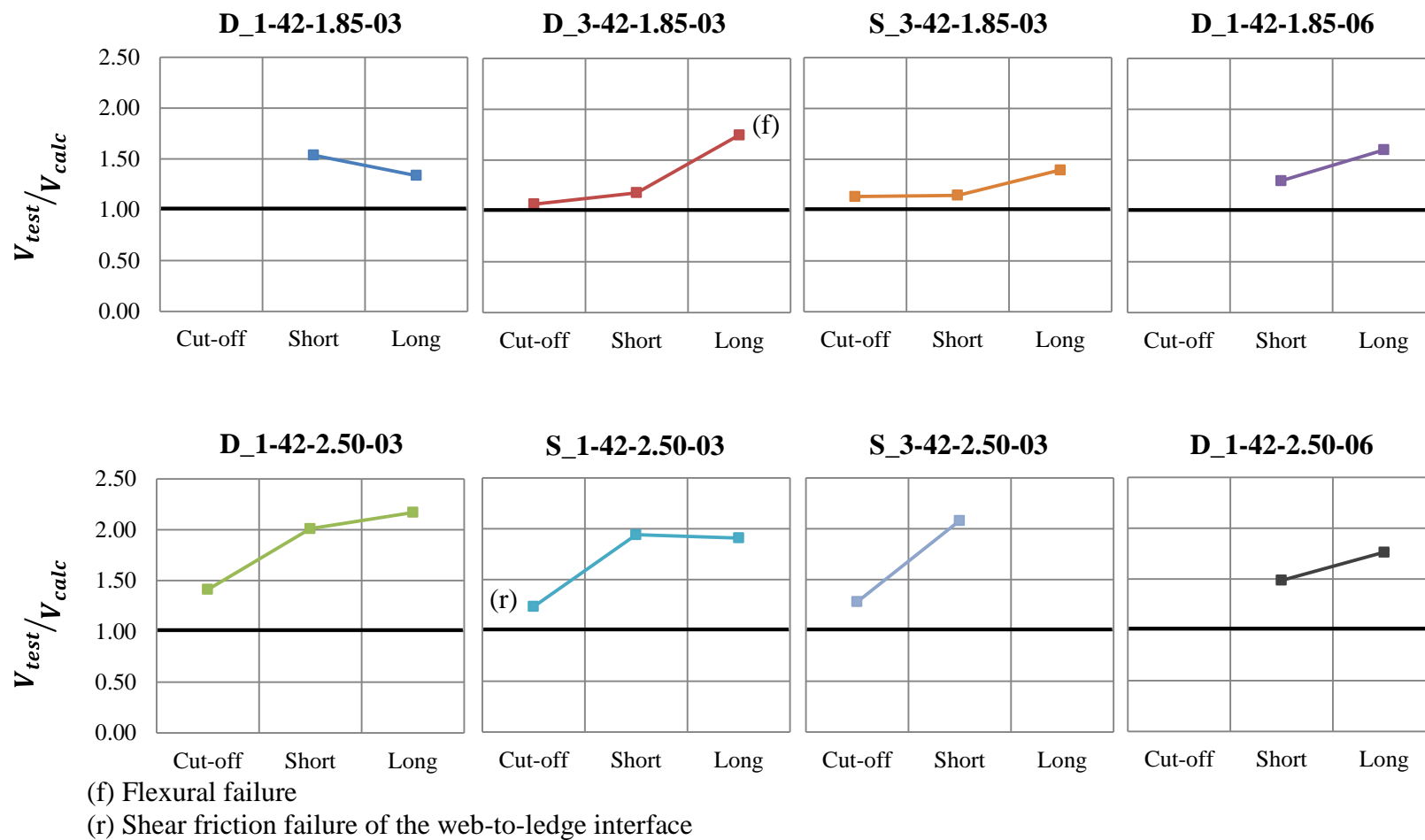
Figure 5-6: Series I: Ledge Length- Direct comparisons of experimental capacity with TxDOT Project 0-5253 STM calculations

As shown in Figure 5-6, the ratio of experimental shear strength to nominal capacity values varied between 1.07 and 2.17. A clear trend can be observed in the directly comparable specimens where the conservatism increases as the ledge length increases. There are a couple of cases that did not follow this trend, but that can be attributed to variability in shear tests. Considering the large number of tests presented in this series, it is evident that longer ledges provide additional strength not captured by the STM provisions.

This observation is confirmed when a more general comparison of thirty three tests from the experimental program is made. The ratio of the experimental to calculated shear strengths are summarized by ledge length and a/d ratio in Table 5-4 and Figure 5-7. The minimum, maximum, and average V_{test}/V_{calc} values increase with the ledge length suggesting that the STM provisions do not fully take into account the beneficial effect of longer ledges on the strength of inverted-T beams. It can be seen in Table 5-4 that the conservatism increases with ledge length for both a/d ratios; with strength estimates for beam tested at an a/d ratio of 2.50 being more conservative than those tested at 1.85. It is also important to note that the highest strength ratio (2.17) was found for a long ledge specimen and the lowest (1.05) corresponded to a cut-off ledge specimen. The cut-off ledges also had the lowest average V_{test}/V_{calc} value of 1.14.

Table 5-4: Series I: Ledge Length- STM summary by a/d ratio.

$\dfrac{V_{test}}{V_{calc}}$	Cut-off Ledge Length			Short Ledge Length			Long Ledge Length		
	a/d 1.85	a/d 2.50	Avg	a/d 1.85	a/d 2.50	Avg	a/d 1.85	a/d 2.50	Avg
	7 tests	3 tests	10 tests	7 tests	8 tests	15 tests	5 tests	3 tests	8 tests
Min	1.05	1.23	1.05	1.15	1.24	1.15	1.34	1.76	1.34
Max	1.26	1.41	1.41	1.92	2.08	2.08	1.76	2.17	2.17
Mean	1.14	1.31	1.19	1.44	1.74	1.60	1.57	1.95	1.71
STDV	0.08	0.09	0.11	0.31	0.30	0.33	0.20	0.21	0.27
COV*	0.07	0.07	0.09	0.22	0.17	0.16	0.12	0.11	0.16

* COV = Coefficient of Variation (Standard Deviation / Mean)
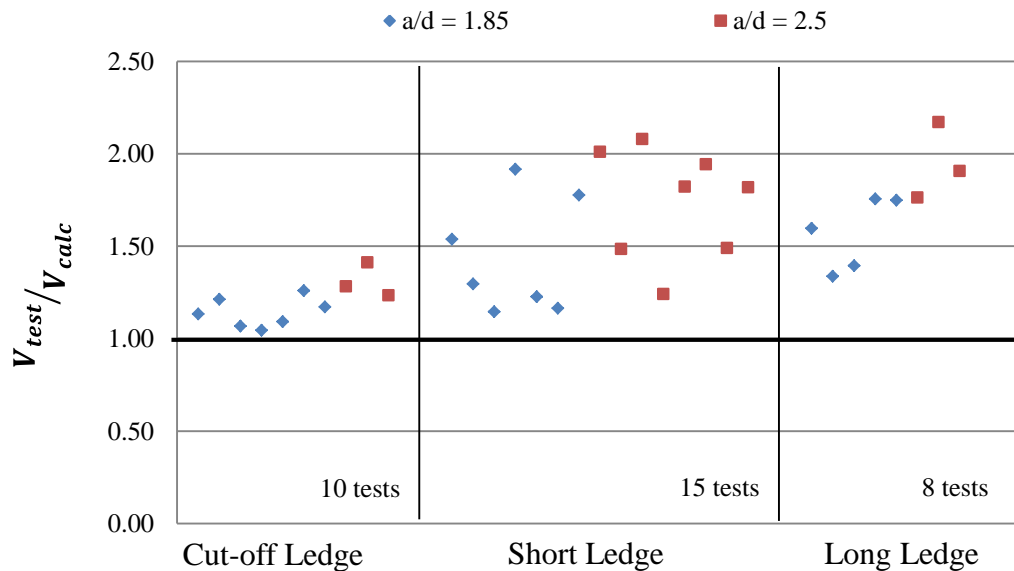
Figure 5-7: Series I: Ledge Length- STM strength predictions.

Results in this section indicate that using cut-off ledges reduces the conservatism of the STM provisions, nevertheless each model resulted in a safe estimate of the capacity of the specimens. Given the relatively low conservatism for cut-off ledges, it may be preferable to avoid cut-off ledges in practice.

5.2.3.2 Effects of Ledge Depth

Two ledge depths were tested: a shallow depth equal to one third the total height of the member and a deep ledge depth equal to one half of the member's height. The depths were chosen to encompass the range observed in the field and still ensure a web-shear failure without punching through the ledge. A summary of the experimental shear strength, V_{test}, and the nominal capacity, V_{calc}, calculated per the TxDOT Project 0-5253 STM provisions for the beams in the ledge depth series is provided in Table 5-5.

Table 5-5: Series II: Ledge Depth

Comparison	Specimen	f'_c (psi)	V_{test} (kip)	V_{calc} (kip)	$\dfrac{V_{test}}{V_{calc}}$
_C1-42-1.85-03	SC1-42-1.85-03 (le)	4303	463	443	1.05
	DC1-42-1.85-03	4330	517	474	1.09
_C1-42-1.85-03b	SC1-42-1.85-03b	2996	456	362	1.26
	DC1-42-1.85-03b	3013	424	362	1.17
_S1-42-1.85-03	SS1-42-1.85-03	5721	583	501	1.16
	DS1-42-1.85-03	5258	712	463	1.54
_C3-42-1.85-03	SC3-42-1.85-03	5873	483	427	1.13
	DC3-42-1.85-03	4568	395	370	1.07
_S3-42-1.85-03	SS3-42-1.85-03	5891	523	456	1.15
	DS3-42-1.85-03	4568	454	370	1.23
_L3-42-1.85-03	SL3-42-1.85-03	5037	571	409	1.39
	DL3-42-1.85-03 (f)	4202	629	359	1.75
_C1-42-2.50-03	SC1-42-2.50-03 (r)	4281	319	259	1.23
	DC1-42-2.50-03	4035	365	259	1.41
_S1-42-2.50-03	SS1-42-2.50-03	5703	398	205	1.94
	DS1-42-2.50-03	5389	406	202	2.01
_L1-42-2.50-03	SL1-42-2.50-03	4281	498	261	1.91
	DL1-42-2.50-03	4929	510	235	2.17
_S3-42-2.50-03	SS3-42-2.50-03	5891	447	215	2.08
	DS3-42-2.50-03	5687	430	236	1.82

(le) Horizontal ledge tie failure in cross section model

(f) Flexural failure

(r) Shear friction failure of the web-to-ledge interface

The V_{test}/V_{calc} values from twenty tests are plotted in ten pairs of directly comparable specimens to investigate the effect of the ledge height in Figure 5-8. Every variable in each group is held constant except for the depth of the ledge. No clear trend could be distinguished when examining the capacity ratio plots in Figure 5-8.
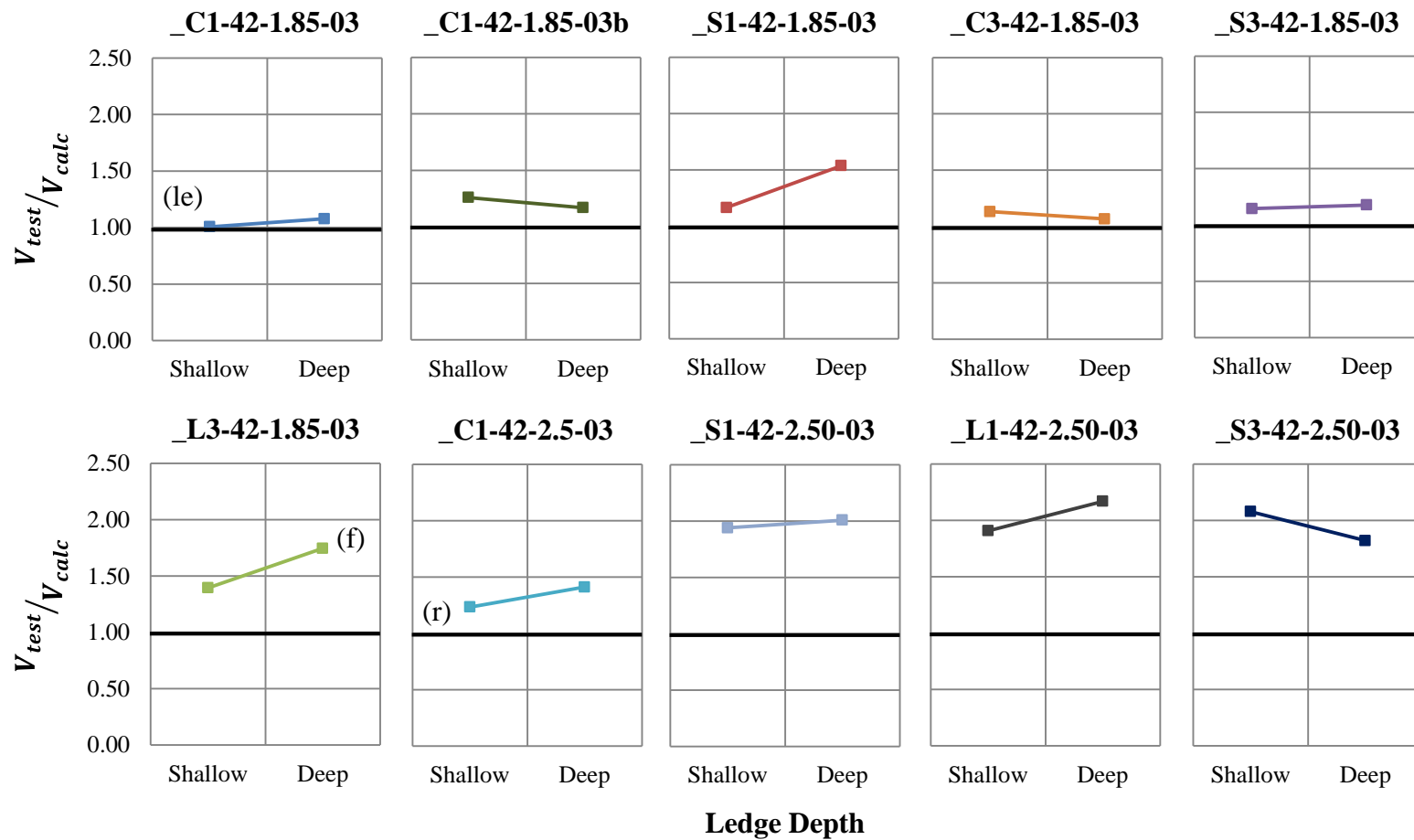
_C1-42-1.85-03   **_C1-42-1.85-03b**   **_S1-42-1.85-03**   **_C3-42-1.85-03**   **_S3-42-1.85-03**

_L3-42-1.85-03   **_C1-42-2.5-03**   **_S1-42-2.50-03**   **_L1-42-2.50-03**   **_S3-42-2.50-03**

(le) Horizontal ledge tie failure in cross section model

(f) Flexural failure

(r) Shear friction failure of the web-to-ledge interface

Figure 5-8: Series II: Ledge Depth- Direct comparisons of experimental capacity with TxDOT Project 0-5253 STM calculations

127

The ratio of the experimental to calculated shear strengths are summarized by ledge depth and a/d ratio in Table 5-6 and Figure 5-9. When examining the collection of all the tests in the experimental program, it is apparent that the ledge depth has no appreciable effect on the accuracy or conservatism of the strut-and-tie models. Only a slight difference is noted between the average conservatism for the two a/d ratios. One can conclude then that the effect of the ledge depth on web-shear strength of inverted-T beams is adequately captured by the strut-and-tie model; i.e., no bias is introduced by the design procedure.

Table 5-6: Series II: Ledge Depth- STM summary by a/d ratio.

$\dfrac{V_{test}}{V_{calc}}$	Shallow Ledge Depth			Deep Ledge Depth		
	a/d = 1.85	a/d = 2.50	Avg	a/d = 1.85	a/d = 2.50	Avg
	8 tests	7 tests	15 tests	11 tests	7 tests	18 tests
Min	1.13	1.23	1.13	1.07	1.41	1.07
Max	1.92	2.08	2.08	1.78	2.17	2.17
Mean	1.38	1.64	1.50	1.37	1.74	1.51
Standard deviation	0.30	0.37	0.35	0.25	0.29	0.32
COV**	0.22	0.23	0.23	0.19	0.17	0.21

** COV = Coefficient of Variation (Standard Deviation / Mean)
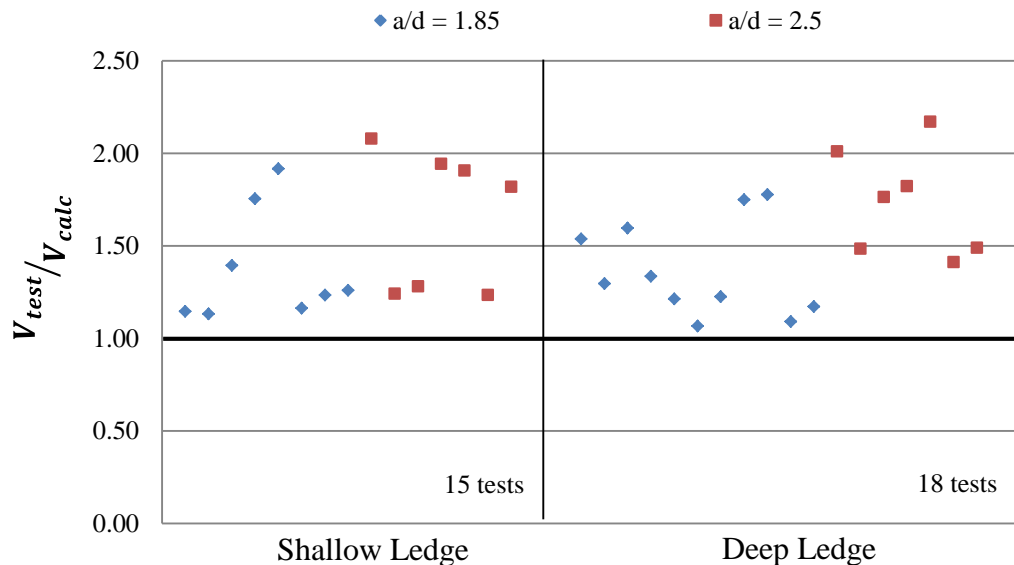
Figure 5-9: Series II: Ledge Depth- STM and LRFD strength predictions

The STM provisions mandate a minimum angle of 25 degrees between a strut and a tie and thus a minimum ledge depth is implicit in the provisions. Given the lack of bias in the strength estimates when ledge depth is considered, no further recommendations are

made about ledge depth by the current study. The few beams that sustained ledge failures all had shallow ledges and were loaded with a single point load. These beams did however fail at a substantially higher load than the ledge strength estimated by the STM provisions.

5.2.3.3 Effects of Web Reinforcement

It was shown in Section 4.5 that increasing the web reinforcement ratio from 0.3% to 0.6% in both orthogonal directions increased the strength of inverted-T beams. Larger amounts of web reinforcement were also found to affect the serviceability behavior of the beam as additional reinforcement better restrained the widths of the diagonal cracks.

A summary of the experimental shear strength, V_{test}, and the nominal capacity, V_{calc}, calculated per the TxDOT Project 0-5253 STM provisions for the fourteen directly comparable specimens investigated in Section 4.5 is presented in Table 5-7.

Table 5-7: Series III: Web Reinforcement Ratio

Comparison	Specimen	f'_c (psi)	V_{test} (kip)	V_{calc} (kip)	$\dfrac{V_{test}}{V_{calc}}$
DS1-42-1.85-_	DS1-42-1.85-03	5258	712	463	1.54
	DS1-42-1.85-06/03	4173	739	416	1.78
	DS1-42-1.85-06	5024	621	479	1.30
DL1-42-1.85-_	DL1-42-1.85-03	4929	626	468	1.34
	DL1-42-1.85-06	4830	741	464	1.60
SL3-42-1.85-_	SL3-42-1.85-03	5037	571	409	1.39
	SL3-42-1.85-06	5250	744	424	1.76
DS1-42-2.50-_	DS1-42-2.50-03	5389	406	202	2.01
	DS1-42-2.50-06/03	4173	539	362	1.49
	DS1-42-2.50-06	5088	503	339	1.48
DL1-42-2.50-_	DL1-42-2.50-03	4929	510	235	2.17
	DL1-42-2.50-06	4986	622	353	1.76
SS3-42-2.50-_	SS3-42-2.50-03	5891	447	215	2.08
	SS3-42-2.50-06 (f)	6255	516	415	1.24

(f) Flexural failure

The ratio of test shear capacity to that calculated using the strut-and-tie models is shown in Figure 5-10 for the beams in this series. Each of the six groups is a direct comparison of two or three specimens in which every parameter was kept constant except the reinforcement ratio.

DS1-42-1.85-_

DL1-42-1.85-_

SL3-42-1.85-_

$\rho_v = 0.3\%$ 0.6% 0.6%
$\rho_h = 0.3\%$ 0.3% 0.6%

$\rho_v = 0.3\%$ $\rho_v = 0.6\%$
$\rho_h = 0.3\%$ $\rho_h = 0.6\%$

$\rho_v = 0.3\%$ $\rho_v = 0.6\%$
$\rho_h = 0.3\%$ $\rho_h = 0.6\%$

DS1-42-2.50-_

DL1-42-2.50-_

SS3-42-2.50-_

$\rho_v = 0.3\%$ 0.6% 0.6%
$\rho_h = 0.3\%$ 0.3% 0.6%

$\rho_v = 0.3\%$ $\rho_v = 0.6\%$
$\rho_h = 0.3\%$ $\rho_h = 0.6\%$

$\rho_v = 0.3\%$ $\rho_v = 0.6\%$
$\rho_h = 0.3\%$ $\rho_h = 0.6\%$

(f) Flexural failure
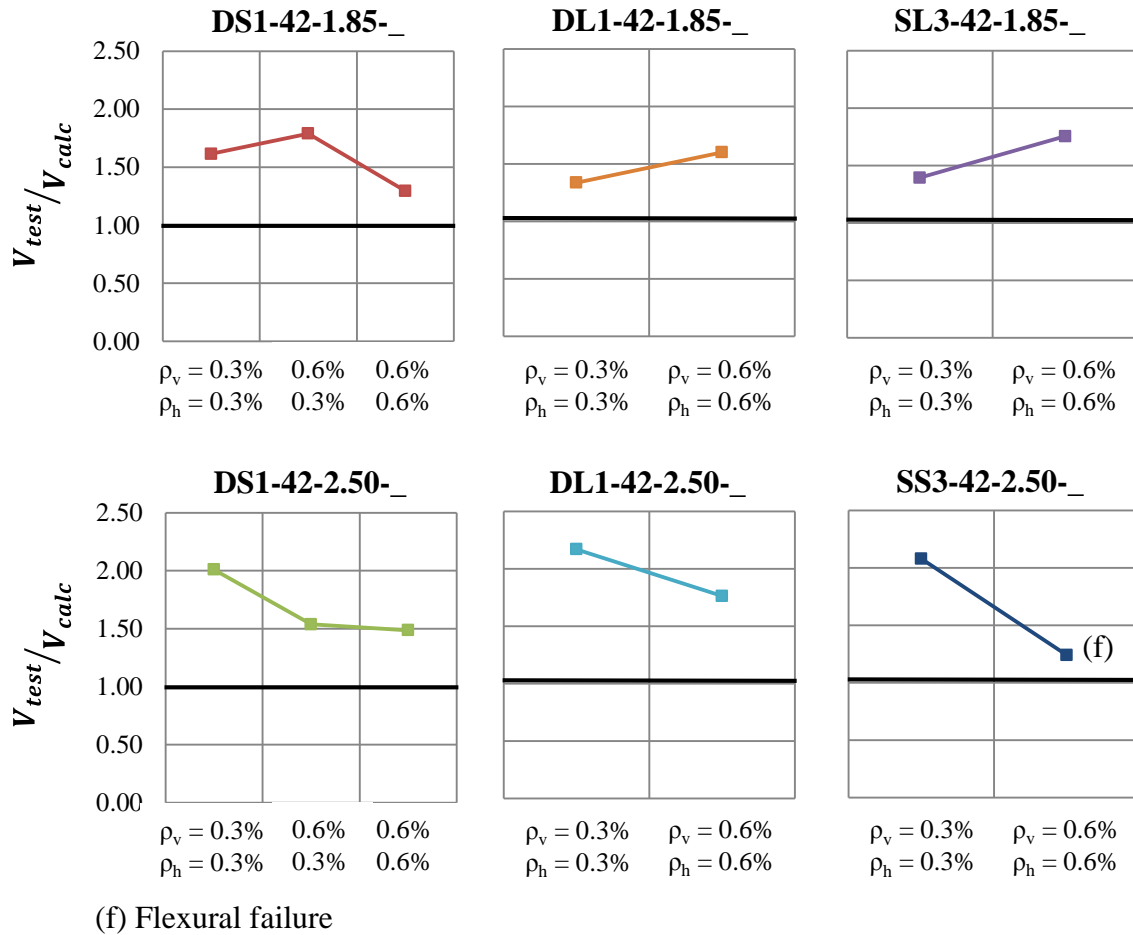
Figure 5-10: Series III: Web Reinforcement- Direct comparisons of experimental capacity with TxDOT Project 0-5253 STM calculations

The V_{test}/V_{calc} ratios varied between 1.24 and 2.17 for the beams in the reinforcement ratio series. Except for one point, an increase in conservatism was observed as the reinforcement ratio is increased for the specimens with an a/d ratio of 1.85. For the beams with the larger a/d ratio of 2.50, the opposite was true with decreased conservatism observed with increasing reinforcement ratio.

Using the TxDOT Project 0-5253 STM provisions, the specimens tested at an a/d ratio of 1.85 were estimated to fail by crushing of the direct strut or the strut-to-node interface. The STM provisions do not increase the strength of struts or nodes based on the amount of distributed reinforcement. Since higher strengths were observed for higher reinforcement ratio in specimens with an a/d of 1.85, and increase in conservatism in the STM provisions is observed here with increasing reinforcement ratio. The observed increase in shear strength with increasing amounts of web reinforcement could be due to additional crack control and confinement provided to the node by the additional

reinforcement. By contrast, the specimens with an a/d ratio of 2.50 failed due to yielding of the transverse reinforcement (intermediate tie) in the shear span. The STM provisions relate web shear capacity to the transverse reinforcement ratio; i.e., doubling the amount of reinforcement doubles the predicted contribution of that steel to shear capacity. Test results however have shown that doubling the amount of transverse reinforcement less than doubled the percentage of the steel contribution to the shear capacity; as evidenced by the lower conservatism of STM provision for the higher web reinforcement ratio. It is possible that the considered tie width is dependent on the amount of steel and may be narrower than estimated.

Similar observations can be made when results from all test specimens are considered (Table 5-8, Figure 5-11).

Table 5-8: Series III: Web Reinforcement Ratio- STM summary

$\dfrac{V_{test}}{V_{calc}}$	$\rho_v = \rho_h = 0.3\%$			$\rho_v = \rho_h = 0.6\%$		
	a/d = 1.85	a/d = 2.50	Avg	a/d = 1.85	a/d = 2.50	Avg
	14 tests	10 tests	24 tests	4 tests	3 tests	7 tests
Min	1.05	1.23	1.05	1.21	1.24	1.21
Max	1.92	2.17	2.17	1.76	1.49	1.76
Mean	1.30	1.77	1.50	1.47	1.39	1.43
Standard deviation	0.26	0.34	0.37	0.25	0.13	0.20
COV**	0.20	0.19	0.25	0.17	0.10	0.14

** COV = Coefficient of Variation (Standard Deviation / Mean)
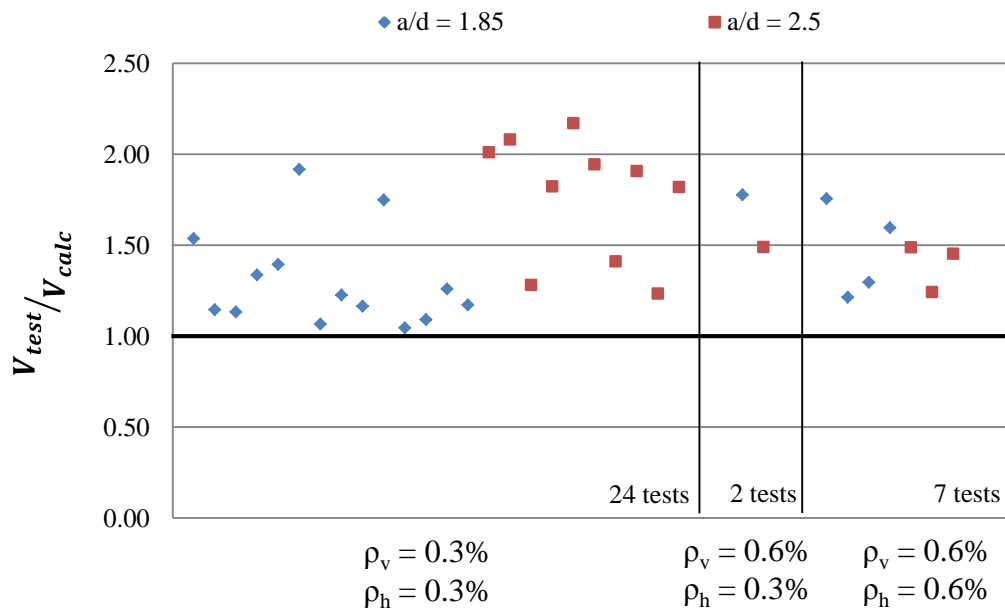
Figure 5-11: Series III: We Reinforcement Ratio- STM capacity results

Overall though, the strut-and-tie provisions produced accurate and reasonably conservative estimates of strength for all the inverted-T specimens. It is therefore not recommended to introduce adjustments to the provisions to account for the effects of reinforcement ratios.

5.2.3.4   Effects of Number of Point Loads

As discussed in Section 4.6, specimens with different number of point loads were investigated to determine what effect the loading condition had on the strength and serviceability of inverted-T beams. A slight but otherwise insignificant decrease in strength and first cracking load was observed for beams tested with multiple point loads. Results thus indicate that the conclusions from one-point load tests may be extended to multiple point loads; which is the case for the vast majority of bent caps in the field.

In order to examine the applicability of TxDOT Project 0-5253 STM provisions for inverted-T beams subjected to multiple loads, results from specimens that were tested with one and three loading points are compared. The capacities from twelve directly comparable specimens, in which every variable (ledge geometry, reinforcement ratio, a/d ratio) was kept constant, are summarized in Table 5-9.

132

Table 5-9: Series IV: Number of Point Loads

Comparison	Specimen	f'_c (psi)	V_{test} (kip)	V_{calc} (kip)	$\dfrac{V_{test}}{V_{calc}}$
SS_-42-1.85-03	SS1-42-1.85-03	5721	583	501	1.16
	SS3-42-1.85-03	5891	523	456	1.15
DS_-42-1.85-03	DS1-42-1.85-03	5258	712	463	1.54
	DS3-42-1.85-03	4568	454	370	1.23
DL_-42-1.85-03	DL1-42-1.85-03	4929	626	468	1.34
	DL3-42-1.85-03 (f)	4202	629	359	1.75
SC_-42-2.50-03	SC1-42-2.50-03 (r)	4281	319	259	1.23
	SC3-42-2.50-03	5873	329	257	1.28
SS_-42-2.50-03	SS1-42-2.50-03	5703	398	205	1.94
	SS3-42-2.50-03	5891	447	215	2.08
DS_-42-2.50-03	DS1-42-2.50-03	5389	406	202	2.01
	DS3-42-2.50-03	5687	430	236	1.82

(f) Flexural failure

(r) Shear friction failure

It can be inferred from Table 5-9 that many of the V_{test}/V_{calc} values are similar amongst the number of point load comparisons. The ratios are plotted in Figure 5-12 in six pairs of directly comparable specimens in order to better illustrate this point. The V_{test}/V_{calc} ratios varied between 1.15 and 2.08. No clear trend resulting from different number of loads is seen in the figure. Such observations suggest that no bias is introduced in the STM design provisions when multiple point loads are considered.
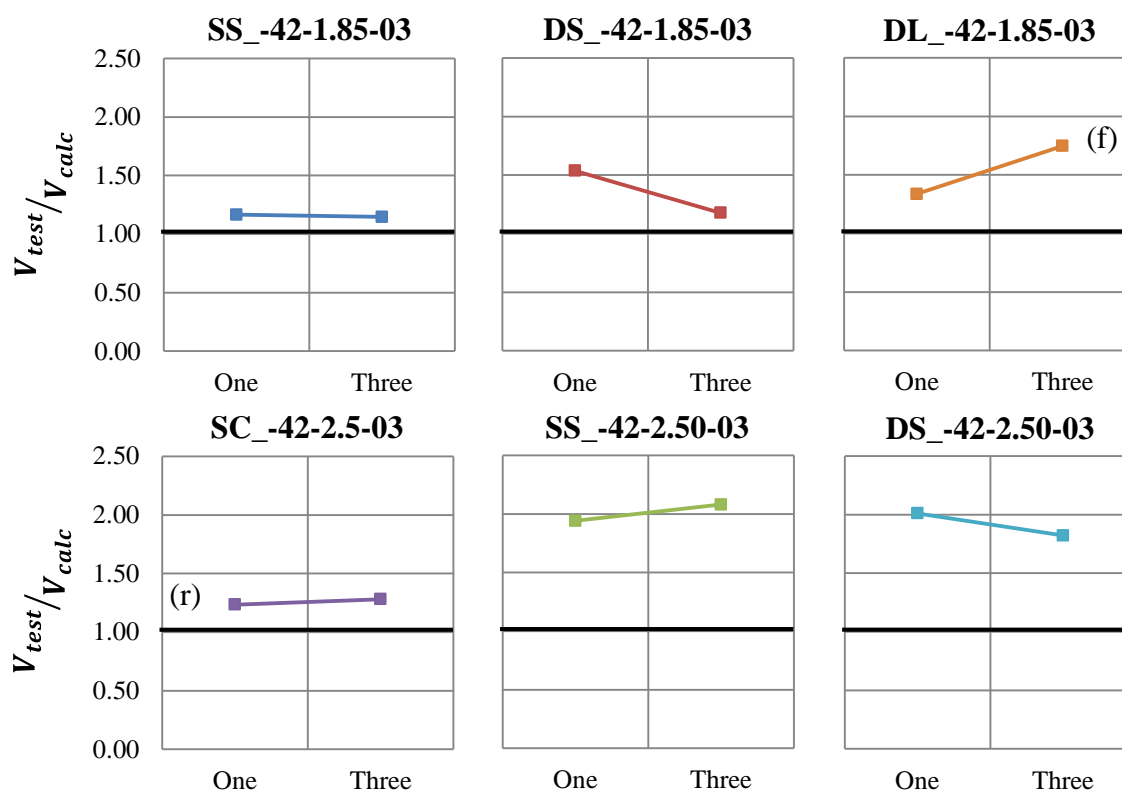
(f) Flexural failure
(r) Shear friction failure of the web-to-ledge interface

Figure 5-12: Series IV: Number of Point Loads- Direct comparisons of experimental capacity with TxDOT Project 0-5253 STM calculations.

Similar observations can be made when results from all test specimens are considered (Table 5-10 and Figure 5-13).

Table 5-10: Series IV: Number of Point Loads- STM summary.

$\dfrac{V_{test}}{V_{calc}}$	One Point Load			Three Point Loads		
	a/d = 1.85	a/d = 2.50	Avg	a/d = 1.85	a/d = 2.50	Avg
	12 tests	10 tests	22 tests	7 tests	4 tests	11 tests
Min	1.05	1.23	1.05	1.07	1.24	1.07
Max	1.92	2.17	2.17	1.76	2.08	2.08
Mean	1.37	1.72	1.53	1.35	1.61	1.44
Standard deviation	0.28	0.30	0.34	0.29	0.41	0.34
COV**	0.20	0.18	0.22	0.22	0.26	0.24

** COV = Coefficient of Variation (Standard Deviation / Mean)

134
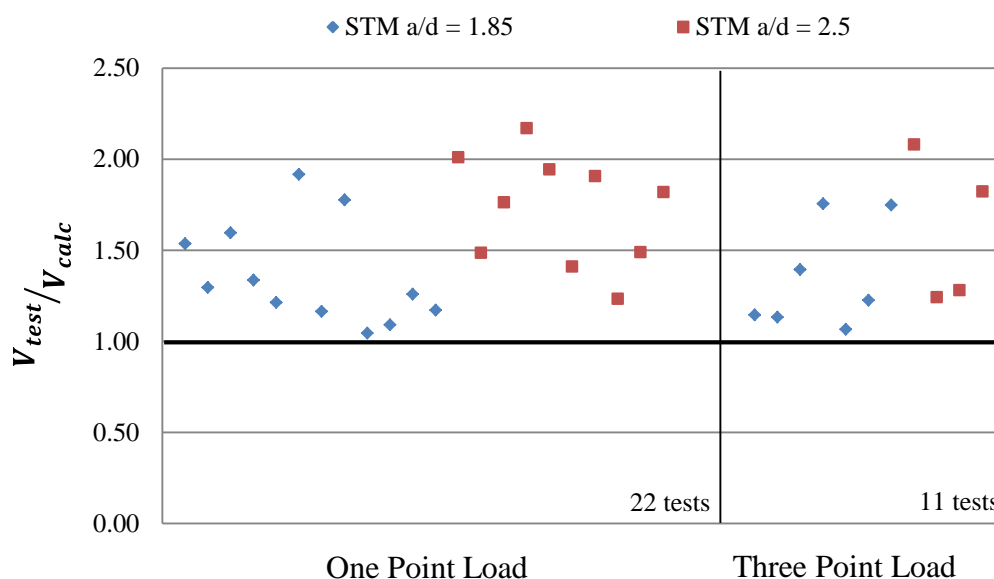
Figure 5-13: Series IV: Number of Point Loads- STM strength predictions

The STM design provisions of TxDOT Project 0-5253 thus provided accurate and acceptably conservative estimates of strength for the specimens evaluated in this series and adequately captured the behavior regardless of the number of point loads used in testing.

5.2.3.5 *Effects of Web Depth*

In order to ensure that the TxDOT Project 0-5253 STM provisions are applicable to larger inverted-T beams, a series investigating different web depths was developed. Most of the specimens in the experimental program were constructed with a total web height of 42 in. Two beams were constructed with a total depth of 75 in. and are investigated in this section. As mentioned previously, laboratory testing limitations prevented testing additional beams with web depths of 75 in. The web height is the only variable that is changed between the direct comparisons provided in Table 5-11. All beams were loaded on short, shallow ledges and their estimated strengths are presented in Table 5-11.

Table 5-11: Series V: Web Depth

Comparison	Specimen	f'_c (psi)	V_{test} (kip)	V_{calc} (kip)	$\dfrac{V_{test}}{V_{calc}}$
SS1-_-1.85-03	SS1-42-1.85-03	5721	583	501	1.16
	SS1-75-1.85-03	2867	745	389	1.92
SS1-_-2.50-03	SS1-42-2.50-03	5703	398	205	1.94
	SS1-75-2.50-03 (p)	5158	649	357	1.82

(p) Punching shear failure

The ratio of the shear capacity obtained from testing to that predicted by the STM is shown in Figure 5-14 for the two pairs of comparisons in this series. Although there are not enough comparisons to draw firm conclusions on the effect of web depth, it is important to note that strut-and-tie models were used to estimate conservative results for specimens of both depths. An increase in conservatism was noted for larger beams tested at an a/d of 1.85 and a negligible decrease was observed for larger beams tested at an a/d ratio of 2.50.
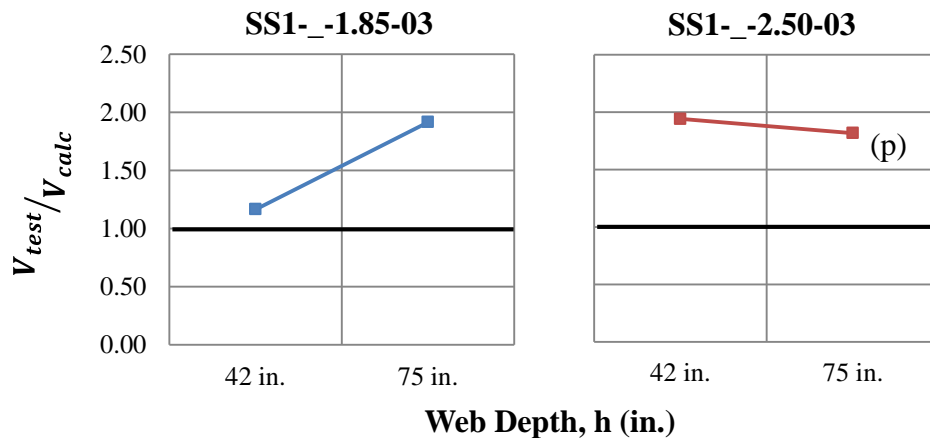
(p) Punching shear failure

Figure 5-14: Series V: Web Depth- Direct comparisons of experimental capacity with TxDOT Project 0-5253 STM calculations

5.2.3.6   Effects of Compression- and Tension-Chord Loading

The difference in STM strength estimates between tension- and compression-chord loaded beams is investigated here. For direct comparison with specimens tested in this project, only the compression-chord loaded rectangular beams with 21 in. web width, 42 in. or 75 in. web depth, 0.3% web reinforcement, and a/d ratios of 1.85 and 2.50 are included in this series from Project 0-5253. As no beams were tested with 0.6% web

reinforcement in the previous project, a compression-chord loaded beam, C1-42-1.85-06, was tested in the current experimental program to fill that gap.

Table 5-12: Series VI: Loaded Chord

Comparison	Specimen	f'_c (psi)	V_{test} (kip)	V_{pred} (kip)	$\dfrac{V_{test}}{V_{pred}}$
_1-42-1.85-03	DC1-42-1.85-03	4303	517	474	1.09
	DS1-42-1.85-03	5258	712	463	1.54
	DL1-42-1.85-03	4929	626	468	1.34
	SC1-42-1.85-03 (le)	4330	463	443	1.05
	SS1-42-1.85-03	5721	583	501	1.16
	III-1.85-03[1]	4990	412	374	1.10
	III-1.85-03b[1]	3300	471	258	1.83
	I-03-2[1]	5240	569	381	1.49
	I-03-4[1]	5330	657	382	1.72
_1-75-1.85-03	SS1-75-1.85-03	2867	745	389	1.92
	IV-2175-1.85-03[1]	4930	842	501	1.68
_1-42-1.85-06	DC1-42-1.85-06	3727	519	428	1.21
	DS1-42-1.85-06	5024	621	479	1.30
	DL1-42-1.85-06	4830	741	464	1.60
	C1-42-1.85-06[2]	3727	637	428	1.49
_1-42-2.50-03	DC1-42-2.50-03	4035	365	259	1.41
	DL1-42-2.50-03	4929	510	235	2.17
	SC1-42-2.50-03 (r)	4281	319	259	1.23
	SS1-42-2.50-03	5703	398	205	1.94
	SL1-42-2.50-03	4281	498	261	1.91
	III-2.5-03[1]	5030	516	282	1.83

(le) Ledge tie failure

(r) Shear friction failure

[1] Compression-chord loaded beam from TxDOT Project 0-5253

[2] Compression-chord loaded beam from TxDOT Project 0-6416

Estimated shear strength ratios V_{test}/V_{calc} are summarized in The difference in STM strength estimates between tension- and compression-chord loaded beams is investigated here. For direct comparison with specimens tested in this project, only the compression-chord loaded rectangular beams with 21 in. web width, 42 in. or 75 in. web depth, 0.3% web reinforcement, and a/d ratios of 1.85 and 2.50 are included in this series from Project 0-5253. As no beams were tested with 0.6% web reinforcement in the previous project, a

compression-chord loaded beam, C1-42-1.85-06, was tested in the current experimental program to fill that gap.

Table 5-12 for this series. The strength ratios are also plotted in Figure 5-15 for each of the four comparison groups. Horizontal lines indicate the mean value for each group in the figure.
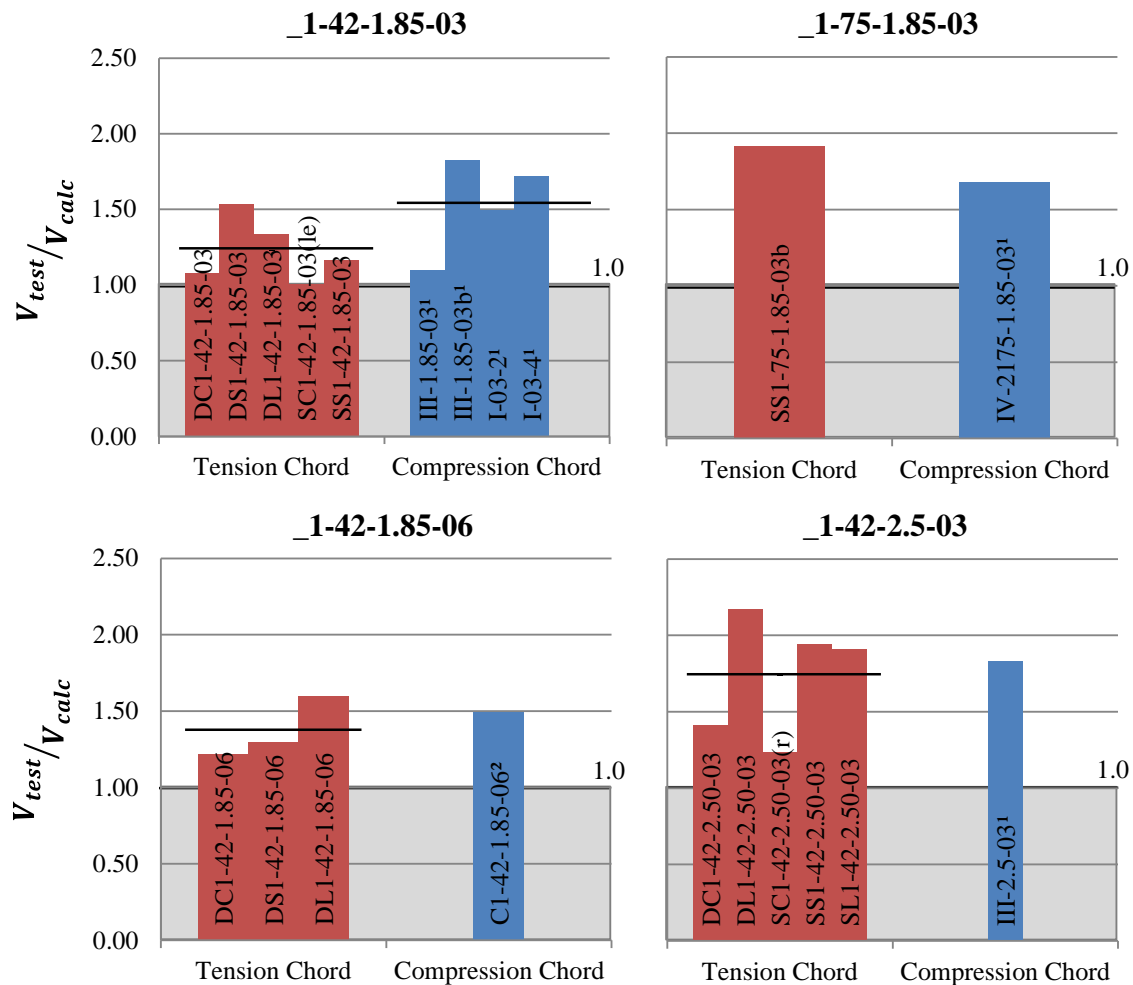
Figure 5-15: Series VI: Loaded Chord- Direct comparisons of experimental capacity with TxDOT Project 0-5253 STM calculations.

The V_{test}/V_{calc} ratios varied between 1.05 and 2.17 for tension-chord loaded (inverted-T) beams and 1.10 to 1.83 for compression-chord loaded beams. It is important to note that all capacity ratios were above 1.0, indicating a conservative strength estimation for all specimens. As shown in Figure 5-15, the conservatism with respected to the loaded chord varied depending on the shear span to depth ratio, web depth, and reinforcement ratio. For 42 in. deep beams tested at an a/d of 1.85, the STM provisions were slightly more

138

conservative (the capacity ratio was higher) for compression-chord loaded specimens with either reinforcement ratio. The opposite was true for 75 in. deep beams with a reinforcement ratio of 0.3% in both directions; however with such few shear tests at that web depth, a definitive conclusion cannot be made. For the 42 in. deep beams tested at an a/d ratio of 2.50 and 0.3% reinforcement in both directions, the strut-and-tie models for the tension-chord loaded beams were slightly more conservative. Overall the STM models appear to estimate relatively accurately shear strength with little bias toward loading chord and with only two tests having V_{test}/V_{calc} values over 2.0.

When comparing all of the specimens in this series without grouping, a slight decrease in the conservatism in the models is seen with the tension-chord loaded specimens (V_{test}/V_{calc} = 1.50) versus the compression-chord loaded specimens (V_{test}/V_{calc} = 1.59) as summarized in Table 5-13 and Figure 5-16. This trend is true for beams tested at an a/d ratio of 1.85, as the average V_{test}/V_{calc} is 1.37 for tension-chord loaded beams and 1.83 for compression-chord loaded beams. The opposite is true for specimens tested at an a/d ratio of 2.50 as the conservatism of the inverted-T beams is higher than that of the rectangular beams, but there are fewer results to compare. Given the conflicting trends for various parameter groups and only a slight overall difference observed between compression- and tension-chord loaded specimens, it can be concluded that the STM provisions show little bias towards compression- or tension-chord loading.

Table 5-13: Series VI: Loaded Chord STM summary.

V_{test} / V_{calc}	Tension Chord			Compression Chord		
	all	**a/d = 1.85**	**a/d = 2.50**	**all**	**a/d = 1.85**	**a/d = 2.50**
	14 tests	**9 tests**	**5 tests**	**7 tests**	**6 tests**	**1 tests**
Min	1.05	1.05	1.23	1.10	1.10	1.83
Max	2.17	1.92	2.17	1.83	1.83	1.83
Mean	1.49	1.35	1.73	1.59	1.55	1.83
STDV	0.36	0.28	0.39	0.26	0.26	
COV*	0.24	0.21	0.23	0.16	0.17	

* COV = Coefficient of Variation (Standard Deviation / Mean)
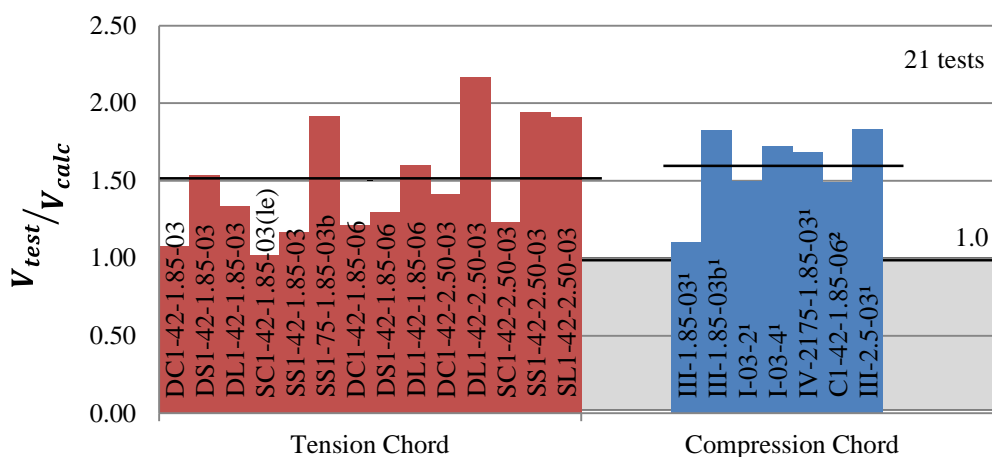
Figure 5-16: Series VI: Loaded Chord- STM conservatism

5.2.4 Summary of Strength Results

The strut-and-tie provisions developed by TxDOT Project 0-5253 and implemented for inverted-T beams as described in Chapter 2 produced reasonably conservative estimates of the strength of all the inverted-T specimens. The STM procedures offer a more rational approach to designing inverted-T deep beams than sectional design, as they inherently consider all failure modes for the ledges, web, and bearing points. A summary of the comparisons of V_{test}/V_{calc} from the strut-and-tie models for all specimens tested is provided in Figure 5-17 and Table 5-14.

The STM provisions showed no bias to ledge depth, number of point loads, beam depth, or chord loading; i.e., they captured the effects of these variables adequately. The provisions did however show limited bias to ledge length and reinforcement ratio, but produced conservative results in all cases with reasonable safety margins. The strength results from the thirty three tests in the experimental program thus support a recommendation to use TxDOT Project 0-5253 STM provisions for the strength design of inverted-T beams. It is also recommended based on strength observations to avoid cut-off ledges because the specimens were more prone to ledge failures and strengths estimates with lower safety margins.
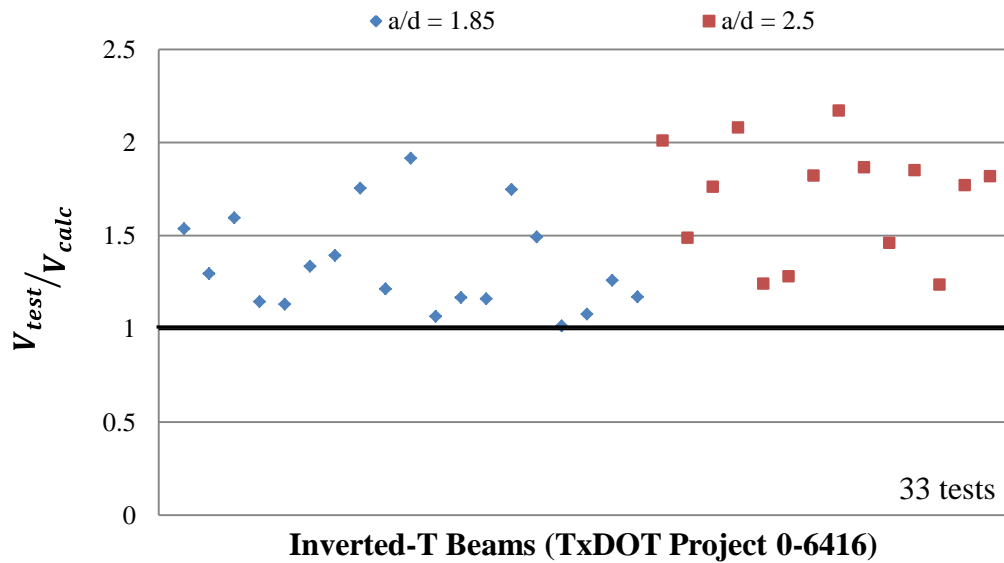
Figure 5-17: Conservatism of STM provisions as applied to inverted-T beams

Table 5-14: Summary of experimental/calculated shear capacity

$\dfrac{V_{test}}{V_{calc}}$	Inverted-T Beams (0-6416) 33 tests	Evaluation Database (0-5253) 179 tests
Min	1.05	0.73
Max	2.17	4.14
Mean	1.50	1.54
Unconservative[*]	0.0%	0.6%
Standard deviation	0.33	0.43
Coefficient of Variation**	0.22	0.28

* Unconservative = % of tests for which $V_{test}/V_{calc} < 1.0$

** Coefficient of Variation = Standard Deviation / Mean

5.3   DIAGONAL CRACKING UNDER SERVICE LOADS

In TxDOT Project 0-5253, a recommendation to limit shear stresses in deep beams at service loads was given. Such a limit is useful for the prevention and control of diagonal cracks. The limit was given through a simple and reasonably conservative equation. This equation and its applicability to inverted-T beams is discussed herein.

5.3.1 Background

For durability considerations, it is necessary to limit or prevent diagonal cracking under service loads in reinforced concrete members. In this section, trends between the shear force at first diagonal cracking and pertinent variables are investigated.

The main types of cracks found in inverted-T beams are depicted in Figure 5-18. The focus of the current project is diagonal cracking, including both flexure-shear cracks and web-shear cracks. Flexure-shear cracks form after or simultaneously with the flexural cracks and extend from the tip of the flexural crack towards the load or, as in the case of inverted-T beams, to the compression chord directly above the load. Web-shear cracks occur independently from flexural cracking and form when the principal tension stress in the web of the member exceeds the tensile strength of the concrete. In deep beams, transverse tensile stresses develop due to the spreading of compressive stresses in bottle-shaped struts and also contribute to the width of flexure-shear cracks (MacGregor and Wight, 2005).
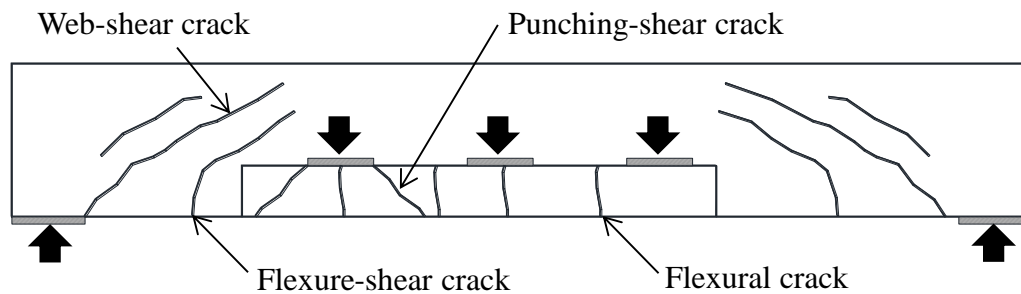
Figure 5-18: Types of cracks in reinforced concrete inverted-T deep beams.

With regard to the current project, no distinction was made between flexure-shear or web-shear cracks when evaluating the serviceability behavior of the test specimens. Both were treated as diagonal cracks.

ACI-ASCE Committee 326 report (1962) identified the major variables that affect the diagonal cracking load of reinforced concrete beams. These variables are: section size ($b_w d$), tensile strength of concrete (that can be taken as a function of ($\sqrt{f_c'}$)), longitudinal reinforcement ratio (ρ_l), and moment to shear ratio at the critical section (M/V). Since M/V is constant in the main shear span of beams loaded with concentrated loads, the shear span-to-depth ratio (a/d) can be used in lieu of M/V.

In TxDOT Project 0-5253, the effects of these variables ($b_w d$, $\sqrt{f_c'}$, a/d, ρ_l, d) on the diagonal cracking load of deep beams was assessed with data from the experimental program and the literature. The resulting information was then used to recommend an

equation that estimates a load below which service loads must remain to limit diagonal cracking.

As with all cracking data, considerable scatter was observed in diagonal cracking loads of deep beams. The deep beam project showed that the primary variables affecting the diagonal cracking load were the section size, the tensile strength of the concrete, and the a/d ratio. The longitudinal reinforcement ratio was not explicitly examined as part of the experimental program and although it may contribute to the diagonal cracking load to some degree, there was insufficient data to fully evaluate the variable. The effect of the section depth was found to be small and erratic based on test results and data from the literature. The quantity of web reinforcement was also not found to have a significant effect on the load at first diagonal cracking as the steel is not typically engaged until after the section cracks.

Two approaches to limit diagonal cracking under service loads were considered in TxDOT Project 0-5253. The first was associated with the strut-and-tie models and involved limiting the force generated in the diagonal strut by service loads to a specified percentage of its unfactored capacity. This was, in effect, a separate service-load strut-and-tie analysis that could be integrated easily with the ultimate-strength since the same model would be used with different applied loads and efficiency factors.

It was decided not to recommend this approach however due to a fundamental flaw. Strut-and-tie modeling is a lower-bound approach and therefore is intended to be used in design to provide a safe estimate for ultimate strength. In order for a member to reach the ultimate capacity estimated by the STM, redistribution of forces and cracking is expected to occur. The analysis procedure is not intended to accurately estimate service level stresses or limit cracking. Thus the researchers of TxDOT Project 0-5253 concluded that a STM-based approach to limit diagonal cracking under service loads would not be appropriate.

The resulting recommendation was a separate service load check. A reasonably conservative equation was developed to estimate the diagonal cracking load of deep beams based on data from the experimental program and the deep beam database. This check was simple and more theoretically justified than the STM approach. In this task, the applicability of the deep beam diagonal cracking load estimate is evaluated for use with inverted-T beam design.

5.3.2   Diagonal Cracking in Inverted-T Beams

Several experimental variables were evaluated to determine the effect on the diagonal cracking load of inverted-T deep beams. Along with the section size ($b_w d$), the tensile

strength of the concrete ($\sqrt{f'_c}$), and the a/d ratio, the effect of the ledge geometry, reinforcement ratio, and number of point loads were assessed.

The effect of section size on the diagonal cracking load of the specimens in the experimental program is shown in Figure 5-19. As expected, the diagonal cracking load increases as the shear area (b_wd) increases. Prior to diagonal cracking, the member behaves elastically and thus the entire section contributes to the diagonal cracking strength. As the specimen cracks the layout and material strength influence the ultimate capacity of the inverted-T beams.
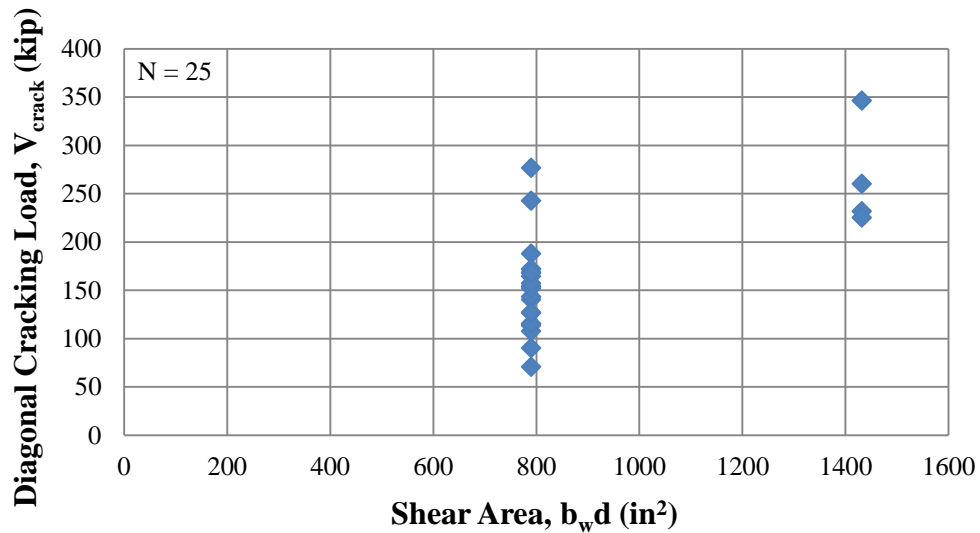
Figure 5-19: Effect of section size on diagonal cracking load of inverted-T beams.

There is scatter within each section size in Figure 5-19, which is likely a result of the other variables that contribute to the diagonal cracking load of deep beams. To determine the effect of the tensile strength of the concrete, the diagonal cracking load was normalized by the shear area and plotted versus $\sqrt{f'_c}$ in Figure 5-20.

144
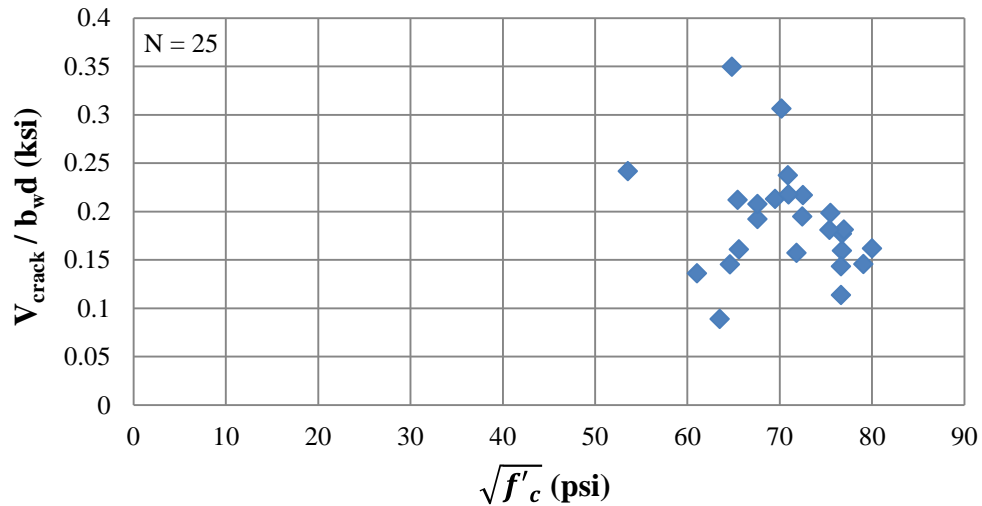
Figure 5-20: Effect of tensile strength on diagonal cracking load of inverted-T beams.

It has been widely accepted that the diagonal cracking load is a function of the square root of the compressive strength of concrete; the cracking load is expected to increase with the tensile strength of the concrete that is a function of the square root of the compressive strength of concrete. The data plotted in Figure 5-20 shows considerable scatter without a clear trend between the diagonal cracking load and the square root of the compressive strength of the concrete. It is important to note here that concrete strengths did not vary substantially across test specimens and therefore the variable could not be adequately assessed using the inverted-T specimens.

Based on past research and TxDOT Project 0-5253, the diagonal cracking loads are normalized by the shear area times the square root of the compressive strength of concrete; i.e., the influence of section size and concrete strength on cracking were included in the analyses.

The effect of the shear span-to-depth ratio on the diagonal cracking load of inverted-T beams is shown in Figure 5-21. In the figure, the normalized diagonal cracking load can be seen to decrease as the a/d ratio increases. This observed trend is similar to that observed for compression-chord loaded beams in the TxDOT Project 0-5253. As discussed in Birrcher et al. (2008), the downward trend is related to the change in principle tensile stress distribution that occurs when the a/d ratio changes. Lower a/d ratios are subjected to a more complex state of stress due to the proximity of the applied load to the support. As a result there is considerable scatter at an a/d ratio of 1.85. As the a/d ratio exceeds 2, the beam tends more towards slender beam behavior and diagonal cracking strengths are concentrated at $2\sqrt{f_c'}b_wd$ (in psi units).
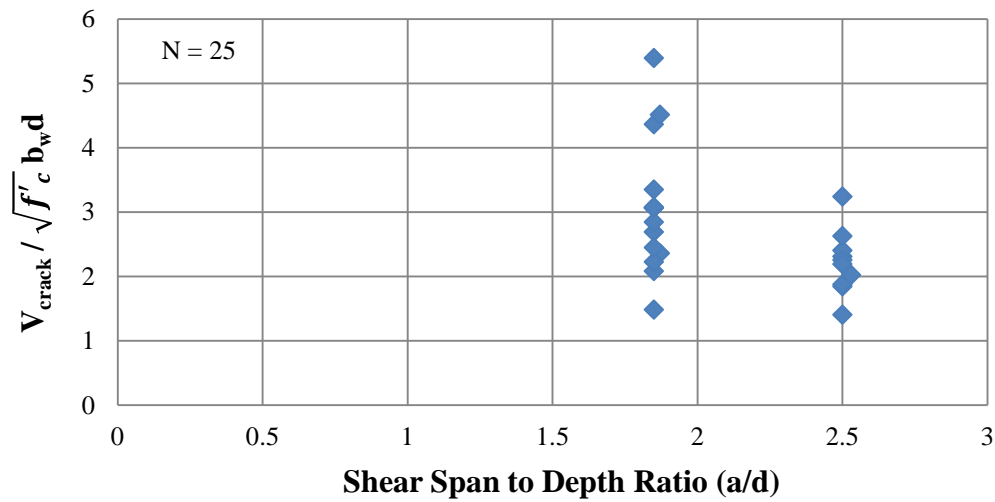
Figure 5-21: Effect of a/d ratio on diagonal cracking load of inverted-T beams.

As the longitudinal reinforcement ratio in the current study was not varied significantly, the effect of that parameter could not be assessed with respect to crack width. The effect of beam depth on the diagonal cracking load was evaluated in both projects. The results from TxDOT Project 0-5253 indicate that the diagonal cracking load decreased with increasing beam depth, but the effect was small and erratic. Other deep beam literature sources revealed conflicting results. No clear trend is revealed by plotting the data from the current inverted-T beam experimental program in Figure 5-22. No depth effect was apparent at the different a/d ratios.
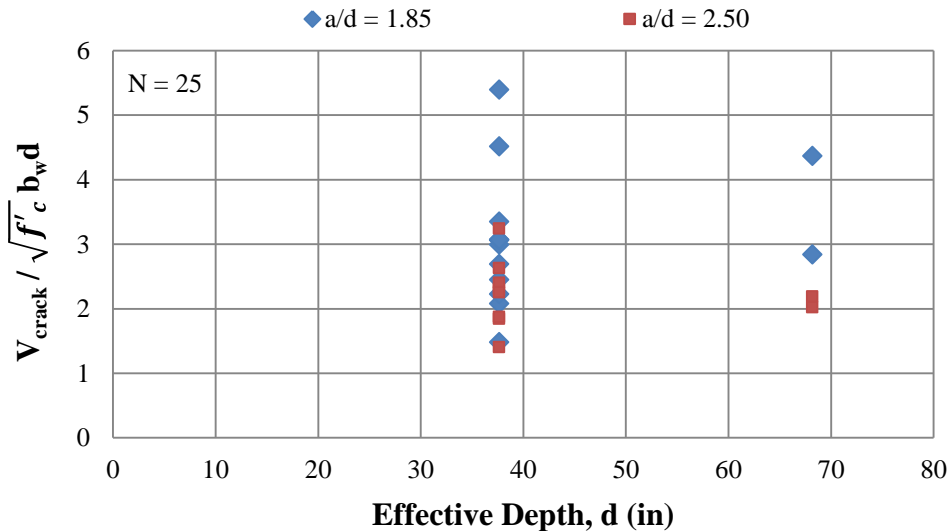
Figure 5-22: Effect of depth on the diagonal cracking load of beams of inverted-T beams.

The effect of web reinforcement ratio was also evaluated in the experimental program of the current project. As discussed in Section 4.5, a slight decrease in diagonal cracking

load was observed for the directly comparable inverted-T beams; illustrated in Figure 5-23. Three out the four comparisons show this trend, however, due to the limited number of direct comparisons and the weak trend observed it can be concluded that web reinforcement ratio has a negligible effect on the load at first diagonal cracking. A similar observation can be made when the normalized diagonal cracking loads for all test specimens are examined (Figure 5-24). Likewise, no significant effect of web reinforcement ratio on the diagonal cracking load of deep beams was observed in Project 0-5253.
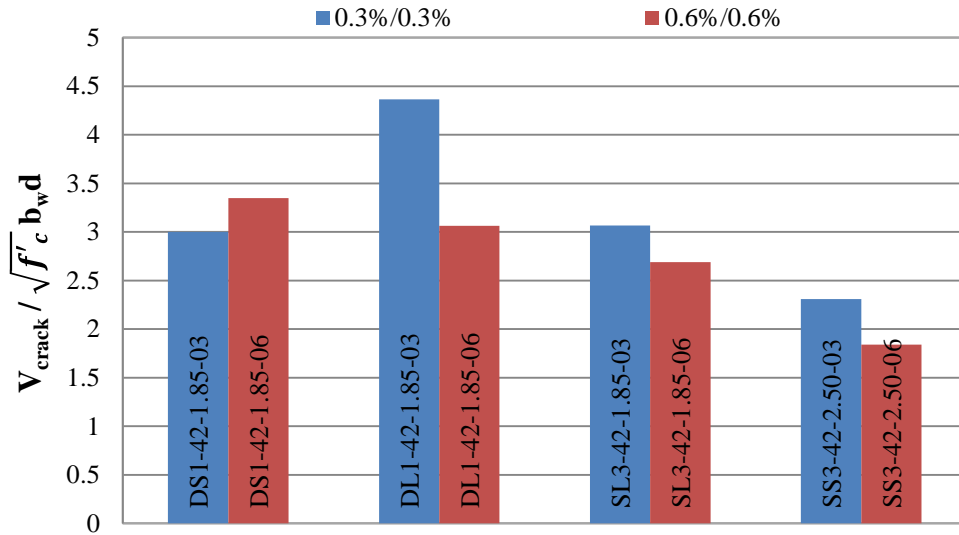
Figure 5-23: Effect of web reinforcement on the diagonal cracking load of directly comparable inverted-T specimens.
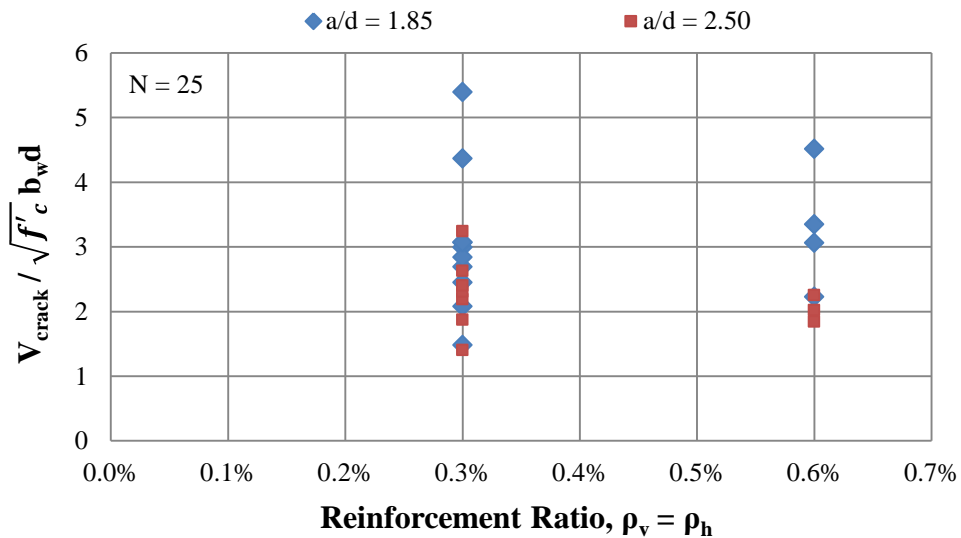
Figure 5-24: Effect of web reinforcement on diagonal cracking load of inverted-T beams.

147

The variables unique to the current experimental program, including ledge length, ledge depth, and the number of point loads, were also investigated to determine their effect on the diagonal cracking load of inverted-T beams.

As discussed in Section 4.3, the length of the ledge on the inverted-T specimens was found to have a positive effect on the diagonal cracking load. An increase in the normalized cracking load was observed with increasing ledge lengths between directly comparable beams. As shown in Figure 5-25, the trend can also be seen when all cracking loads in the experimental program are considered. Even with the scatter in the data there is a clear increase in diagonal cracking load with longer ledge lengths for both a/d ratios. Thus the cracking load results reinforce the strength-based recommendation for avoiding the use of cut-off ledges in practice. Not only do cut-off ledges generate relatively low web-shear strengths compared to other ledge lengths, but they also cause adjacent webs to crack at lower shear stresses than with longer ledges.

Thus given the recommendation not to use cut-off ledges and the inherent scatter in test results, it was decided to consider a conservative limit on shear stress at diagonal cracking that encompasses short and long ledges without explicitly accounting for ledge length.
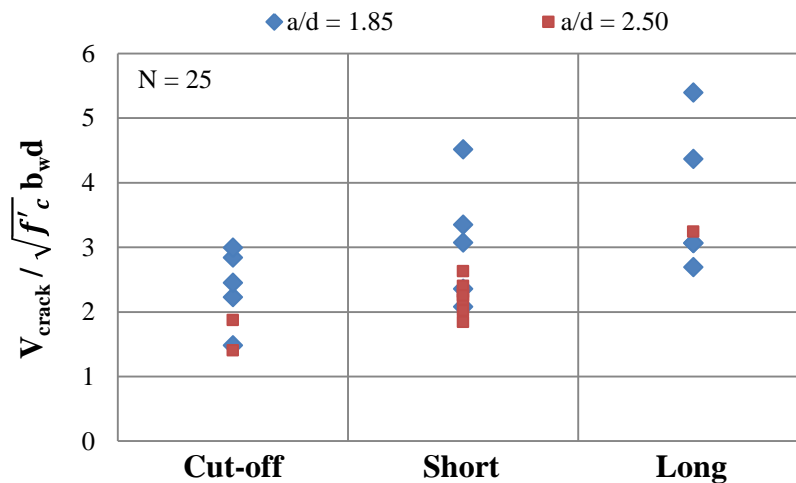
Figure 5-25: Effect of ledge length on the diagonal cracking load of inverted-T beams.

A weaker trend between diagonal cracking load and ledge depths was noted in Section 4.4. According to the results of the direct comparisons, deeper ledges tended to experience a slightly higher normalized cracking load than shallow ledges. The general comparison shown in Figure 5-26 supports this observation for beams tested at an a/d ratio of 1.85, but there is no apparent trend for the beams tested at an a/d ratio of 2.50. The observed trends however are relatively weak and the depth of the ledge is not

considered to be a primary variable affecting the diagonal cracking load of inverted-T beams.
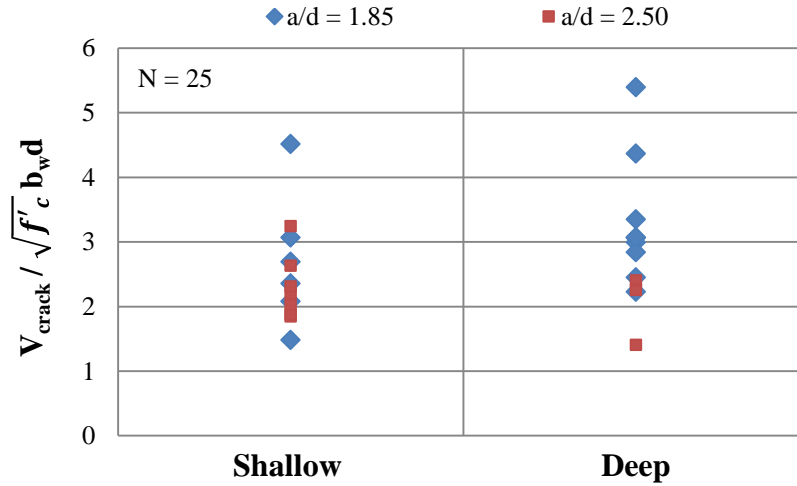
Figure 5-26: Effect of ledge depth on the diagonal cracking load of inverted-T beams.

A third variable unique to this study is the number of point loads. The direct comparisons relating to the number of point loads did not reveal an effect on the diagonal cracking load as discussed in Section 4.6. As shown in Figure 5-27, no significant trend can be observed from the general comparison of data from all tests of the experimental program.
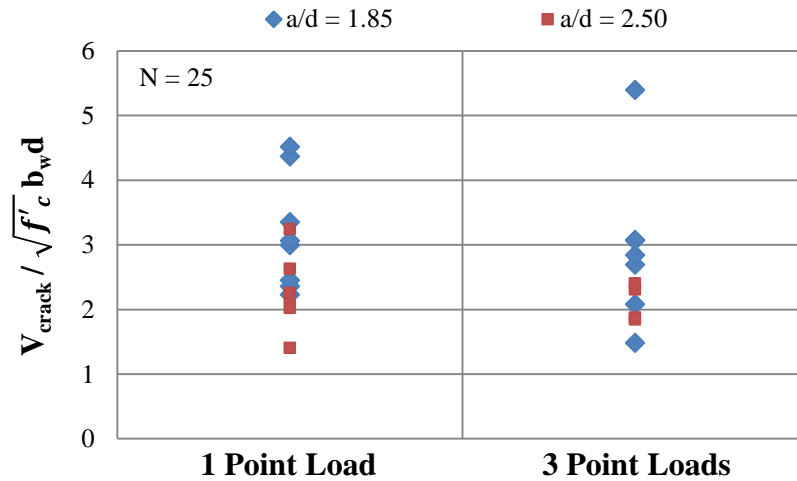
Figure 5-27: Effect of multiple point loads on the diagonal cracking load of inverted-T beams.

In summary, the primary variables found to affect the diagonal cracking loads were the shear area, $b_w d$, and the shear span-to-depth ratio, a/d. The tensile strength of the concrete, represented by $\sqrt{f_c'}$, was also considered for normalization purposes although

no clear trend was observed in this data set. Ledge length showed some influence on the load at first diagonal cracking; the influence was however not large enough to warrant including it in limits on service-load shear stresses. Cut-off ledges tended to crack at lower loads than beams with other ledge lengths. Such an observation reinforces the strength-based recommendation for not using cut-off ledges in practice.

Estimating Diagonal Cracking Loads

TxDOT Project 0-5253 examined empirical equations from the deep beam literature and determined that they did not have the level of accuracy and conservatism required for the current task. Many of these equations only applied to slender beams or those of considerably smaller shear area and thus were not applicable to the compression-chord loaded bent caps under investigation in that project. Very limited data was available prior to this project of crack width progression for inverted-T beams.

In TxDOT project 0-5253, a simple and reasonably conservative equation was selected for determining the diagonal cracking load as is was deemed the most reasonable approach given the scatter in the data. The equation proposed in TxDOT Project 0-5253 is compared to diagonal cracking data of a deep beam database (from Project 0-5253) and results for this project's experimental program (Project 0-6416) in Figure 5-28.

As shown in Figure 5-28, the TxDOT Project 0-5253 equation estimates a lower bound on shear stress at first diagonal cracking not only for compression-chord loaded beams but also for inverted-T beams. The four inverted-T beams that showed diagonal cracking at shear stresses lower than estimated by the equation had shallow and/or cut-off ledges (SC1-42-1.85-03, SL1-42-1.85-03, SC3-42-1.85-03, SC3-42-2.50-03). Such an observation strengthens the recommendation for eliminating cut-off ledges in practice based on strength. If cut-off ledges were not used, the given equation would be conservative for all but one of the inverted-T specimens. Overall the performance was comparable to the compression-chord loaded beams for which it was developed. It is therefore concluded that the existing equation for limiting shear stress at service loads in rectangular beams is equally applicable to inverted-T beams.
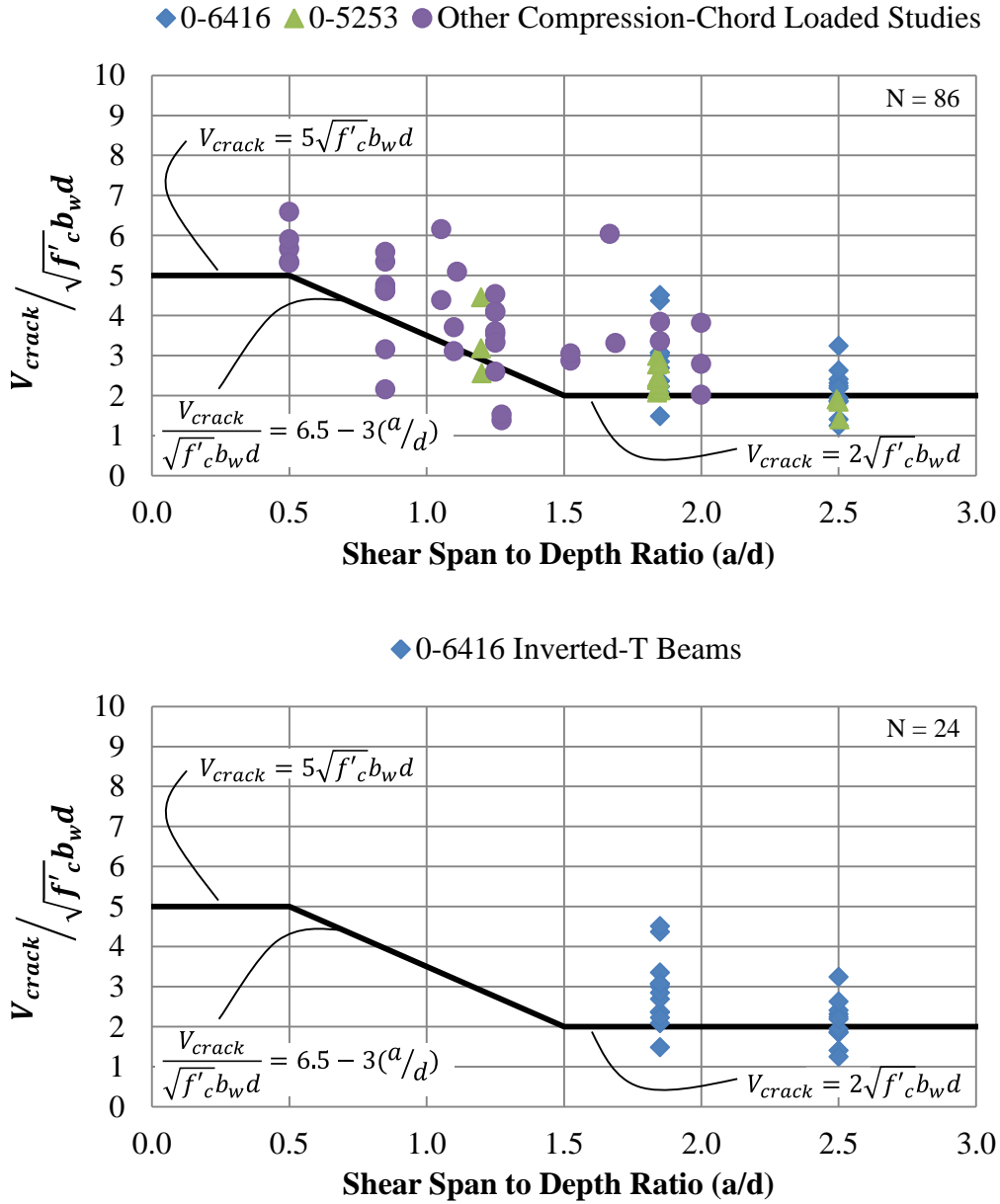
Figure 5-28: Assessment of proposed equation for estimate of diagonal cracking.

5.3.3 Design Implications

To limit diagonal cracking in inverted-T bent caps under service loads, the following approach should be taken. The shear in the member due to unfactored service loads should be computed and compared to the estimated diagonal cracking load given by the following equation:

$$V_{crack} = [6.5 - 3(\tfrac{a}{d})]\sqrt{f'_c} b_w d \qquad\qquad (5.1)$$

but not greater than $5\sqrt{f'_c} b_w d$ nor less than $2\sqrt{f'_c} b_w d$

with a = shear span (in.) (Refer to Figure 3-2)
         d = effective depth of the member (in.)
         f'_c = compressive strength of concrete (psi)
         b_w = web width of the member (in.)

A member is not expected to crack under normal loading conditions if the service level shear is less than the estimated diagonal cracking load. If the service-load shear is greater, the design of the member can be altered to increase the value of the diagonal cracking load. The section size ($b_w d$) of the member can be increased, but a greater depth will reduce the a/d ratio for a member with a fixed span length. Theoretically, a higher concrete strength can also be specified to increase the tensile capacity of the concrete but based on the lack of trend observed in Figure 5-20, this is likely more beneficial for compression-chord loaded beams than inverted-T beams. If these options are not practical, additional web reinforcement can be provided to help restrain the diagonal crack widths under service loads. Note that, as discussed in Section 4.5.3, there are lesser benefits of supplying additional web reinforcement for the purpose of crack width control, especially around service level loads.

The service load check provides an indication of the likelihood of the formation of diagonal cracks in service. As discussed in Birrcher et al. (2009), the proposed equation can also be used to determine at what load an inverted-T or deep beam is expected to crack, if the service load shear exceeds the expected diagonal cracking load. This will indicate if a bent cap can be expected to crack under dead loads alone; a scenario that should be avoided.

5.3.4 Summary and Conclusions
The variables that affect the diagonal cracking load of inverted-T beams were investigated with data from the current experimental program. The primary variables were found to be the shear area, $b_w d$, and the a/d ratio of the member. Web reinforcement ratio and ledge length were found to have limited influence with the exception of several beams with cut-off ledges. The diagonal cracking load recorded in inverted-T beam tests compared well with the lower-bound empirical equation developed for rectangular beams. Only four of the inverted-T beams showed lower diagonal cracking loads than estimated by the equation but their values were well within the acceptable range of scatter. Those beams had mostly cut-off ledges. Given the relatively low diagonal cracking load recorded for specimens with cut-off ledges, it is not recommended to design inverted-T beams with cut-off ledges.

It is recommended to use the same diagonal cracking equation for inverted-T beams and rectangular beams. Limiting the shear stresses at service loads to below values estimated by the equation will reduce the likelihood of diagonal cracking at service loads but will not guarantee that a reinforced concrete inverted-T beam will remain uncracked under service loads. Inconsistencies in design assumptions and actual field conditions can result in stresses higher than those accounted for in this equation. However, the process is simple and should significantly reduce diagonal cracking in service. It also draws the attention of the designer to the serviceability aspect of design for inverted-T beams, which is lacking in the AASHTO LRFD Design Specifications and TxDOT Bridge Design Manual as both of these methods only limit the stress in the hanger reinforcement at service loads.

5.4 CORRELATION OF MAXIMUM IN-SERVICE DIAGONAL CRACK WIDTH WITH ULTIMATE SHEAR STRENGTH

As discussed in Chapter 1, diagonal cracking has been observed in multiple inverted-T straddle bent caps in existing structures. During field inspections, engineers are tasked with assessing the amount of damage in the members. Currently there is little information in the literature that presents a reliable method for relating the width of diagonal cracks to the amount of distress in an inverted-T beam. In this section, a method for comparing the maximum width of an in-service diagonal crack with the residual capacity of an inverted-T straddle bent caps is developed.

TxDOT Project 0-5253 created a simple chart that related the maximum diagonal crack width on a deep beam to the load on the member. Unlike an analytical approach which would require complex models and multiple assumptions to estimate diagonal crack widths, the empirically-based chart can easily be used by engineers in the field. That chart is currently not approved for use with inverted-T beams.

5.4.1 Background

Limited crack width data was available in the literature, none of which could be used to relate crack widths to load levels in inverted-T beams. Only results from this study were applicable to inverted-T beams. The following presents an overview of crack width data for deep rectangular beams to frame the issue for inverted-T beams.

Birrcher et al. (2009) reviewed the few studies on deep beam shear that included the serviceability information to determine what factors affected the crack widths. Although none of the specimens were loaded on the tension chord, the conclusions were made on deep beams and have some relevance to the current task.

Effect of web reinforcement on the diagonal crack widths of rectangular deep beams

The review of deep beam literature by Birrcher et al. (2009) revealed that distributed web reinforcement was reported as being the most important variable in controlling diagonal crack widths. From limited test data in which crack widths were reported, additional vertical reinforcement beyond a certain minimum was found to have little effect on further restraining the diagonal crack widths in the service load range. Above 50% of the load capacity however, Bracci et al., (2000) and Young et al., (2002) found that specimens with 0.6% reinforcement in the vertical direction had narrower crack widths than those with 0.3% reinforcement. These results were obtained from full-scale (33 in. x 36 in.) specimens and agree well with the findings for inverted-T specimens. It was observed for the inverted-T specimens that increasing the amount of web reinforcement from 0.3% to 0.6% had limited effect on the diagonal crack widths at typical service load levels, but was found to make a significant difference at higher loads as discussed in Chapter 4.

TxDOT Project 0-5253 came to a similar conclusion when evaluating the diagonal crack widths for deep beams. In general the amount of transverse reinforcement was found to have limited effect on the maximum width of the diagonal crack at first cracking and more significantly at higher loads. Additionally, the spacing of the stirrups was found in that study not to significantly affect the width of diagonal shear cracks as long as the existing spacing limit of d/4 or 12 in. in Section 5.13.2.3 of AASHTO LRFD 2012 was upheld.

Effect of a/d ratio on the diagonal crack widths of rectangular deep beams

A review of the literature on reinforced concrete deep beams resulted in mixed observations on the effect of the a/d ratio on diagonal crack widths. A few studies discussed in Birrcher et al. (2009) observed some increases in diagonal crack widths as the a/d ratio increased, but the data was not conclusive. Others saw no trend between the diagonal crack widths and a/d ratio. In their own work, Birrcher et al. saw a trend when examining some sets of comparable beams and no trend in others. When all of the specimens were plotted collectively, a slight trend with the a/d ratio was observed but it was attributed more to the scatter in diagonal crack width data. It was therefore concluded that the a/d ratio did not have a significant effect on the diagonal crack widths of rectangular deep beams.

5.4.2 Diagonal Crack Widths in Inverted-T Beams

All of the test specimens of the current project are listed in Table 5-15. The specimens that failed in punching shear or flexure were also included as they had reached their predicated shear capacity at failure. The results of thirty three inverted-T beam shear tests

were used in the current task. Nineteen specimens were tested at an a/d ratio of 1.85 and fourteen were tested at an a/d ratio of 2.50. The overall height of the specimens was either 42 or 75 in. and the width was constant at 21 in. The ledge depth and length varied as discussed in Section 3.2. The web reinforcement was either 0.3% or 0.6% in both orthogonal directions. Two specimens were tested with 0.6% reinforcement in the vertical and 0.3% in the horizontal direction. Several different bearing plate sizes were used as shown in Table 5-15.

The measured maximum diagonal crack widths were plotted versus the percent of maximum applied load in the figures included in this section. Plotting the crack data from the experimental program in this manner enabled specimens of different size, ledge geometries, and concrete strength to be compared. It also enabled a correlation to be made between the maximum diagonal crack width and the percent of the ultimate capacity. The size of the bearing plates were assumed to have no effect on the width of the diagonal cracks.

Table 5-15: Specimens used in correlating crack width to capacity.

Specimen	b in.	h in.	d in.	Ledge Depth	Ledge Length	Point Loads	Support Plate in.	Load Plate in.	ρ_v	ρ_h	a/d ratio
DS1-42-1.85-03	21	42	37.6	h/2	Short	1	16 x 20	26 x 9	0.3%	0.3%	1.85
DS1-42-2.50-03	21	42	37.6	h/2	Short	1	16 x 20	26 x 9	0.3%	0.3%	2.50
DS1-42-1.85-06	21	42	37.6	h/2	Short	1	16 x 20	26 x 9	0.6%	0.6%	1.85
DS1-42-2.50-06	21	42	37.6	h/2	Short	1	16 x 20	26 x 9	0.6%	0.6%	2.50
DL1-42-1.85-06	21	42	37.6	h/2	Long	1	16 x 20	26 x 9	0.6%	0.6%	1.85
DL1-42-2.50-06	21	42	37.6	h/2	Long	1	16 x 20	26 x 9	0.6%	0.6%	2.50
SS3-42-1.85-03	21	42	37.6	h/3	Short	3	16 x 20	18 x 9	0.3%	0.3%	1.85
SS3-42-2.50-03	21	42	37.6	h/3	Short	3	16 x 20	18 x 9	0.3%	0.3%	2.50
SS3-42-2.50-06 (f)	21	42	37.6	h/3	Short	3	16 x 20	18 x 9	0.6%	0.6%	2.50
SC3-42-1.85-03	21	42	37.6	h/3	Cut-off	3	16 x 20	18 x 9	0.3%	0.3%	1.85
SC3-42-2.50-03	21	42	37.6	h/3	Cut-off	3	16 x 20	18 x 9	0.3%	0.3%	2.50
DS3-42-2.50-03	21	42	37.6	h/2	Short	3	16 x 20	18 x 9	0.3%	0.3%	2.50
DL1-42-1.85-03	21	42	37.6	h/2	Long	1	16 x 20	26 x 9	0.3%	0.3%	1.85
DL1-42-2.50-03	21	42	37.6	h/2	Long	1	16 x 20	26 x 9	0.3%	0.3%	2.50
SL3-42-1.85-03	21	42	37.6	h/3	Long	3	16 x 20	18 x 9	0.3%	0.3%	1.85
SL3-42-1.85-06	21	42	37.6	h/3	Long	3	16 x 20	18 x 9	0.6%	0.6%	1.85
DC1-42-1.85-06	21	42	37.6	h/2	Cut-off	1	30 x 21	30 x 10	0.6%	0.6%	1.85
SS1-75-1.85-03	21	75	68.2	h/3	Short	1	16 x 20	30 x 10	0.3%	0.3%	1.85
DC3-42-1.85-03	21	42	37.6	h/2	Cut-off	3	16 x 20	18 x 9	0.3%	0.3%	1.85
DS3-42-1.85-03	21	42	37.6	h/2	Short	3	16 x 20	18 x 9	0.3%	0.3%	1.85
SS1-42-1.85-03	21	42	37.6	h/3	Short	1	16 x 20	26 x 9	0.3%	0.3%	1.85
SS1-42-2.50-03	21	42	37.6	h/3	Short	1	16 x 20	26 x 9	0.3%	0.3%	2.50
DC1-42-2.50-03	21	42	37.6	h/2	Cut-off	1	16 x 20	26 x 9	0.6%	0.6%	1.85
DL3-42-1.85-03 (f)	21	42	37.6	h/2	Long	3	16 x 20	18 x 9	0.3%	0.3%	1.85
SL1-42-2.50-03	21	42	37.6	h/3	Long	1	16 x 20	26 x 9	0.3%	0.3%	2.50
SC1-42-2.50-03 (r)	21	42	37.6	h/3	Cut-off	1	16 x 20	26 x 9	0.3%	0.3%	2.50
DS1-42-1.85-6/3	21	42	37.6	h/2	Short	1	16 x 20	26 x 9	0.6%	0.3%	1.85
DS1-42-2.50-6/3	21	42	37.6	h/2	Short	1	16 x 20	26 x 9	0.6%	0.3%	2.50
SC1-42-1.85-03 (le)	21	42	37.6	h/3	Cut-off	1	30 x 21	18 x 9	0.3%	0.3%	1.85
DC1-42-1.85-03	21	42	37.6	h/2	Cut-off	1	30 x 21	18 x 9	0.3%	0.3%	1.85
SC1-42-1.85-03b	21	42	37.6	h/3	Cut-off	1	30 x 21	30 x 10	0.3%	0.3%	1.85
DC1-42-1.85-03b	21	42	37.6	h/2	Cut-off	1	30 x 21	30 x 10	0.3%	0.3%	1.85
SS1-75-2.50-03	21	75	68.2	h/3	Short	1	16 x 20	30 x 10	0.3%	0.3%	2.50

(f) Flexural failure

(r) Shear friction failure of the web-to-ledge interface

(le) Ledge tie failure

5.4.2.1 Effect of test variables on the diagonal crack widths of inverted-T beams

As discussed in Section 5.3.1, two different types of diagonal cracks exist in reinforced concrete deep beams: flexure-shear cracks and web-shear cracks. In the analysis of the crack width data, no distinction was made between the two types of diagonal cracks. The variables that are suspected of affecting the width of the diagonal cracks in the inverted-T beams were explored using test results of this experimental program.

The maximum diagonal crack widths were examined using directly comparable beam sets in Chapter 4. In general, the amount of web reinforcement was found to affect the maximum width of diagonal cracks throughout the loading history; as illustrated in the two sets of comparisons in Figure 5-29. Specimens subjected to a given percent of ultimate load were found to have wider crack widths when reinforced with 0.3% web reinforcement ratio than those with 0.6%. In other words, the larger reinforcement ratio resulted in greater diagonal crack width restraint.
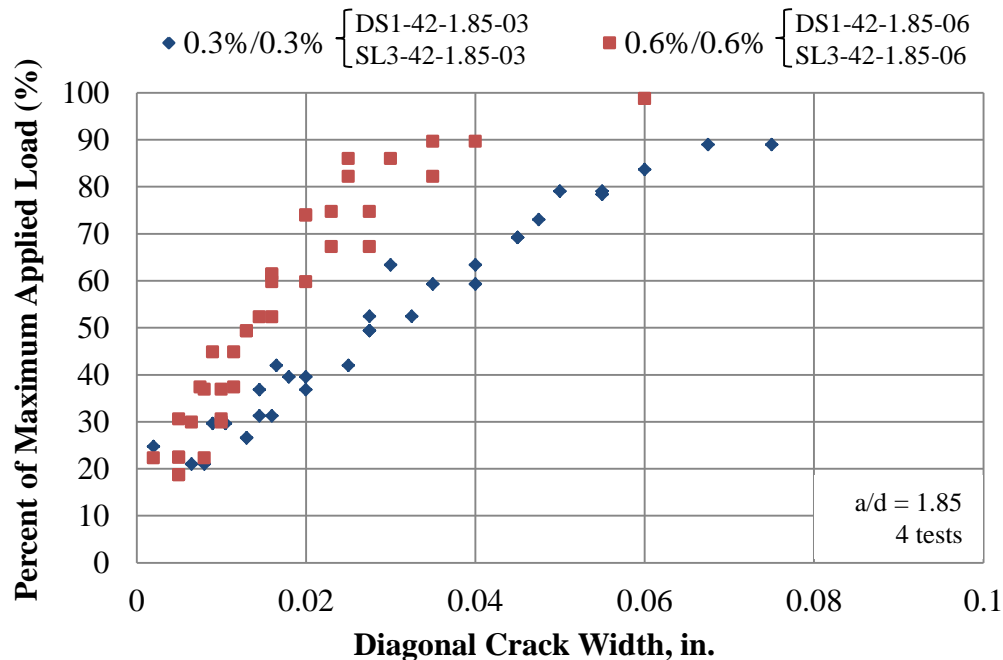
Figure 5-29: Effect of web reinforcement on diagonal crack widths of test specimens.

The serviceability effects of the other variables in the experimental program were also considered in Chapter 4. Except for the web reinforcement ratio, the direct comparisons did not reveal any appreciable trends between the inverted-T variables and the crack width progression. To some extent, the ledge length contributed to the width of diagonal cracks. However, the effect was small in relation to the scatter associated with the crack widths of similar specimens. The other variables investigated in the experimental

program, including a/d ratio, ledge depth, number of point loads, and web depth, did not have a significant effect on the width of the diagonal cracks. Thus, a chart correlating the diagonal crack width to the residual capacity of the inverted-T beams was developed considering the quantity of web reinforcement as the primary variable; as was done in TxDOT Project 0-5253.

5.4.2.2 *Correlation of Crack Width to Residual Capacity*

The crack width data from the thirty three specimens used in the current task are plotted in the following figures. Each of the nineteen beams included in Figure 5-30 were tested at an a/d ratio of 1.85. Figure 5-31 contains the crack width data from fourteen beams tested at an a/d ratio of 2.5. In both plots the data was separated into three groups by the quantity of web reinforcement: 0.3% reinforcement in each direction, 0.6% vertical reinforcement and 0.3% horizontal reinforcement, and 0.6% reinforcement in each direction.

As shown in Figure 5-30, there is a consistent trend between the maximum diagonal crack width and the amount of web reinforcement for an a/d ratio of 1.85. A power function trend line was fitted through the data for beams with equal reinforcement ratios in each direction . The square of the correlation coefficient, R^2, was provided next to each tend line. This value quantifies the error between the trend line and the data points, with an R^2 value of 1.0 representing a perfect fit. In Figure 5-30, it is shown that the R^2 value increases as the quantity of web reinforcement increases. This indicated that with a smaller amount of reinforcement there was more scatter in the diagonal crack width data for beams tested at an a/d ratio of 1.85. As the amount of web reinforcement was increased from 0.3% to 0.6% in each direction, the maximum width of diagonal cracks was more consistent. This observation was in agreement with the crack width findings for rectangular reinforced concrete deep beams in TxDOT Project 0-5253.

One specimen was constructed with 0.6% in the vertical and 0.3% in the horizontal direction with an a/d ratio of 1.85. At lower loads, below 60% of the maximum applied load, its crack widths resembled those of beams with 0.3% reinforcement in both directions. As the load increased past 60% of maximum, the diagonal crack widths tended more towards an average of the crack widths of specimens with 0.3% or 0.6% reinforcement ratios exclusively. Such findings suggest that a beam constructed with mixed reinforcement would mimic the behavior of a beam with equal reinforcement in both directions corresponding to approximately the average of the vertical and horizontal reinforcement ratios.
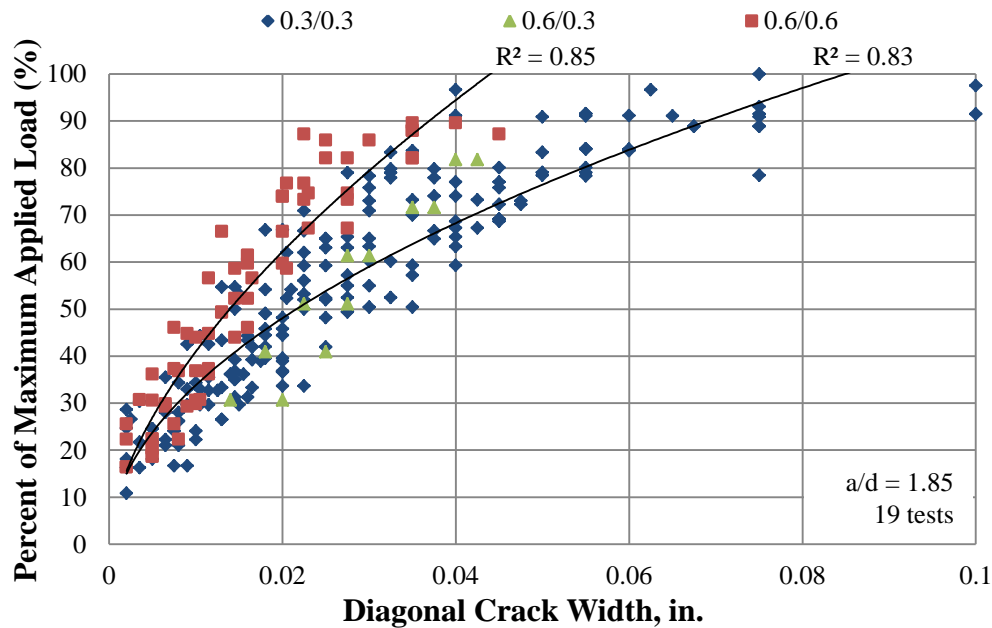
Figure 5-30: All crack width data at an a/d ratio of 1.85 used in this task with trend lines.

Crack width data from fourteen tests with an a/d ratio of 2.5 was also examined. As shown in Figure 5-31, the trend for the reinforcement ratios is consistent with that shown for an a/d ratio of 1.85. In fact, there is even less scatter in the beams tested at an a/d of 2.50 than those at 1.85 for specimens with 0.3% reinforcement in each direction, as indicated by the higher R^2 value. Higher amounts of web reinforcement showed lower scatter in the diagonal crack width data for a/d = 2.5 as well. One specimen with a vertical reinforcement ratio of 0.6% and horizontal reinforcement ratio of 0.3% was tested at an a/d ratio of 2.50. Similarly to the specimen tested at an a/d=1.85 with unequal reinforcement ratios, the crack width progression of this beam corresponded roughly to that of a beam that would be tested with equal reinforcement ratios in both directions equal to the average of both reinforcement ratios.
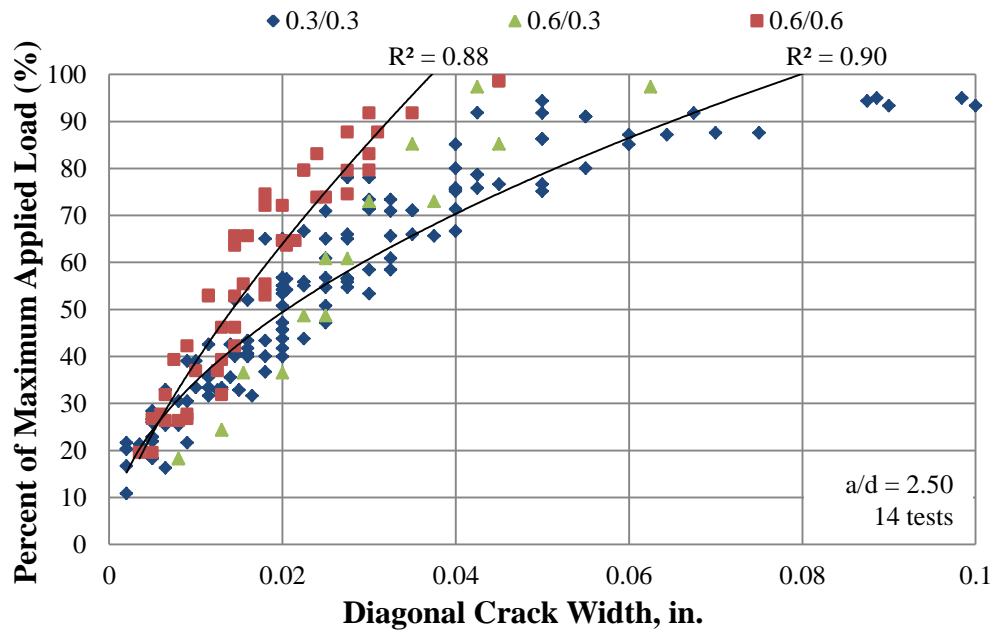
Figure 5-31: All crack width data at an a/d ratio of 2.50 used in this task with trend lines.

In Figure 5-32 and Figure 5-33, the power function trend lines were replaced with straight line segments for a/d=1.85 and a/d=2.5 respectively. Combining the two figures in Figure 5-34 showed minimal differences between trend lines for beams tested at the two a/d ratios. The diagonal crack widths were found to vary primarily due to the amount of web reinforcement present in the beam, and a/d ratios have little effect.
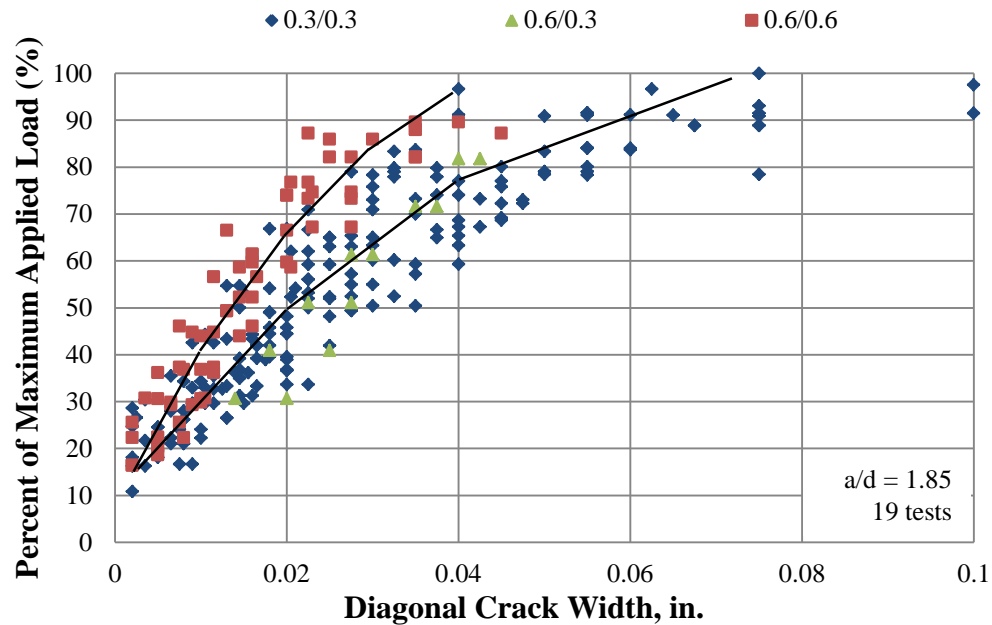
Figure 5-32: All crack width data at an a/d ratio of 1.85 with straight line approximations.
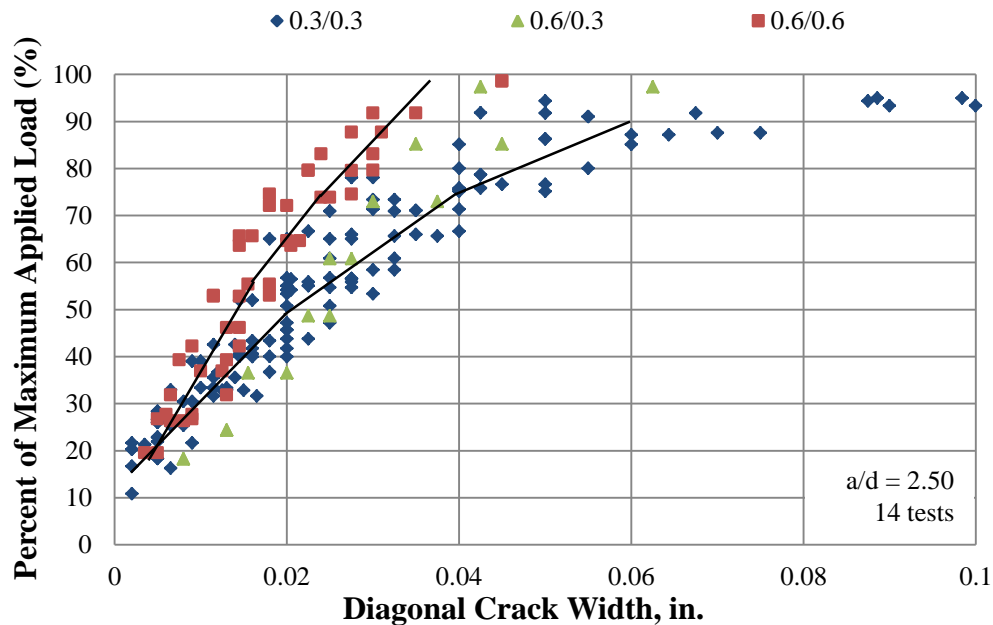
Figure 5-33: All crack width data at an a/d ratio of 2.50 with straight line approximations.

Several percentages of ultimate capacity were tabulated along with their corresponding maximum diagonal crack width values. For each percentage of ultimate load selected, a range of scatter based on the variance of the crack widths in the plot was also assigned. The resulting chart comparing the percent of ultimate capacity of a member to a measured crack width with respect to the member's reinforcement ratio is included in Figure 5-35.
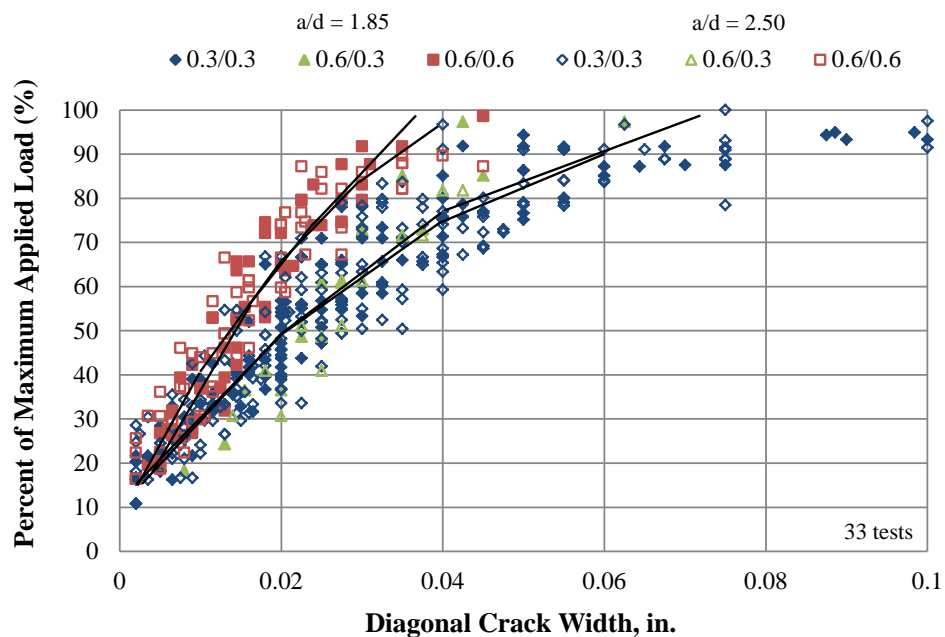
Figure 5-34: All crack width data with straight line approximations.

Load on the Member, Quantified as a Percent of Ultimate Capacity on Average (± scatter)						
Reinforcement \ w_{max} (in.)	0.01	0.02	0.03	0.04	0.05	0.06
$\rho_v = 0.003$ $\rho_h = 0.003$	30 (± 10)	50 (± 15)	65 (± 15)	75 (± 15)	80 (± 15)	90 (± 10)
$\rho_v = 0.006$ $\rho_h = 0.006$	40 (± 10)	65 (± 10)	85 (± 10)	~ Ultimate	~ Ultimate	~ Ultimate

Notation:
w_{max} = maximum measured diagonal crack width (in.)
ρ_v = reinforcement ratio in vertical direction ($\rho_v = A_v / bs_v$)
ρ_h = reinforcement ratio in horizontal direction ($\rho_h = A_v / bs_h$)
A_v & A_h = total area of stirrups or horizontal bars in one spacing (in.^{2})
s_v & s_h = spacing of stirrups or horizontal (skin reinf.) bars (in.)
b = width of web (in.)

Directions:
1). Determine ρ_v and ρ_h for bent cap
2). Measure maximum diagonal crack width, w_{max}, in inches
3). Use chart with w_{max}, ρ_v, and ρ_h to estimate % of capacity. Interpolate for intermediate values ρ_v and ρ_h. For unequal ρ_v and ρ_h use the average of the two when reading off the chart.

Important Notes:
In this chart, the maximum width of the primary diagonal crack in a shear-critical member is linked to the load on the member, quantified as a percent of its ultimate capacity. The intent of this chart is to aid field engineers in evaluating residual capacity in diagonally-cracked, reinforced-concrete bent caps subject to concentrated loads at a/d ratios between 1.0 and 2.5. This chart was developed from crack width data from 33 tests of simply supported reinforced concrete inverted-T beams with overall heights between 42" and 75". The testing was conducted at a/d ratios of 1.85 and 2.5.

This chart should be used in conjunction with sound engineering judgment with consideration of the following limitations:
 - variability in crack widths in general (± scatter)   -differences between field and laboratory conditions
 - members loaded at a/d < 1.85 may be at slightly higher % of capacity   -implications of an unconservative estimate of capacity

This chart is intended to be used for inverted-T bent caps. Not applicable with reinforcement ratios above 0.6%

Figure 5-35: Proposed chart that links diagonal crack width to percent of ultimate capacity of inverted-T bent caps.

The inverted-T diagonal crack width chart indicates a larger percent maximum load for a given crack width than that developed by TxDOT Project 0-5253 for compression-chord loaded deep beams with reinforcement ratios of 0.3%. It appears that the presence of tension in the web of the inverted-T members affects the width of the diagonal cracks.

The chart was developed with data from specimens constructed with the minimum reinforcement ratio of 0.3% and an upper bound of 0.6% in both directions. The percentage of ultimate capacity for inverted-T bent caps with less than 0.3% reinforcement can be conservatively estimated using the crack width data for the lower bound. This chart should be used with caution and sound engineering judgment for inverted-T bent caps that are constructed with reinforcement ratios greater than 0.6%. It is assumed that the crack widths will continue to decrease with increased amounts of reinforcement at a given percent of ultimate capacity, but specimens with greater than 0.6% reinforcement in either direction were not tested as part of the current project. Likewise, no bent cap inspected in this project was constructed with a web reinforcement ratio greater than 0.6%.

For the distressed in-service inverted-T bent caps that fall within the reinforcement ratio range given in Figure 5-35, it is acceptable to interpolate between the tabulated values. It is also acceptable to take an average of the reinforcement ratios in each orthogonal direction when using the chart. Using the chart with an assumed reinforcement ratio greater than the actual cap ratio will lead to a conservative estimate of the percent of ultimate capacity.

It should be emphasized that this chart should always be used in conjunction with sound engineering judgment. The conditions in the field can vary drastically from those seen in the laboratory. The chart is an estimate and its accuracy can change due to the variability in crack width data, the limited variables in the chart, and the differences between field and laboratory conditions. Thus the chart should only be viewed as a useful guide to making informed decisions regarding the level of distress in a diagonally cracked inverted-T bent cap.

5.4.3   Summary and Conclusions

In this section, variables that affect the maximum width of diagonal cracks in shear-critical inverted-T deep beams were discussed. Test results indicate that the amount of web reinforcement crossing the diagonal crack is the primary variable influencing the crack widths examined in this study. The a/d ratio was found to have little effect on the maximum width of the diagonal cracks. From the experimental data, a chart was produced that correlates the maximum width of a diagonal crack to the load acting on a member in terms of a percent of ultimate capacity. Results from thirty three full-scale

tests on specimens with varying ledge lengths, ledge depths, reinforcement ratios, number of point loads, and web depths were used to develop the chart. The chart should be used with sound engineering judgment because crack widths generally have high variability, the chart only accounts for a limited set of variables, and differences may exist between field and laboratory conditions.

CHAPTER 6
In-Service Inverted-T Bridge Bents

6.1 BACKGROUND

In this chapter, critical design characteristics and conditions of the investigated inverted-T straddle bent caps is presented. The residual capacity of each bent cap is then estimated with comparisons to the measured crack widths obtained during the field inspection.

6.2 INSPECTION REPORTS

The following sections include the reports from the field inspections of eight reinforced concrete inverted-T straddle bent caps at four cities in the state of Texas. The location of each straddle bent, date of inspection, key design characteristics, and crack widths are provided. Additional figures are included to document the condition of the structures.

6.2.1 Austin (TX-290 and I-35)

Three reinforced concrete inverted-T straddle bent caps in the I-35/TX-290 interchange on the north side of Austin were found to have significant diagonal cracks. The location of the straddle bents are shown in Figure 6-1. Completed in November of 2001, the bridges were just over 8 years old when they were inspected by the TxDOT Project 0-6416 research team. Shear cracks were observed on both faces of the bent caps near the supports but due to the high traffic in the area not all sides could be accessed for inspection.

Figure 6-1: Location of inverted-T straddle bent caps in Austin (Mapquest)

A summary of the data from the bridge drawings that is of interest to this project is provided in Table 6-1. The same parameters were collected for each bent cap inspected to allow comparisons among inverted-T bent caps in the field and the specimens tested in the experimental program. The individual bent caps are discussed in detail in the following sections.

Table 6-1: Important characteristics of Austin straddle bents (6K, 3M, 28K)

Bent	Location	ρ_v	ρ_h	a/d	Ledge Length	Ledge Height / Cap Height	No. of Girders
6K	(30.326788, -97.706456)	0.43%	0.37%	1.7	Short	35%	2
3M	(30.322401, -97.702838)	0.43%	0.37%	1.4	Short	35%	3
28K	(30.321920, -97.703878)	0.43%	0.37%	1.4	Short	35%	3

The individual bent caps are identified by their GPS location (latitude, longitude). The reinforcement ratios, ρ_v and ρ_h, were calculated at the location of the shear cracks (between the column and the exterior girder). The shear span to depth ratio, a/d, was taken as the distance from the center of the column to the center of the bearing of the exterior girder divided by the effective depth of the member as calculated from the bridge drawings. The ledge length was determined by the distance the ledge extended past the exterior girder. If the ledge was continuous across the bottom of the beam to the column it was considered "long". If the ledge terminated a short distance from the edge of the girder, but enough to allow the 45° load spread, then it was considered "short". A short ledge is the typical detail of most bent caps in this inspection. If the ledge stopped immediately after the exterior girder it was considered "cut-off". The ledge height was determined by comparing the height of the ledge to the total height of the bent cap. A ledge height of 25-38% of the total height of the cap was considered "shallow" and 39-50% was "deep". These characteristics reflect variables considered in the experimental portion of the current project.

6.2.1.1 Austin Bent 6K

Austin Bent 6K, located along the southbound feeder of I-35, provided access to eastbound TX-290 over an I-35 on-ramp. Two U-beams were supported by the bent cap. Shear cracks were observed between the exterior girders and columns on both faces but only the northwest corner, outlined in Figure 6-2, could be accessed for crack measurements due to traffic and site restrictions.
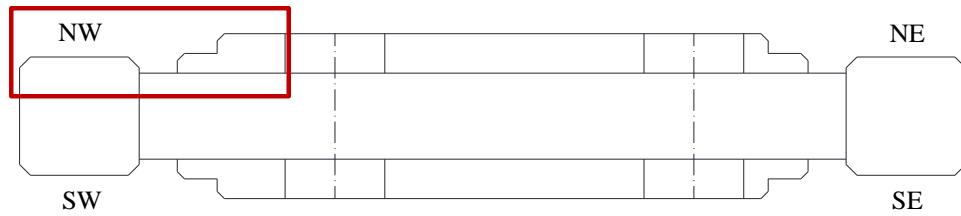
Figure 6-2: Plan View of Austin Bent 6K

A picture of the investigated shear span along with a sketch showing the size and location of observed cracks is provided in Figure 6-3. The cracks were highlighted in the photographs to better show their position. The largest shear crack, which measured 0.016 in. at its widest point, ran from mid face of the U-beam to the end of the ledge as shown in the sketch. Other cracks, with widths up to 0.013 in., were observed along the top and side of the web-ledge interface. A crack was also observed to extend under the beam.
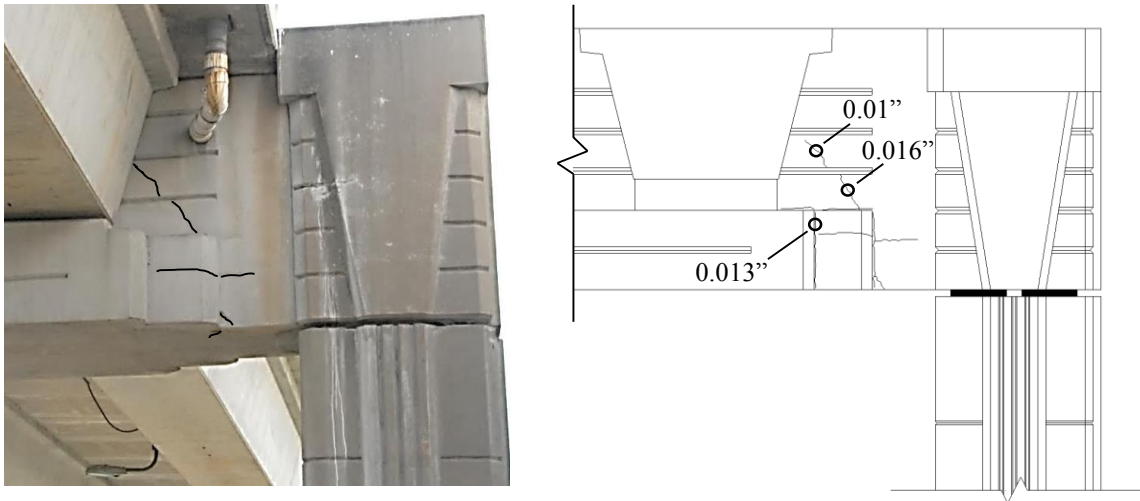
Figure 6-3 Photograph and Sketch of Northwest Corner of Austin Bent 6K

6.2.1.2   Austin Bent 3M

Bent 3M, located along the westbound feeder of TX-290 on the north side of Austin, provided access to southbound I-35 over a TX-290 on-ramp. Three U-beams were supported by the bent caps. Shear cracks, similar to those present on Bent 6K, were observed on both faces of Bent 3M but only the southwest corner could be accessed as shown in Figure 6-4.
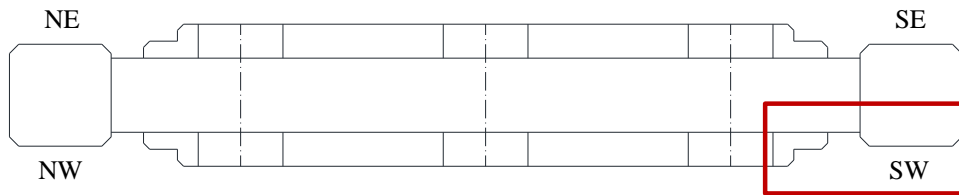
Figure 6-4: Plan View of Austin Bent 3M

A photograph and a sketch of the cracks on southwest corner of Bent 3M is provided in Figure 6-5. The largest shear crack, measuring 0.02 in., ran from above the end of the ledge to the column near the bottom of the beam. Only hairline cracking was observed along the web-ledge interface.

The northeast corner of Bent 3M appeared to have much larger cracks but access for the purpose of crack measurements was not possible. Crack sizes of up to 0.03 in. were approximated from ground observation by The University of Texas at Austin researchers.
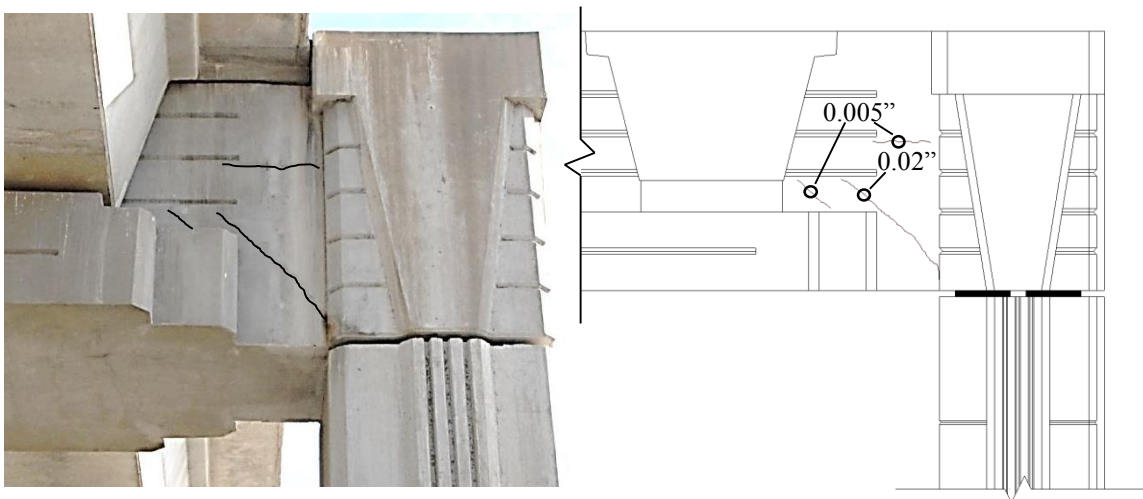
Figure 6-5: Photograph and Sketch of Southwest corner of Austin Bent 3M

6.2.1.3   Austin Bent 28K

Bent 28K provided access to eastbound TX-290 from northbound I-35 over the TX-290 feeder road. Three U-beams were supported on each side of the inverted-T bent cap. Shear cracks were also observed on both faces of Bent 28K. The northwest and northeast corners, shown in Figure 6-6, were investigated
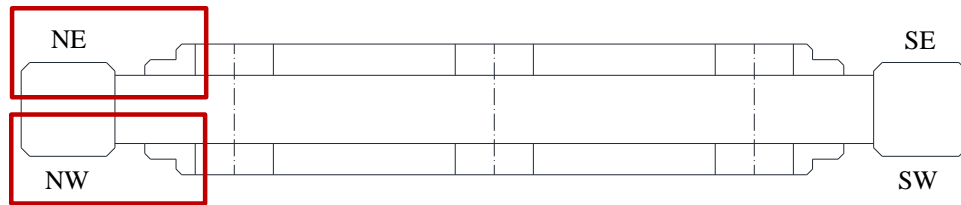
Figure 6-6: Plan View of Austin Bent 28K

A photograph and sketch of the location and widths of the cracks on the northwest corner of Bent 28K are provided in Figure 6-7. Two shear cracks were observed in the web of the bent with one extending from mid face of the U-beam to the ledge and measuring 0.016 in. The second crack was larger, 0.03 in., and ran parallel to and above the first. This crack was recorded as measuring 0.025 in. during a previous inspection. Cracking measuring up to 0.03 in. was also observed along the web-ledge interface and on the top side of the ledge. This was considerably larger than the 0.016 in. that was measured previously.
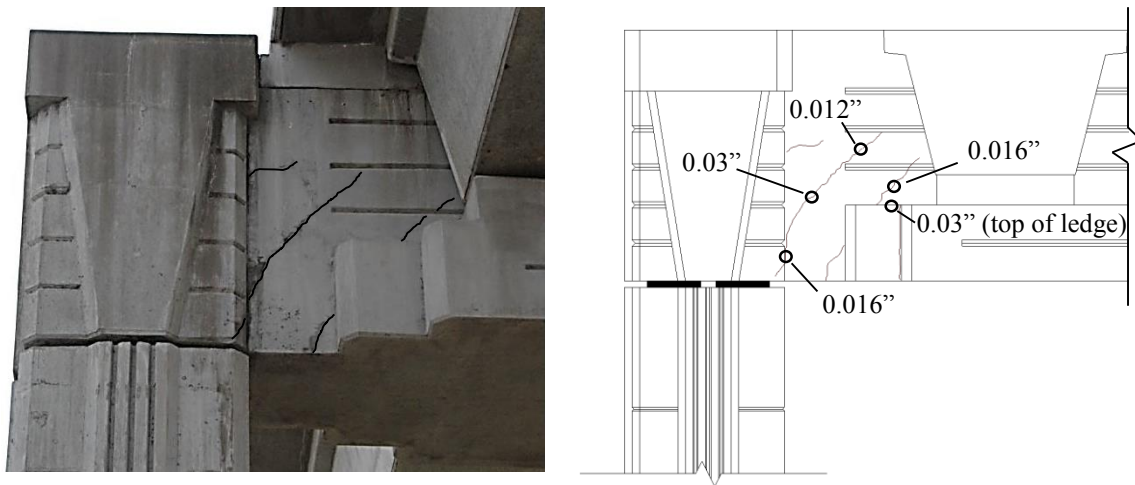
Figure 6-7 Photograph and Sketch of Northwest Corner of Austin Bent 28K

The northeast corner of the beam had a similar cracking pattern, as shown in Figure 6-8, with the two cracks measuring 0.012 and 0.02 in. Cracks of comparable width to the previous inspection (0.012 in.) were also observed along the web-ledge interface. Also, torsion did not appear to be an issue because the cracks ran in the same direction on each side of the bent cap. If the cracks were to spiral around the bent cap, angled one way on the east side of the beam and the opposite direction on the west, then torsional effects would need to be considered.
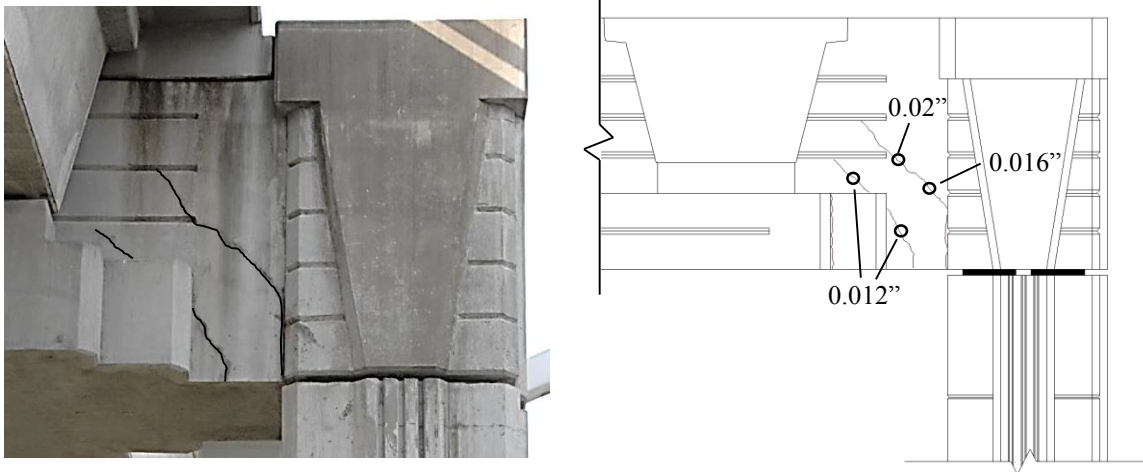
Figure 6-8: Crack size and location on the northeast corner of Austin bent 28

6.2.2 San Antonio (I-35 S)

Shear cracks were observed on one reinforced concrete inverted-T straddle bent cap on the I-35 southbound frontage road just north of San Antonio. The location of the straddle bent is shown in Figure 6-9. Five TxDOT Type C I-girders were supported by the bent. The bridge was inspected by TxDOT Project 0-6416 members on July 26th, 2010.
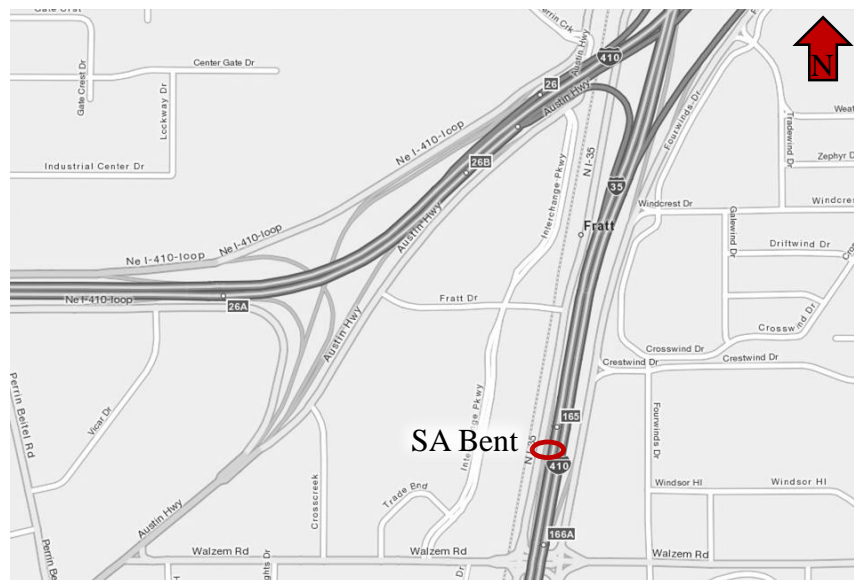
Figure 6-9: Location of inverted-T straddle bent cap in San Antonio (Mapquest)

Table 6-2 summarizes the data collected from the bridge drawings that is of interest to this project. The reinforcement ratio, shear span, and ledge data were unknown or approximated from the visual inspection. No bridge plans were available to the researchers at The University of Texas at Austin.

Table 6-2: Important Characteristics of San Antonio Straddle Bents

Bent	Location	ρ_v	ρ_h	a/d	Ledge Length	Ledge Height / Cap Height	No. of Girders
SA	(29.512478, -98.397567)	Unavailable		1.85	Long	33%	5

Shear cracks were observed on both faces of the bent caps near the columns but due to site restrictions only three corners, shown in the plan view in Figure 6-10, could be accessed by the bucket truck. Cracks associated with a moment connection between the column and bent cap were observed at the frame corners and an impact mark was found on the north side of the bent.
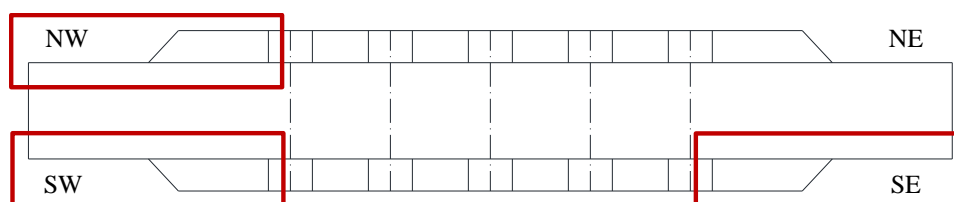
Figure 6-10: Plan View of San Antonio Bent Cap

The northwest corner of the bent had a single shear crack that measured 0.01 in. The cracks extended from the top of the exterior I-girder to the corner of the web-ledge interface as shown in Figure 6-11. A flexure crack measuring 0.01 in. was also observed at the end of the bent cap (i.e. the frame corner). Evidence of spalling was present near the beam-deck interface on the northwest corner of the bent.
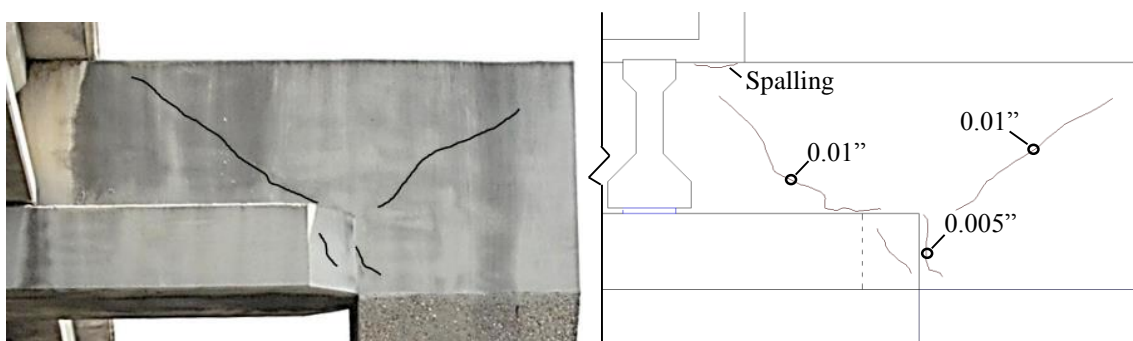
Figure 6-11: Crack Size and Location on the Northwest Corner of the San Antonio Bent

The southwest corner of the bent was nearly identical to the northwest with a shear crack measuring 0.01 in. that extended from the end of the ledge to the top of the I-girder. A similar width flexure crack was observed in the corner of the beam, suggesting the presence of a moment connection, and is shown in Figure 6-12.

171
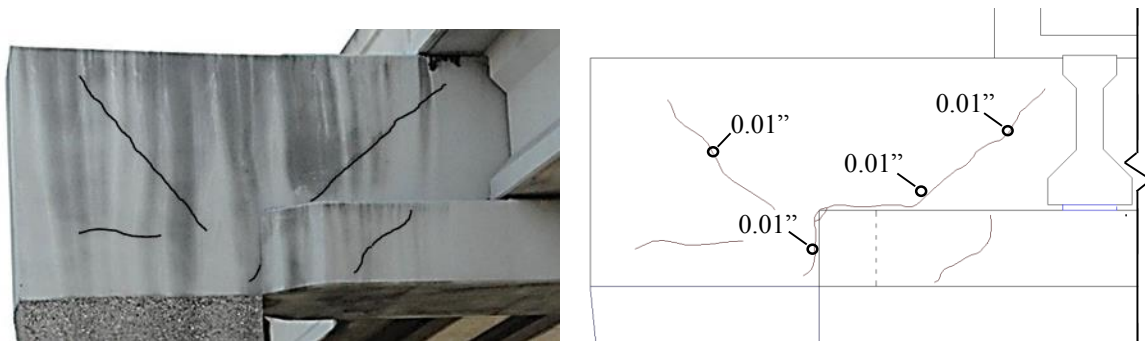
Figure 6-12: Crack Size and Location on the Southwest Corner of the San Antonio Bent

The southeast corner had a slightly different cracking pattern as shown in Figure 6-13. The cracks were larger than the west side of the beam with a maximum width of 0.015 in and no significant flexure cracking was observed in the corner of the bent. Due to the lack of bridge drawings it was not possible to draw conclusions on the effects of reinforcement as it was unknown and the shear span-to-depth ratios appeared very similar under a visual observation.
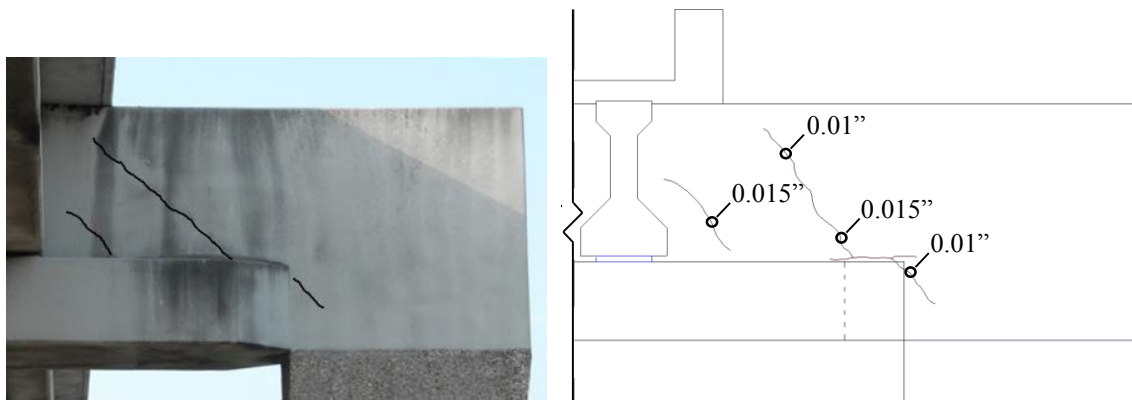
Figure 6-13: Crack size and location on the southeast corner of the San Antonio bent

6.2.3 El Paso (I-10 E Geronimo Drive Exit)

Two inverted-T straddle bent caps located on the feeder road of the I-10 East to Gateway Blvd East connector in El Paso were identified as having significant diagonal shear cracks. The off-ramp is located just west of Geronimo Drive as shown in the map in Figure 6-14.
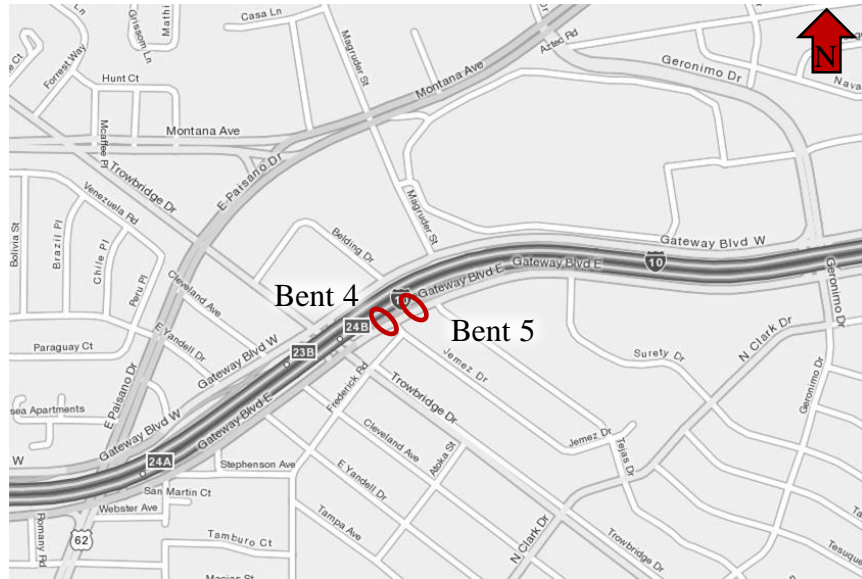
Figure 6-14: Location of inverted-T straddle bent caps in El Paso (Mapquest)

The bridge was inspected by TxDOT Project 0-6416 members from the University of Texas on August 17th, 2010. Before the site visit, relevant geometric and design information was gathered from the original bridge drawings and recorded in Table 6-3.

Table 6-3: Important Characteristics of El Paso Straddle Bents

Bent	Location	ρ_v	ρ_h	a/d	Ledge Length	Ledge Height / Cap Height	No. of Girders
4	(31.78047, -106.41612)	0.57%	0.19%	1.7	Cut Off	29%	5/6
5	(31.78055, -106.41599)	0.57%	0.19%	3.4	Cut Off	29%	6

The cut off ledge in these straddle bent caps raised some concern in the current project because it does not allow the load entering the ledge to spread as much as a longer ledge (Section 3.2.2). The resulting concentrated tensile zone could have resulted in the larger crack widths seen in the El Paso structures. Further discussion on the characteristics and crack widths for various ledge lengths can be found in Chapter 4.

6.2.3.1   El Paso Bent 4

A plan view of Bent 4 is shown in Figure 6-15 with the inspected regions highlighted in red. The north end of the straddle bent was not investigated because it was built directly into a retaining wall and thus had no measurable shear span.
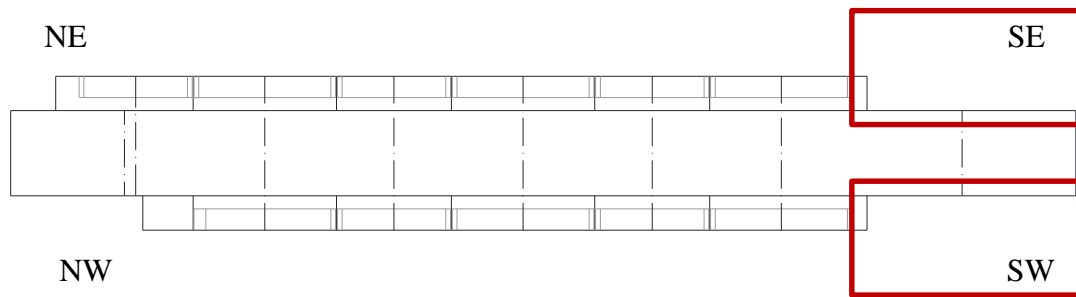
Figure 6-15: Plan View of El Paso Bent 4

The southwest corner Bent 4 had a large shear crack that was highly visible to passing traffic. The crack extended from mid height of the exterior girder to the lower corner of the cap-to-column connection and measured 0.04 in. at its widest point. Minor spalling was observed at two locations along the length of the crack. The concrete directly next to the problematic areas was labeled "11-8-95" suggesting that it had been a concern during a previous investigation. A picture and sketch of the cracks observed during the field inspection are provided in Figure 6-16.

Unlike the bent cap investigated in Austin, the El Paso inverted-T caps were cast monolithically with the columns and the reinforcement was detailed to create a moment connection. This was confirmed by the existence of fairly large (0.02 in. wide) cracks shown at the frame corners as depicted in Figure 6-16 and Figure 6-17. These cracks were horizontal on the columns, vertical on the bent cap, and ran from the top outside corner to the bottom inside corner- opposite to the direction of the shear cracks at the beam-column connection. Similar, yet less significant cracking patterns were observed in the San Antonio inverted-T straddle bent cap.
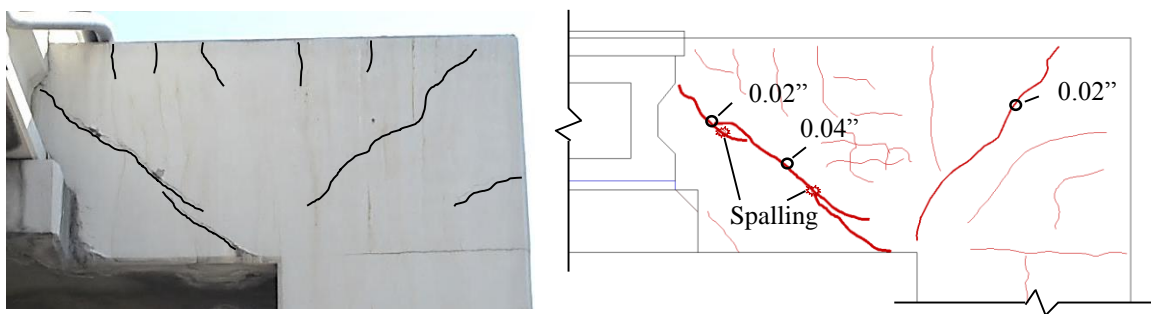
Figure 6-16: Crack Size and Location on the Southwest Corner of El Paso Bent 4

The southeast corner appeared to be slightly less distressed with a maximum crack width of 0.03 in. as shown in Figure 6-17. Overall the cracking pattern was very similar with a large shear crack and multiple smaller moment cracks in the corner of the beam.

174

Five prestressed concrete box beams framed into the west face of the Bent 4 and were approximately 83 ft. long. Six framed into the east side and were 61 ft. The difference in span lengths, and thus applied load, was likely a factor for the variance in crack widths measured on the two sides of the bent cap.
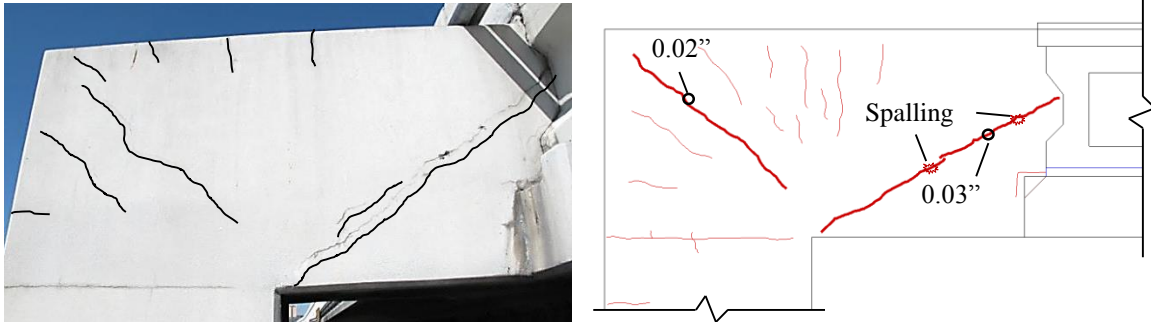
Figure 6-17: Crack Size and Location on the Southeast Corner of El Paso Bent 4

6.2.3.2 El Paso Bent 5

The plan view of Bent 5 from the Geronimo exit off of I-10 in El Paso is given in Figure 6-18 with the inspected northeast and northwest corners highlighted in red. The south side of the bent was not inspected due to the fact that the box beams extended all the way to the column on the south side of the straddle bent.
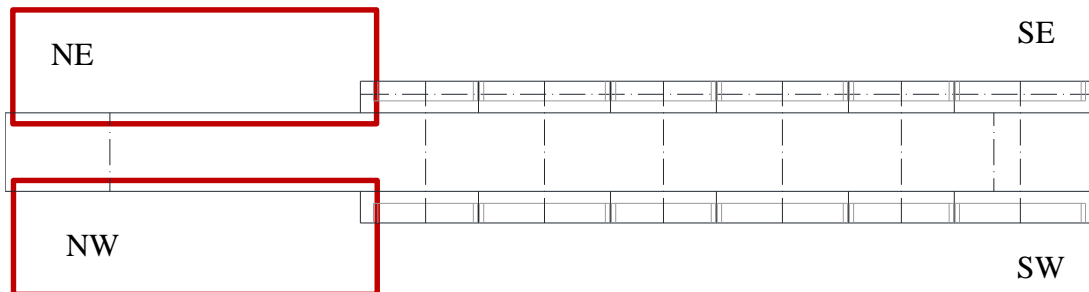
Figure 6-18: Plan View of El Paso Bent 5

A photograph and sketch of the cracks on the northeast corner of Bent 5 is shown in Figure 6-19. Due to the longer shear span, the cracks were more typical of a bent cap exhibiting sectional shear behavior. The cracks in this inverted-T straddle bent were also fewer in number and narrower in width than those observed on Bent 4. This was due in part to the longer shear span (a/d of 3.4 vs 1.7 seen in Bent 4) and the fact that most of the box beams in this bridge were closer to the south support, thus reducing the load on the north side of the straddle bent. The widths of the two largest shear cracks on the northeast corner of the bent measured 0.01 in.
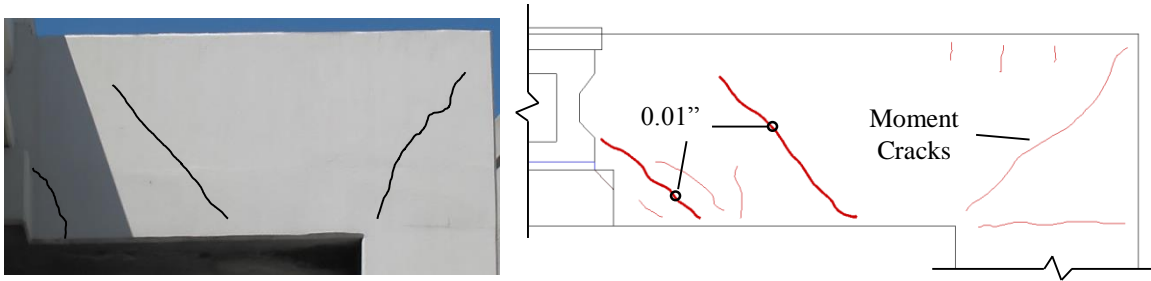
Figure 6-19: Crack Size and Location on the Northeast Corner of El Paso Bent 5

The northwest corner, shown in Figure 6-20, appeared to experience slightly more distress. The shear crack closer to the exterior girder was twice the width of that seen on the opposite side of the beam. Nevertheless with a maximum shear crack width of 0.02 in., Bent 5 was found to be subjected to less distress than the El Paso Bent 4.
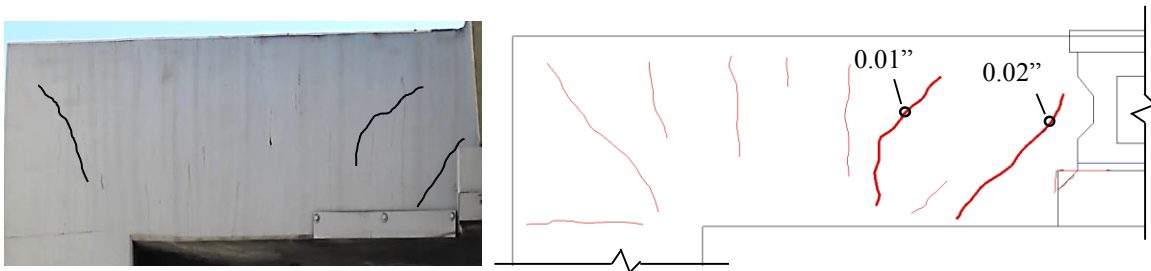
Figure 6-20: Crack Size and Location on the Northwest Corner of El Paso Bent 5

6.2.4 Waco (TX-6 E and I-35N)

Two inverted-T straddle bent caps in the recently completed TX-6 East to I-35 North connector in Waco (refer to Figure 6-21) were found to have developed diagonal cracks. The 6-year-old flyover was inspected by TxDOT Project 0-6416 researchers on January 11th, 2010. Shear cracks were observed on both faces of the two bent caps in the region of the shear span. All cracks were inspected except for those on the east side of Bent 17 due to traffic and site restrictions.
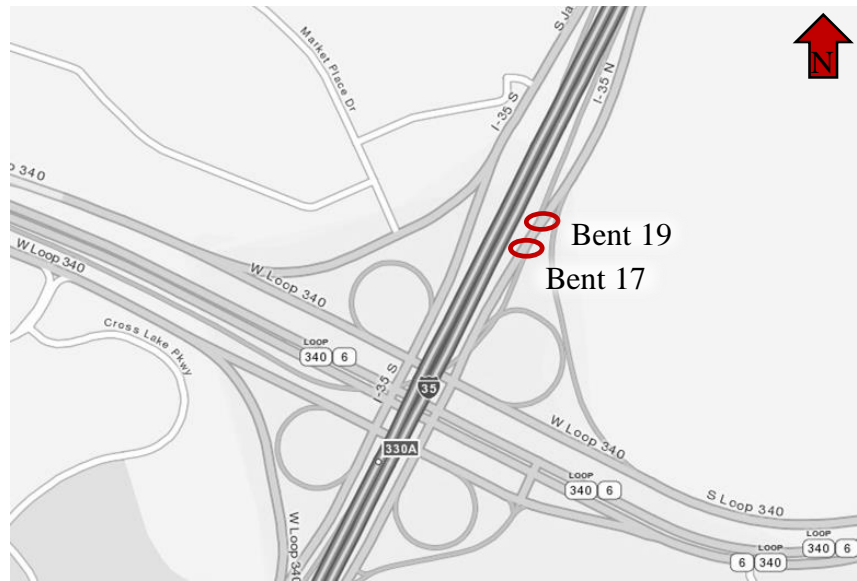
Figure 6-21: Location of inverted-T Straddle Bent Caps in Waco (Mapquest)

The location, reinforcement ratio, shear span, ledge data and number of girders supported on the ledges located at each side of the straddle bents are presented in Table 6-4.

Table 6-4: Important Characteristics of Waco Straddle Bents

Bent	Location	ρ_v	ρ_h	a/d	Ledge Length	Ledge Height / Cap Height	No. of U-Beams
17	(31.496031, -97.148663)	0.46%	0.30%	2.5	Short	36%	3
19	(31.496476, -97.148489)	0.46%	0.30%	2.5	Short	36%	3

6.2.4.1 Waco Bent 17

The Waco Bent 17 bent crossed an off-ramp feeding onto the I-35 North frontage road. Only the northwest and southwest corners of the bent, highlighted in red in Figure 6-22, were inspected due to site restrictions.
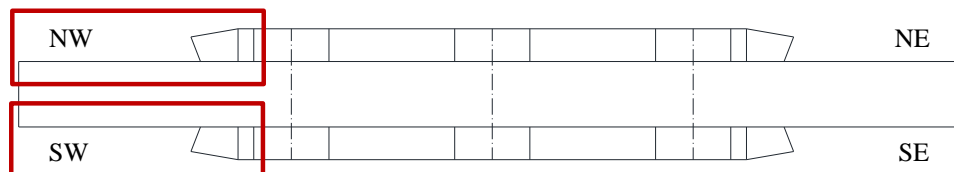
Figure 6-22: Plan View of Waco Bent 17

The diagonal cracks on Bent 17 appeared larger in the photographs due to efflorescence. The buildup was scraped off the bent cap before crack widths were measured as shown in

177

Figure 6-23. It was important to ensure accuracy and not allow the stained concrete to affect the results of the field inspection. The scraping and measuring process was repeated for various cracks to obtain a good record of the condition of the straddle bent.

Figure 6-23: Scraping off Efflorescence and Measuring Diagonal Cracks

A photograph and a sketch showing the diagonal cracking on the southwest corner of Bent 17 is provided in Figure 6-24. All of the cracks extended from the column support to the top of the cap behind the exterior U-beam. This pattern was typical of all bent caps inspected in this report and of the beams tested in the experimental portion of the current project. No flexureal cracking was observed near the supports- confirming the simply supported bearing condition in the bridge drawings. Overall the shear cracks on this bent were relatively small with the largest measuring 0.01 in.

Figure 6-24: Crack Size and Location on the Southwest Corner of Waco Bent 17

The northwest corner of Bent 17, shown in detail in Figure 6-25, had similar diagonal crack sizes and patterns. Cracks ranging from hairline to 0.005 and 0.01 in. extended from the column to the top of the bent cap next to the U-beam. Overall the distress in this inverted-T straddle bent cap was found to be moderate, despite the large amount of staining and efflorescence.
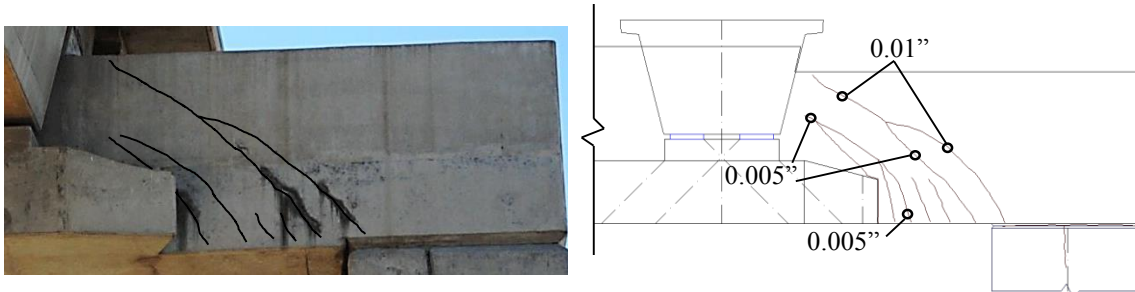
Figure 6-25: Crack Size and Location on the Northwest Corner of Waco Bent 17

6.2.4.2 Waco Bent 19

All four corners of Bent 19 could be accessed and were inspected as shown in the Figure 6-26 plan view. The straddle bent cap was built on relatively level ground without any roadway or traffic interference as at the time of the inspection the exit road had yet to be constructed under the bent. Unlike the previous straddle bent, there was very little staining or efflorescence overemphasizing the size and extent of the diagonal cracking as shown in the figures in this section.
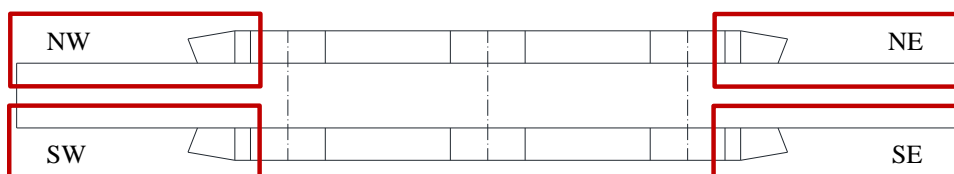
Figure 6-26: Plan View of Waco Bent 19

The cracking pattern was similar to that seen in the previous Waco bent but the cracks themselves were slightly wider. The largest crack measured on Bent 17 was 0.01 in. whereas a crack on the northwest corner of Bent 19 was found to have a width of 0.015 in. as shown in Figure 6-27.
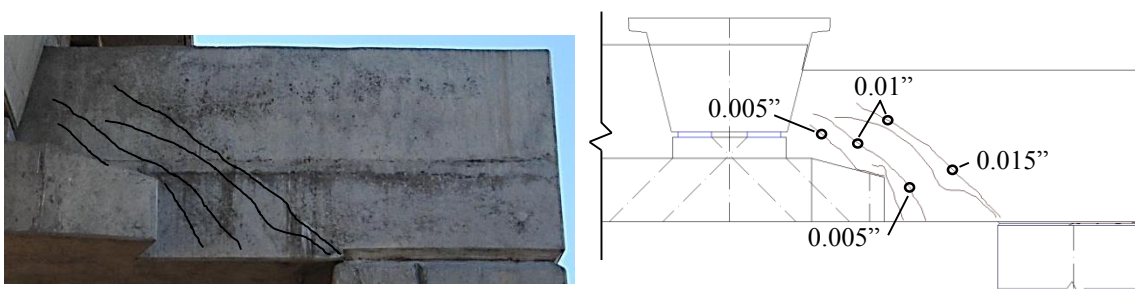
Figure 6-27: Crack Size and Location on the Northwest Corner of Waco Bent 19

The southwest corner of Bent 19, shown in Figure 6-28, was subjected to a similar cracking pattern with a series of cracks that extended from the column to the exterior U-

179

beam. However, the largest cracks on the southwest corner were found to have a smaller width of 0.01 in.
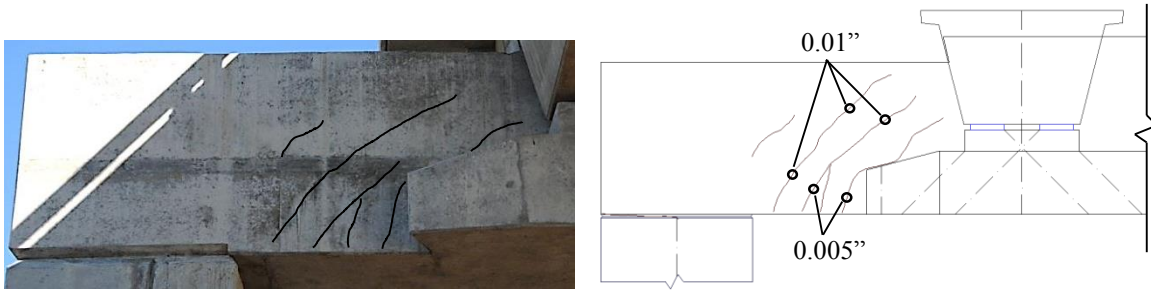
Figure 6-28: Crack Size and Location on the Southwest Corner of Waco Bent 19

A similar pattern was observed when comparing the southeast and northeast corners. The southeast shear span had cracks ranging from hairline to widths of 0.005 and 0.01 in. as shown in Figure 6-29. The northeast corner, shown in Figure 6-30, had a maximum crack width of only 0.005 in. It appeared that a difference in span lengths on either side of the bent cap could be responsible for the varying crack widths between the north and south sides of the inverted-T straddle bent cap.
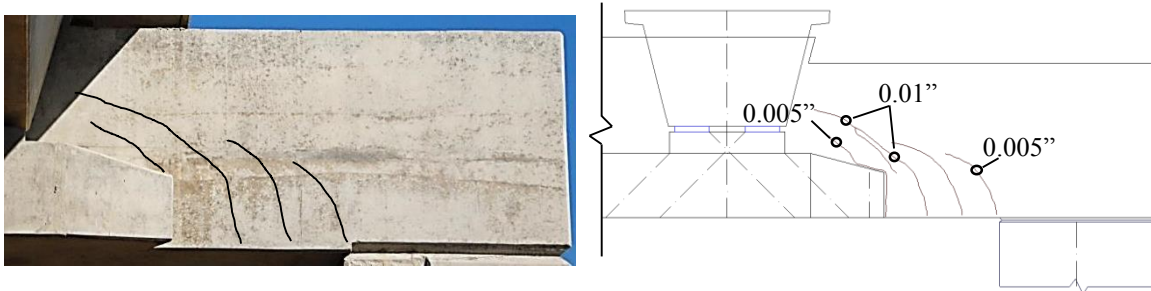
Figure 6-29: Crack Size and Location on the Southeast Corner of Waco Bent 19
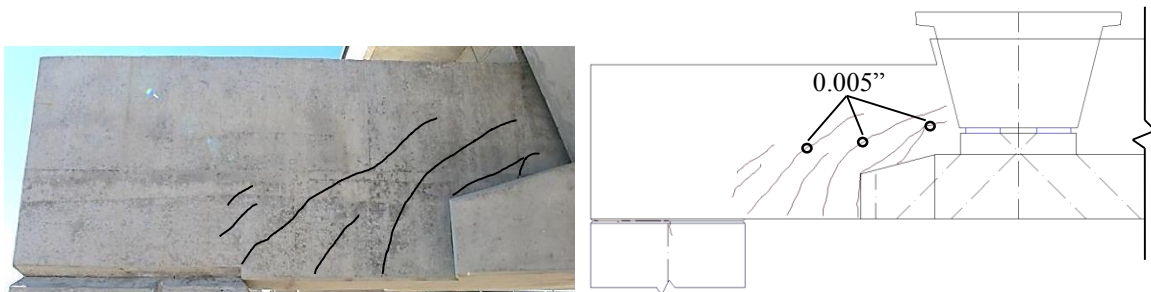
Figure 6-30: Crack Size and Location on the Northeast Corner of Waco Bent 19

Comparing the west corners of the bent cap to the east also suggests that one side has incurred more distress. The measured cracks on the west corners in Figure 6-27 and

Figure 6-28 range from 0.005 to 0.015 in. The east corner, however, has only a few cracks over 0.005 in. as shown in Figure 6-29 and Figure 6-30.

6.2.5 Findings from the Field Inspection

A visual inspection could not reveal all factors contributing to shear cracking in and inverted-T straddle bent cap. No coring or destructive testing was performed to assess the strength of the structures. One of the goals of the current project was to construct and test comparable inverted-T beams in a laboratory setting. The observations made from the results of these beams will aid inspectors in determining the significance of cracking through the use of the diagonal crack width and ultimate capacity comparison chart presented in Figure 5-31.

By varying different parameters found in the field, including shear reinforcement ratios, shear span-to-depth ratios, and ledge geometry, this report aimed to determine what factors influence the size and extent of the shear cracks. Summarized in Table 6-5 are the variables from the different bent caps in this inspection report accompanied with the corresponding maximum crack size. As discussed in Chapter 5, the reinforcement ratio had the most significant effect on the width of the diagonal cracks.

Table 6-5: Inverted-T Crack Width Summary

Bent	ρ_v	ρ_h	a/d	Ledge Length	Ledge Height / Cap Height	Max Crack
Austin IH-35 / Tx-290 Bent 6K	0.43%	0.37%	1.7	Short	35%	0.016 in.
Austin IH-35 / Tx-290 Bent 3M	0.43%	0.37%	1.4	Short	35%	0.02 in.
Austin IH-35 / Tx-290 Bent 28K	0.43%	0.37%	1.4	Short	35%	0.03 in.
San Antonio IH-35 S Exit 165	Unavailable		1.85*	Long	33%*	0.015 in.
El Paso IH-10 / Geronimo Bent 4	0.57%	0.19%	1.7	Cut-Off	29%	0.04 in.
El Paso IH-10 / Geronimo Bent 5	0.57%	0.19%	3.4	Cut-Off	29%	0.02 in.
Waco IH-35 / LP340 Bent 17	0.46%	0.30%	2.5	Short	36%	0.01 in.
Waco IH-35 / LP340 Bent 19	0.46%	0.30%	2.5	Short	36%	0.015 in.

* Approximated based on field observations

181

A few observations could be made on the geometry of the inverted-T straddle bent caps and their respective maximum crack widths. The largest crack width was measured on Bent 4 in El Paso. Two of the factors contributing to the size of this crack, the ledge height and ledge length, are recorded in Table 6-5. Compared to every other bent cap in this investigation, El Paso Bent 4 had the shortest and shallowest ledge along with the smallest horizontal web reinforcement ratio. Bent 5 had an identical ledge geometry but a larger shear span-to-depth ratio (a/d) and was arranged so that most of the load from the box beams was transferred directly to the opposite support (refer to Figure 6-19). Nevertheless the maximum crack size measured on Bent 5 was also larger than many of those observed in this survey.

The San Antonio bent had the longest ledge and some of the smallest shear cracks, 0.015 in., of any cap inspected in this report. Similarly, the Waco straddle bent experienced some of the smallest shear cracks. The largest shear cracks measured on the Waco Bent 17 and Bent 19 were 0.010 and 0.015 in., respectively. The reinforcement ratios and shear span-to-depth ratios were comparable to the other beams investigated in this study.

6.3   SERVICEABILITY BEHAVIOR

6.3.1   Diagonal Cracking under Service Loads

One of the tasks of the current project was to develop a means to prevent or limit diagonal cracking for inverted-T beams subjected to service level loads. A previously derived equation from the deep beam study. TxDOT Project 0-5253, was evaluated with diagonal cracking loads from the inverted-T experimental program. It was concluded that the existing recommendation to estimate the diagonal cracking load based on a simple equation was valid for inverted-T beams as well as rectangular bent caps.

The diagonal cracking load was found to be a function of the shear area, $b_w d$, the tensile strength of the concrete, $\sqrt{f_c'}$, and the a/d ratio of the member as shown in Equation 6-1.

$$V_{crack} = [6.5 - 3(\tfrac{a}{d})]\sqrt{f_c'}b_w d \tag{6.1}$$

but not greater than $5\sqrt{f_c'}b_w d$ nor less than $2\sqrt{f_c'}b_w d$

where a = shear span (in.)
   d = effective depth of the member (in.)
   f'_c = compressive strength of concrete (psi)
   b_w = web width of the member (in.)

In order to evaluate the performance of the in-service beams inspected as part of the current project, the service load of the inspected bents was compared to the calculated

diagonal cracking load as shown in Figure 6-31. CAP18, A TxDOT Bent Cap Analysis Program, was used to determine the maximum bending and shear force envelopes on the simply supported bridge bent caps. Loads assigned to the bent caps were calculated in accordance with the bridge drawings and AASHTO LRFD Bridge Design Specifications, 4th Ed. (2007) and the 2008 Interim Revisions as prescribed by TxDOT LRFD Bridge Design Manual (July 2008). A design example provided by the TxDOT bridge division aided in the determination of loads and proper use of the analysis program.
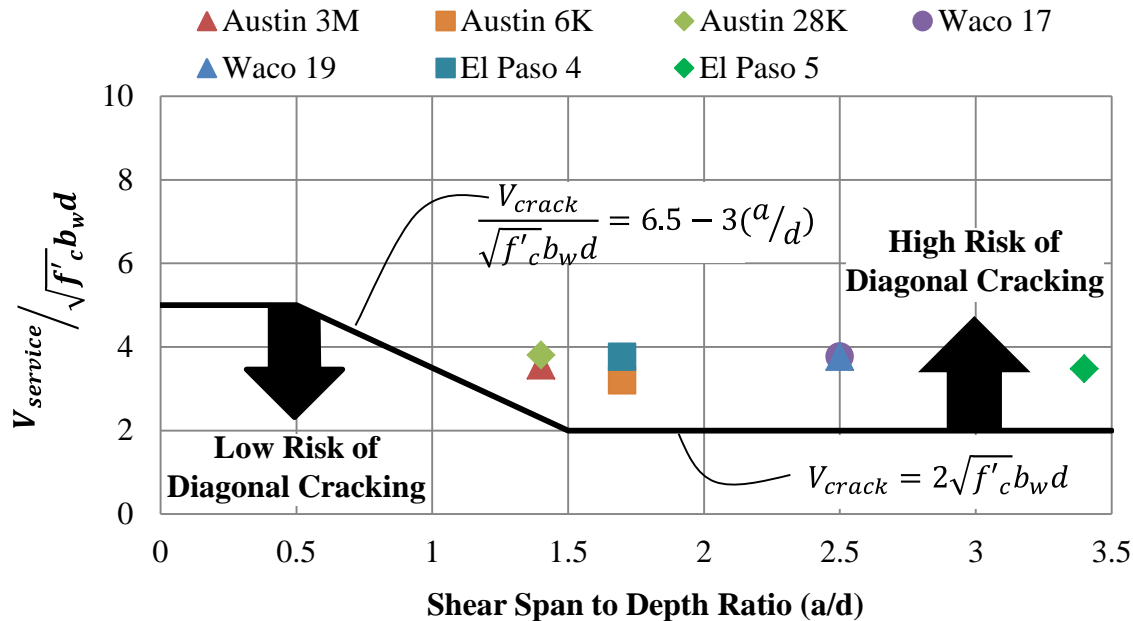
Figure 6-31: Assessment of in-service bent caps with the proposed equation for diagonal cracking estimation

In this figure, any point below the diagonal cracking line would indicate a bent cap with a low risk of diagonal cracking- i.e., the service level shear is below the cracking load. Any point above this line would represent a bent cap that is very likely to crack when subjected to its corresponding service level load. According to the cracking equation, increasing the section size or the concrete compressive strength would decrease the risk of diagonal cracking.

Based on the proposed equation, the service level shear was greater than the estimated diagonal cracking load for each in-service bent cap inspected as part of the current project. Therefore the inverted-T bents had a high risk of diagonal cracking when subjected to service level loads. Overloads and other unexpected conditions would only increase this chance.

For future designs it is recommended that the bent caps be sized according to Equation 6-1 to limit the risk of diagonal cracking. If those options are not available due to geometry

restrictions the designer is encouraged to increase the compressive strength of the concrete and provide additional web reinforcement to control crack widths.

6.3.2 Maximum Diagonal Crack Widths

Another task for the current project was to develop a chart that could be used to correlate the maximum diagonal crack width on an inverted-T beam to the load on the member, quantified as a percent of the ultimate capacity. A similar chart was developed in TxDOT Project 0-5253 for use with rectangular deep beams but was not approved for use with tension-chord loaded members. The inverted-T chard and its development are presented in Section 5.4.

The diagonal crack width to capacity chart provided in Figure 5-31 was applied to the in-service members inspected in the current project. Based on the measured maximum crack width and the web reinforcement ratio, the capacities in the following table were estimated. It should be noted that conditions in the field can vary from those seen in the laboratory and chart results should only be viewed as a useful guide to determining the level of distress in a diagonally cracked inverted-T bent cap.

Table 6-6: Estimated percent of ultimate capacity for in-service bent caps

Bent	ρ_v	ρ_h	Maximum Crack Width	Ultimate Capacity
Austin IH-35 / Tx-290 Bent 6K	0.43%	0.37%	0.016 in.	45 (±15)%
Austin IH-35 / Tx-290 Bent 3M	0.43%	0.37%	0.02 in.	55 (±15)%
Austin IH-35 / Tx-290 Bent 28K	0.43%	0.37%	0.03 in.	70 (±15)%
San Antonio IH-35 S Exit 165	Unavailable		0.015 in.	40-50%*
El Paso IH-10 / Geronimo Bent 4	0.57%	0.19%	0.04 in.	85 (±15)%
El Paso IH-10 / Geronimo Bent 5	0.57%	0.19%	0.02 in.	55 (±15)%
Waco IH-35 / LP340 Bent 17	0.46%	0.30%	0.01 in.	35 (±15)%
Waco IH-35 / LP340 Bent 19	0.46%	0.30%	0.015 in.	45 (±15)%

*Unknown reinforcement ratio, the range represents $\rho_v = \rho_h = 0.3\%$ to $\rho_v = \rho_h = 0.6\%$

The chart presented in Chapter 5 provides capacity estimations based on select crack widths and reinforcement ratios of 0.3% or 0.6% in each orthogonal direction. As shown in Table 6-6, inverted-T bent caps typically fall within this range so the capacity values need to be interpolated. For the in-service inverted-T beams the vertical and horizontal reinforcement ratios were averaged and then the percent of ultimate capacity was calculated by linear interpolating values from the chart based on the maximum crack width. For example, the average reinforcement ratio of Austin Bent 6k was 0.4% which is ⅓ the difference between the 0.3% and 0.6% values. The maximum crack width of 0.016 in. is located roughly halfway in-between the provided values of 0.01 and 0.02 in.

Therefore the percent of ultimate capacity should be about ⅓ the difference between 40% and 53% resulting in an estimated load of 45% of the ultimate capacity of the member.

For the San Antonio bent cap, no information was available to determine the web reinforcement ratio. Therefore the provided range corresponds to the values obtained for 0.3% to 0.6% in each orthogonal direction. The ±15% scatter should also be considered.

6.4   SUMMARY

Field inspections revealed inverted-T bent caps subjected to varying levels of distress across the state of Texas. Pertinent information including ledge geometry, a/d ratio, reinforcement ratio, and number of girders was collected for each structure. Photographs were taken and crack width measured to document the condition of each bent.

The in-service structures were then compared to the diagonal cracking load estimate discussed in Section 5.3. It was found that based on the section size, a/d ratio, and concrete strength, each of the inverted-T bent caps inspected as part of the current study had a high risk of cracking under service level loads.

Using the data gathered in the field inspections, the load on the bent caps, quantified as the percent of ultimate capacity, was determined with the diagonal crack width chart provided in Figure 5-31. It was then concluded that several of the existing structures had been subjected to loads up to 70-85% of their ultimate capacity.

Based on the analysis of results from the inverted-T experimental program and the conditions of the in-service bent caps, it is recommended to design such structures in the future based on the recommendations of this project that are summarized in Chapter 7.

CHAPTER 7
Design Recommendations

7.1   INTRODUCTION

The design recommendations presented in this chapter reflect the conclusions drawn as a result of the extensive experimental program on inverted-T beams and assessing the accuracy and applicability of currently available STM procedures that were calibrated with compression-chord loaded beam test results, as implemented in Chapter 2 of this report.

7.2   PROPOSED CHANGES TO TXDOT DESIGN SPECIFICATIONS

7.2.1   General Design Recommendations

The following recommendations for designing inverted-T beams resulted from the experimental work performed in this project. Examples of inverted-T design using strut-and-tie modeling are presented in Williams et al. (2011).

1- ***Use STM design procedures for designing inverted-T bent caps***. Almost all inverted-T beams should be classified as deep beams because they are mostly made up of disturbed regions. These areas of nonlinear strain are the result of point loads (girders or column supports) and geometric discontinuities (ledges) as illustrated in Figure 7-1. It is therefore inappropriate to use the sectional shear approach to design inverted-T beams and thus strut-and-tie models should be used.

2- ***Determine the following tie widths when implementing the STM provisions for inverted-T beams.*** The load spread under the loading points defines the hanger tie width and should be taken as the width of the bearing pad plus two times the effective depth of the ledge. The width of the horizontal ledge tie at the top of the ledge is smaller and should be taken as the bearing pad width plus five times the distance from the center of the pad to the face of the web. This is consistent with current AASHTO recommendations for ledge design. These recommendations are discussed in Chapter 2 and highlighted in examples in TxDOT Project 5-5253.

3- ***Avoid using cut-off ledges***. Cut-off ledges were shown to result in lower web shear strengths than longer ledges. Cut-off ledges were also found to reduce the load at first diagonal cracking in the web. Moreover, cut-off ledges increased the risk of ledge failures.

4- ***Size member to limit web shear stresses at service loads.*** Based on the shear span to depth ratio, the concrete compressive strength, and the web width, estimate the

diagonal cracking load using Equation 5-1. This provision is essential to limit diagonal cracking at service load levels.

5- ***Provide a minimum of 0.3% web reinforcement ratio in each direction***. This minimum ratio should be used to limit diagonal crack widths at service loads. As demonstrated by experimental results, should a beam sustain diagonal cracking at service load levels, providing the recommended minimum reinforcement ratio will ensure narrow crack widths. Furthermore, this minimum ratio is needed to fully mobilize strut and node strengths.
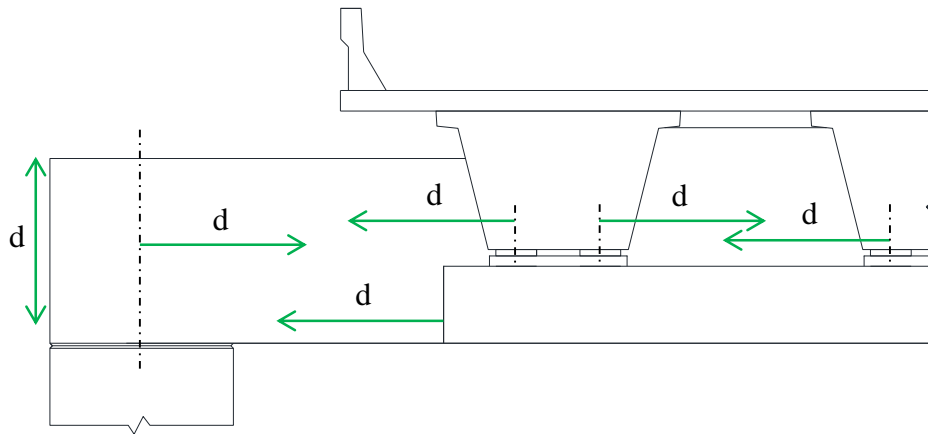
Figure 7-1: D-regions in inverted-T bent caps

7.2.2   Strut-and-Tie Model Design Procedure

The following outlines a series of steps typically followed when designing a deep structural component using the STM procedure developed as part of Project 0-5253. The procedure can be adapted to the particular design scenarios as necessary and it should be noted that the steps are sometimes performed simultaneously. The STM procedure is presented in a flow-chart format in Figure 7-2.

1. Separate B- and D-regions – Determine which regions of the structural component are expected to exhibit deep beam behavior or if the entire component should be designed using STM. For inverted-T bent caps, D-regions typically account for most if not all of the beam.

2. Define load case – Calculate the factored loads acting on the structural component, and if necessary, make simplifying assumptions to develop a load case that can be applied to a reasonable STM.

3. Analyze structural component – Solve for the structural component's support reactions assuming linear elastic behavior.

4. <u>Size structural component using the shear serviceability check</u> – Determine the initial geometry of the structural component by using the shear serviceability check presented in Section 5.3 to prevent or limit diagonal cracking at service loads.

5. <u>Develop strut-and-tie model</u> – Position struts and ties to represent the actual flow of forces within the structural component, and determine the forces in the struts and ties.

6. <u>Proportion ties</u> – Specify the reinforcement needed to carry the force in each tie.

7. <u>Perform nodal strength checks</u> – Define the geometries of the critical nodes, and ensure the strength of each face is adequate to resist the applied forces determined from the analysis of the STM.

8. <u>Proportion crack control reinforcement</u> – Specify the required crack control reinforcement to restrain diagonal cracks formed by the transverse tensile stresses of bottle-shaped struts. As discussed in Section 4.5, 0.3% reinforcement orthogonal in both directions is the minimum recommended for inverted-T bent caps.

9. <u>Provide necessary anchorage for ties</u> – Ensure reinforcement is properly anchored at the nodal regions.

```
┌─────────────────────────────────────────┐
│        Separate B- and D-Regions          │
└─────────────────────────────────────────┘
                    ↓
┌─────────────────────────────────────────┐
│             Define Load Case              │
└─────────────────────────────────────────┘
                    ↓
┌─────────────────────────────────────────┐
│       Analyze Structural Component        │
└─────────────────────────────────────────┘
                    ↓
┌─────────────────────────────────────────┐
│         Size Structural Component         │
└─────────────────────────────────────────┘
                    ↓
┌─────────────────────────────────────────┐
│       Develop Strut-and-Tie Model         │
└─────────────────────────────────────────┘
                    ↓
┌─────────────────────────────────────────┐
│             Proportion Ties               │
└─────────────────────────────────────────┘
                    ↓
┌─────────────────────────────────────────┐
│       Perform Nodal Strength Checks       │
└─────────────────────────────────────────┘
                    ↓
┌─────────────────────────────────────────┐
│   Proportion Crack Control Reinforcement  │
└─────────────────────────────────────────┘
                    ↓
┌─────────────────────────────────────────┐
│     Provide Necessary Anchorage for Ties  │
└─────────────────────────────────────────┘
```
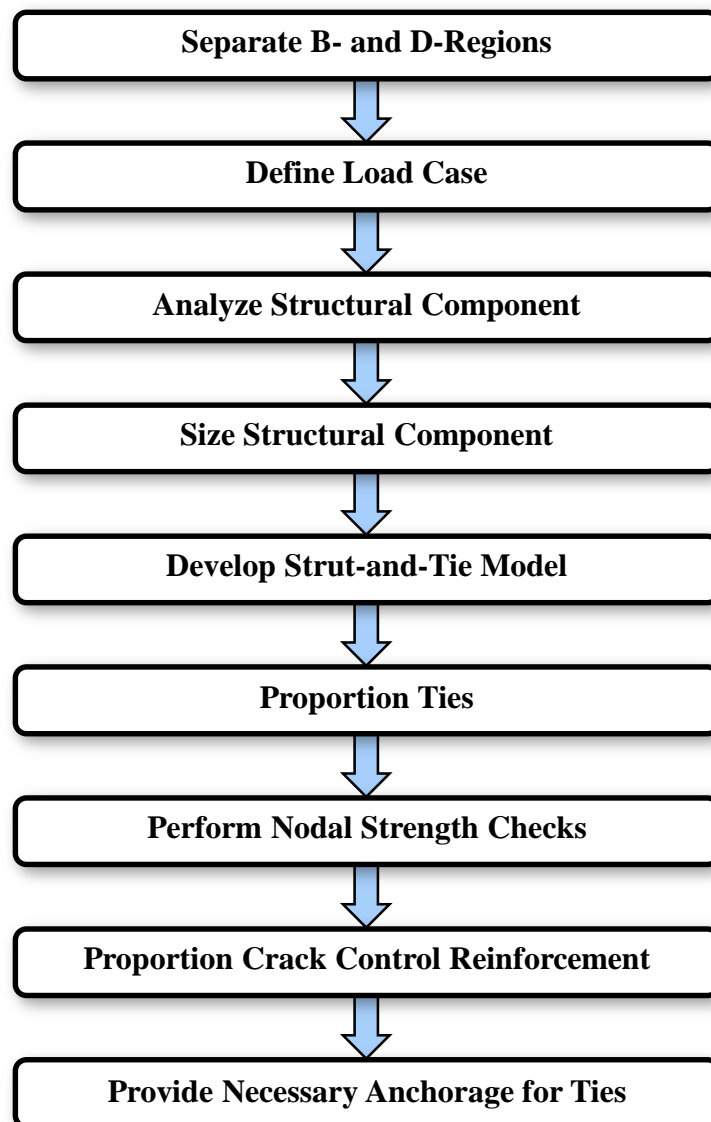
Figure 7-2: Strut-and-tie model design procedure (adapted from TxDOT Report 5-5253)

For the sake of brevity, additional details for each step in the strut-and-tie model design procedure can be found in TxDOT Report 5-5253. The proposed revisions to the AASHTO LRFD Bridge Design Specifications for strut-and-tie modeling are also presented before the design examples for ease of reference in the report.

7.2.3 TxDOT Report 5-5253 Design Examples

Detailed design examples for inverted-T straddle bent caps are provided in TxDOT Report 5-5253. The design examples explicitly note the difference between the design of an inverted-T and a rectangular beam. These differences were highlighted in Chapter 2 of

this report. As the girder loads are applied to the ledge of inverted-T beams, vertical ties (stirrups) are necessary to transfer the loads through the web to the compression chord. This results in tension across the width of the beam that must be resisted by transverse ledge reinforcement. In order to account for the flow of forces through the cross section and along the beam length, a three-dimensional STM must be developed for the design of an inverted-T bent cap.

A moment frame and a simply supported bent cap were investigated in Project 5-5253 to compare the influence of boundary condition assumptions. The struts and nodes within the bent cap are illustrated in Figure 7-3. For the moment frame example, the bent was modeled to allow the forces to "turn" around the frame corners. This required the use of a curved-bar node at the top corners of the bent, which occurs at a frame corner where a diagonal strut is equilibrated by two ties that represent curved continuous reinforcing bars (Klien, 2008). This type of node is not unique to inverted-T beams and as moment frame specimens were not tested, it was not investigated in the current experimental program.
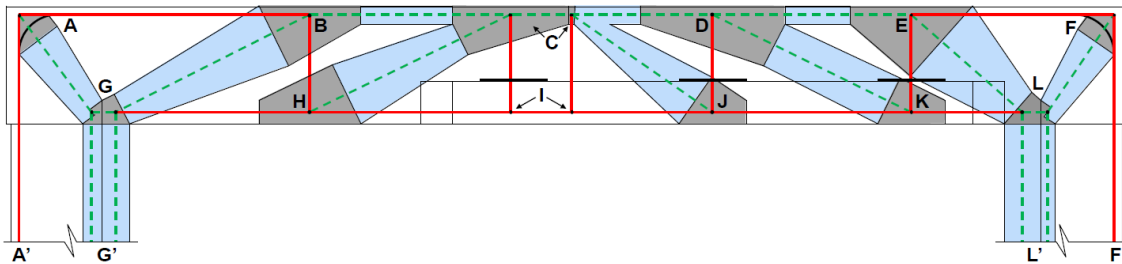
Figure 7-3: Illustration of struts and nodes within the moment frame inverted-T bent cap (Williams 2011).

For the simply supported design example, the basic principles were the same but the geometry of the STM, the member forces, and the resulting reinforcement layout were different from those of the moment frame structure. The reinforcement details for the moment frame design allowed for the flow of forces around the frame corners and permitted moment to be transferred between the columns and the bent cap. For the simply supported case, only vertical reactions were assumed to be transferred between the cap and the columns. Due to the fixity of the structure, the moment at the midspan of the moment frame bent cap was significantly smaller than the simply supported bent cap which required more reinforcement in the bottom chord. Additional stirrups were also required for the simply supported member due to the reduced truss depth. These design differences are expected between simply supported and moment frame structures.

The design examples were modeled after a moment frame inverted-T bent cap that was originally designed using TxDOT sectional procedure. Although not inspected as part of the current project, the in-service bent cap was reported to have significant diagonal

cracking in the shear spans as shown in Figure 7-4. The shear serviceability check developed by TxDOT Project 0-5253 and evaluated in the current project indicated that diagonal cracking was likely for the structure. An increase in cross-sectional dimensions and/or concrete strength would have been necessary to limit cracking. Flexural cracking was also observed at the outside of the frame corners, which would indicate that the bend radius of the longitudinal bars was too small. In the moment frame example, it was discovered that a larger bend radius was required for the longitudinal bars in the corners of the frame, once again verifying the applicability of the recommended STM design procedure.

Figure 7-4: US-59/ N W. Little York Bent #4, Houston Texas

CHAPTER 8
Summary and Conclusions

8.1 SUMMARY

Diagonal cracking in the shear span of inverted-T bent caps prompted an investigation into the design of such structures from a strength and serviceability standpoint. A previous research project, TxDOT Project 0-5253, investigated rectangular deep beams loaded on the compression chord. In this project recommendations were made for the design of such structures through strut-and-tie modeling provisions. Serviceability recommendations were also made to limit diagonal cracking and relate maximum crack width to deep beam residual capacity. These provisions proved useful to TxDOT engineers but were not approved for tension-chord loaded structures such as inverted-T bent caps.

Due to scarcity of experimental investigations on inverted-T beams, a comprehensive experimental program was undertaken to examine the behavior of such structural elements and assess the accuracy and validity of implementing the TxDOT Project 0-5253 STM design provisions. In order to accomplish the aforementioned goal, the scope of the project was divided into the following tasks:

1. Conduct a comprehensive literature review to expose the current state of knowledge on inverted-T beams.

2. Conduct a detailed assessment of the condition of distressed in-service bent caps

3. Conduct experimental investigations to uncover the main factors affecting the web diagonal cracking behavior of inverted-T beams:

    i. Determine the influence that the length of the ledge has on the strength and serviceability behavior of an inverted-T beam (Section 4.3).

    ii. Determine the influence that the depth of the ledge has on the strength and serviceability behavior of an inverted-T beam (Section 4.4).

    iii. Determine the influence that the web reinforcement ratio has on the strength and serviceability behavior of an inverted-T beam (Section 4.5).

    iv. Determine the influence that the number of point loads has on the strength and serviceability behavior of an inverted-T beam (Section 4.6).

    v. Determine the influence that the depth of the web has on the strength and serviceability behavior of an inverted-T beam (Section 4.7).

    vi. Determine the effect of tension-chord loading on the strength and serviceability of deep beams (Section 4.8).

4. Make a recommendation on the application of TxDOT Project 0-5253 STM provisions for the design of inverted-T bent caps (Section 5.2).

5. Make a recommendation on the feasibility of limiting diagonal cracking under service loads (Section 5.3).

6. Make a recommendation for relating the maximum diagonal crack width of an inverted-T beam to its residual capacity (Section 5.4).

An exhaustive database was assembled to evaluate all relevant results on inverted-T beams test from the literature and the current experimental program. It was discovered that research in this field is scarce. Of the 130 beam tests compiled, most were of beams not comparable to in-service structures. Complicated support conditions, unrealistic geometry, impractical reinforcement layouts, and unrealistically small dimensions precluded the use of all inverted-T specimens in the literature.

An extensive experimental program was therefore undertaken to achieve the project objectives. Thirty three full-scale inverted-T specimens were tested as part of this project. The cross-sectional dimensions of the specimens included: 21 in. web widths and 42 in. or 75 in. web heights. Ledge width for all specimens was 10.5 in. on each side. Length and depth of the ledges were varied as per the projects tasks. During the tests, measurements of the applied load, deflection along the beam, the strain at various locations, and diagonal crack widths were recorded. With the data from these tests the eight primary objectives of the current project were addressed.

8.2   CONCLUSIONS

The conclusions of the current study, based on data from the experimental program, are presented in this section.

8.2.1   Effects of Ledge Length

The effects of the length of the ledge on the shear strength and serviceability of inverted-T beams were investigated experimentally. Specimens in the experimental program were constructed with one of three different ledge lengths: cut-off, where the ledge was terminated directly after the bearing plate, short, where the ledge was extended a distance equal to the ledge depth from the edge of the bearing plate, and long ledges that extended all of the way to the support. Twenty tests were conducted on eight groups of directly comparable specimens in which every variable was kept constant except for the length of the ledge. The following could be concluded from test results:

- **Increasing the length of the ledge increases the web shear strength of inverted-T beams and delays the appearance of first diagonal cracking in the web.** Based on the experimental results specimens with cut-off ledges were found to have the lowest normalized shear strength and were more likely to crack at lower loads. It is

recommended to extend the ledge at least a distance equal to its depth past the bearing plate of the exterior girder.

- **The length of the ledge has no appreciable effect on the width of diagonal cracks..** Once the inverted-T specimen cracked, no further trend was observed between the length of the ledge and the diagonal crack width as crack width expansion due to increasing load was not a function of ledge length.

8.2.2 Effects of Ledge Depth

The effects of the depth of the ledge on the strength and serviceability of inverted-T beam webs were investigated experimentally. Specimens in the experimental program were constructed with either deep ledges or shallow ledges; with depths equal to one half or one third of the height of the beam. Twenty tests were conducted on ten groups of directly comparable specimens. The following could be concluded from test results:

- **Increasing the depth of the ledge had no appreciable effect on the strength or serviceability behavior of the webs of inverted-T specimens.** No trends were observed between the depth of the ledge and the normalized shear strength of the webs. Although deeper ledges did increase the diagonal cracking load slightly, they had no effect on the progression of crack widths with applied load.

8.2.3 Effects of Web Reinforcement Ratio

The effects of the web reinforcement ratio on the strength and serviceability behavior of reinforced concrete inverted-T beams were investigated experimentally. The minimum reinforcement ratio recommended by TxDOT Project 0-5253 was also evaluated to ensure adequate performance. Several distributions of web reinforcement were investigated on 42-in. deep beams. The majority of test specimens had either 0.3% or 0.6% reinforcement in each orthogonal direction. Two specimens were constructed with 0.6% in the vertical direction (shear stirrups) and 0.3% in the horizontal (skin reinforcement). Fourteen tests were conducted on six groups of directly comparable specimens. The following could be concluded from test results:

- **Increasing the horizontal and vertical web reinforcement ratio from 0.3% to 0.6% increased the shear strength for specimens tested at a/d ratios of 1.85 and 2.50.** The specimens tested at an a/d ratio of 1.85 failed in a manner consistent with a single-panel, direct-strut mechanism. While this mechanism depends mostly on the strength of the concrete it appeared that additional reinforcement served to reinforce the strut and the corresponding strut-to-node interface. The specimens tested at an a/d ratio of 2.50 generally failed in a manner that was consistent with a sectional-shear model, or a multiple panel STM. At this longer shear span, increasing the vertical reinforcement was expected to increase the strength of the member as the vertical web tie was the weakest element.

- **Increasing the horizontal and vertical web reinforcement ratio from 0.3% to 0.6% had little influence on the shear at first cracking of the webs but did reduce diagonal crack widths at larger levels of load.**

- **To adequately restrain the maximum diagonal crack widths in the webs at service loads, a minimum of 0.3% web reinforcement ratio should be provided and spaced evenly in each orthogonal direction within the effective strut area.** The maximum diagonal crack width of specimens with 0.3% reinforcement in each direction were found to satisfy the 0.016 in. limit at estimated service level loads. The 0.3% web reinforcement ratio is consistent with the recommendations in TxDOT Project 0-5253 and with the current AASHTO LRFD provision (Article 5.6.3.6, 2012).

8.2.4 Effects of Multiple Loading Points

The effects of multiple point loads on the strength and serviceability behavior of inverted-T beams were investigated experimentally. Specimens were loaded on the ledge at either one or three points. Twelve tests were conducted on six pairs of directly comparable specimens in which every parameter was kept constant except the number of load points. The following could be concluded from test results:

- **The number of point loads did not influence the strength or serviceability behavior of the inverted-T specimens.** No appreciable trends were observed when the shear strengths were compared between specimens loaded at one or three points and the diagonal cracking load was essentially unchanged. Multiple loading points did not significantly influence the progression of diagonal crack widths with applied load. The results therefore lend support to extending experimental findings from single-point loaded specimens to multi-point loaded bent caps in the field.

8.2.5 Effects of Web Depth

The effects of web depth on the strength and serviceability performance of reinforced concrete inverted-T beams were investigated experimentally. Tests were conducted at a/d ratios of 1.85 and 2.50 on specimens with 42 in. and 75 in. deep webs and 0.3% web reinforcement in each direction. A single load was applied to short, shallow ledges for all directly comparable specimens. The following could be concluded from test results:

- **Within the full-scale web depth range tested, web depth did not influence the strength or serviceability behavior of the inverted-T specimens.** No appreciable trends were observed when the calculated and experimental shear strengths were compared between specimens of different depths and the diagonal cracking load was essentially unchanged. Web depth did not significantly influence the progression of diagonal crack widths with applied load.

8.2.6 Effects of Tension Chord Loading

The effects of tension chord loading on the strength and serviceability performance of reinforced concrete deep beams were investigated by comparing inverted-T beams from the current study with rectangular bent caps from TxDOT Project 0-5253.

- **No strength effects were observed due to tension-chord loading, but the tension field does affect crack width.** The inverted-T beams were observed to crack at higher levels of load and sustain smaller crack widths throughout loading. Thus an inverted-T beam with the same crack width as a compression-chord loaded beam would be closer to its ultimate capacity.

8.2.7 Proposed STM Design Provisions

The STM design provisions developed by TxDOT Project 0-5253 were evaluated for the design of inverted-T bent caps. The following recommendations were issued for the design of inverted-T beams:

- **TxDOT Project 0-5253 STM provisions are recommended for the design of inverted-T bent caps.** A comparison between the ultimate shear capacity obtained from the test result and the nominal shear capacity from the calculations revealed conservative strength estimates for every specimen. Furthermore, the strut-and-tie models accurately predicted the ultimate failure mode for twenty eight of the thirty three specimens. For the five that did not fail in shear, the calculated shear capacity was exceeded and the actual failure mode was the second weakest element in the model. Within these provisions, a minimum web reinforcement ratio is given as 0.3% in each orthogonal direction. That minimum worked well in inverted-T beams both in terms of developing strut/node strengths and in terms of limiting diagonal crack widths at service levels. It is recommended to provide that minimum ratio in inverted-T beams.

- **Recommendations were given in Chapter 2 for implementing the STM provisions for inverted-T beams.** The geometry of inverted-T beams requires the use of a three-dimensional STM model or two complimentary two-dimensional models. Recommendations were given to aid in developing these models. The width over which the load is assumed spreads under the loading points defines the hanger tie width and was defined. The width of the tie at the top of the ledge was also defined based on current AASHTO design procedures for ledges.

- **Cut-off ledges are not recommended.** Cut-off ledges were shown to result in lower web shear strengths than longer ledges. Cut-off ledges were also found to reduce the load at first diagonal cracking in the web. Moreover, cut-off ledges increased the risk of ledge failures.

Application of the STM provision to the design of one of the inverted-T beam specimens is given in Appendix A. Two detailed design examples of inverted-T beams are given in the final report of Project 5-5253 (Williams et al. (2011)).

8.2.8   Limiting Diagonal Cracking under Service Loads

Along with strength design provisions, a service-load shear check to limit diagonal cracking was given.

- **The simple and reasonably conservative equation to estimate the diagonal cracking load of deep beams is recommended for use with inverted-T beams.** As in the deep beam project, the diagonal cracking load of inverted-T beams was found to be mainly a function of the shear area, the square root of the compressive strength of concrete, and the a/d ratio. With this equation the service level shear in the member can be sized to limit diagonal cracking. If the service level shear (full dead load plus live load) exceeds the estimated diagonal cracking load, the design of the section can be modified to increase section size and/or additional web reinforcement can be provided to control diagonal crack widths. This check encourages the designer to consider the likelihood of diagonal cracking in service.

- **Longitudinal post tensioning could be investigated for structures that do not pass service checks**. It has been shown in rectangular beams that post-tensioning reduces crack widths and may increase shear strength. It is likely it would have a similar result for inverted-T beams, however, this has not been directly investigated.

8.2.9   Correlation of Maximum Diagonal Crack Width to Web-Shear Strength

Diagonal crack widths were measured and compared to applied load to help field engineers evaluate the residual capacity of a diagonally-cracked inverted-T bent caps.

- **A simple chart was developed to correlate the maximum diagonal crack width in a deep beam to the load acting on the member, quantified as a percent of its ultimate capacity.** As the other variables investigated in the experimental program had limited effects on the width of the diagonal cracks, the chart is only a function of the amount of web reinforcement in the member. It is similar to the one produced for the compression-chord loaded deep beams, but for a given percentage of resulting residual strength, cracks in inverted-T beams were found to be smaller than those in rectangular beams. This chart is a simple means to make an informed decision regarding the amount of distress in a diagonally-cracked inverted-T bent cap when a more sophisticated means of evaluation is unavailable.

8.3   CONCLUDING REMARKS

In this research project, the behavior of inverted-T webs was studied through a comprehensive experimental program. Thirty three tests were conducted on large-scale

specimens, some of which are amongst the largest deep beams, and certainly inverted-T beams, ever tested in the history of shear research. From the analysis of this data, the effect of the following parameters on the strength and serviceability behavior of inverted-T beam webs was determined: the length of the ledge, the depth of the ledge, the quantity of web reinforcement, the number of point loads, the depth of the member, and the shear span-to-depth ratio.

With the results obtained from examining the effect of these parameters, the strut-and-tie provisions proposed by TxDOT Project 0-5253 were assessed for applicability to inverted-T beams. The design provisions were found to yield accurate and reasonably conservative results for tension-chord loaded beams. The recommended minimum web reinforcement ratio adequately restrained the width of diagonal cracks and the service-load check for limiting the formation of diagonal cracks under service loads was suitable for inverted-T beams as well as the deep beams for which they were developed. The knowledge obtained from this study was also used to improve the evaluation of bent caps in the field as diagonal crack widths of inverted-T beams were found to correspond to a greater percentage of ultimate capacity than their compression-chord loaded counterpart. This report provides a comprehensive summary of the parameters affecting the behavior of inverted-T beams with which the condition of in-service bent caps can be properly assessed.

References

AASHTO LRFD, *Bridge Design Specifications*, American Association of State Highway and Transportation Officials, Washington, D.C., 2012.

ACI Committee 224, "Control of Cracking in Concrete Structures" (ACI 224R-01), *ACI Manual of Concrete Practice*, American Concrete Institute, Farmington Hills, MI, 2008.

ACI Committee 318-11, *Building Code Requirements for Reinforced Concrete (ACI 318-11)*, American Concrete Institute, Farmington Hills, MI, 2011.

ACI-ASCE Committee 326, "Shear and Diagonal Tension," American Concrete Institute, Farmington Hills, MI, 1962.

ACI-ASCE Joint Committee 426-73, *The Shear Strength of Reinforced Concrete Members (ACI-ASCE 426-72)*, American Concrete Institute, Detroit, MI, 1973.

ACI-ASCE Joint Committee 445, *Recent Approaches to Shear Design of Structural Concrete (ACI 445R-99)*, American Concrete Institute, Farmington Hills, MI, 1999.

ASTM A 370 – 08a, *Standard Test Methods and Definitions for Mechanical Testing of Steel Products*, American Society for Testing and Materials, West Conshohocken, PA, May 2008.

ASTM A 615/A 615M – 08, *Standard Specification for Deformed and Plain Carbon-Steel Bars for Concrete Reinforcement*, American Society for Testing and Materials, West Conshohocken, PA, March 2008.

ASTM C 143/C 143M – 08, *Standard Test Method for the Slump of Hydraulic-Cement Concrete*, American Society for Testing and Materials, West Conshohocken, PA, March 2008.

ASTM C 31/C 31M – 08a, *Standard Practice for Making and Curing Concrete Test Specimens in the Field*, American Society for Testing and Materials, West Conshohocken, PA, April 2008.

ASTM C 39/C 39M – 05, *Standard Test Method for Compressive Strength of Cylindrical Concrete Specimens*, American Society for Testing and Materials, West Conshohocken, PA, November 2005.

Bergmeister, K.; Breen, J. E.; Jirsa, J. O.; and Kreger, M. E., *Detailing for Structural Concrete*, Report No. 1127-3F, Center for Transportation Research, University of Texas at Austin, Austin, Texas, May 1993.

Birrcher, D., Tuchscherer, R., Huizinga, M., Bayrak, O., Wood, S., & Jirsa, J. *Strength and Serviceability Design of Reinforced Concrete Deep Beams.* Austin, TX: Center for Transportation Research, The University of Texas at Austin. 2009.

Bracci, J. M., Keating, P. B., and Hueste, M. B. D., *Cracking in RC Bent Caps*, Research Report 1851-1, Texas Transportation Institute, The Texas A&M University System, College Station, Texas, Oct. 2000, 257 pp.

Brown, M. D.; Sankovich, C. L.; Bayrak, O.; Jirsa, J. O.; Breen, J. E.; and Wood, S. L., *Design for Shear in Reinforced Concrete Using Strut-and-Tie Models*, Report No. 0-4371-2, Center for Transportation Research, University of Texas at Austin, Austin, Texas, Apr. 2006.

Cussens, A. R., & Besser, I. I. Shear strength of reinforced concrete wall-beams under combined top and bottom loads. *The Structural Engineer, 63B*(3), Steptember 1985. 50-56 pp.

Fereig, S. M., & Smith, K. N. Indirect Loading on Beams with Short Shear Spans. *ACI Journal, 74*(5), May 1, 1977, pp. 220-222.

Ferguson, P. M. Some Implications of Recent Diagonal Tension Tests. *Journal of the American Concrete Institute, 53*(8), 1956, pp. 157-172.

Fernández-Gómez, E., Larson, N., Garber, D., Ghannoum, W., & Bayrak, O. Strength and Serviceability of Reinforced Concrete Inverted-T Straddle Bent Caps. *PCI/NBC Proceedings.* 2011

FIB, *Structural Concrete, Textbook on Behaviour, Design, and Performance*, Volume 3, International Federation for Structural Concrete, Lausanne, Switzerland, 1999, 269 pp.

Furlong, R. W., & Mirza, S. A. *153-1F - Strength and Serviceability of Inverted T-Beam Bent Caps Subject to Combined Flexure, Shear, and Torsion.* Austin: Center for Highway Research, University of Texas at Austin.1974.

Furlong, R. W., Ferguson, P. M., & Ma, J. S. *113-4 - Shear and anchorage study of reinforcement in inverted-T beam bent cap girders.* Austin TX: Center for highway research at The University of Texas at Austin. 1971.

Galal, K., & Sekar, M. Rehabilitation of RC inverted-T girders using anchored CFRP sheets. (S. Direct, Ed.) *Composites: Part B - Engineering, 39*(4), June 1, 2007, pp. 604-617.

Garber, D. B. *Shear Cracking in Inverted-T Straddle Bents.* Master's Thesis, University of Texas at Austin. August 2011.

Graf, O., Brenner, E., & Bay, H. Versuche mit einem wandartigen Trager aus Stahlbeton. *Deutscher Ausschuss fur Stahlbeton, 99*, 1943, pp. 41-54.

Huizinga, M. R., *Strength and Serviceability Performance of Large-Scale Deep Beams: Effect of Transverse Reinforcement*, Master's Thesis, University of Texas at Austin, August 2007, 232 pp.

Leonhardt, F., & Walther, R. (1966). Wandartige Träger. *Deutscher Ausschuss furStahlbeton, 178*.

Ma, J. S. PhD Dissertation: *Behavior of reinforced concrete inverted T-beams.* Austin, TX: University of Texas at Austin. 1971.

MacGregor, J. G. and Wight, J. K., *Reinforced Concrete, Mechanics and Design*, 4th Edition, Pearson Prentice Hall, New Jersey, 2005, 1132 pp.

MacGregor, J. G., "Derivation of Strut and Tie Models for the 2002 ACI Code," *ACI SP-208 Examples for the Design of Structural Concrete with Strut-and-Tie Models*, American Concrete Institute, Michigan, 2002, 242 pp.

Mitchell, D., and Collins, M.P., "Diagonal Compression Field Theory – A Rational Model for Structural Concrete in Pure Torsion," *ACI Journal*, Vol. 71, No. 8, August 1974, pp. 396-408.

Ramirez, J.A., and Breen, J.E., *Proposed Design Procedures for Shear and Torsion in Reinforced and Prestressed Concrete*, Report No. 248-4F, Center for Transportation Research, University of Texas at Austin, Austin, Texas, 1983.

Schlaich, J., Schäfer, K. and Jennewein, M., "Toward a Consistent Design of Structural Concrete," *PCI Journal*, Vol. 32, No. 3, May-June 1987, pp.74-150.

Schütt, H. Über das Tragvermögen wandartiger Stahlbetonträger. *Beton und Stahlbetonbau, 10*, October 1956, pp. 220-224.

Smith, K. N., & Fereig, S. M. "Effect Of Loading And Supporting Condidtions On The Shear Strength Of Deep Beams". *ACI, SP 42*, January 1, 1974, pp. 441-460.

Tan, K. H., Kong, F. K., & Weng, L. W. (1997, June 3). High strength concrete deep beams subjected to combined top-and bottom-loading. *The Structural Engineer, 75*(11), 191-197.

Taylor, R. Some shear tests on reinforced concrete beams without shear reinforcement. *Magazine of Concrete Research, 12*(36), November 1960, pp. 145-154.

TxDOT. *Bridge Design Manual - LRFD.* 2011

TxDOT, Texas Department of Transportation Standard Bridge Drawings, 2008.

Wight, J.K., and Parra-Montesinos, G., "Use of Strut-and-Tie Model for Deep Beam Design as per ACI 318 Code," *ACI Concrete International,* Vol. 25, No. 5, May 2003, pp. 63-70

Williams, C. S. *Strut-and-Tie Model Design Examples for Bridges.* Master's Thesis, University of Texas at Austin. 2011

Young, B. S., Bracci, J. M., Keating, P. B., and Hueste, M. B., "Cracking in Reinforced Concrete Bent Caps," *ACI Structural Journal*, Vol. 99, No. 4, July-August 2002, pp. 488-498.

Zhang, N. and Tan, K. H., "Size effect in RC deep beams: Experimental investigation and STM verification," *Engineering Structures*, Vol. 29, 2007, pp. 3241-3254.

Zhu, R. R.-H., Dhonde, H., & Hsu, T. T. *TxDOT Project 0-1854: Crack Control for Ledges in Inverted "T" Bent Caps*. University of Houston. 2003.

APPENDIX A. Design Example

A.1 Overview

A detailed strut-and-tie design example of one of the specimens in the experimental program is provided in this appendix. The STM design provisions recommended in this project for inverted-T beams were used.
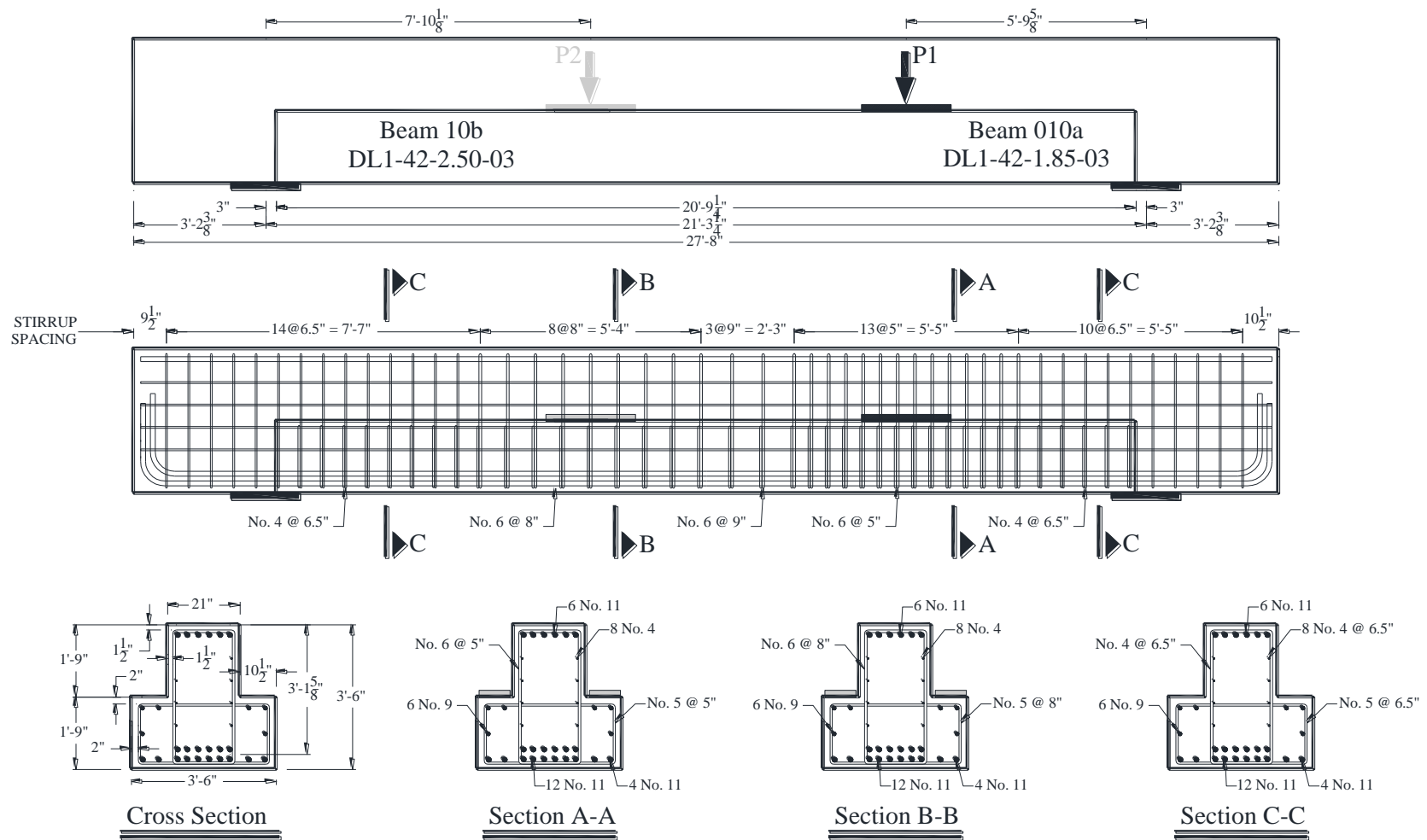

Figure A-1: Beam DL1-42-1.85-03

Beam 10a: DL1-42-1.85-03, shown in Figure A-1, was designed to fail in shear. The shear-span-to-depth ratio was 1.85 and the predicted failure mode was crushing of the strut-to-node interface at the support closest to the load point. Therefore the objective of this design example was to ensure that all other elements in the strut-and-tie model do not govern the capacity of the beam. This is thus not a typical design where a beam is dimensioned to resist a certain combination of loads. Rather this beam was designed to fail in shear while its strength remained within laboratory testing capacities.

As mentioned in Chapter 3, all of the beams in the experimental program were constructed with the same web width of 21 in. and ledge width of 10.5 in. The total height of this beam was 42in. As this was to be a "long, deep ledge" specimen, the ledge was constructed with a depth of 21 in. and continued from the edge of the bearing plate to the support. The ledge dimensions and the final reinforcement layout are shown in Figure A-2.

Originally the beam was designed with a specified concrete compressive strength of $f'_c = 4$ ksi and steel tensile strength of $f_y = 60$ ksi. The values shown in the following example are the actual measured material strengths, as presented in Chapter 3. Examining the strut-and-tie model using these values enables a direct comparison between the calculated strength of the specimen and the actual strength obtained through testing; as discussed in Chapter 5.

Figure A-2: Elevation and cross-sectional details of DL1-42-1.85-03.

A.2 Defining the Beam

The following calculations outline the steps taken to develop a strut-and-tie model to determine the capacity of DL1-42-1.85-03.

Gross Section Properties

First the gross dimensions of the beam are determined as presented in Figure A-2.

$$L = 255\frac{1}{4} \text{ in}$$ Length of the beam between supports

$$L_1 = 69\frac{5}{8} \text{ in}$$ Near support to load

$$L_2 = 185\frac{5}{8} \text{ in}$$ Far support to load

$$b = 21 \text{ in}$$ Web width

$$h_l = 21 \text{ in}$$ Ledge height

Load and Support Plate Properties

The next step is to define the load and support plate sizes as these determine the size of their respective nodes and influence the strength of the strut-and-tie model. Once the size of the load plate is known, the distance the load will spread over the length of the ledge can also be calculated.

$$w_l := 9 \text{in}$$ Load plate width

$$l_l := 26 \text{in}$$ Load plate length

$$w_s := 20 \text{in}$$ Support plate width

$$l_s := 16 \text{in}$$ Support plate length

$$d_l := h_l - 1.5\text{in} - 0.5d_5 = 19\frac{3}{16} \cdot \text{in}$$ Distance from the top of ledge to compression reinforcement

$$l_{sp} := l_l + 2 \cdot d_l = 64\frac{3}{8} \cdot \text{in}$$ Resulting load spread
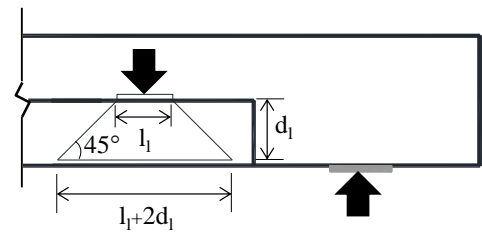
Material Properties

The beam was originally designed with specified material strengths of $f'_c = 4$ ksi and $f_y = 60$ ksi. This example, however, will consider the measured material strengths to get a better estimate of the actual strength of the beam.

$$f'_c := 4.93 \text{ksi}$$

$$f_{y\_11} := 71.0075 \text{ksi} \quad A_{11} := 1.56 \text{in}^2 \quad d_{11} := 1.41 \text{in}$$

$$f_{y\_6} := 61.9 \text{ksi} \quad A_6 := 0.44 \text{in}^2 \quad d_6 := 0.75 \text{in}$$

$$f_{y\_5} := 64.285 \text{ksi} \quad A_5 := 0.31 \text{in}^2 \quad d_5 := 0.625 \text{in}$$

$$f_{y\_4} := 64.425 \text{ksi} \quad A_4 := 0.20 \text{in}^2 \quad d_4 := 0.5 \text{in}$$

STM Nodal Factors

As discussed in Chapter 2, the strength of the node depends on the elements (struts and/or ties) framing into it as well as the particular face under consideration. A concrete efficiency factor, *v*, is applied to the concrete strength, *f'c*, to limit the compressive stress at the face of each node.

$$f_{cu} := m \cdot v \cdot f'_c$$

$$v_{CCC\_b} := 0.85 \qquad\qquad\qquad \text{Bearing and back face of CCC node}$$

$$v_{CCT\_b} := 0.7 \qquad\qquad\qquad \text{Bearing and back face of CCT node}$$

$$v_{CCT\_stn} := \begin{vmatrix} 0.45 & \text{if} & \left(0.85 - \dfrac{f'_c}{20 \text{ksi}}\right) < 0.45 = 0.604 \\[2em] 0.65 & \text{if} & \left(0.85 - \dfrac{f'_c}{20 \text{ksi}}\right) > 0.65 \\[2em] 0.85 - \dfrac{f'_c}{20 \text{ksi}} & \text{otherwise} \end{vmatrix} \qquad \text{CCC and CCT strut-to-node interface}$$

A confinement modification factor, *m*, is also used to increase the allowable bearing stress in a node to account for the effects of confinement provided by the concrete when the loaded area, *A₁*, is smaller than the supported area, *A₂*. In this case the support plate is only 20 in. wide whereas the beam is 21 in. wide.

$$A_1 := w_s \cdot l_s = 320 \, \text{in}^2$$

$$A_2 := (w_s + 1\text{in})(l_s + 1\text{in}) = 357 \cdot \text{in}^2$$

$$m := \sqrt{\frac{A_2}{A_1}} = 1.056$$

A.3 Longitudinal Strut-and-Tie Model

The next step is to determine the location of the struts and ties as shown in Figure A-3. The horizontal flexure tie, Tie AH, is positioned at the center of the longitudinal reinforcement. The

horizontal strut at the top of the beam, Strut BF, is located at the center of the compression stress block, determined from a standard flexural analysis. Tie BC is located at the center of the hanger reinforcement at the load point. Tie DE and Tie FG were then located at third points between the edge of the hanger bar spread and the line projected at a 25 degree angle from the edge of the support plate at Node H to the top of the beam as shown in Figure 2-14.
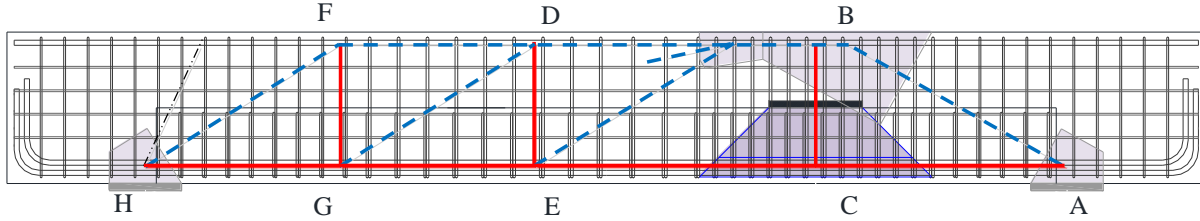
Figure A-3: Strut-and-tie model for DS1-42-1.85-03

$A'_s := 6 \cdot A_{11} = 9.36\,in^2$ Compression Steel

$A_s := 12 A_{11} = 18.72\,in^2$ Flexure Steel

$w_{flex} := 2 \cdot 4.365\,in = 8.73\,in$ Flexure Tie Width

$a := \dfrac{A_s \cdot f_{y\_11} - A'_s \cdot f_{y\_11}}{0.85\,b \cdot f'_c} = 7.553\,in$ Compression Stress Block

$d := 42\,in - \dfrac{w_{flex}}{2} = 37.635\,in$ Top of beam to center of flexural reinforcement

$h := d - \dfrac{a}{2} = 33.859\,in$ Moment arm

$a_d := \dfrac{L_1}{d} = 1.85$ Shear span-to-depth ratio

With the locations of the struts and ties determined, the size of the nodes can be defined. The length of Node B in the longitudinal direction is determined by the spread length of the hanger tie, l_{sp}. It is then divided proportionally to the amount of the applied load that acts on the left and right side of the node to obtain l_e and l_a respectively. The depth of the node is taken as the depth of the compression stress block, a, determined above.

209
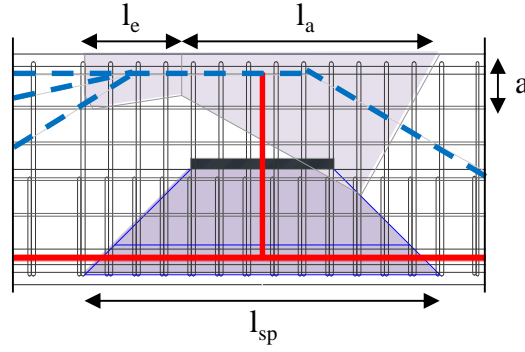
Figure A-4: Geometry of CCT Node B

$$l_a := l_{sp} \cdot \left(\frac{L_2}{L} \right) = 46.813 \text{in} \qquad \text{Portion of the load spread length, lsp, on the left side of Node B}$$

$$l_e := l_{sp} \cdot \left(1 - \frac{L_2}{L} \right) = 17.562 \text{in} \qquad \text{Portion of the load spread length, lsp, on the right side of Node B}$$

To determine the angle of each of the struts, the arctangent is taken of the distance from the center of the flexural steel to the center of the compression stress block divided by the horizontal length of the node.

$$l_{ab} := 0.5 l_a + l_e - 0.5 l_{sp} = 8.781 \text{in} \qquad \text{Distance from center of length la to location of Tie BC}$$

$$l_{be} := l_a + 0.5 l_e - 0.5 l_{sp} = 23.407 \text{in} \qquad \text{Distance from center of length le to location of Tie BC}$$

$$l_{2.5} := \frac{L_2 - l_{be}}{3} = 54.07 \text{in} \qquad \text{Distance from the edge of the load spread, lsp, to Support H}$$

$$\theta_A := \text{atan}\left(\frac{h}{L_1 - l_{ab}} \right) = 0.508 \qquad \Theta_A := \theta_A \cdot \frac{180}{\pi} = 29.092 \qquad \text{Angle between Strut AB and Tie AC}$$

$$\theta_E := \text{atan}\left(\frac{h}{l_{2.5}} \right) = 0.559 \qquad \Theta_E := \theta_E \cdot \frac{180}{\pi} = 32.055 \qquad \text{Angle between Strut BE and Tie DE}$$

$$\theta_G := \text{atan}\left(\frac{h}{l_{2.5}} \right) = 0.559 \qquad \Theta_G := \theta_G \cdot \frac{180}{\pi} = 32.055 \qquad \text{Angle between Strut DG and Tie EG}$$

$$\theta_H := \text{atan}\left(\frac{h}{l_{2.5}} \right) = 0.559 \qquad \Theta_H := \theta_H \cdot \frac{180}{\pi} = 32.055 \qquad \text{Angle between Strut FH and Tie GH}$$

Node Capacities

The strength of each node is dependent on the area of the face of the node and the limited compressive stress, f_{cu}. The area of each node face is equal to its length, calculated according to Figure 2-12 or Figure 2-13, multiplied by the beam width, *b*, or the plate width, if applicable. For the nodes defined by the support or bearing plates the concrete modification factor is applied. Only the critical nodes, the support Nodes A and H, and the hanger Node B are checked in the longitudinal model. For each critical node, the capacity of the strut-to-node interfaces (STNI)

and bearing surfaces are determined. For Node A, the notation R_A refers to the bearing strength at the support at A as shown in Figure A-4. AB_A refers to the capacity of the strut-to-node interface of Strut AB at Node A. Likewise AB_B is the capacity of the strut-to-node interface of strut AB at Node B, BD_B is the strength of the strut-to-node interface of strut BD, etc. P_L is the total bearing capacity at the load point, considering both ledges. The ν factors in the following equations reflect the respective type of node face.
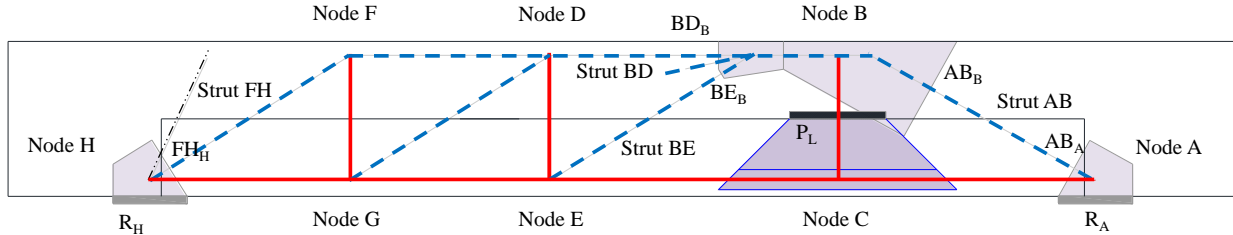
Figure A-5: Strut and node notation

Node A
$$R_A := m \cdot \nu_{CCT\_b} \cdot f_c \cdot w_s \cdot l_s = 1166.418 \text{kip}$$

$$AB_A := m \cdot \nu_{CCT\_stn} \cdot w_s \cdot \left(l_s \cdot \sin(\theta_A) + w_{flex} \cdot \cos(\theta_A)\right) \cdot f_c = 968.409 \text{kip}$$

Node B
$$BD_B := \nu_{CCT\_stn} \cdot b \cdot a \cdot f_c + A'_s \cdot f_{y\_11} = 1136.518 \text{kip}$$

$$BE_B := \nu_{CCT\_stn} \cdot b \cdot \left[\left(l_e + a \cdot \tan(\theta_E)\right)\sin(\theta_E) - \frac{a}{\cos(\theta_E)}\right] \cdot f_c = 182.417 \text{kip}$$

$$AB_B := \nu_{CCT\_stn} \cdot b \cdot \left(l_a \cdot \sin(\theta_A) + a \cdot \cos(\theta_A)\right) \cdot f_c = 1834.463 \text{kip}$$

Node H
$$FH_H := m \cdot \nu_{CCT\_stn} \cdot w_s \cdot \left(l_s \cdot \sin(\theta_H) + w_{flex} \cdot \cos(\theta_H)\right) \cdot f_c = 998.751 \text{kip}$$

$$R_H := m \cdot \nu_{CCT\_b} \cdot f_c \cdot w_s \cdot l_s = 1166.418 \text{kip}$$

Load
$$P_L := 2 \cdot m \cdot \nu_{CCT\_b} \cdot f_c \cdot w_l \cdot l_l = 1705.886 \text{kip}$$

Member Forces

The purpose of the experimental program was to examine the shear capacity and behavior of the inverted-T beams. Therefore each beam was designed to fail in shear. For an a/d ratio of 1.85, the expected failure mechanism is crushing of the nodes at the ends of the direct strut. Therefore, the beam was detailed with that as its weakest element. For DS1-24-1.85-03, the strut-to-node interface of Strut AB at Node A controlled with the smallest capacity of 968.4 kips. The low capacity value of the STNI of Strut BE at Node B is misleading as it can be combined with the STNI of BD (discussed later on). The design check is then performed with the applied load, *P*, that would result in a force of 968.4 kip in Strut AB. The resulting force in each member is donated as "$F_{element}$" such as F_{AB} for the force in Strut AB or F_{AC} for the force in Tie AC. For the critical nodes, the ratio of capacity to force is highlighted in the following calculations. As long as that ratio is greater than 1.0, the element is not expected to control the strength of the beam

$$P := AB_A \cdot \sin(\theta_A) \cdot \left(\frac{L}{L_2}\right) = 647.49 kip \qquad \boxed{P = 647 \cdot kip}$$

Design Beam to Fail at Strut-to-Node Interface at Node H

Node A

$$F_{RA} := \left(\frac{L_2}{L}\right) P = 470.848 kip \qquad \boxed{\frac{R_A}{F_{RA}} = 2.477}$$

$$F_{AB} := \frac{F_{RA}}{\sin(\theta_A)} = 968.409 kip \qquad \boxed{\frac{AB_A}{F_{AB}} = 1} \qquad \boxed{\frac{AB_B}{F_{AB}} = 1.894}$$

$$F_{AC} := F_{AB} \cdot \cos(\theta_A) = 846.238 kip$$

Node H

$$F_{RH} := \left(\frac{L_1}{L}\right) P = 176.639 kip \qquad \boxed{\frac{R_H}{F_{RH}} = 6.603}$$

$$F_{FH} := \frac{F_{RH}}{\sin(\theta_H)} = 332.821 kip \qquad \boxed{\frac{FH_H}{F_{FH}} = 3.001}$$

$$F_{GH} := F_{FH} \cos(\theta_H) = 282.079 kip$$

Node F

$$F_{DF} := F_{FH} \cos(\theta_H) = 282.079 kip$$

$$F_{FG} := F_{FH} \sin(\theta_H) = 176.639 kip$$

Node G

$$F_{DG} := \frac{F_{FG}}{\sin(\theta_G)} = 332.821 kip$$

$$F_{EG} := F_{DG} \cos(\theta_G) + F_{GH} = 564.159 kip$$

Node D

$$F_{BD} := F_{DG} \cos(\theta_G) + F_{DF} = 564.159 \text{kip}$$

$$F_{DE} := F_{DG} \sin(\theta_G) = 176.639 \text{kip}$$

Node E

$$F_{BE} := \frac{F_{DE}}{\sin(\theta_E)} = 332.821 \text{kip}$$

$$F_{CE} := F_{BE} \cos(\theta_E) + F_{EG} = 846.238 \text{kip}$$

Node B

$$F_{BC} := F_{BE} \sin(\theta_E) + F_{AB} \cdot \sin(\theta_A) = 647.487 \text{kip}$$

$$\frac{BD_B}{F_{BD}} = 2.015 \qquad \frac{BE_B}{F_{BE}} = 0.548$$

Try combining Strut BE and Strut BD (shallow angle)

Checks

$$F_{RH} + F_{RA} - P = 0 \cdot \text{kip} \qquad F_{AC} - F_{CE} = -0 \cdot \text{kip}$$

$$F_{BD} + F_{BE} \cos(\theta_E) - F_{AB} \cdot \cos(\theta_A) = 0 \cdot \text{kip}$$

Two comparisons are highlighted red in the above calculations. The first is the ratio of the strength of the strut-to-node interface at Node A to the force in Strut AB. That ratio is equal to 1.0, confirming that the applied load was determined based on the capacity of that element. The second red highlight is for the strut-to-node interface of Strut BE at Node B. Based on the above calculations it would appear that the node does not have the capacity to carry the applied node. This is not true, however because of the shallow angle between the two, Strut BE and Strut BD can be combined when they intersect Node B. As they move away from each other, Strut BE can spread and thus will not be critical to the capacity of the beam.

Modified Node face at Strut BE and BD

$$\theta_{mod} := \operatorname{atan}\left(\frac{F_{BE} \sin(\theta_E)}{F_{BD} + F_{BE} \cos(\theta_E)}\right) = 0.206 \qquad \Theta_{mod} := \theta_{mod} \cdot \frac{180}{\pi} = 11.79$$

$$F_x := F_{BD} + F_{BE} \cos(\theta_E) = 846.238 \text{kip} \qquad F_y := F_{BE} \sin(\theta_E) = 176.639 \text{kip}$$

$$F_{mod} := \sqrt{F_x^2 + F_y^2} = 864.477 \text{kip}$$

$$mod_F := v_{CCT\_str} \cdot b \cdot (l_a \cdot \sin(\theta_{mod}) + a \cdot \cos(\theta_{mod})) \cdot f_c + A'_s \cdot f_{y\_11} \cdot \cos(\theta_{mod}) = 1710.185 \text{kip}$$

$$\frac{mod_F}{F_{mod}} = 1.978 \qquad \text{ok!}$$

Tie Requirements

In order to ensure a shear failure due to node crushing, enough reinforcement must be provided in each tie to carry the applied load without yielding. For each of the 42 in. beams in the experimental program, twelve No. 11's were provided as the flexural reinforcement. If this proved insufficient steps were taken to ensure a shear failure, such as decreasing the compressive strength of the concrete. From the truss forces calculated above, the remaining ties were detailed as follows. The number of stirrups (No. 4 bars) and spacing was predetermined based on the reinforcement ratio for each beam. The hanger ties, however, were designed specifically to resist the force in the member, "F", with "T" representing the tensile capacity of the strut based on the total area and yield strength of the steel. For example, the force in hanger Tie BC from the applied load P would be F_{BC} determined in the previous section, and the capacity of the tie is T_{BC} determined by the steel provided to resist that force.

Flexural Reinforcement- #11 bars

$$F_{flex} := max\left(F_{AC}, F_{CE}, F_{EG}, F_{GH}\right) = 846.238 kip$$

$$T_{flex} := A_s \cdot f_{y\_11} = 1329.26 kip$$

$$\frac{T_{flex}}{F_{flex}} = 1.571$$

Hanger Bars- #6 stirrups

$$T_{BC} := 28 A_6 \cdot f_{y\_6} = 762.608 kip$$

$$\frac{T_{BC}}{F_{BC}} = 1.178$$

Tie FG- #5 stirrups and #6 hangers

$$T_{FG} := 14 A_4 \cdot f_{y\_4} + 6 A_6 \cdot f_{y\_6} = 343.806 kip$$

$$\frac{T_{FG}}{F_{FG}} = 1.946$$

Tie DE- #6 hangers

$$T_{DE} := 16 A_6 \cdot f_{y\_6} = 435.776 kip$$

$$\frac{T_{DE}}{F_{DE}} = 2.467$$

A.4 Cross-Sectional Strut-and-Tie Model

A similar detailing process is repeated for the cross-sectional strut-and-tie model. The overall dimensions are set by the type of inverted-T beam being designed. DS1-42-1.85-03 is a 42 in. deep beam with 21 in. deep ledges as show in Figure A-2. The resulting strut-and-tie model is detailed in Figure A-6. Strut BC is located at the depth of the longitudinal flexure tie. Hanger Tie BF and EC are aligned with the vertical hanger bars and Tie AD is aligned with the horizontal ledge bars. Struts AB and DC allow the load to be transferred from the ledge to the bottom of the web.
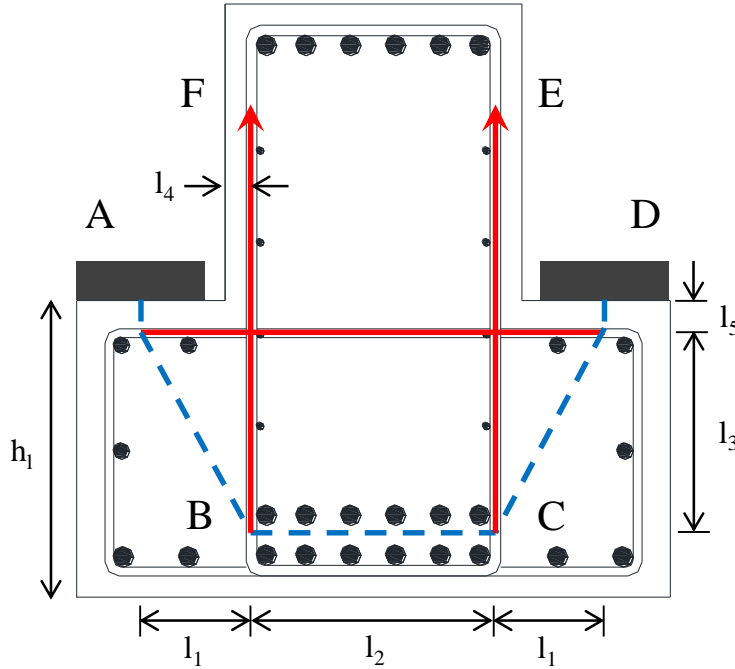
Figure A-6: Cross-Sectional Strut-and-Tie Model

Truss Geometry

$$l_4 := \left(1.5 + \frac{3}{8}\right) in$$

$$l_1 := l_4 + 1in + 0.5w_1 = 7.375in$$

$$l_3 := h_1 - 0.5w_{flex} - l_5 = 14.322in$$

$$\theta := atan\left(\frac{l_3}{l_1}\right) = 1.095$$

$$l_2 := b - 2l_4 = 17.25in$$

$$l_5 := \left(2 + \frac{5}{16}\right) in = 2.313in$$

$$l_n := l_{sp} - w_{flex}$$

$$\Theta := \theta \cdot \frac{180}{\pi} = 62.755$$

Because the cross section and loading is symmetric, only one side needs to be considered. The capacity of Node A and Node B are calculated in the same manner as those in the longitudinal strut-and-tie model with R_a referring to the bearing capacity at Node A and ab_a to the capacity of the STNI of Strut AB at Node A.

Node a

$$R_a := v_{CCT\_b} f_c \cdot w_l \cdot l_l = 807.534 \text{kip}$$

$$ab_a := v_{CCT\_stn} l_l \cdot (w_l \cdot \sin(\theta) + 2l_5 \cdot \cos(\theta)) \cdot f_c = 782.758 \text{kip}$$

Node b

$$ab_b := v_{CCT\_stn} l_{sp} \cdot (w_{flex} \cdot \cos(\theta) + 2l_4 \cdot \sin(\theta)) \cdot f_c = 1404.031 \text{kip}$$

$$bc_b := v_{CCT\_stn} l_n \cdot w_{flex} \cdot f_c = 1445.322 \text{kip}$$

Next the forces in the cross-sectional strut-and-tie model are determined by applying half of the load, P, from the longitudinal model to the bearing pads on each ledge. It is important to ensure that the ratio of the capacity of each node face is greater than the applied force so that a ledge failure does not occur. Once again, the "F" denotes the force in the member due to the applied load, *P*.

$$F_{Ra} := \frac{P}{2} = 323.771 \text{kip} \qquad \boxed{\frac{R_a}{F_{Ra}} = 2.494}$$

$$F_{ab} := \frac{F_{Ra}}{\sin(\theta)} = 364.174 \text{kip} \qquad \boxed{\frac{ab_b}{F_{ab}} = 3.855}$$

$$F_{dc} := F_{ab} = 364.174 \text{kip}$$

$$F_{bc} := F_{ab} \cdot \cos(\theta) = 166.717 \text{kip} \qquad \boxed{\frac{bc_b}{F_{bc}} = 8.669}$$

$$F_{ad} := F_{ab} \cdot \cos(\theta) = 166.717 \text{kip}$$

$$F_{bf} := F_{ab} \cdot \sin(\theta) = 323.771 \text{kip}$$

$$F_{ce} := 0.5 F_{BC} = 323.771 \text{kip}$$

$$F_{bf} - F_{ce} = -0 \cdot \text{kip} \qquad \text{Load check}$$

The final step in the design process is to detail the steel in the ledge. The hanger bars were checked in the longitudinal strut-and-tie model and do not need to be examined here. Enough horizontal ledge bars need to be provided to prevent a ledge failure and ensure the performance of the beam such that $T_{ad} > F_{ad}$.

$$T_{ad} := 12 A_5 \cdot f_{y\_5} = 239.14 \text{kip} \qquad \boxed{\frac{T_{ad}}{F_{ad}} = 1.434}$$